Hokkaido University

Study on Assembled Structures and Physical Properties of Luminescent Lanthanide(III) Complexes

A Thesis

By

Yuichi Hirai

Graduate School of Chemical Sciences and Engineering

Submitted in partial fulfillment of the requirements

For the degree of Doctor, Engineering

List of publications

[1] Y. Hirai, T. Nakanishi, K. Miyata, K. Fushimi, Y. Hasegawa, “Thermo-sensitive luminescent materials composed of Tb(III) and Eu(III) complexes,” *Mater. Lett.*, **2014**, *130*, 91-93.

[2] Y. Hirai, T. Nakanishi, Y. Kitagawa, K. Fushimi, T. Seki, H. Ito, H. Fueno, K. Tanaka, T. Satoh, Y. Hasegawa, “Luminescent Coordination Glass: Remarkable Morphological Strategy for Assembled Eu(III) Complexes,” *Inorg. Chem.*, **2015**, *54*, 4364-4370.

[3] Y. Hirai, T. Nakanishi, Y. Hasegawa, “Organo-lanthanide luminophores bridged by phosphine oxide ligands,” *J. Lumin.*, **2016**, *170*, 801-807.

[4] Y. Hirai, T. Nakanishi, Y. Kitagawa, K. Fushimi, T. Seki, H. Ito, Y. Hasegawa, “High energy transfer efficiency of Eu(III) coordination polymers with thiophene-derivative bridge,” *Angew. Chem. Int. Ed.*, **2016**, *170*, 801-807.

[5] Y. Hirai, P.P. Ferreira da Rosa, T. Nakanishi, Y. Kitagawa, K. Fushimi, Y. Hasegawa, “Amorphous Formability and Temperature-Sensitive Luminescence of Lanthanide Coordination Glasses Linked by Thienyl, Naphthyl, and Phenyl Bridges with Ethynyl Groups," *Bull. Chem. Soc. Jpn.,* **2017***, 90*, 322-326.

[6] Y. Hirai, T. Nakanishi, Y. Kitagawa, K. Fushimi, T. Seki, H. Ito, Y. Hasegawa, “Cracking the Code of Triboluminescence Using Lanthanide Coordination Polymers with Face-to-Face Arranged Substituents," *in contribution*.

Other publications

[1] H. Kataoka, T. Kitano, T. Takizawa, Y. Hirai, T. Nakanishi, Y. Hasegawa, “Photo- and Thermo-stable Luminescent Beads Composed of Eu(III) Complexes and PMMA for Enhancement of Silicon Solar Cell Efficiency”, *J. Alloys Compd.*, **2014**, *611*, 293-297.

[2] Y. Hasegawa, N. Sato, Y. Hirai, T. Nakanishi, Y. Kitagawa, A. Kobayashi, M. Kato, T. Seki, H. Ito, K. Fushimi, “Enhanced Electric Dipole Transition in Lanthanide Complexes with Organometallic Ruthenocene Units”, *J. Phys. Chem. A*, **2015**, *119*, 4825-4833.

[3] S. Rungrodnimitchai, D. Kotatha, C. Dokbua, Y. Hasegawa, T. Nakanishi, Y. Hirai, T. Kawai: NOVEL SYNTHESIS OF EU2+ DOPED CAF2 NANOCRYSTALS AND EU2+ DOPED SRF2 NANOCRYSTALS IN LIQUID AMMONIA, *Acad. J. Sci.*, **2015**, *04*, 223-232.

[4] M. Hatanaka, Y. Hirai, Y. Kitagawa, T. Nakanishi, Y. Hasegawa, K. Morokuma: Organic linkers control the thermosensitivity of the emission intensities from Tb(III) and Eu(III) in a chameleon polymer, *Chem. Sci.*, **2017**, *8*, 423-429.

List of presentations

[1] Y. Hirai, T. Nakanishi, T. Satoh, T. Kakuchi, K. Fushimi, Y. Hasegawa : 「Synthesis and photophysical properties of supramolecular Eu(III) complex」 14th Chitose International Forum on Photonics Science & Technology（2013 年 7 月, 千歳）

[2] 平井悠一, 中西貴之, 佐藤敏文, 覚知豊次, 伏見公志, 長谷川靖哉: 「超分子型 Eu(III)錯体の発光特性とアモルファス特性」第 25 回配位化合物の光化学討論会 (2013 年 8 月, 唐津)

[3] 平井悠一, 中西貴之, 佐藤敏文, 覚知豊次, 伏見公志, 長谷川靖哉:「超分子型 Eu(III)錯体の発光特性と構造転移」2013 年光化学討論会, (2013 年 9 月, 松山)

[4] 平井悠一, 中西貴之, 伏見公志, 長谷川靖哉: 「超分子型 Eu(III)錯体の構造転移と光物性」第 3 回 CSJ 化学フェスタ, (2013 年 10 月, 船堀)

[5] 平井悠一, 中西貴之, 関朋宏, 伊藤肇, 佐藤敏文, 伏見公志, 長谷川靖哉: 「Eu(III)配位複合体の組織構造と発光特性」錯体化学会第 63 回討論会, (2013 年 11 月, 那覇)

[6] Y. Hirai, T. Nakanishi, K. Fushimi, Y. Hasegawa :「Unusual photophysical properties of lanthanide coordination polymers composed of Tb(III) ions and a small amount of Eu(III) ions」27^{TH} Rare earth research conference 2014 (2014 年 6 月, Reno, USA)

[7] 平井悠一, 宮田康平, 中西貴之, 伏見公志, 長谷川靖哉: 「Tb(III)と Eu(III)から構成される配位高分子の光物性」日本化学会北海道支部会 2014 年夏季研究発表会, (2015 年 7 月, 苫小牧)

[8] 平井悠一, 中西貴之, 関朋宏, 伊藤肇, 佐藤敏文, 伏見公志, 長谷川靖哉: 「位置異性配位子を有する発光性 Eu(III)錯体の形態制御」錯体化学会第 64 回討論会, (2015 年 9 月, 東京)

[9] Y. Hirai, T. Nakanishi, T. Satoh, T. Kakuchi, K. Fushimi, Y. Hasegawa : 「Photo and thermophysical properties of Eu(III) complexes with bidentate phosphine oxide ligands」15th Chitose International Forum on Photonics Science & Technology (2014 年 10 月, 千歳)

[10] 平井悠一, 中西貴之, 関朋宏, 伊藤肇, 伏見公志, 長谷川靖哉:「自己集積型 Eu(III)錯体の構造制御と光物性」2014 年光化学討論会, (2014 年 11 月, 札幌)

[11] 平井悠一, 中西貴之, 北川裕一, 伏見公志, 関朋宏, 伊藤肇, 笛野博之, 田中一義, 長谷川靖哉: 「希土類錯体の形態制御および光物性評価」新学術領域「元素ブロック高分子材料の創出」第 3 回合同修論発表会, (2015 年 3 月, 京都)

[12] 平井悠一, 中西貴之, 北川裕一, 伏見公志, 長谷川靖哉: 「チオフェン誘導体で架橋した Eu(III)錯体の物性評価」第 32 回希土類討論会, (2015 年 5 月, 鹿児島)

[13] Y. Hirai, T. Nakanishi, Y. Kitagawa, T. Seki, H. Ito, K. Fushimi, Y.

Hasegawa: 「Thermo-stable and Strong Luminescence Properties of Lanthanide Coordination Polymers Linked with Thiophene Derivative Units」錯体化学会第 65 回討論会, (2015 年 9 月, 奈良)

[14] Y. Hirai, T. Nakanishi, Y. Kitagawa, K. Fushimi, Y. Hasegawa: 「Morphological Strategy for Assembled Eu(III) Complexes with Strong Luminescence and Amorphous Formability」16th Chitose International Forum on Photonics Science & Technology (CIF 16), (2015 年 10 月, 千歳)

[15] 平井悠一・中西貴之・北川裕一・伏見公志・長谷川靖哉: 「熱耐久性およびアモルファス特性を有する希土類錯体の発光」第 11 回学際領域における分子イメージングフォーラム, (2015 年 11 月, 東京)

[16] Y. Hirai, T. Nakanishi, Y. Kitagawa, K. Fushimi, Y. Hasegawa: 「Construction of luminescent lanthanide coordination glass」The 2nd International Workshop on Luminescent Materials (LumiMat2016), (2015 年 12 月, 京都)

[17] Y. Hirai, T. Nakanishi, Y. Kitagawa, K. Fushimi, Y. Hasegawa: 「High emission quantum yields and energy transfer efficiency of Eu(III) coordination polymers with heteroaromatic bridge」日本化学会第 96 春季年会, (2016 年 3 月, 京都)

[18] Y. Hirai, T. Nakanishi, Y. Kitagawa, K. Fushimi, Y. Hasegawa: 「Development of luminescent Eu(III) coordination compounds with glass-forming ability」International Symposium on Lanthanide Coordination Chemistry (ISLCC2016), (2016 年 6 月, 神奈川)

[19] Y. Hirai, T. Nakanishi, Y. Kitagawa, K. Fushimi, Y. Hasegawa: 「Design and synthesis of luminescent Eu(III) coordination glass」International Conference on Coordination Chemistry, (2016 年 7 月, Brest, France)

[20] Y. Hirai, T. Nakanishi, Y. Kitagawa, K. Fushimi, Y. Hasegawa:「Photo- and tribo-luminescence of lanthanide coordination polymers with (hetero)aromatic bridges」錯体化学会第 66 回討論会, (2016 年 9 月, 福岡)

[21] Y. Hirai, T. Nakanishi, Y. Kitagawa, K. Fushimi, Y. Hasegawa: 「Strong Photoluminescence and Thermal Stability of Eu(III) Coordination Polymers with Thiophene-Based Bridge」Pacific Rim Meeting on Electrochemical and Solid-State Science (PRiME2016), (2016 年 10 月, Hawaii, USA)

[22] 平井悠一・中西貴之・北川裕一・伏見公志・長谷川靖哉: 「温度・励起波長・機械刺激に応答して発光を示す希土類錯体ポリマー」第 12 回学際領域における分子イメージングフォーラム, (2016 年 11 月, 東京)

[23] 平井悠一, 中西貴之, 伏見公志, 長谷川靖哉: 「希土類錯体ポリマーの多刺激に応答した発光特性」第 6 回 CSJ 化学フェスタ, (2016 年 11 月, 船堀)

List of patents

[1] 長谷川靖哉, 平井悠一, 中西貴之, 伏見公志:「配位子及び希土類錯体」特願 2013-141994 (2013.07.05)

[2] Yasuchika Hasegawa, Yuichi Hirai, Takayuki Nakanishi, Koji Fushimi:「Ligand, and rare earth complex」PCT / JP2014 / 067861

[3] 中西貴之, 平井悠一, 長谷川靖哉, 北川裕一, 伏見公志:「希土類錯体ポリマー」　特願 2016-092667

List of awards

[1] 平成 25 年 7 月
14th Chitose International Forum on Photonics Science & Technology (CIF14)において、Best Poster Award を受賞

[2] 平成 25 年 8 月
第 25 回配位化合物の光化学討論会において、優秀ポスター賞を受賞

[3] 平成 25 年 10 月
第 3 回 CSJ 化学フェスタにおいて、優秀ポスター発表賞を受賞

[4] 平成 26 年 10 月
15th Chitose International Forum on Photonics Science & Technology (CIF15)において、Poster Award を受賞

[5] 平成 27 年 3 月
新学術領域研究「元素ブロック高分子材料の創出」第 3 回合同修論発表会において、優秀発表賞を受賞

[6] 平成 27 年 8 月
錯体化学若手の会夏の学校 2015 において、優秀ポスター賞を受賞

[7] 平成 27 年 8 月
第 3 回 TIA ナノグリーン・サマースクールにおいて、奨励賞を受賞

[8] 平成 27 年 9 月
錯体化学会第 65 回討論会において、ポスター賞を受賞

[9] 平成 28 年 3 月
日本化学会第 96 春季年会において、学生講演賞を受賞

[10] 平成 28 年 6 月
International Symposium on Lanthanide Coordination Chemistry (ISLCC2016)において、Best Poster Award を受賞

[11] 平成 28 年 11 月
第 6 回 CSJ 化学フェスタにおいて、優秀ポスター発表賞を受賞

CONTENTS

CHAPTER 3

Luminescent lanthanide(III)-mixed coordination polymers for tunable temperature-sensitivity

CHAPTER 4

Construction of luminescent lanthanide(III) coordination glass

CHAPTER 5

Amorphous formability and temperature-sensitive luminescence of lanthanide(III) coordination glasses

CHAPTER 6

Triboluminescence of lanthanide(III) coordination polymers

CHAPTER 7

Summary and outlook

Chapter 1

General introduction

Abstract

Luminescent materials play a vital role in our lives. There has been significant progress in the development of inorganic and organic phosphors. Assembled lanthanide (Ln(III)) coordination compounds have attracted much attention as promising candidates for luminescent materials due to their unique photophysical properties derived from f-f transitions. In this thesis, the relationships between assembled Ln(III) coordination compounds and photophysical, thermal, and mechanical properties are focused on for the development of novel luminescent materials. The molecular designs of organic bridging ligands to control the assembled structures and physical properties of Ln(III) coordination compounds are shown.

1.1 Introduction

The development of efficient and bright luminescent materials has broadened the range and time of activities of human beings, who rely to a large extent on visual perception. After the emergence of incandescent lamps, the first electric light invented by Thomas Edison, artificial light sources have contributed greatly to lifestyle changes.[1-3] The first commercial light-emitting diode (LED) was developed by Holonyak and Bevacqua based on GaAsP.[4] Kido and Adachi then successfully fabricated efficient emitters for white LEDs based on lanthanide complexes and organic compounds.[5-7] Numerous types of inorganic and organic luminescent materials are now used in various applications such as displays, lightings, lasers, and optical communication systems (Figure 1-1).[8-11]

Figure 1-1. Typical luminescent materials in our daily lives.

Inorganic phosphors are composed of host materials and dopants that serve as activators, sensitizers, and impurities. The photophysical properties of these materials are usually tuned by varying the host/dopant combinations or the concentrations of dopants, and these materials have advantages of stability due to the rigid inorganic frameworks. Schnick and co-workers recently developed a narrow-band red nitride phosphor, $Sr[LiAl_3N_4]$:Eu(II).[12]

Organic luminophores, on the other hand, are generally aromatic compounds with extended π-electron systems as represented by perylenes and coumarins.[13-15] Physical properties of these compounds can be controlled by expansion/reduction of π-electron systems and modification of substituents. These classes of compounds have been used in soft and flexible optical devices such as organic displays and lightings.[16-18]

In addition to the materials mentioned above, coordination compounds are also attractive because of their various combinations of metal ions and organic ligands. Coordination compounds form polyhedral, cluster, and polymer structures depending on metal ions and the moiety of organic ligands, which result in varied chemical and physical properties.[19] These features make them possible to be next-generation luminescent materials with novel functions.

1.2 Luminescence of lanthanide(III) ions

Among these materials mentioned above, lanthanide(III) (Ln(III)) coordination compounds assembled from Ln(III) ions and organic ligands have attracted attention due to their versatile photophysical properties arising from characteristic 4f-4f transitions.[20-26] They generally show line-like emission and long emission lifetimes, different from *d*-block transition metal complexes or organic compounds (Figure 1-2a). It is also known that the emission wavelength varies depending on Ln(III) ions from the visible (VIS) to near-infrared (NIR) region (Figure 1-2b, Table 1-1).[27,28] VIS emission from Tb(III), Eu(III), Dy(III), or Sm(III) ions has long been used for applications such as LEDs and other lighting devices.[6,7,29] NIR emitters such as Pr(III), Ho(III), Yb(III), Nd(III), and Er(III) compounds have also been used in various applications such as optical signal amplifiers in telecommunication networks, laser systems, and biomedical imaging sensors.[30-33]

The electronic configuration of the most common +III oxidation state of lanthanide ions (Ln(III)) is [Xe]$4f^{n-1}$, and the 4f orbitals are filled from La(III) ($4f^0$) to Lu(III) ($4f^{14}$). Since the radial charge density distribution of Ln(III) ions is smaller than the filled 5s and 5p orbitals, the 4f orbitals are shielded from the coordination environments by these orbitals. Although lanthanides bind mostly via ionic interactions, these characteristic electronic structures of Ln(III) ions provide minimal perturbation of the ligand field upon 4f orbitals. The ligand field, however, can affect the emission spectra of Ln(III) ions.

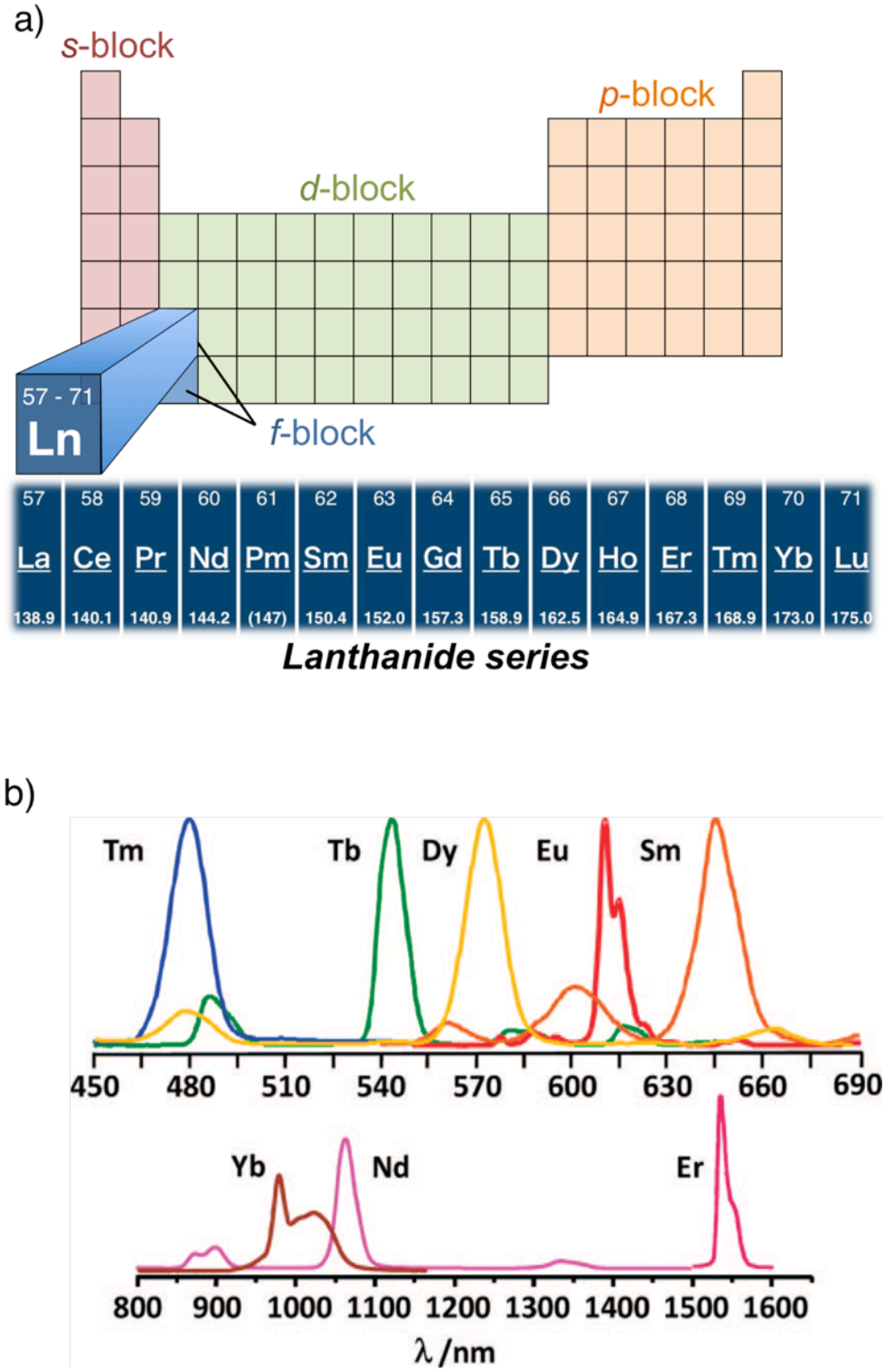

Figure 1-2. a) Lanthanide elements in periodic table, and b) emission spectra of Ln(III) tris(*β*-diketonate) compounds.[27]

Table 1-1. Most common emissive f-f transitions of Ln(III) ions.[28]

Element	Transition	Wavelength / nm
Pr	$^1D_2 \rightarrow {}^3F_4$	1000
	$^1D_2 \rightarrow {}^1G_4$	1440
	$^1D_2 \rightarrow {}^3H_J$ (J = 4, 5)	600, 690
	$^3P_0 \rightarrow {}^3H_J$ (J = 4 - 6)	490, 545, 615, 640
	$^3P_0 \rightarrow {}^3F_J$ (J = 2 - 4)	700, 725
Nd	$^4F_{3/2} \rightarrow {}^4I_J$ (J = 9/2 - 13/2)	900, 1060, 1350
Sm	$^4G_{5/2} \rightarrow {}^6H_J$ (J = 9/2 - 13/2)	560, 595, 640, 700, 775
	$^4G_{5/2} \rightarrow {}^6F_J$ (J = 1/2 - 9/2)	870, 887, 926, 1010, 1150
Eu	$^5D_0 \rightarrow {}^7F_J$ (J = 0 - 6)	580, 590, 615, 650, 720, 750, 820
Gd	$^6P_{7/2} \rightarrow {}^8S_{7/2}$	315
Tb	$^5D_4 \rightarrow {}^7F_J$ (J = 6 - 0)	490, 540, 580, 620, 650, 660, 675
Dy	$^4F_{9/2} \rightarrow {}^6H_J$ (J = 15/2 - 9/2)	475, 570, 660, 750
	$^4I_{15/2} \rightarrow {}^6H_J$ (J = 15/2 - 9/2)	455, 540, 615, 695
Ho	$^5S_2 \rightarrow {}^5I_J$ (J = 8, 7)	545, 750
	$^7F_5 \rightarrow {}^5I_J$ (J = 8, 7)	650, 965
Er	$^4S_{3/2} \rightarrow {}^4I_J$ (J = 15/2 - 13/2)	545, 850
	$^4F_{9/2} \rightarrow {}^4I_{15/2}$	660
Tm	$^1D_2 \rightarrow {}^3F_4, {}^3H_4, {}^3F_J$ (J = 3, 2)	450, 650, 740, 775
	$^1G_4 \rightarrow {}^3H_6, {}^3F_4, {}^3H_5$	470, 650, 770
	$^3H_4 \rightarrow {}^3H_6$	800
Yb	$^2F_{5/2} \rightarrow {}^2F_{7/2}$	980

1.3 Enhancement of luminescence efficiency

1.3.1 The antenna effect

Since the 4f-4f transitions are parity-forbidden, the absorption coefficients of Ln(III) ions are small (ε < 10 L mol^{-1} cm^{-1}), and this is why sensitized emission through the ligand-to-metal energy transfer (ET) mechanism is desired for the development of highly emissive compounds.

The sensitized emission of Ln(III) compounds was first reported by Weissman in 1942.[34] When Eu(III) complexes with salicylaldehydes or benzoylacetonates were excited in the region of light absorption associated primarily with the ligands, strong line-like “atomic” emission from Eu(III) ions was observed. According to the findings, organic ligands with large absorption coefficients and a suitable energy level for ET were called “antenna ligands,” and the corresponding sensitization process named “antenna effect” was confirmed (Figure 1-3). Then Crosby and co-workers extensively studied these mechanisms to establish the path of the energy migration process in Ln(III) complexes.[35-37] The process is explained in three steps (Figure 1-3b): i) singlet-singlet absorption of antenna ligands, ii) intersystem crossing (ISC) from the singlet excited state (^{1}S) to the triplet excited state (^{3}T), and iii) energy transfer (ET) to the Ln(III) excited state, and then iv) Ln(III)-centered emission (Em) is observed.

Organic chromophores such as β-diketonate and pyridine derivatives have been utilized as ideal antenna ligands to sensitize Ln(III)-centered luminescence (Figure 1-3).[38-40] Typical examples of β-diketonates are hexafluoroacetylacetonates (hfa) and 2-thenoyltrifluoroacetylacetonates (tta), and strong luminescence of these Ln(III)-(β-diketonates) compounds has been

reported by Bünzli and others.[41-43] The group of Bettencourt also reported luminescence of Eu(III) and Tb(III) compounds with a series of pyridine-bis(oxazoline) (Pybox) derivatives.[44-46]

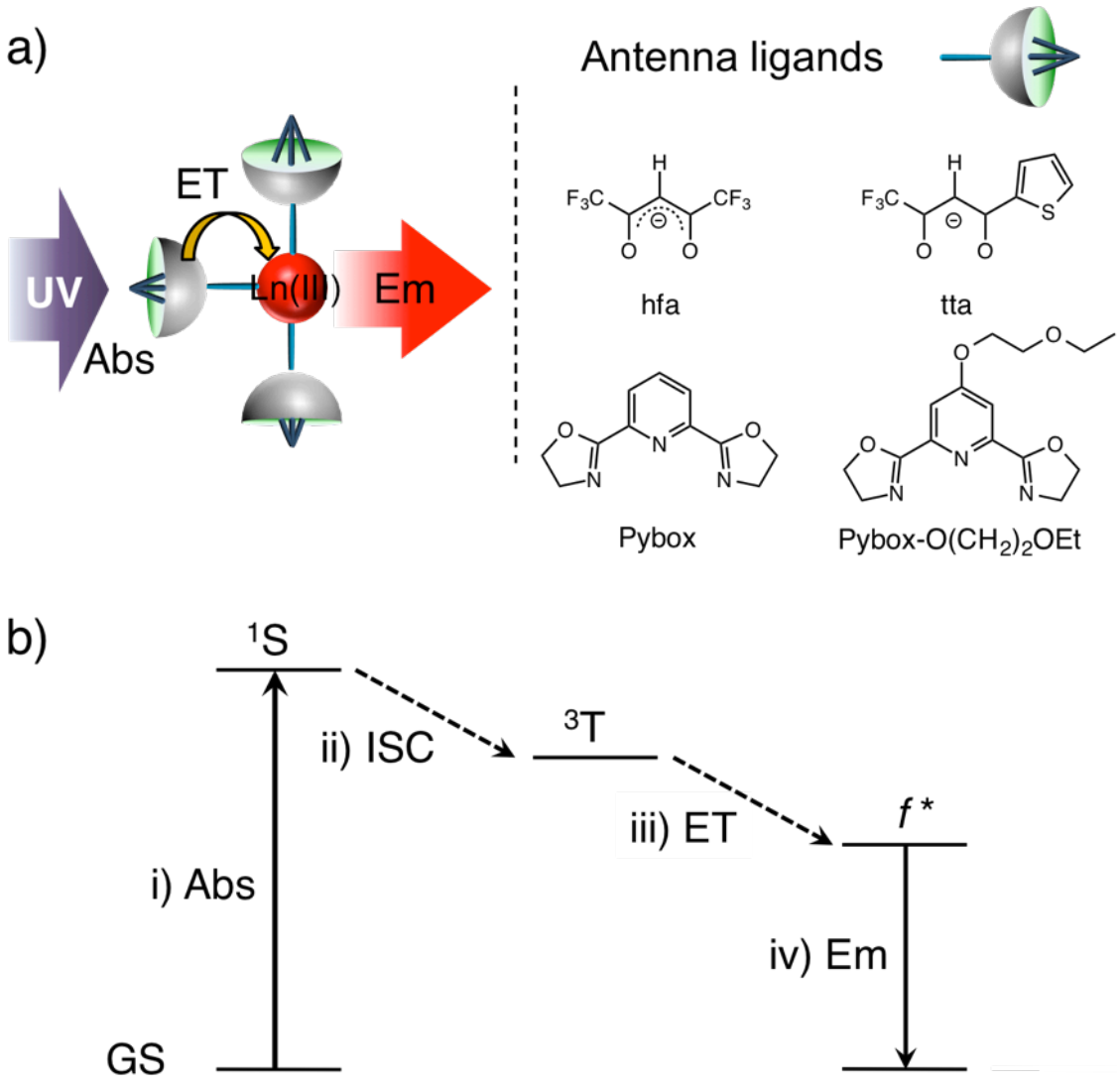

Figure 1-3. a) A schematic representation of antenna effect (left) and chemical structures of reported antenna ligands (right). b) A simplified diagram of sensitized luminescence (Abs: absorption, ET: energy transfer, Em: emission, GS, ground state, ^{1}S: singlet excited state, ^{3}T: triplet excited state, ISC: intersystem crossing, *f* *: emissive level of Ln(III) ions).

1.3.2 Promotion of 4f-4f transitions

As already mentioned, 4f-4f transitions are intrinsically forbidden. First, these transitions accompany a change in spin, and spin is therefore forbidden. Second, since both the electric dipole operator and f orbitals have *ungerade* (odd) symmetry, electric dipole transitions are parity forbidden. However, the spin-orbit coupling invalidates the total spin quantum number *S* to relax the spin rule, and the effects of ligand field upon 4f-5d mixing also partially allow electric dipole transitions.[47] A mixture of opposite parities via crystal fields accompanied by partially allowed transitions was independently proposed by Brian Judd and George Offelt around the same time.[48,49] The radiative rate constants (k_r) of these transitions are strongly affected by the symmetry around Ln(III) ions. The 4f-4f transition probabilities have been enhanced by reducing the geometrical symmetry around Ln(III) ions.[50-53]

Hasegawa and co-workers reported the enhancement of luminescence by introducing an eight-coordinated square anti-prism (8-SAP), a dodecahedron (8-TDH: D_{2d}) and a nine-coordinated monocapped square-antiprism (9-SAP: C_{4v}).[54-57] In addition, seven-coordinated monocapped octahedron (7-MCO: C_{3v}) structures have recently been reported for further enhancement of 4f-4f transitions.[58]

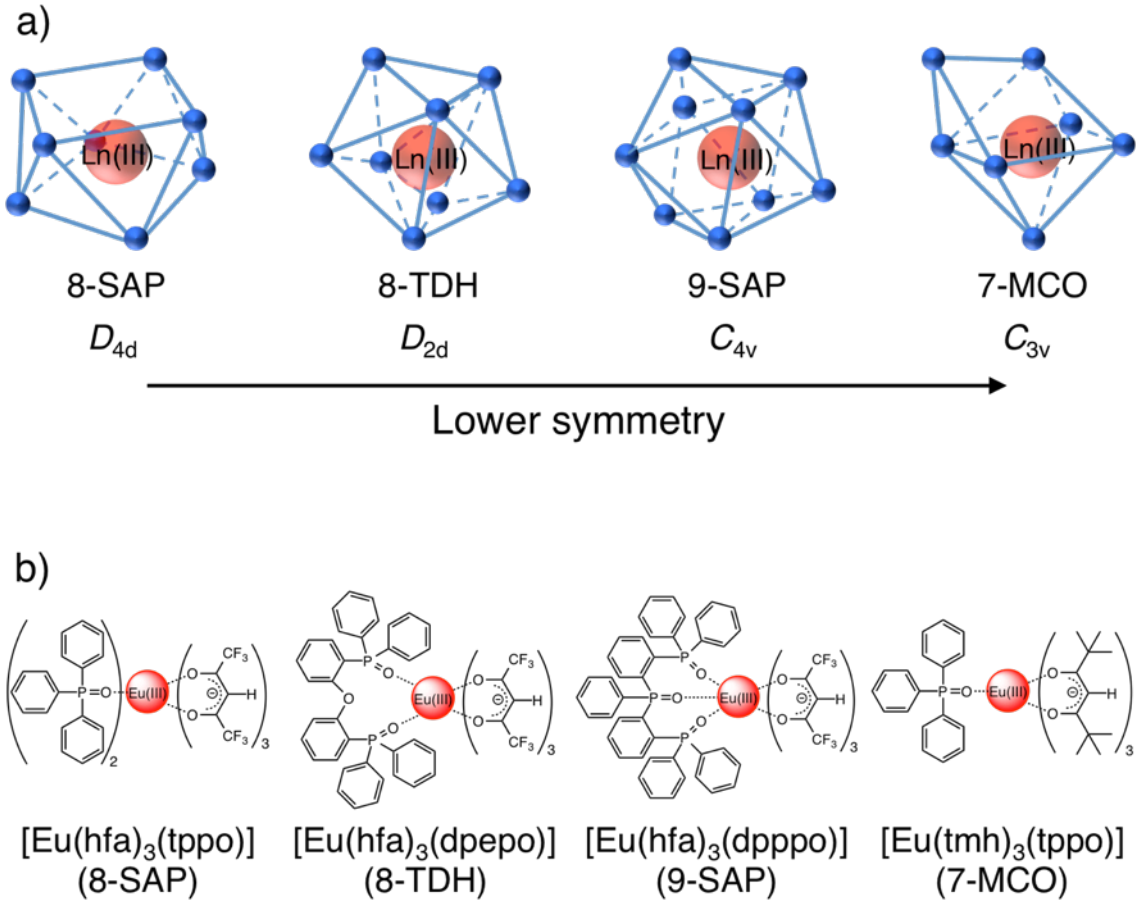

Figure 1-4. a) Ideal coordination geometrical structures of eight-coordinated square anti-prism (8-SAP), dodecahedron (8-TDH: D_{2d}), nine-coordinate monocapped square-antiprism (9-SAP: C_{4v}), and seven-coordinated monocapped octahedron (7-MCO: C_{3v}). b) Chemical structures of reported asymmetrical Eu(III) coordination compounds.[54-58]

1.3.3 Suppression of vibrational relaxation

Suppression of the non-radiative process is also essential for strong emission since Ln(III)-centered emission is easily quenched through vibrational relaxation. When the energy gaps between emissive and ground states of Ln(III) ions correspond well to the vibration of chemical bonds with higher vibrational quantum numbers (v > 1), Ln(III)-centered emission is non-radiatively quenched. Therefore, compounds with high vibrational frequency bonds such as O-H (3600 cm^{-1}), N-H (3300 cm^{-1}), and C-H (2900 cm^{-1}) are usually known to be quenchers. Instead of these bonds, introduction of C=O (1650 cm^{-1}), C-F (1200 cm^{-1}), P=O (1120 cm^{-1}), O-D (2200 cm^{-1}), or C-D (2100 cm^{-1}) bonds is effective for suppressing the non-radiative relaxation, since higher vibrational quanta are needed and the process becomes inefficient (Figure 1-5a).

Based on these molecular designs, Hasegawa and co-workers first succeeded in observing Nd(III)-centered luminescence in an organic solvent.[59] In their work, the deuterated hexafluoroacetylacetonato (hfa-D) ligand played an important role in providing an ideal antenna effect and eliminating high-vibrational C-H and O-H bonds (Figure 1-5b, left). Pikramenou and co-workers demonstrated long emission lifetimes of Yb(III) coordination compounds formed by fully fluorinated imidodiphosphinate ligands (*N*-(*P*,*P*-di(pentafluorophinoyl))-*P*,*P*-dipentafluorophenylphosphinimidic acid: HF_{20}tpip), due to the absence of high energy X-H vibrations (Figure 1-5b, center).[60] Binnemans and co-workers reported strong NIR luminescence of Er(III) complexes consisting of Er(III) ions, bis(perfluoroalkylsulfonyl)imides, and 1,10-phenanthroline [$Er(pos)_3(phen)$] (Figure 1-5b, right).[61]

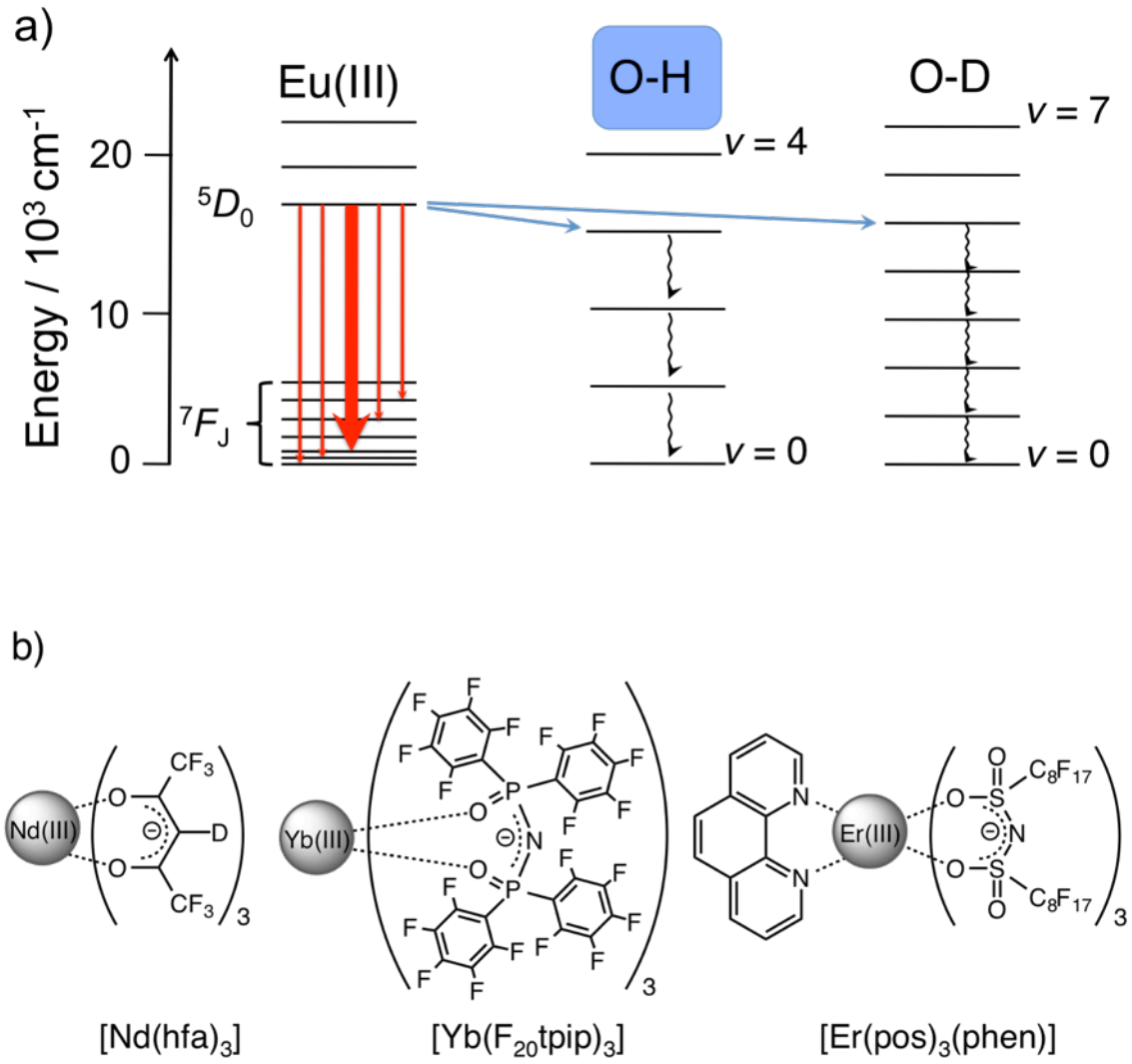

Figure 1-5. a) Radiative and non-radiative vibrational quenching process focused on Eu(III) ions. b) Chemical structures of reported low-vibrational Ln(III) coordination compounds.[59-61]

1.4 Assembled structures of coordination compounds

In addition to the geometrical design around metal ions, control of the entire molecular morphology of coordination compounds is also required to explore their potential as functional materials. Precisely controlled assembly of multi-metal ions and organic bridging ligands provides novel physical or chemical properties that do not appear in individual components, and this precisely controlled assembly has recently become a common idea, particularly for transition metal coordination systems.[62-66]

In 1990, Fujita and co-workers reported the formation of planar-squared Pd(II) coordination compounds $[(en)Pd(4,4'\text{-}bpy)]_4(NO_3)_8$ (en: ethylenediamine, bpy: bipyridine) by mixing Pd(II) ions and organic ligands at room temperature through a self-assembly mechanism (Figure 1-6).[67] The Pd(II) complex also has the ability to recognize an organic molecule in an aqueous medium. These results suggested that finite and single substrate was formed via self-assembly.

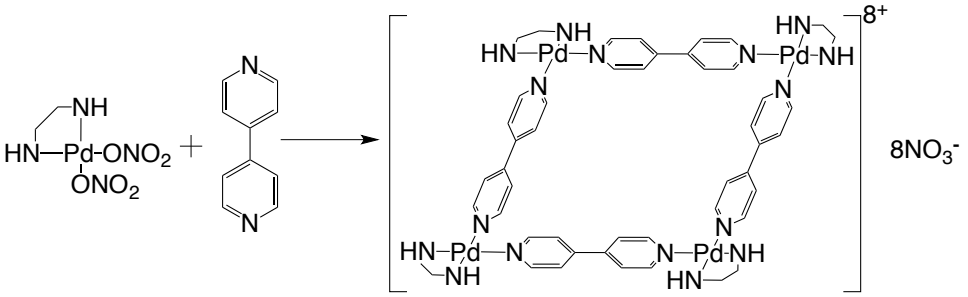

Figure 1-6. A synthetic scheme of a planar-squared Pd(II) complex.[67]

Coordination polymers in particular form characteristic assembled 1-D chains, 2-D sheets, and 3-D networks depending on the moiety of organic bridging ligands.[68,69] These structural features can provide additional functions such as electrical conductivity, redox activity, and specific ion or compound sensitivity

as well as photophysical properties.[70-75] Niu and co-workers reported temperature-dependent magnetic susceptibility and photoluminescence of 2-D organic-inorganic architectures composed of Ln(III)-Cu(II) heterometallic phosphotungstates.[76] Wang developed Mg(II), Ni(II), and Co(II)-based 3-D networks linked by dibenzoic acid derivatives for highly sensitive and selective detection of heterocyclic compounds.[77] Vittal and co-workers also reported that 2-D sheets of emissive Zn(II) coordination compounds were assembled to 3-D networks via [2+2] cycloaddition reaction of bridging ligands.[78]

These studies have exploited the designs of organic bridging ligands for construction and modification of a wide variety of multi-nuclear complexes, coordination polymers, and metal organic frameworks (MOFs). Thus, much larger and complicated assemblies with additional features can be expected with appropriate designs of molecules.

1.5 Assembled Ln(III) coordination compounds

Recently, Ln(III)-based coordination polymers or MOFs have attracted attention due to their rigid scaffolds with versatile photophysical properties.[79] Carlos and co-workers have reported the series of luminescent MOFs based on Ln(III) ions, and they showed that the MOFs have the ability to sense anions, cations, and specific molecules.[80] Reddy reported thermally stable Eu(III) coordination polymers.[81] Hasegawa and co-workers also succeeded in providing thermal stability (> 300˚C) and high luminescence efficiency (70%) by introducing intermolecular hydrogen bonds.[82] Numerous studies on Ln(III)-mixed MOFs have recently been carried out due to the stability and ease of tuning photophysical properties.[83-87] This class of materials has the advantage of being composed of thermodynamically stable backbones; however, these rigid frameworks are also known to allow adsorption of organic solvents and to suppress the coordination of ideal antenna ligands such as *β*-diketonates. Therefore, the design of assembled Ln(III) coordination compounds without inhibiting strong luminescence properties is highly desired.

Since the history of development of Ln(III) coordination polymers is relatively short and an integrated approach to molecular designs for strong luminescent materials with novel functions are still in progress, there is much room for improvement of photophysical, thermal, and mechanical properties derived from specific assembled structures.

1.6 Objectives

An appropriate design of organic bridging ligands makes it possible to control the entire structures of assembled Ln(III) coordination compounds, thus providing novel photophysical, thermal, and mechanical properties.

For this thesis, control of the morphology of assembled Ln(III) coordination compounds was studied in order to achieve enhanced luminescence efficiency and further provide novel functions such as glass-formability and temperature- and shock-sensitivity (Figure 1-7). The author achieved i) high energy transfer efficiencies in densely packed structures, ii) tunable temperature sensitivity using Ln(III) mixed systems, iii) glass-forming ability with hard-to-crystallize structures, and iv) shock-sensitivity by introducing a specific disordered arrangement of substituents between molecules.

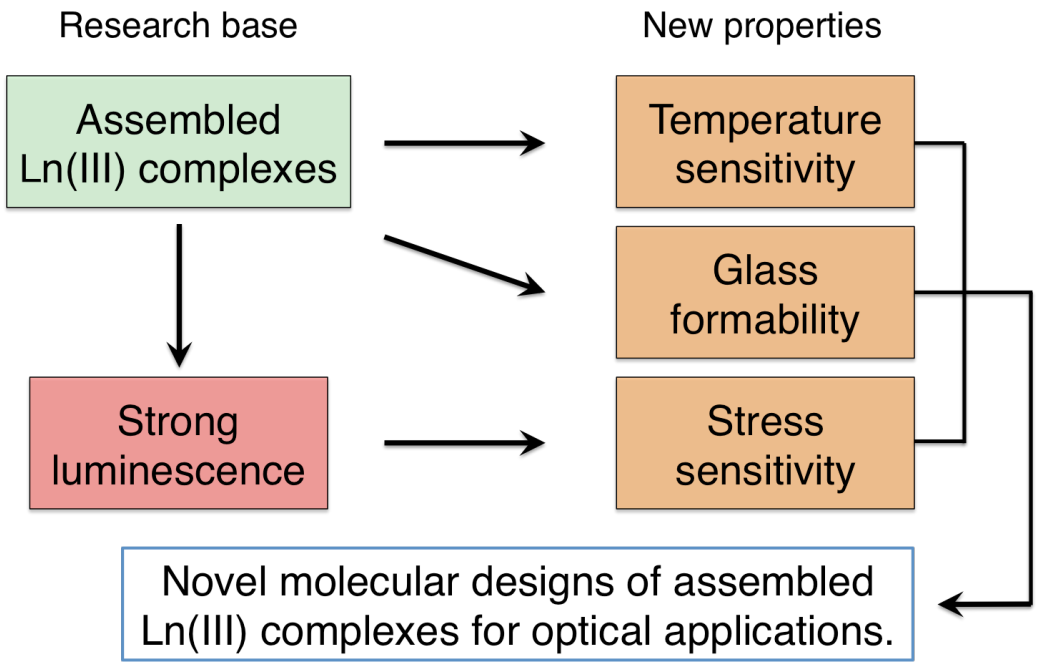

Figure 1-7. A conceptual diagram of this thesis.

1.7 Contents of this thesis

This thesis consists of seven chapters.

In **Chapter 1**, previous studies on Ln(III) complexes and assembled coordination systems are reviewed, and the purpose of this study is described.

In **Chapter 2**, a packing system named “coordination zippers” that is achieved by introducing thiophene-based bridging ligands is proposed. Highly zipped coordination structures with intermolecular hydrogen bonds were constructed for a densely packed structure, resulting in dramatically improved photoluminescence (PL) efficiency via ligand excitation and thermal stability.

In **Chapter 3**, the control of photophysical properties in Tb/Eu mixed coordination polymers for tunable temperature sensitivity is described.

In **Chapter 4**, the strategy for construction of luminescent lanthanide coordination compounds with glass-formability, “lanthanide coordination glasses,” is described. Bent-angled bridging ligands with ethynyl groups are introduced to suppress crystal packing.

Based on the strategy suggested in Chapter 3 and Chapter 4, extension of the molecular designs of coordination glasses and their temperature-responsive luminescence in a glassy state are demonstrated in **Chapter 5**.

In **Chapter 6**, the design of coordination polymers with triboluminescence (TL) properties is described. Strong TL materials were fabricated by inducing an intermolecular disordered arrangement of substituents. A significant PL/TL spectral difference was observed. The mechanisms of these phenomena are discussed on the basis of observations of Tb/Eu mixed coordination polymers.

Finally, in **Chapter 7**, summary and outlook of these studies are given.

1.8 References

[1] E.F. Schubert, J.K. Kim, *Science* **2005**, *308*, 1274-1278.

[2] T.P. Yoon, M.A. Ischay, J.N. Du, *Nat. Chem.* **2010**, *2*, 527-532.

[3] F. Bonaccorso, Z. Sun, T. Hasan, A.C. Ferrari, *Nat. Photonics* **2010**, *4*, 611-622.

[4] N. Holonyak, S.F. Bevacqua, *Appl. Phys. Lett.* **1962**, *1*, 82-83.

[5] C. Adachi, M.A. Baldo, M.E. Thompson, S.R. Forrest, *J. Appl. Phys.* **2001**, *90*, 5048-5051.

[6] J. Kido, H. Hayase, K. Hongawa, K. Nagai, K. Okuyama, *Appl. Phys. Lett.* **1994**, *65*, 2124-2126.

[7] J. Kido, K. Nagai, Y. Ohashi, *Chem. Lett.* **1990**, 657-660.

[8] C.D. Muller, A. Falcou, N. Reckefuss, M. Rojahn, V. Wiederhirn, P. Rudati, H. Frohne, O. Nuyken, H. Becker, K. Meerholz, *Nature* **2003**, *421*, 829-833.

[9] K. Kuriki, Y. Koike, Y. Okamoto, *Chem. Rev.* **2002**, *102*, 2347-2356.

[10] M.A. Baldo, D.F. O'Brien, Y. You, A. Shoustikov, S. Sibley, M.E. Thompson, S.R. Forrest, *Nature* **1998**, *395*, 151-154.

[11] J.M. Phillips, M.E. Coltrin, M.H. Crawford, A.J. Fischer, M.R. Krames, R. Mueller-Mach, G.O. Mueller, Y. Ohno, L.E.S. Rohwer, J.A. Simmons, J.Y. Tsao, *Laser Photonics Rev.* **2007**, *1*, 307-333.

[12] P. Pust, V. Weiler, C. Hecht, A. Tücks, A.S. Wochnik, A.-K. Henß, D. Wiechert, C. Scheu, P.J. Schmidt, W. Schnick, *Nat. Mater.* **2014**, *13*, 891-896.

[13] C. Joblin, F. Salama, L. Allamandola, *J. Chem. Phys.* **1999**, *110*, 7287-7297.

[14] J. Donovalova, M. Cigan, H. Stankovicova, J. Gaspar, M. Danko, A. Gaplovsky, P. Hrdlovic, *Molecules* **2012**, *17*, 3259-3276.

[15] K. Hara, Z.S. Wang, T. Sato, A. Furube, R. Katoh, H. Sugihara, Y. Dan-Oh, C. Kasada, A. Shinpo, S. Suga, *J. Phys. Chem. B* **2005**, *109*, 15476-15482.

[16] M.-C. Choi, Y. Kim, C.-S. Ha, *Prog. Polym. Sci.* **2008**, *33*, 581-630.

[17] M.H. Park, T.H. Han, Y.H. Kim, S.H. Jeong, Y. Lee, H.K. Seo, H. Cho, T.W. Lee, *J. Photon. Energy* **2015**, *5*.

[18] T.H. Han, Y. Lee, M.R. Choi, S.H. Woo, S.H. Bae, B.H. Hong, J.H. Ahn, T.W. Lee, *Nat. Photonics* **2012**, *6*, 105-110.

[19] M.D. Ward, P.R. Raithby, *Chem. Soc. Rev.* **2013**, *42*, 1619-1636.

[20] S.V. Eliseeva, J.C.G. Bünzli, *Chem. Soc. Rev.* **2010**, *39*, 189-227.

[21] J.-C.G. Bünzli, C. Piguet, *Chem. Soc. Rev.* **2005**, *34*, 1048-1077.

[22] K. Binnemans, *Chem. Rev.* **2009**, *109*, 4283-4374.

[23] S.J. Butler, D. Parker, *Chem. Soc. Rev.* **2013**, *42*, 1652-1666.

[24] S. Petoud, G. Muller, E.G. Moore, J. Xu, J. Sokolnicki, J.P. Riehl, U.N. Le, S.M. Cohen, K.N. Raymond, *J. Am. Chem. Soc.* **2007**, *129*, 77-83.

[25] S. Petoud, S.M. Cohen, J.-C.G. Bünzli, K.N. Raymond, *J. Am. Chem. Soc.* **2003**, *125*, 13324-13325.

[26] J.-C.G. Bünzli, S. Comby, A.S. Chauvin, C.D.B. Vandevyver, *J. Rare Earths*, **2007**, *25*, 257-274.

[27] S.V. Eliseeva, M. Ryazanov, F. Gumy, S.I. Troyanov, L.S. Lepnev, J.-C.G. Bünzli, N.P. Kuzmina, *Eur. J. Inorg. Chem.* **2006**, 4809-4820.

[28] A. de Bettencourt-Dias, *Curr. Org. Chem.* **2007**, *11*, 1460-1480.

[29] A. de Bettencourt-Dias, *Dalton Trans.* **2007**, 2229-2241.

[30] J.-C.G. Bünzli, *Chem. Rev.* **2010**, *110*, 2729-2755.

[31] Y. Ohishi, T. Kanamori, T. Kitagawa, S. Takahashi, E. Snitzer, G.H. Sigel, *Opt. Lett.* **1991**, *16*, 1747-1749.

[32] L.H. Slooff, A. Polman, M.P.O. Wolbers, F. van Veggel, D.N. Reinhoudt, J.W. Hofstraat, *J. Appl. Phys.* **1998**, *83*, 497-503.

[33] L. Armelao, S. Quici, F. Barigelletti, G. Accorsi, G. Bottaro, M. Cavazzini, E. Tondello, *Coord. Chem. Rev.* **2010**, *254*, 487-505.

[34] S.I. Weissman, *J. Chem. Phys.* **1942**, *10*, 214-217.

[35] G.A. Crosby, *Mol. Cryst.* **1966**, *1*, 37-81.

[36] G.A. Crosby, R.E. Whan, *J. Chem. Phys.* **1962**, *36*, 863-865.

[37] G.A. Crosby, R.E. Whan, R.M. Alire, *J. Chem. Phys.* **1961**, *34*, 743-748.

[38] K. Binnemans, *Chapter 225* - Rare-earth beta-diketonates, in: J.-C.G.Bünzli, K.A. Gschneidner, K.P. Vitalij (Eds.) *Handbook on the Physics and Chemistry of Rare Earths*, Elsevier, **2005**, 107-272.

[39] A. de Bettencourt-Dias, S. Bauer, S. Viswanathan, B.C. Maull, A.M. Ako, *Dalton Trans.* **2012**, *41*, 11212-11218.

[40] E.S. Andreiadis, N. Gauthier, D. Imbert, R. Demadrille, J. Pécaut, M. Mazzanti, *Inorg. Chem.* **2013**, *52*, 14382-14390.

[41] S.V. Eliseeva, D.N. Pleshkov, K.A. Lyssenko, L.S. Lepnev, J.C.G. Bünzli, N.P. Kuzminat, *Inorg. Chem.* **2010**, *49*, 9300-9311.

[42] N.B.D. Lima, S.M.C. Goncalves, S.A. Junior, A.M. Simas, *Sci. Rep.* **2013**, *3*.

[43] S.V. Eliseeva, O.V. Kotova, F. Gumy, S.N. Semenov, V.G. Kessler, L.S. Lepnev, J.-C.G. Bünzli, N.P. Kuzmina, *J. Phys. Chem. A*, **2008**, *112*, 3614-3626.

[44] A. de Bettencourt-Dias, P.S. Barber, S. Viswanathan, D.T. de Lill, A. Rollett, G. Ling, S. Altun, *Inorg. Chem.* **2010**, *49*, 8848-8861.

[45] A. de Bettencourt-Dias, P.S. Barber, S. Bauer, *J. Am. Chem. Soc.* **2012**, *134*, 6987-6994.

[46] A. De Bettencourt-Dias, S. Viswanathan, A. Rollett, *J. Am. Chem. Soc.* **2007**, *129*, 15436-15437.

[47] B.G. Wybourne, *Mol. Phys.* **2003**, *101*, 899-901.

[48] B.R. Judd, *Phys. Rev.* **1962**, *127*, 750-761.

[49] G.S. Ofelt, *J. Chem. Phys.* **1962**, *37*, 511-520.

[50] S.F. Mason, R.D. Peacock, B. Stewart, *Chem. Phys. Lett.* **1974**, *29*, 149-153.

[51] A.F. Kirby, F.S. Richardson, *J. Phys. Chem.* **1983**, *87*, 2544-2556.

[52] M. Montalti, L. Prodi, N. Zaccheroni, L. Charbonnière, L. Douce, R. Ziessel, *J. Am. Chem. Soc.* **2001**, *123*, 12694-12695.

[53] K. Driesen, P. Lenaerts, K. Binnemans, C. Gorller-Walrand, *Phys. Chem. Chem. Phys.* **2002**, *4*, 552-555.

[54] T. Harada, Y. Nakano, M. Fujiki, M. Naito, T. Kawai, Y. Hasegawa, *Inorg. Chem.* **2009**, *48*, 11242-11250.

[55] T. Harada, H. Tsumatori, K. Nishiyama, J. Yuasa, Y. Hasegawa, T. Kawai, *Inorg. Chem.* **2012**, *51*, 6476-6485.

[56] K. Miyata, T. Nakagawa, R. Kawakami, Y. Kita, K. Sugimoto, T. Nakashima, T. Harada, T. Kawai, Y. Hasegawa, *Chem. Eur. J.* **2011**, *17*, 521-528.

[57] K. Miyata, Y. Hasegawa, Y. Kuramochi, T. Nakagawa, T. Yokoo, T. Kawai, *Eur. J. Inorg. Chem.* **2009**, 4777-4785.

[58] K. Yanagisawa, T. Nakanishi, Y. Kitagawa, T. Seki, T. Akama, M. Kobayashi, T. Taketsugu, H. Ito, K. Fushimi, Y. Hasegawa, *Eur. J. Inorg. Chem.* **2015**, 4769-4774.

[59] Y. Hasegawa, T. Ohkubo, K. Sogabe, Y. Kawamura, Y. Wada, N.

Nakashima, S. Yanagida, *Angew. Chem. Int. Ed.* **2000**, *39*, 357-360.

[60] P.B. Glover, A.P. Bassett, P. Nockemann, B.M. Kariuki, R. Van Deun, Z. Pikramenou, *Chem. Eur. J.* **2007**, *13*, 6308-6320.

[61] R. Van Deun, P. Nockemann, C. Gorller-Walrand, K. Binnemans, *Chem. Phys. Lett.* **2004**, *397*, 447-450.

[62] M. Burnworth, L.M. Tang, J.R. Kumpfer, A.J. Duncan, F.L. Beyer, G.L. Fiore, S.J. Rowan, C. Weder, *Nature* **2011**, *472*, 334-U230.

[63] H. Furukawa, K.E. Cordova, M. O'Keeffe, O.M. Yaghi, *Science* **2013**, *341*, 974.

[64] A.V. Zhukhovitskiy, M.Z. Zhong, E.G. Keeler, V.K. Michaelis, J.E.P. Sun, M.J.A. Hore, D.J. Pochan, R.G. Griffin, A.P. Willard, J.A. Johnson, *Nat. Chem.* **2016**, *8*, 33-41.

[65] T. Fukino, H. Joo, Y. Hisada, M. Obana, H. Yamagishi, T. Hikima, M. Takata, N. Fujita, T. Aida, *Science* **2014**, *344*, 499-504.

[66] A. Tsuda, Y. Nagamine, R. Watanabe, Y. Nagatani, N. Ishii, T. Aida, *Nat. Chem.* **2010**, *2*, 977-983.

[67] M. Fujita, J. Yazaki, K. Ogura, *J. Am. Chem. Soc.* **1990**, *112*, 5645-5647.

[68] T.R. Cook, Y.R. Zheng, P.J. Stang, *Chem. Rev.* **2013**, *113*, 734-777.

[69] S. Kitagawa, R. Kitaura, S. Noro, *Angew. Chem. Int. Ed.* **2004**, *43*, 2334-2375.

[70] A. Gallego, O. Castillo, C.J. Gomez-Garcia, F. Zamora, S. Delgado, *Inorg. Chem.* **2012**, *51*, 718-727.

[71] M.I.J. Polson, E.A. Medlycott, G.S. Hanan, L. Mikelsons, N.L. Taylor, M. Watanabe, Y. Tanaka, F. Loiseau, R. Passalacqua, S. Campagna, *Chem. Eur. J.* **2004**, *10*, 3640-3648.

[72] F. Puntoriero, S. Campagna, A.M. Stadler, J.M. Lehn, *Coord. Chem. Rev.*

2008, *252*, 2480-2492.

[73] A. Rana, S.K. Jana, T. Pal, H. Puschmann, E. Zangrando, S. Dalai, *J. Solid State Chem.* **2014**, *216*, 49-55.

[74] J.N. Hao, B. Yan, *J. Mater. Chem. A* **2015**, *3*, 4788-4792.

[75] L.N. Zhang, A.L. Liu, Y.X. Liu, J.X. Shen, C.X. Du, H.W. Hou, *Inorg. Chem. Commun.* **2015**, *56*, 137-140.

[76] S.S. Shang, J.W. Zhao, L.J. Chen, Y.Y. Li, J.L. Zhang, Y.Z. Li, J.Y. Niu, *J. Solid State Chem.* **2012**, *196*, 29-39.

[77] Y.X. Guo, X. Feng, T.Y. Han, S. Wang, Z.G. Lin, Y.P. Dong, B. Wang, *J. Am. Chem. Soc.* **2014**, *136*, 15485-15488.

[78] R. Medishetty, R. Tandiana, L.L. Koh, J. Vittal, *Chem. Eur. J.* **2014**, *20*, 1231-1236.

[79] Y. Hasegawa, T. Nakanishi, *Rsc Adv.* **2015**, *5*, 338-353.

[80] J. Rocha, L.D. Carlos, F.A.A. Paz, D. Ananias, *Chem. Soc. Rev.* **2011**, *40*, 926-940.

[81] A.R. Ramya, D. Sharma, S. Natarajan, M.L.P. Reddy, *Inorg. Chem.* **2012**, *51*, 8818-8826.

[82] K. Miyata, T. Ohba, A. Kobayashi, M. Kato, T. Nakanishi, K. Fushimi, Y. Hasegawa, *Chempluschem* **2012**, *77*, 277-280.

[83] K.A. White, D.A. Chengelis, K.A. Gogick, J. Stehman, N.L. Rosi, S. Petoud, *J. Am. Chem. Soc.* **2009**, 131 18069-18071.

[84] J.Y. An, C.M. Shade, D.A. Chengelis-Czegan, S. Petoud, N.L. Rosi, *J. Am. Chem. Soc.* **2011**, *133*, 1220-1223.

[85] Y.J. Cui, H. Xu, Y.F. Yue, Z.Y. Guo, J.C. Yu, Z.X. Chen, J.K. Gao, Y. Yang, G.D. Qian, B.L. Chen, *J. Am. Chem. Soc.* **2012**, *134*, 3979-3982.

[86] X.T. Rao, T. Song, J.K. Gao, Y.J. Cui, Y. Yang, C.D. Wu, B.L. Chen, G.D.

Qian, *J. Am. Chem. Soc.* **2013**, *135*, 15559-15564.

[87] Y.J. Cui, B.L. Chen, G.D. Qian, *Coord. Chem. Rev.* **2014**, *273*, 76-86.

Chapter 2

Luminescent Eu(III) coordination polymers with dense structures for high energy transfer efficiencies

Abstract

Novel Eu(III) coordination polymers $[Eu(hfa)_3(dpt)]_n$ (dpt: 2,5-bis(diphenylphosphoryl)thiophene) and $[Eu(hfa)_3(dpedot)]_n$ (dpedot: 3,4-bis(diphenylphosphoryl)ethylenedioxythiophene) were designed for dense structures with high energy transfer efficiency. The zig-zag orientation of single polymer chains induced the formation of densely packed coordination structures with multiple inter-molecular hydrogen bonds. These polymers exhibited high intrinsic emission quantum yields (≈ 80%) due to their asymmetrical and low-vibrational coordination structures. The significantly high energy transfer efficiencies of up to 80% were also achieved.

Based on
Luminescent Europium(III) Coordination Zippers Linked with Thiophene-Based Bridges
Y. Hirai, T. Nakanishi, Y. Kitagawa, K. Fushimi, T. Seki, H. Ito, and Y. Hasegawa, *Angew. Chem. Int. Ed.* **2016**, *55*, 12059-12062.

2.1 Introduction

Developing luminescent molecular materials with high quantum efficiencies is required for applications in light-emitting devices, bio-probes, chemical and physical sensors.[1-7] There have been many reports on luminescent organic and coordination compounds. Swager and co-workers developed amplifying fluorescent conjugated polymers for biological and chemical sensors such as highly explosive trinitrotoluene in seawater.[8] Adachi et al. reported very high phosphorescence efficiency of Ir(III) coordination compounds in organic light-emitting devices.[9]

Among these materials, Ln(III) coordination compounds are promising candidates for pure and strong luminophores as described in Chapter 1.[10-17] The overall emission quantum yields of these compounds are described as:

$$\Phi_{total} = \Phi_{ff} \times \eta_{sens} = \frac{k_r}{k_r + k_{nr}} \times \eta_{sens} \quad \cdots (1)$$

where Φ_{ff} is Ln(III)-centered emission quantum yields, η_{sens} is efficiency of the sensitization process, and k_r and k_{nr} are radiative and non-radiative rate constants, respectively.

Ln(III) coordination compounds with high Φ_{ff} have been successfully synthesized by introducing asymmetrical and low-vibrational coordination structures, resulting in large k_r and small k_{nr} values[18,19] In order to advance these compounds for industrial use, Ln(III) coordination polymers with rigid multi-dimensional networks have been developed over the past two decades.[20-22] The reported Ln(III) coordination polymers exhibit high Φ_{ff} (> 70%) and thermal stability (> 200˚C);however, their energy transfer efficiencies from antenna ligands to Ln(III) ions (η_{sens}) are estimated to be approximately 50%.[23,24] Ln(III) coordination polymers with high η_{sens} are required for ideal

optical devices.

The author here focused on the intra-ligand charge transfer (ILCT) states via charge redistribution of hfa ligands in Ln(III) coordination polymers to enhance the energy transfer efficiency. The ILCT states are formed under specific packing structures and found to contribute to the photosensitization process in Ln(III) complexes.[25] Eliseeva and co-workers recently reported the considerable enhancement of ligand-to-metal energy transfer efficiency for both VIS and NIR emissive Ln(III) coordination compounds, under existence of low-lying ILCT states.[26,27] Hasegawa and co-workers have also demonstrated efficient photosensitized luminescence of Eu(III) coordination polymers with ILCT band.[28] The formation of ILCT states should affect the efficiency of energy transfer from ligands to Ln(III) ions in solid systems. Since these ligand-based electronic effects are characteristic in solid state, dense and tight coordination structures in crystal units may induce the formation of ILCT states, leading to high Φ_{tot}. The author here considers that luminescent Ln(III) coordination polymers with specific ILCT states can be constructed by zig-zag chained polymers, “coordination zippers.”

In this chapter, the novel thiophene-based bridging ligands, 2,5-bis(diphenylphosphoryl)thiophene) (dpt), 3,4-bis(diphenylphosphoryl)ethylenedioxithiophene) (dpedot), and corresponding Eu(III) coordination polymers ($[Eu(hfa)_3(dpt)]_n$ and $[Eu(hfa)_3(dpedot)]_n$, respectively, Figure 2-1a) were prepared to form zig-zag polymer chains with close-packed structures in solid state. Small aromatic core and bent angles of thiophene-based bridges are expected to reduce the distances between $Eu(hfa)_3$ units in single polymer chains. The zig-zag polymer moiety are also expected to induce interdigitation between polymer chains,

leading to intermolecular CH/F and CH/π interactions through bridging ligands and antenna ligands. The Eu(III) coordination polymer with linear-typed bridges ($[Eu(hfa)_3(dpbp)]_n$,[24] Figure 2-1b) was also prepared for comparison. Their photophysical properties were estimated by UV/Vis absorption, emission, and excitation spectra. Thermal stability is discussed on the basis of the results of thermogravimetric analyses and single crystal X-ray diffraction.

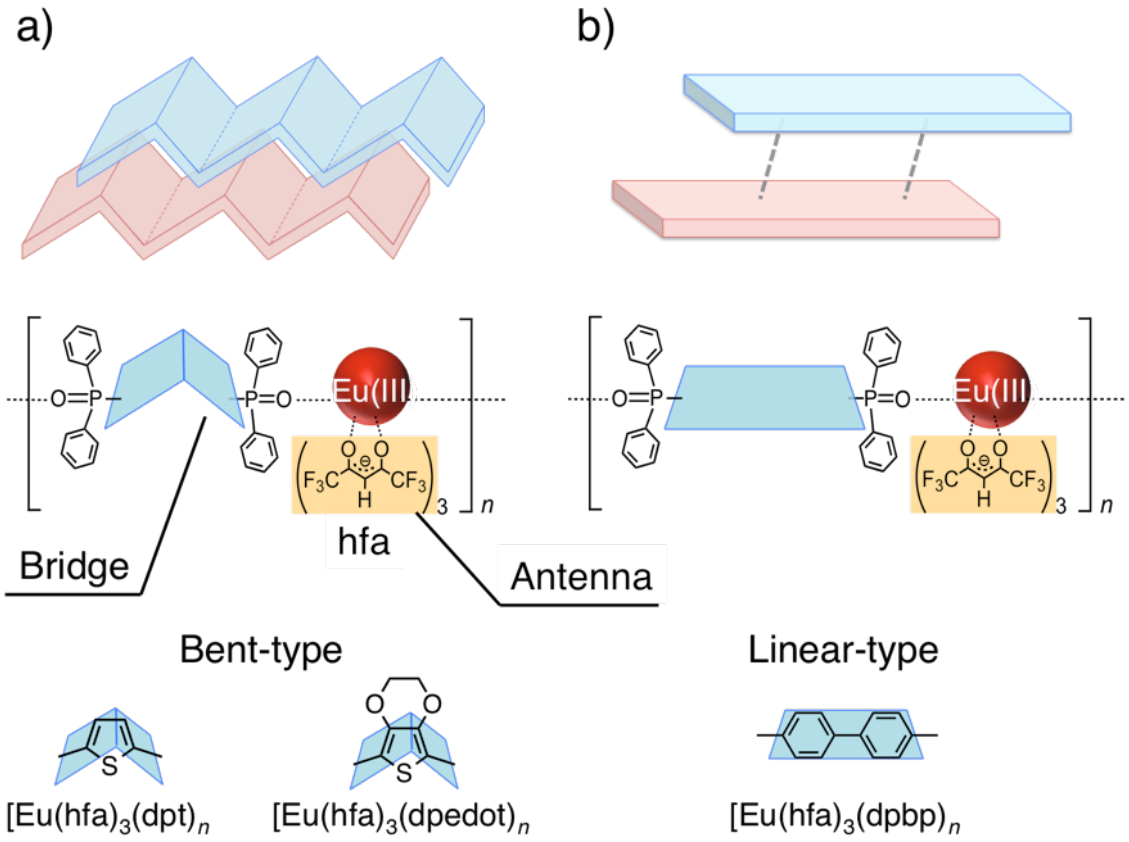

Figure 2-1. Diagram of a) Eu(III) coordination zippers with bent-type bridges and b) Eu(III) coordination polymers with linear-type bridges.

2.2 Experimental Section

2.2.1 Materials

Europium acetate *n*-hydrate (99.9%), *n*-BuLi (in *n*-hexane, 1.6 M), and hydrogen peroxide were purchased from Kanto Chemical Co., Inc. 2,5-Dibromothiophene, 3,4-ethylenedioxythiophene, and chlorodiphenylphosphine (PPh_2Cl) were obtained from Tokyo Chemical Industry Co., Ltd. All other chemicals and solvents were reagent grade and were used without further purification.

2.2.2 Apparatus

^1H NMR (400 MHz) spectra were recorded on a JEOL ECS400. Chemical shifts were reported in δ ppm, referenced to an internal tetramethylsilane standard for ^1H NMR spectroscopy. Infrared spectra were recorded on a JASCO FTIR-420 spectrometer using KBr pellets. Elemental analyses were performed by an Exeter Analytical CE440. Mass spectrometry was performed by a Thermo Scientific Exactive (ESI-MS) and a JEOL JMS-700TZ (FAB-MS). Thermogravimetric analysis (TGA) was performed on a Seiko Instruments Inc. EXSTAR 6000 (TG-DTA 6300) in an argon atmosphere at a heating rate of 5˚C min^{-1}.

2.2.3 Syntheses

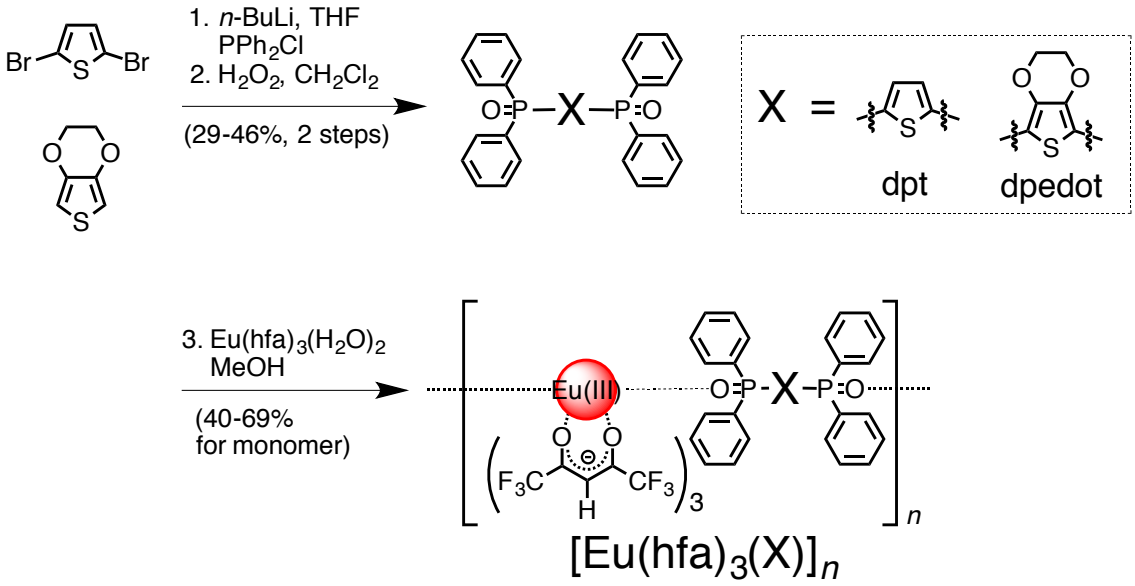

Scheme 2-1. Synthetic schemes of phosphine oxide ligands and Eu(III) coordination polymers.

Preparation of $[Eu(hfa)_3(H_2O)]_2$:

Europium acetate *n*-hydrate (2.0 g, 5.8 mmol) was dissolved in distilled water (30 mL). Hexafluoroacetylacetone (4.0 g, 19 mmol) was added dropwise to the solution and let stirred for 3 h at room temperature to form pale yellow precipitates. The reaction mixture was filtered and washed with distilled water and chloroform for several times. The resulting powder was used without further purification for the next step.

Yield 4.1 g (89%). IR (KBr): 1650 (st, C=O), 1258-1145 (st, C-F) cm^{-1}. Anal. Calcd for $C_{15}H_7EuF_{18}O_8$: C, 22.27; H, 0.87%. Found: C, 22.12; H, 1.01%.

Preparation of 2,5-bis(diphenylphosphoryl)thiophene (dpt):

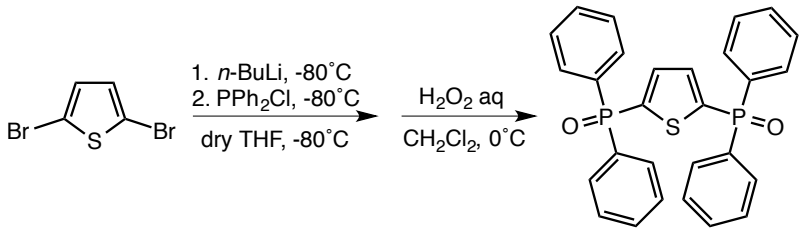

In a degassed 3-neck round-bottomed flask (300 mL vol.), 2,5-dibromothiophene (2 mL, 17.7 mmol) was dissolved in dry THF (70 mL) under argon atmosphere, then stirred until a homogeneous solution was formed at room temperature. A solution of *n*-BuLi (28 mL, 44 mmol) was added dropwise to the solution at −80˚C. The addition was completed in ca. 15 min. The mixture was allowed to stir for 3 h, after which a PPh_2Cl (8.0 mL, 45 mmol) was added dropwise at −80˚C, then the solution became cloudy. The mixture was gradually brought to room temperature, and stirred for 14 h to form clouded yellow solution. The product was extracted with dichloromethane and dried over anhydrous $MgSO_4$. The solvent was concentrated and dissolved in dichloromethane (50 mL) in a flask. The solution was cooled to 0˚C and then 30% H_2O_2 aqueous solution (24 mL) was added to it. The reaction mixture was stirred for 2 h. The product was extracted with dichloromethane and the obtained crude powder was washed with ethyl acetate for several times to afford white powder.

Yield: 2.3 g (29%). ^1H NMR (400 MHz, $CDCl_3$, 25˚C) δ 7.79-7.86 (m, 8H, -CH), δ 7.64-7.67 (m, 2H, -CH), δ 7.43-7.49 (m, 6H, -CH), δ 7.35-7.41 (m, 8H, -CH) ppm. ESI-Mass (*m*/*z*): calcd for $C_{28}H_{23}O_2P_2S$ $[M+H]^+$, 485.09; found, 485.09. Anal. Calcd for $C_{28}H_{22}O_2P_2S$: C, 69.41; H, 4.58%. Found: C, 68.90; H, 4.57%.

Preparation of 3,4-bis(diphenylphosphoryl)ethylenedioxythiophene (dpedot):

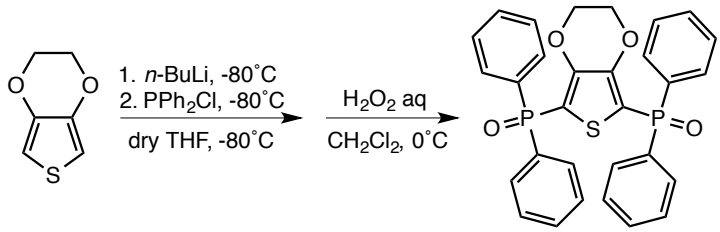

In a degassed 3-neck round-bottomed flask (300 mL vol.), 3,4-ethylenedioxythiophene (2 mL, 18.5 mmol) was dissolved in dry THF (80 mL) under argon atmosphere, then stirred until a homogeneous solution was formed at room temperature. A solution of *n*-BuLi (29 mL, 46 mmol) was added dropwise to the solution at −80˚C. The addition was completed in ca. 15 min. The mixture was allowed to stir for 2 h, after which a PPh_2Cl (8.5 mL, 46 mmol) was added dropwise at −80˚C. The mixture was gradually brought to room temperature, and stirred for 4 h. The product was extracted with dichloromethane and dried over anhydrous $MgSO_4$. The solvent was concentrated and dissolved in dichloromethane (50 mL) in a flask. The solution was cooled to 0˚C and then 30% H_2O_2 aqueous solution (25 mL) was added to it. The reaction mixture was stirred for 2 h. The product was extracted with dichloromethane and the obtained crude powder was washed with ethyl acetate for several times to afford pale brown powder.

Yield: 4.6 g (46%). ^1H NMR (400 MHz, $CDCl_3$, 25˚C) δ 7.68-7.74 (m, 8H, -CH), δ 7.51-7.55 (m, 4H, -CH), δ 7.42-7.46 (m, 8H, -CH), δ 4.12 (s, 4H, $-CH_2$) ppm. ESI-Mass (*m*/*z*): calcd for $C_{30}H_{25}O_4P_2S$ $[M+H]^+$, 543.09; found, 543.09. Anal. Calcd for $C_{30}H_{24}O_4P_2S$: C, 66.42; H, 4.46%. Found: C, 66.04; H, 4.53%.

Preparation of $[Eu(hfa)_3(dpt)]_n$:

Phosphine oxide ligand (0.39 g, 0.80 mmol) and $Eu(hfa)_3(H_2O)_2$ (0.64 g, 0.80 mmol) were dissolved in methanol (40 mL), respectively. The solutions were mixed and refluxed for 3 h to form white precipitates. The obtained white solid was washed with methanol.

Yield: 0.40 g (40% for monomer). IR (KBr): 1655 (st, C=O), 1143 (st, P=O) cm^{-1}. FAB-Mass (*m*/*z*): calcd for $C_{38}H_{24}EuF_{12}O_6P_2S$ $[M\text{-}hfa]^+$: 1051.0, found, 1050.8. Anal. Calcd for $C_{43}H_{25}EuF_{18}O_8P_2S$: C, 41.07; H, 2.00%. Found: C, 40.91; H, 2.12%.

Preparation of $[Eu(hfa)_3(dpedot)]_n$:

Phosphine oxide ligand (0.43 g, 0.80 mmol) and $Eu(hfa)_3(H_2O)_2$ (0.64 g, 0.80 mmol) were dissolved in methanol, respectively. The solutions were mixed and refluxed for 3 h. The reaction mixture was concentrated and washed with chloroform. The solvent was evaporated and re-dissolved in 50˚C methanol for recrystallization. The obtained crystals were washed with −20˚C methanol.

Yield: 0.73 g (69% for monomer). IR (KBr): 1657 (st, C=O), 1145 (st, P=O) cm^{-1}. FAB-Mass (*m*/*z*): calcd for $C_{40}H_{26}EuF_{12}O_8P_2S$ $[M\text{-}hfa]^+$: 1109.0, found, 1109.0. Anal. Calcd for $C_{45}H_{27}EuF_{18}O_{10}P_2S$: C, 41.08; H, 2.07 %. Found: C, 40.92; H, 2.37%.

2.2.4 Crystallography

Single crystals of $[Eu(hfa)_3(dpt)]_n$ were prepared by liquid-liquid diffusion of dpt / dichloromethane solution and $Eu(hfa)_3(H_2O)_2$ / methanol solution. A colorless needle-like crystal of $[Eu(hfa)_3(dpt)]_n$ was mounted on a MicroLoop 75 μm using Paratone-N. The measurement was performed on a Rigaku XtaLAB P200 diffractometer using multi-layer mirror monochromated Mo-Kα radiation. Single crystals of $[Eu(hfa)_3(dpedot)]_n$ were prepared by slow evaporation of $[Eu(hfa)_3(dpedot)]_n$ / methanol solution. A colorless block-shaped single crystal of $[Eu(hfa)_3(dpedot)]_n$ was mounted on a MiTiGen micromesh using Paratone-N. The measurement was performed on a Rigaku R-AXIS RAPID diffractometer using graphite monochromated Mo-Kα radiation. Non-hydrogen atoms were refined anisotropically. Hydrogen atoms were refined using the riding model. All calculations were performed using the CrystalStructure crystallographic software package. CIF data was confirmed by using the checkCIF/PLATON service. Supplementary crystallographic data for this paper can be obtained free of charge from the Cambridge Crystallographic Data Centre via www.ccdc.cam.ac.uk/data_request/cif (CCDC-1477386 for $[Eu(hfa)_3(dpt)]_n$ and CCDC-1048291 for $[Eu(hfa)_3(dpedot)]_n$, respectively).

2.2.5 Assignment of coordination geometry

To describe the geometry of Ln(III) complexes and to evaluate the degree of distortion from ideal geometry, the "shape measure" criterion *S*,[29] suggested by Raymond and co-workers, is estimated using the following method (Figure 2-2) and equation (2) on the basis of crystal data.

$$S = \min \sqrt{\left(\frac{1}{m}\right)\sum_{i=1}^{m}(\delta_i - \theta_i)^2} \quad \cdot \cdot \cdot (2)$$

1. Ln(III) ions and O atoms in the first coordination sphere are connected by lines.
2. The observed dihedral angle δ_i (angle between the normal and adjacent faces) along the *i*th edge and θ_i (the same angle for the corresponding ideal polyhedral shape) are measured.
3. The squared difference of δ_i and θ_i is estimated.
4. 2 and 3 are executed for all edges, and the sum of squared differences is obtained by dividing the number of edges (*m* = 18 in this study).
5. The square root of 4 is calculated.
6. 2-5 are executed for all possible geometries, and the smallest value is defined as *S* [deg] for the Ln(III) complex.

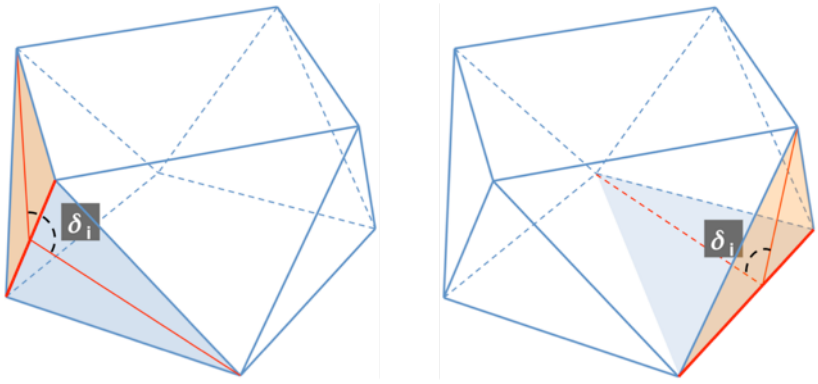

Figure 2-2. The examples of dihedral angles (δi) in an 8-SAP structure.

2.2.6 Optical measurements

UV-Vis absorption spectra were recorded on a JASCO V-670 spectrometer. Emission and excitation spectra were recorded on a HORIBA Fluorolog-3 spectrofluorometer and corrected for the response of the detector system. Emission lifetimes (τ_{obs}) were measured using the third harmonics (355 nm) of a Q-switched Nd:YAG laser (Spectra Physiscs, INDI-50, fwhm = 5 ns, λ = 1064 nm) and a photomultiplier (Hamamatsu photonics, R5108, response time ≤ 1.1 ns). The Nd:YAG laser response was monitored with a digital oscilloscope (Sony Tektronix, TDS3052, 500 MHz) synchronized to the single-pulse excitation. Emission lifetimes were determined from the slope of logarithmic plots of the decay profiles. The emission quantum yields excited at 380 nm (Φ_{tot}) were estimated using JASCO F-6300-H spectrometer attached with JASCO ILF-533 integrating sphere unit (φ = 100 mm). The wavelength dependence of the detector response and the beam intensity of Xe light source for each spectrum were calibrated using a standard light source.

2.2.7 Estimation of intrinsic emission quantum yields

The photophysical parameters such as intrinsic emission quantum yields (Φ_{ff}), radiative (k_r) and non-radiative (k_{nr}) rate constants can be related in the simplified equations (3)-(5) in the case of Eu(III) complexes due to the character of purely magnetic dipole transition $^5D_0 \rightarrow {}^7F_1$.[19,30]

$$\Phi_{ff} = \frac{k_r}{k_r + k_{nr}} = \frac{\tau_{obs}}{\tau_{rad}} \quad \cdot \cdot \cdot (3)$$

$$k_r = \frac{1}{\tau_{rad}} = A_{MD,0} n^3 \left(\frac{I_{tot}}{I_{MD}} \right) \quad \cdot \cdot \cdot (4)$$

$$k_{nr} = \frac{1}{\tau_{obs}} - \frac{1}{\tau_{rad}} \quad \cdot \cdot \cdot (5)$$

τ_{obs} and τ_{rad} are observed and radiative emission lifetimes, where τ_{rad} is defined as an ideal emission lifetime without non-radiative process. $A_{MD,0}$ is the spontaneous emission probability for $^5D_0 \rightarrow {}^7F_1$ transition in vacuo (14.65 s^{-1}), n is the refractive index of the medium (an average index of refraction equal to 1.5 is employed.[31]), and I_{tot}/I_{MD} is the ratio of the total area of the corrected Eu(III) emission spectrum to the area of the $^5D_0 \rightarrow {}^7F_1$ band.

2.3 Results and Discussion

2.3.1 Photophysical properties

The excitation, absorption, and emission spectra of the Eu(III) coordination polymers in solid state are shown in Figure 2-3a. The coordination zippers exhibited bright red luminescence.

The photophysical parameters are summarized in Table 2-1. The intrinsic emission quantum yields (Φ_{ff}) for both polymers were estimated to be as high as that of the previous coordination polymer $[Eu(hfa)_3(dpbp)]_n$, indicating a low-vibrational coordination structure. The larger radiative rate constants (k_r) also indicate that the coordination geometries around Eu(III) ions are greatly distorted. The sharp signals at around 394, 416, 465, 472, 526, and 534 nm in excitation spectra were attributed to the 4f-4f transitions (see Table 2-2 for each assignment). These spectroscopic features also supports the existence of allowed 4f-4f transitions in Eu(III) ions of these compounds, which relates to high intrinsic emission quantum yields. The most remarkable point is that both polymers exhibited twice as large Φ_{tot} values (Φ_{tot} ~ 60%), compared to $[Eu(hfa)_3(dpbp)]_n$ (Φ_{tot} = 29%).

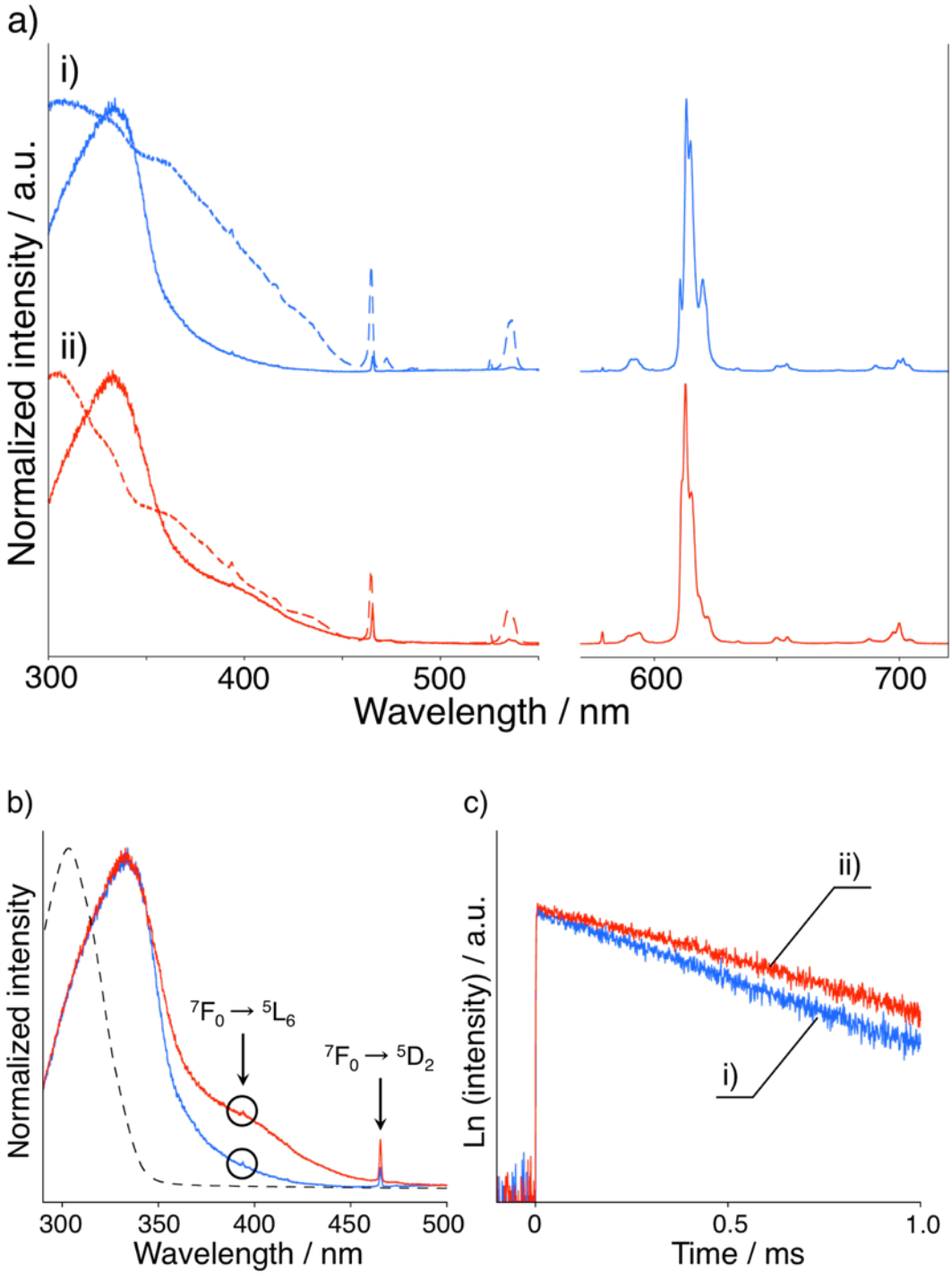

Figure 2-3. a) Diffuse reflectance (solid line), excitation (dotted line, monitored at 613 nm), and emission (solid line, λ_{ex} = 380 nm) spectra. b) An absorption spectrum (10^{-5} M in MeOH for monomer, dashed line) and diffuse reflectance spectra (solid line). c) Emission decay profiles (λ_{ex} = 355 nm) of i) $[Eu(hfa)_3(dpt)]_n$ (blue line) and ii) $[Eu(hfa)_3(dpedot)]_n$ (red line).

Table 2-1. Photophysical parameters of Eu(III) coordination polymers $[Eu(hfa)_3(X)]_n$ in solid state.

Sample	Φ_{tot}[a] / %	Φ_{ff}[b] / %	η_{sens}[a] / %	τ_{obs}[c] / ms	k_r[b] / s^{-1}	k_{nr}[b] / s^{-1}
$[Eu(hfa)_3(dpt)]_n$	60	75	80	0.75	1.0×10^3	3.3×10^2
$[Eu(hfa)_3(dpedot)]_n$	56	85	66	0.93	9.1×10^2	1.6×10^2
$[Eu(hfa)_3(dpbp)]_n$ [d]	29	72	40	0.85	8.5×10^2	3.2×10^2

[a] λ_{ex} = 380 nm. [b] Equation 3-5. [c] λ_{ex} = 355 nm. [d] Reference [24].

Table 2-2. The list of observed peaks in excitation spectra of $[Eu(hfa)_3(X)]_n$ (X = dpt, dpedot) and corresponding 4f-4f transitions that are generally found in absorption spectra of Eu(III) coordination compounds.[32]

Transitions in excitation spectra		Transitions in absorption spectra	
Wavelength / nm	Transitions	Dipole character	Wavelength / nm
394	$^5L_6 \leftarrow {}^7F_0$	ED	390-405
416	$^5D_3 \leftarrow {}^7F_1$	MD	410-420
465	$^5D_2 \leftarrow {}^7F_0$	ED	460-470
472	$^5D_2 \leftarrow {}^7F_1$	ED	470-480
526	$^5D_1 \leftarrow {}^7F_0$	ED	520-530
534	$^5D_1 \leftarrow {}^7F_1$	ED	530-540

ED: induced magnetic dipole transition, MD: magnetic dipole transition.

The η_{sens} of $[Eu(hfa)_3(dpt)]_n$ and $[Eu(hfa)_3(dpedot)]_n$ were estimated to be 80% and 66%, respectively. The author considered the high η_{sens} to be responsible for the formation of low-lying ILCT states induced by the densely packed zig-zag orientation. In order to confirm the formation of ILCT states, an absorption spectrum in methanol and diffuse reflectance spectra in solid state were measured (Figure 2-3b). In 10^{-5} M methanol solution, π-π* transition bands of hfa is observed at around 300 nm. In solid state, both polymers

exhibited small 4f-4f absorption of Eu(III) ions at 394 nm and 465 nm. The broad absorption over UV to VIS regions was observed due to the ligand-based transitions, including π-π* absorption bands at 330 nm and ILCT bands at around 400 nm. The excitation spectra also indicate that the long-wavelength bands also contribute to Eu(III)-centered luminescence.

2.3.2 Coordination structures

The η_{sens} should be related to the formation of ILCT states in solid state as mentioned in introduction. Therefore, single crystals of both polymers were prepared to investigate the coordination structures. The crystal structures were determined to be typical 8-coordination with three hfa and two phosphine oxide ligands (Figure 2-4a, 2-5a). First, the coordination geometry around Eu(III) ions was examined on the basis of crystal data. The shape factor *S* was calculated, and the observed dihedral angles (δ_i), ideal dihedral angles for square antiprism (θ_{SAP}) and trigonal dodecahedron (θ_{TDH}), calculated measure shape criteria, S_{SAP} and S_{TDH} are summarized in Table A2-1 and A2-2. When assuming 8-SAP structure for [Eu(hfa)$_3$(dpedot)]$_n$, the *S* value is much smaller than that for 8-TDH (S_{SAP} = 5.13 < S_{TDH} = 10.6), indicating that the coordination geometry is closer to 8-SAP than to 8-TDH. The geometry of [Eu(hfa)$_3$(dpt)]$_n$ can be defined as distorted 8-SAP structure due to the close *S* values (S_{SAP} = 8.84, S_{TDH} = 9.21).

The orientation and intermolecular interactions of polymer chains were also investigated (Figure 2-4b, 2-5b). [Eu(hfa)$_3$(dpt)]$_n$ showed highly ordered and densely packed structure due to the alternate arrangement of CF_3 and phenyl groups between single polymer chains. The multiple intermolecular CH/F ($d_{CH/F}$ = 2.80 Å (H72/F9), 2.91 Å (H52/F10), 2.81 Å (H54/F6)) and CH/π ($d_{CH/\pi}$ = 2.79

Å (H51/π), 2.91 Å (H53/π)) interactions were observed. In the case of $[Eu(hfa)_3(dpedot)]_n$, intramolecular π/π interactions were identified ($d_{\pi/\pi}$ = 3.56 Å). The number of intermolecular CH/F interactions is much smaller than that for $[Eu(hfa)_3(dpt)]_n$, since the $[Eu(hfa)_3(dpedot)]_n$ forms relatively-disordered polymer chains. The binding energies of CH/F and CH/π interactions are generally known to be 10-30 and 2-10 kJ mol^{-1}, respectively.[33] Thus, $[Eu(hfa)_3(dpt)]_n$ is highly zipped and shows large crystal density (Table 2-3).

In order to precisely evaluate the density of antenna ligands, distances between hfa ligands were estimated (Figure 2-6). The intra-unit, intra-chain, and inter-chain hfa distances are shown in Table 2-4. The intra-chain distances are close in $[Eu(hfa)_3(dpt)]_n$ and $[Eu(hfa)_3(dpedot)]_n$ (smallest: 9 Å, largest: 14 Å). On the other hand, $[Eu(hfa)_3(dpedot)]_n$ and $[Eu(hfa)_3(dpbp)]_n$ exhibited close inter-chain distances (smallest: 7 Å, largest: 16 Å). These results indicate that intra-chain distances greatly affect η_{sens} values. Thus, introduction of thiophene-based bridging ligands is ideal for reducing the intra-chain hfa-hfa distances, resulting in efficient ligand-to-metal energy transfer.

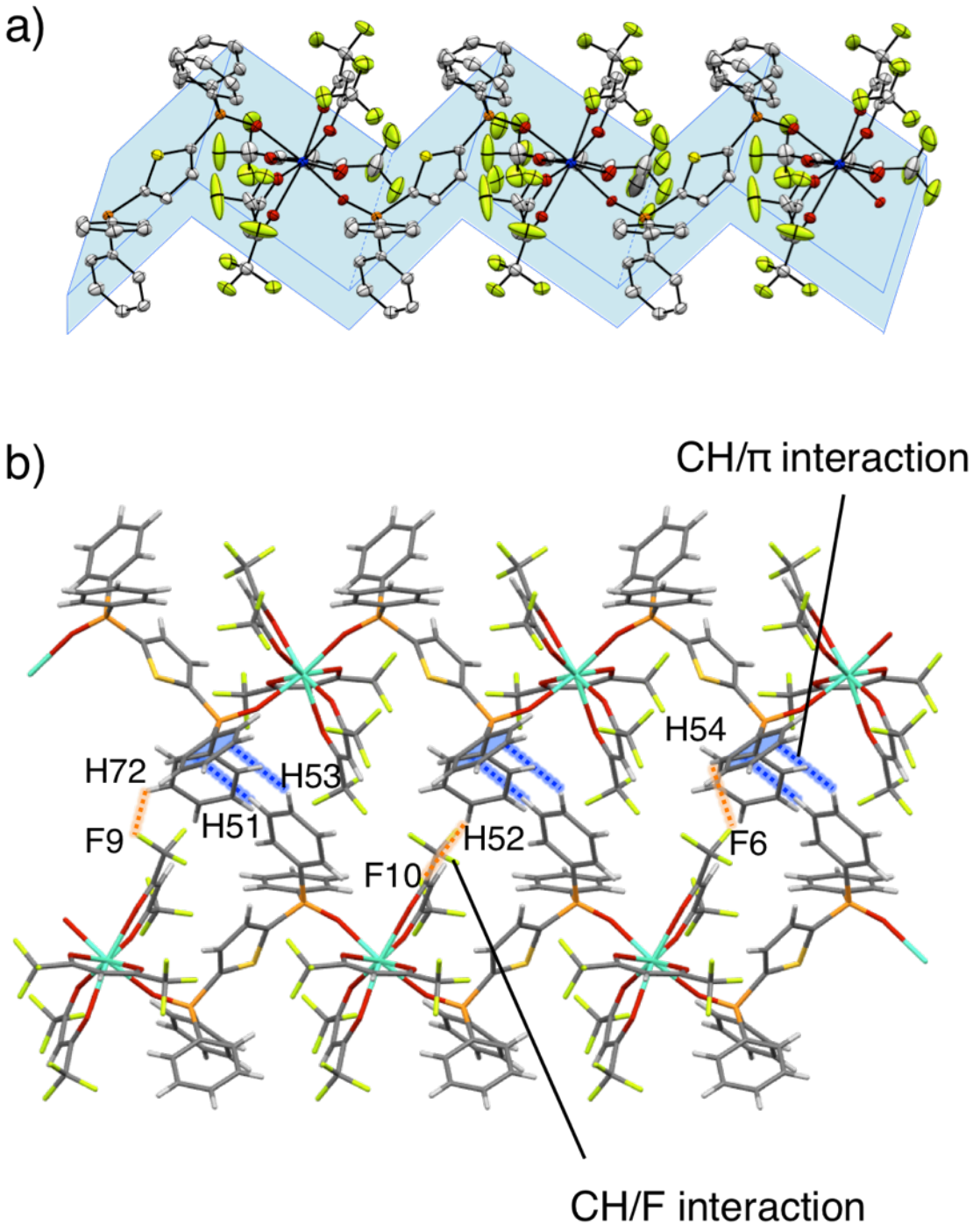

Figure 2-4. a) ORTEP drawing (showing 50% probability displacement ellipsoids) and b) crystal packing structure focused on intermolecular interactions between single polymer chains of $[Eu(hfa)_3(dpt)]_n$.

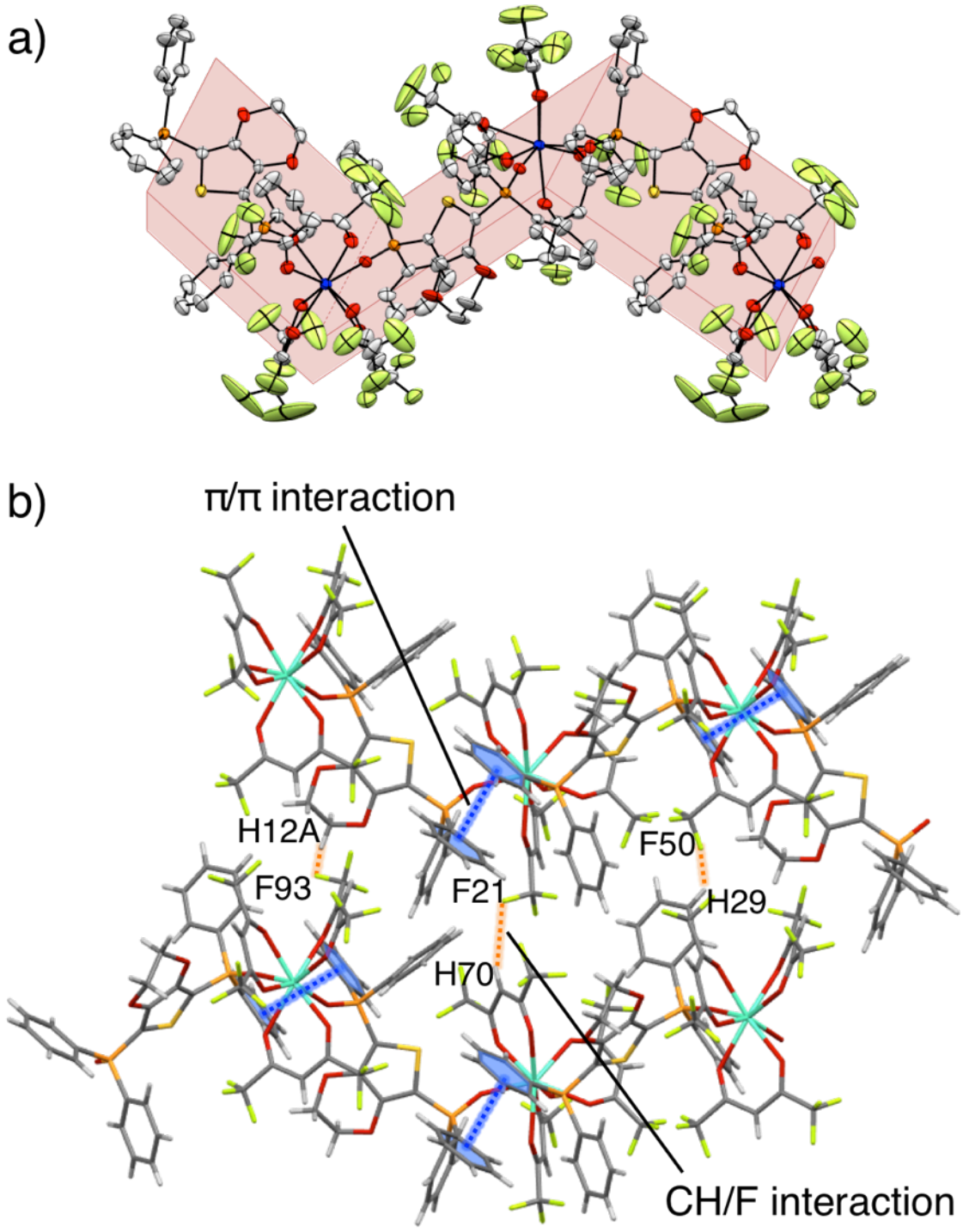

Figure 2-5. a) ORTEP drawing (showing 50% probability displacement ellipsoids) and b) crystal packing structure focused on intermolecular interactions between single polymer chains of $[Eu(hfa)_3(dpedot)]_n$.

Table 2-3. Crystal data of the Eu(III) coordination polymers.

	$[Eu(hfa)_3(dpt)]_n$	$[Eu(hfa)_3(dpedot)]_n$	$[Eu(hfa)_3(dpbp)]_n$[25]
Chemical formula	$C_{43}H_{25}EuF_{18}O_8P_2S$	$C_{45}H_{27}EuF_{18}O_{10}P_2S$	$C_{52}H_{31}EuF_{18}O_8P_2$
Formula weight	1257.60	1315.64	1339.69
Crystal system	Monoclinic	Triclinic	Monoclinic
Space group	$P2_1/n$ (#14)	$P1$ (#1)	$C2/c$ (#15)
a / Å	10.4933(5)	12.2292(14)	23.477(4)
b / Å	21.9927(11)	12.9103(11)	13.367(2)
c / Å	20.4330(11)	18.1033(19)	17.168(3)
α / deg	90.000	89.739(5)	90.000
β / deg	90.654(5)	84.208(4)	95.5749(8)
γ / deg	90.000	63.809(7)	90.000
Volume / Å^3	4715.1(4)	2549.1(5)	5340.5(16)
Z	4	2	4
d_{calc} / g cm^{-3}	1.771	1.714	1.666
Temperature / °C	−180	−150	−123
μ (Mo Ka) / cm^{-1}	15.619	14.516	13.472
max 2θ / deg	55.0	55.0	55.0
Reflections	43336	25115	21091
Independent refle	10696	18962	6099
R_1	0.0492	0.0359	0.0266
wR_2	0.1105	0.0954	0.0668

[a] $R_1 = \sum ||F_o| - |F_c|| / \sum |F_o|$. [b] $wR_2 = [\sum w (F_o^2 - F_c^2)^2 / \sum w (F_o^2)^2]^{1/2}$.

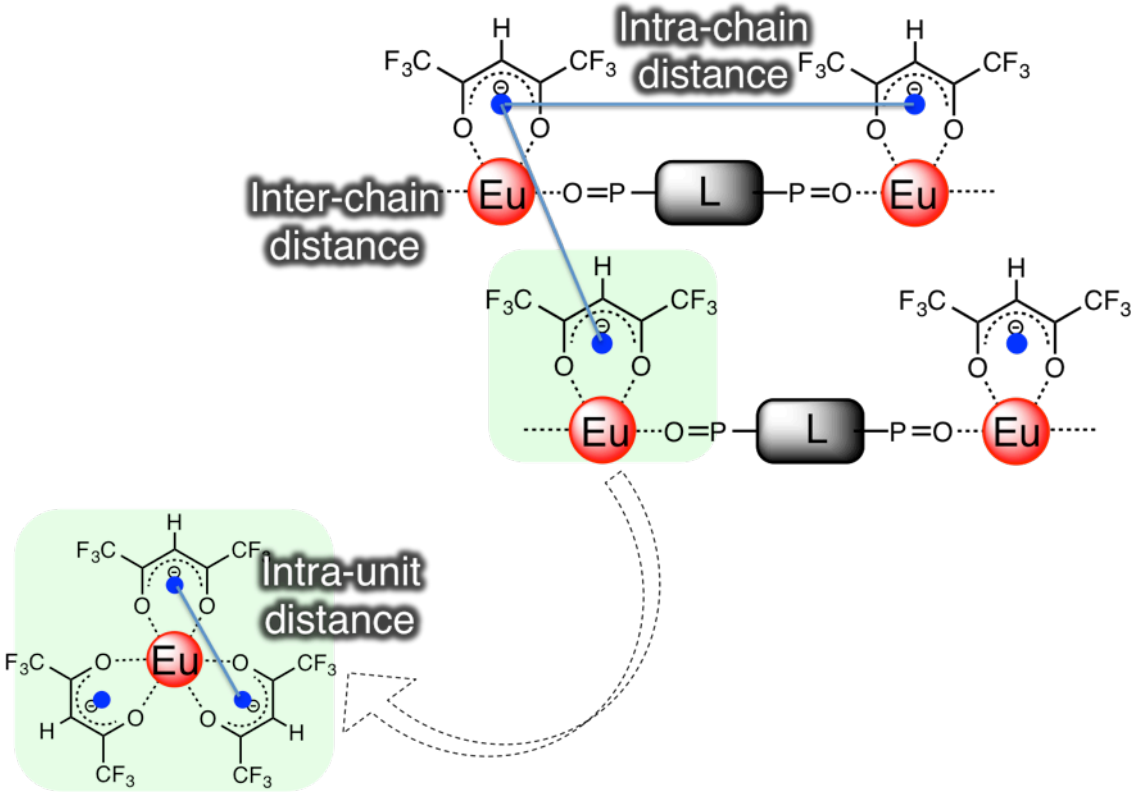

Figure 2-6. A schematic representation of the distances between hfa ligands in Eu(III) coordination polymers.

Table 2-4. Distances between hfa ligands in Eu(III) coordination polymers.

		$[Eu(hfa)_3(dpt)]_n$		$[Eu(hfa)_3(dpedot)]_n$		$[Eu(hfa)_3(dpbp)]_n$
η_{sens} / %		80		66		40
		4.88		4.70		4.67
Intra-unit		4.41		5.20		4.67
distance / Å		5.31		3.54		5.34
	Average	4.87	Average	4.48	Average	4.89
Intra-chain	Smallest	8.90	Smallest	9.19	Smallest	10.24
distance / Å	Largest	14.1	Largest	14.4	Largest	18.0
Inter-chain	Smallest	5.76	Smallest	7.23	Smallest	7.27
distance / Å	Largest	9.98	Largest	15.7	Largest	15.8

2.3.3 Thermal properties

Thermogravimetric analyses were carried out to determine the thermal stability of Eu(III) coordination zippers (Figure 2-7). Thermal decomposition point of $[Eu(hfa)_3(dpt)]_n$ was estimated to be 322˚C, which was higher than $[Eu(hfa)_3(dpbp)]_n$ (308˚C).[24] High thermal stability of $[Eu(hfa)_3(dpt)]_n$ was due to the densely-packed structures between single polymer chains with multiple intermolecular CH/F and CH/π interactions. $[Eu(hfa)_3(dpedot)]_n$ exhibited relatively low decomposition temperature (264˚C). A small drop in the thermogravimetric curve is assumed to be responsible for the degradation of dioxane ring in dpedot ligands, followed by desorption and degradation of hfa ligands.

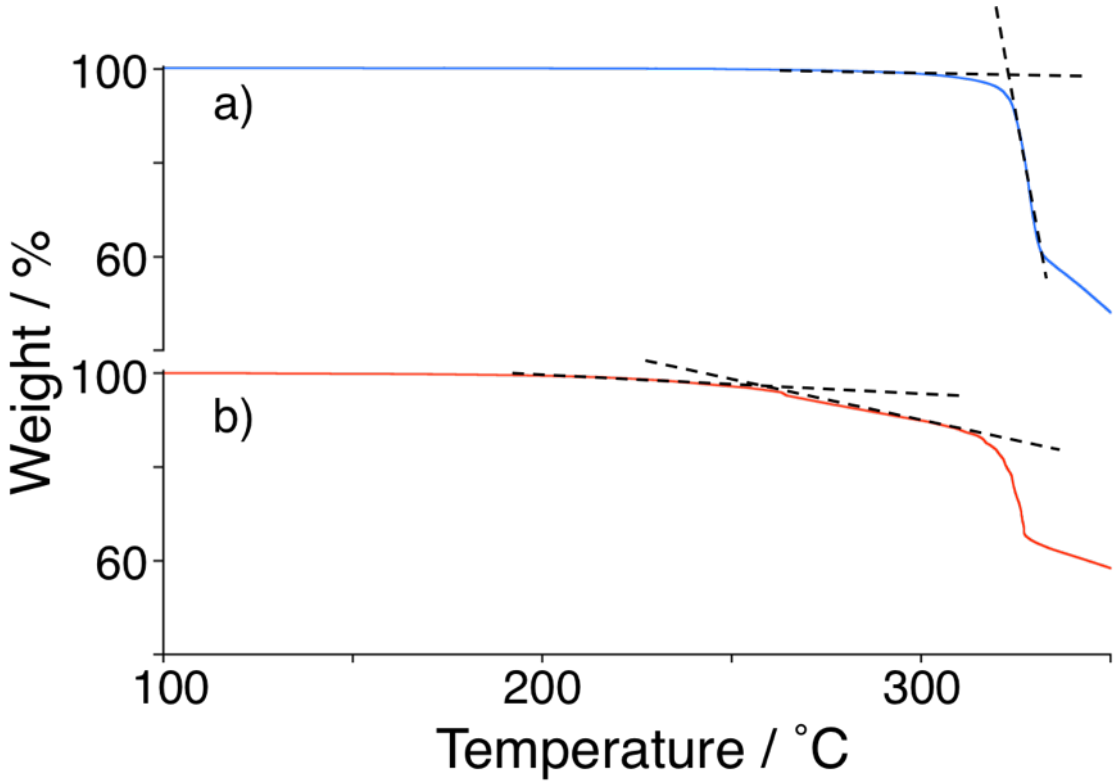

Figure 2-7. TGA thermograms of a) $[Eu(hfa)_3(dpt)]_n$ (blue line) and b) $[Eu(hfa)_3(dpedot)]_n$ (red line) under an argon atmosphere (5˚C min^{-1}).

2.3.4 DFT calculations

The dipole moment D of the bridging ligands was also estimated using DFT calculations [B3LYP 6-31G**] on the basis of CIF data (Figure 2-8). Compared to the previously reported compounds, the bridging ligands in coordination zippers have large D values.

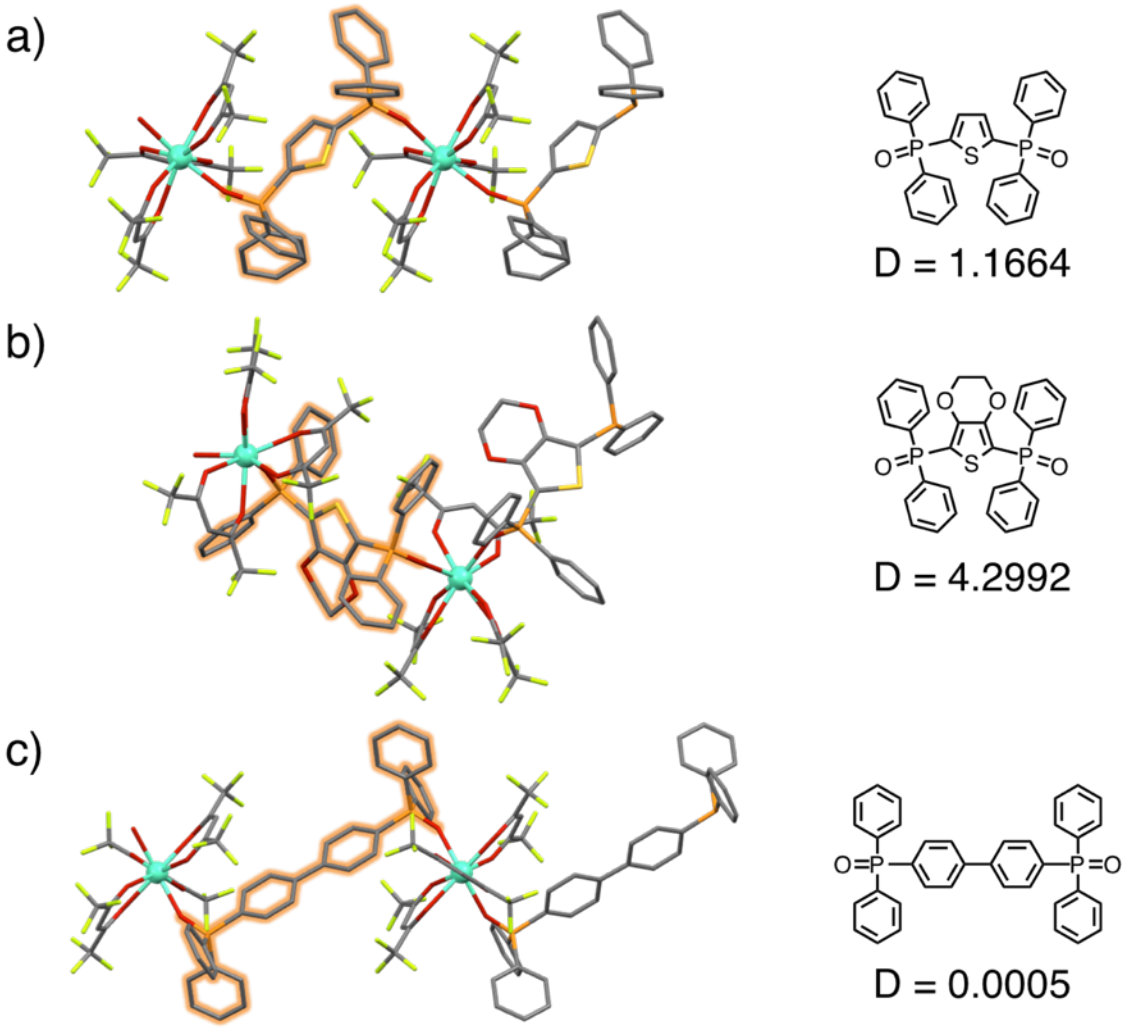

Figure 2-8. Crystal structures of Eu(III) coordination polymers focused on bridging ligands for DFT calculations (left), chemical structures, and calculated D values (right) (a: dpt, b: dpedot, c: dpbp, respectively).

The polar character of bridging ligands probably results in the characteristic alternate arrangement of inter- or intra-polymer chains. Eu(III) coordination polymers with larger D values were also found to show larger Φ_{ff}. Mason and co-workers proposed the “ligand polarization” theory of 4f-4f hypersensitivity, that described the relationship between induced electric dipole moment and dynamic coupling in the Judd-Offelt theory.[34,35] The effect on dipole moment of the ligand in an Ln(III) complex also has been reported.[36,37] The 4f-4f transition probability should be increased by the ligands with large dipole moments, since the polarizability generally describes the strength of field-induced dipoles, and the compounds with large ground state dipole moments tend to exhibit large induced dipole moments. The enhancement of Φ_{ff} in Eu(III) coordination zippers were thus caused by the larger magnitude of the dipole moment in bridging ligands.

2.4 Conclusions

In conclusion, highly emissive and thermally stable Eu(III) coordination polymers $[Eu(hfa)_3(dpt)]_n$ and $[Eu(hfa)_3(dpedot)]_n$ were successfully synthesized by introducing thiophene-based bridges. They exhibit bright red luminescence with energy transfer efficiency up to 80%. Efficient ligand-to-metal energy transfer is achieved by the formation of densely packed coordination zipper structures induced by the small and bent bridging ligands. Incorporation of polar thiophene-based bridges was also found to enhance the 4f-4f transition of Eu(III) ions.

Along with the conventional molecular design of ligand fields around Eu(III) ions, we have provided novel guidelines for a densely packed assembly of luminescent Ln(III) coordination polymers. The reported strategy for coordination zippers would be advantageous for efficient energy transfer and strong luminescence in the solid state, which can be employed in highly emissive and stable materials for optical applications.

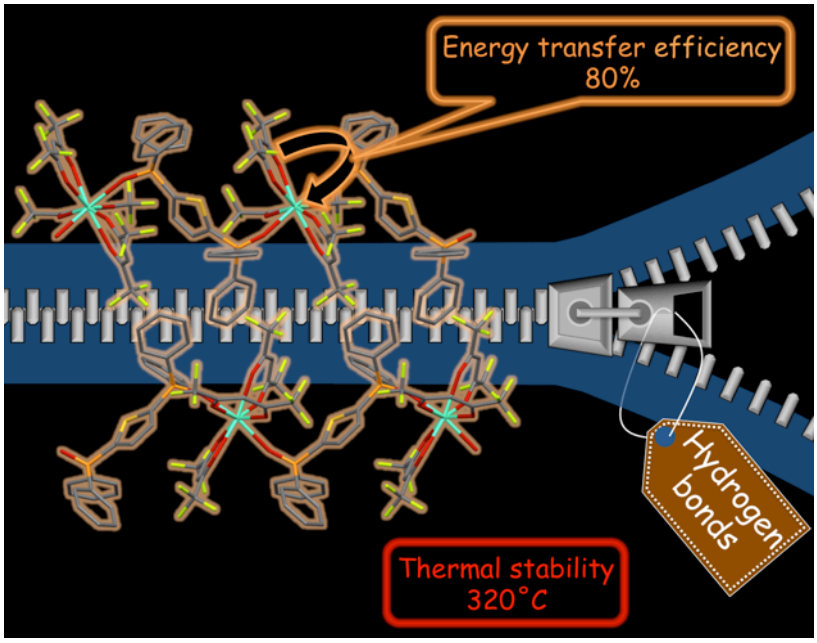

2.5 References

[1] J.H. Burroughes, D.D.C. Bradley, A.R. Brown, R.N. Marks, K. Mackay, R.H. Friend, P.L. Burn, A.B. Holmes, *Nature* **1990**, *347*, 539-541.

[2] C.D. Dimitrakopoulos, P.R.L. Malenfant, *Adv. Mater.* **2002**, *14*, 99-117.

[3] E.G. Moore, A.P.S. Samuel, K.N. Raymond, *Acc. Chem. Res.* **2009**, *42*, 542-552.

[4] S.V. Eliseeva, J.-C.G. Bünzli, *Chem. Soc. Rev.* **2010**, *39*, 189-227.

[5] M. Schaferling, *Angew. Chem. Int. Ed.* **2012**, *51*, 3532-3554.

[6] J.F. Callan, A.P. de Silva, D.C. Magri, *Tetrahedron* **2005**, *61*, 8551-8588.

[7] A.P. de Silva, H.Q.N. Gunaratne, T. Gunnlaugsson, A.J.M. Huxley, C.P. McCoy, J.T. Rademacher, T.E. Rice, *Chem. Rev.* **1997**, *97*, 1515-1566.

[8] S.W. Thomas, G.D. Joly, T.M. Swager, *Chem. Rev.* **2007**, *107*, 1339-1386.

[9] C. Adachi, M.A. Baldo, M.E. Thompson, S.R. Forrest, *J. Appl. Phys.* **2001**, *90*, 5048-5051.

[10] A. de Bettencourt-Dias, *Dalton Trans.* **2007**, *22*, 2229-2241.

[11] J.-C.G. Bünzli, C. Piguet, *Chem. Soc. Rev.* **2005**, *34*, 1048-1077.

[12] K. Binnemans, *Chem. Rev.* **2009**, *109*, 4283-4374.

[13] T. Gunnlaugsson, M. Glynn, G.M. Tocci, P.E. Kruger, F.M. Pfeffer, Coord. *Chem. Rev.* **2006**, *250*, 3094-3117.

[14] G.E. Khalil, K. Lau, G.D. Phelan, B. Carlson, M. Gouterman, J.B. Callis, L.R. Dalton, *Rev. Sci. Instrum.* **2004**, *75*, 192-206.

[15] N.B.D. Lima, S.M.C. Goncalves, S.A. Junior, A.M. Simas, *Sci. Rep.* **2013**, 3.

[16] A. de Bettencourt-Dias, P.S. Barber, S. Viswanathan, *Coord. Chem. Rev.* **2014**, *273*, 165-200.

[17] L. Armelao, S. Quici, F. Barigelletti, G. Accorsi, G. Bottaro, M. Cavazzini, E. Tondello, *Coord. Chem. Rev.* **2010**, *254*, 487-505.

[18] K. Binnemans, R. Van Deun, C. Gorller-Walrand, S.R. Collinson, F. Martin, D.W. Bruce, C. Wickleder, *Phys. Chem. Chem. Phys.* **2000**, *2*, 3753-3757.

[19] M.H.V. Werts, R.T.F. Jukes, J.W. Verhoeven, *Phys. Chem. Chem. Phys.* **2002**, *4*, 1542-1548.

[20] H.B. Zhang, L.J. Zhou, J. Wei, Z.H. Li, P. Lin, S.W. Du, *J. Mater. Chem.* **2012**, *22*, 21210-21217.

[21] M.S. Liu, Q.Y. Yu, Y.P. Cai, C.Y. Su, X.M. Lin, X.X. Zhou, J.W. Cai, *Cryst. Growth Des.* **2008**, *8*, 4083-4091.

[22] J. Rocha, L.D. Carlos, F.A.A. Paz, D. Ananias, *Chem. Soc. Rev.* **2011**, *40*, 926-940.

[23] S.V. Eliseeva, D.N. Pleshkov, K.A. Lyssenko, L.S. Lepnev, J.-C.G. Bünzli, N.P. Kuzmina, *Inorg. Chem.* **2010**, *49*, 9300-9311.

[24] K. Miyata, T. Ohba, A. Kobayashi, M. Kato, T. Nakanishi, K. Fushimi, Y. Hasegawa, *ChemPlusChem* **2012**, *77*, 277-280.

[25] A. D'Aleo, F. Pointillart, L. Ouahab, C. Andraud, O. Maury, *Coord. Chem. Rev.* **2012**, *256*, 1604-1620.

[26] S.V. Eliseeva, O.V. Kotova, F. Gumy, S.N. Semenov, V.G. Kessler, L.S. Lepnev, J.-C.G. Bünzli, N.P. Kuzmina, *J. Phys. Chem. A* **2008**, *112*, 3614-3626.

[27] E.R. Trivedi, S.V. Eliseeva, J. Jankolovits, M.M. Olmstead, S. Petoud, V.L. Pecoraro, *J. Am. Chem. Soc.* **2014**, *136*, 1526-1534.

[28] Y. Hasegawa, R. Hieda, K. Miyata, T. Nakagawa, T. Kawai, *Eur. J. Inorg. Chem.* **2011**, *32*, 4978-4984.

[29] J.D. Xu, E. Radkov, M. Ziegler, K.N. Raymond, *Inorg. Chem.* **2000**, *39*,

4156-4164.

[30] A. Aebischer, F. Gumy, J.-C.G. Bünzli, *Phys. Chem. Chem. Phys.* **2009**, *11*, 1346-1353.

[31] R. Pavithran, N.S.S. Kumar, S. Biju, M.L.P. Reddy, S.A. Junior, R.O. Freire, *Inorg. Chem.* **2006**, *45*, 2184-2192.

[32] K. Binnemans, *Coord. Chem. Rev.* **2015**, *295*, 1-45.

[33] G.R. Desiraju, T. Steiner, *The Weak Hydrogen Bond in Structural Chemistry and Biology*, Oxford Univ. Press, **1999**.

[34] S.F. Mason, R.D. Peacock, B. Stewart, *Chem. Phys. Lett.* **1974**, *29*, 149-153.

[35] S.F. Mason, R.D. Peacock, B. Stewart, *Mol. Phys.* **1975**, *30*, 1829-1841.

[36] T. Nakagawa, Y. Hasegawa, T. Kawai, *J. Phys. Chem. A* **2008**, *112*, 5096-5103.

[37] Y. Hasegawa, N. Sato, Y. Hirai, T. Nakanishi, Y. Kitagawa, A. Kobayashi, M. Kato, T. Seki, H. Ito, K. Fushimi, *J. Phys. Chem. A* **2015**, *119*, 4825-4833.

Appendices

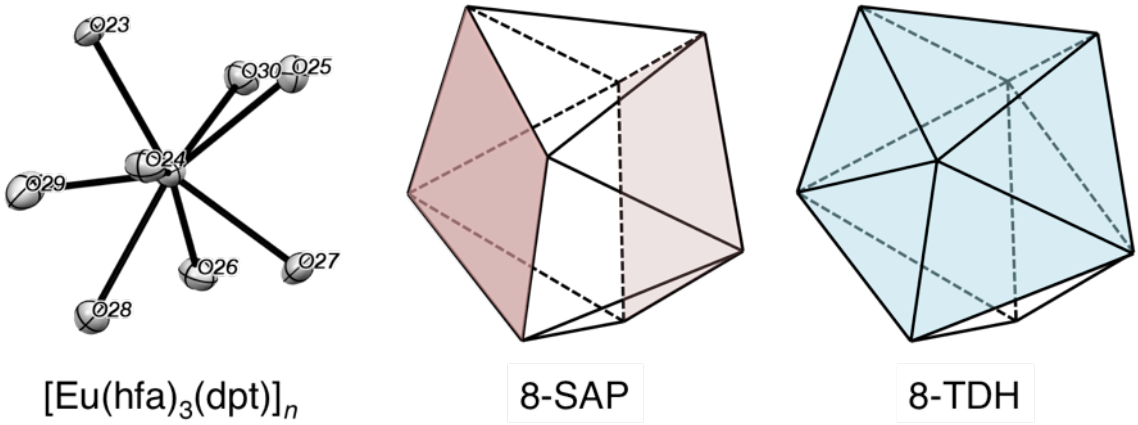

Figure A2-1. Coordination environments around an Eu(III) ion of $[Eu(hfa)_3(dpt)]_n$.

Table A2-1. The observed (δ_i), idealized dihedral angles (θ_{SAP}, θ_{TDH}), and calculated S values (S_{SAP}, S_{TDH}) for $[Eu(hfa)_3(dpt)]_n$.

			SAP			TDH	
	δ_i	θ_{SAP}	$\delta_i - \theta_{SAP}$	$(\delta_i - \theta_{SAP})^2$	θ_{TDH}	$\delta_i - \theta_{TDH}$	$(\delta_i - \theta_{TDH})^2$
O24-O29	5.24	0	5.24	27.46	29.86	-24.62	606.14
O24-O23	68.88	77.1	-8.22	67.57	61.48	7.4	54.76
O24-O28	81.63	77.1	4.53	20.52	74.29	7.34	53.88
O29-O23	80.44	77.1	3.34	11.156	74.29	6.15	37.83
O29-O28	75.37	77.1	-1.73	2.99	61.48	13.89	192.93
O27-O30	19.75	0	19.75	390.06	29.86	-10.11	102.21
O27-O26	66.84	77.1	-10.26	105.27	61.48	5.36	28.73
O27-O25	68.77	77.1	-8.33	69.39	74.29	-5.52	30.47
O30-O25	72.46	77.1	-4.64	21.53	76.62	-4.16	17.31
O30-O26	75.09	77.1	-2.01	4.04	74.84	0.25	0.06
O26-O29	62.58	51.6	10.98	120.56	54.51	8.07	65.12
O26-O28	48.82	51.6	-2.78	7.73	48.09	0.73	0.53
O27-O24	38.83	51.6	-12.77	163.07	47.76	-8.93	79.74
O27-O28	54.06	51.6	2.46	6.05	54.48	-0.42	0.18
O25-O24	62.44	51.6	10.84	117.51	52.57	9.87	97.42
O25-O23	48.77	51.6	-2.83	8.01	52.85	-4.08	16.65
O30-O29	36.18	51.6	-15.42	237.78	47.34	-11.16	124.56
O30-O23	56.74	51.6	5.14	26.42	52.63	4.11	16.89
			S_{SAP} = 8.84			S_{TDH} = 9.21	

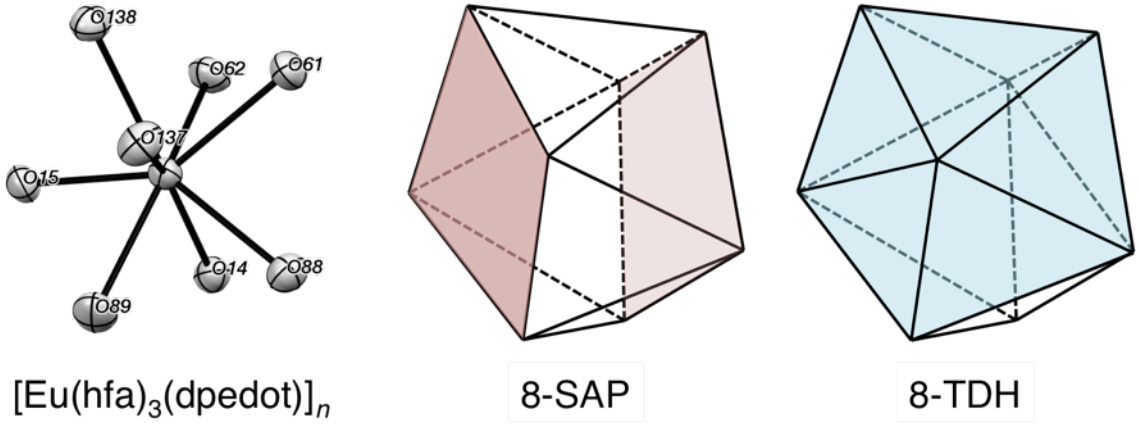

Figure A2-2. Coordination environments around an Eu(III) ion of $[Eu(hfa)_3(dpedot)]_n$.

Table A2-2. The observed (δ_i), idealized dihedral angles (θ_{SAP}, θ_{TDH}), and calculated S values (S_{SAP}, S_{TDH}) for $[Eu(hfa)_3(dpedot)]_n$.

		SAP			TDH		
	δ_i	θ_{SAP}	$\delta_i - \theta_{SAP}$	$(\delta_i - \theta_{SAP})^2$	θ_{TDH}	$\delta_i - \theta_{TDH}$	$(\delta_i - \theta_{TDH})^2$
O137-O15	9.51	0	9.51	90.44	29.86	-20.35	414.12
O137-O138	73.01	77.1	-4.09	16.73	61.48	11.53	132.94
O137-O89	72.78	77.1	-4.32	18.66	74.29	-1.51	2.28
O15-O138	73.68	77.1	-3.42	11.70	74.29	-0.61	0.37
O15-O89	76.15	77.1	-0.95	0.90	61.48	14.67	215.21
O88-O62	2.24	0	2.24	5.02	29.86	-27.62	762.86
O88-O14	77.47	77.1	0.37	0.14	61.48	15.99	255.68
O88-O61	77.83	77.1	0.73	0.53	74.29	3.54	12.53
O62-O61	75.47	77.1	-1.63	2.66	76.62	-1.15	1.32
O62-O14	82.34	77.1	5.24	27.46	74.84	7.5	56.25
O14-O15	53.39	51.6	1.79	3.20	54.51	-1.12	1.25
O14-O89	47.91	51.6	-3.69	13.62	48.09	-0.18	0.03
O88-O137	44.55	51.6	-7.05	49.70	47.76	-3.21	10.30
O88-O89	60.99	51.6	9.39	88.17	54.48	6.51	42.38
O61-O137	54.42	51.6	2.82	7.95	52.57	1.85	3.42
O61-O138	46.58	51.6	-5.02	25.20	52.85	-6.27	39.31
O62-O15	44.37	51.6	-7.23	52.27	47.34	-2.97	8.82
O62-O138	59.28	51.6	7.68	58.98	52.63	6.65	44.22
			S_{SAP} = 5.13			S_{TDH} = 10.6	

Chapter 3

Luminescent lanthanide(III)-mixed coordination polymers for tunable temperature-sensitivity

Abstract

The control of energy transfer efficiency in lanthanide (Ln(III))-mixed coordination polymers is reported. The coordination polymers $[Tb,Eu(hfa)_3(dpbp)]_n$ are composed of Tb(III) and Eu(III) ions, hfa ligands, and bidentate phosphine oxide ligands (dpbp: 4,4'-bis(diphenylphosphoryl)biphenyl). The emission colors were controlled by varying the mixture ratio of Tb(III) and Eu(III) ions (Tb/Eu = 1-1000). The obtained compounds were characterized by XRD, emission spectra, and emission lifetime measurements. The observed spectroscopic features were discussed on the basis of energy transfer efficiency in the solid state.

Based on

Thermo-sensitive luminescent materials composed of Tb(III) and Eu(III) complexes

Y. Hirai, T. Nakanishi, K. Miyata, K. Fushimi, Y. Hasegawa, *Mater. Lett.* **2014**, *130*, 91-93.

3.1 Introduction

In the field of fluid dynamics, visualization of flow fields is a key technique for the development of efficient transportation systems such as cars, ships, and aircraft.[1-5] Flow visualization can provide a straightforward and qualitative assessment of fluid flow on the surface of a material. Some visualization methods using temperature- or pressure-sensitive paint (TSP or PSP) with organic dyes are called molecular imaging techniques and they provide detailed information.[6-9] These techniques have the advantage of describing the entire flow field on objects[10,11] unlike discrete point probes for temperature or pressure that provide point-by-point information, leading to insufficient spatial resolution (Figure 3-1). For unsteady flows in particular, fluid visualization can render details of the flow field far more quickly than conventional measurements.[12]

In molecular imaging techniques, temperature and pressure on the surface of a in the fluid have been detected by thermal and oxygen quenching of the luminescence from organic and coordination compounds.[8,9] However, these compounds intrinsically show broad, mono-colored, weak emission and a relatively low decomposition point (< 200˚C), resulting in a limited temperature-sensitive region. Thermally stable and temperature-sensitive dyes are highly desired for detecting the pressure on airframe surfaces such as atmospheric vehicles and hypersonic jetliners that are subjected to atmospheric re-entry, resulting in a significant temperature elevation due to aerodynamic heating in the hypersonic flow.

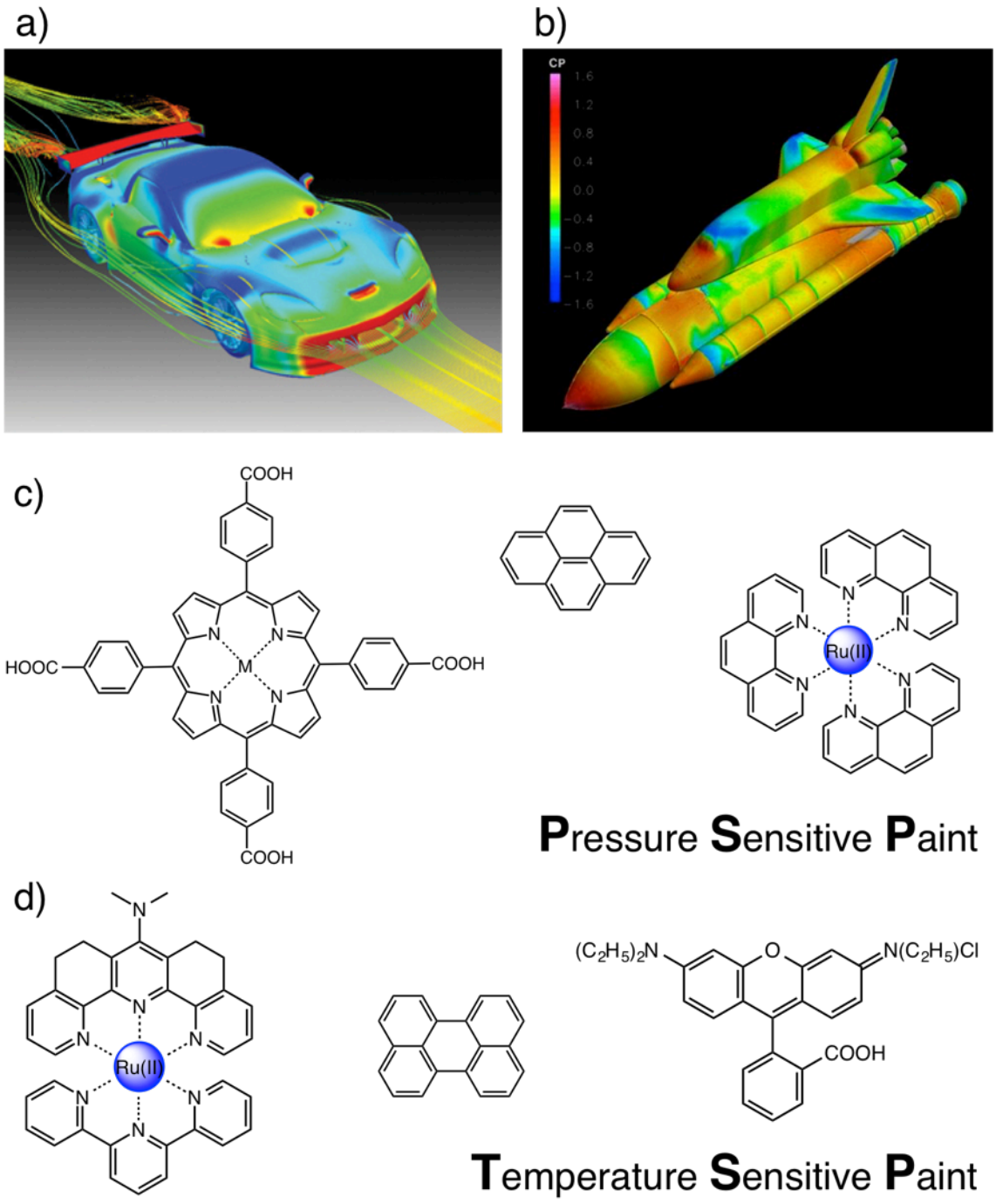

Figure 3-1. a) Simulated flow field using computational fluid dynamics[10] and b) pressure sensitive paint flow visualization data.[11] Chemical structures of c) pressure sensitive paint (PSP) and temperature sensitive paint (TSP).

Luminescent physical sensors based on Ln(III) coordination compounds are attractive in terms of the resolution of signal detection, due to their characteristic sharp and long-lived emission arising from 4f-4f transitions as described in Chapter 1.[13-22]

In 2003, Amao and co-workers first developed luminescent Eu(III) complexes with temperature sensitivity.[23] Wolfbeis demonstrated that Eu(III) *β*-diketonate complexes can be used for high-resolution oxygen profilings.[24] Katagiri reported a Tb(III) complex with effective energy back transfer (BET) from the emitting level of Tb(III) ions to the excited triplet state of hfa ligands, which is suitable for temperature sensors.[25] Hasegawa *et al.* also reported a Tb/Eu mixed system with hfa ligands, $[Tb,Eu(hfa)_3(dpbp)]_n$ (Tb/Eu = 99), that exhibits dramatic color change depending on the temperature from 200 to 500 K.[26] This is due to the BET as well as energy transfer between Ln(III) ions (Figure 3-2). Thermal stability was also achieved by introducing intermolecular hydrogen bonds such as CH/π and CH/F interactions. Since Tb(III) ions are energy donors and Eu(III) ions are energy acceptors in “chameleon luminophore” systems, energy transfer efficiency between lanthanide ions can be tuned by changing the Tb/Eu mixture ratio. The varied energy transfer efficiency should lead to variable emission color and temperature-sensitive regions.

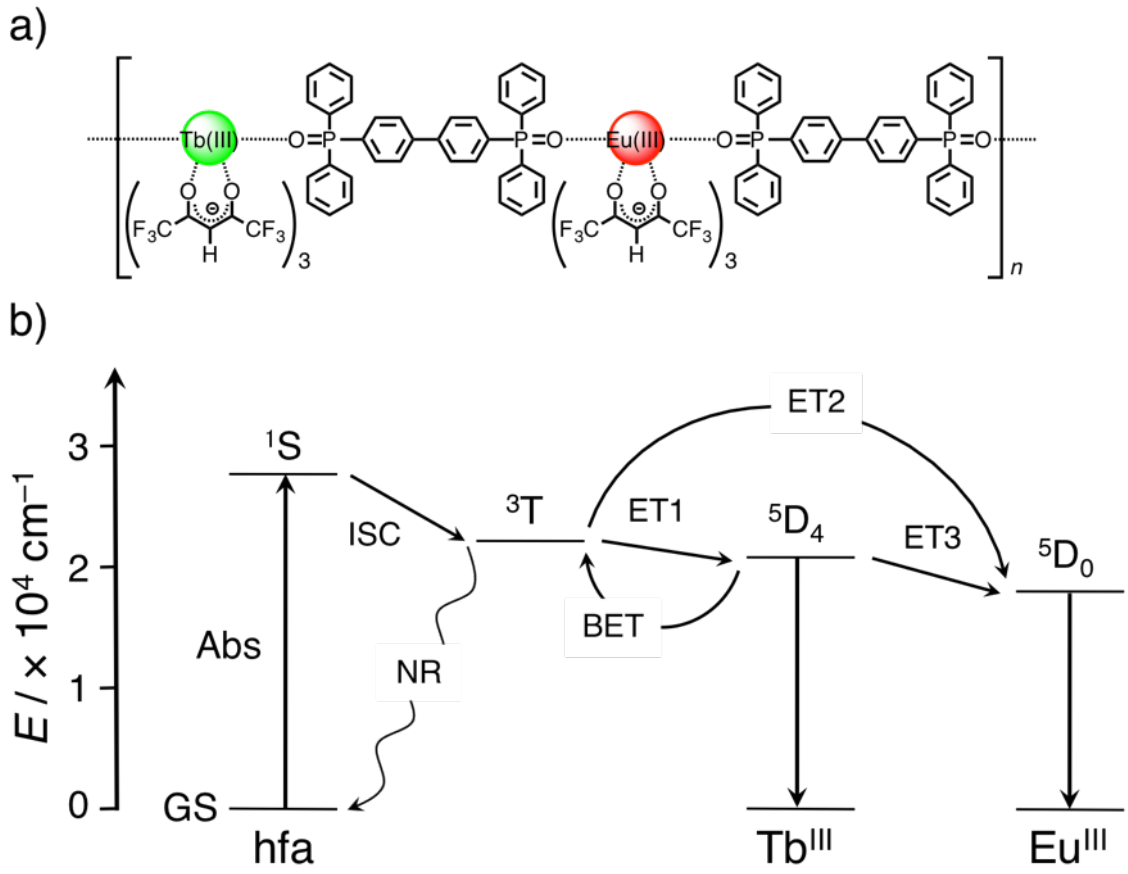

Figure 3-2. a) Chemical structure of Tb(III)/Eu(III) mixed coordination polymer and b) corresponding energy transfer diagram.[26]

Photophysical studies on the energy transfer from Tb(III) to Eu(III) ions are common in mono- and di-nuclear lanthanide complexes in homogeneous organic and aqueous media.[27,28] Recently, carboxylate-based Ln(III)-mixed coordination polymers including MOFs have been extensively developed for luminescent thermometers over a wide temperature range.[29-32] Temperature sensitive region generally depends on organic bridging ligands, and study on the effect of Ln(III) mixture ratios on temperature sensitivity is still in progress. Kinetic analyses of the photophysical properties in solid-state coordination polymers are directly linked to the development of effective thermo-sensors for measurements on the surface of materials.

In this chapter, temperature-dependence of the energy transfer efficiencies between Tb(III) and Eu(III) ions in coordination polymers are described for estimation of luminescence performance. The Tb(III)/Eu(III) mixed coordination polymers, $[Tb,Eu(hfa)_3(dpbp)]_n$, were prepared and characterized by IR and XRD measurements. The energy transfer efficiencies in the range between 100 K and 400 K were estimated using emission spectra and emission lifetime measurements in a cryostat. The characteristic photophysical properties were found in a coordination polymer with Tb(III) ions and a small amount of Eu(III) ions (Tb/Eu = 750). The energy transfer efficiency between Ln(III) ions in solid-state coordination polymers is described for further development of thermo-sensitive luminescent materials.

3.2 Experimental Section

3.2.1 Materials

Europium(III) acetate *n*-hydrate (99.9%) and terbium(III) acetate tetrahydrate (99.9%) were purchased from Wako Pure Chemical Industries Ltd. 4,4'-Dibromobiphenyl, hexafluoroacetylacetone, chlorodiphenylphosphine and ytterbium(III) acetate tetrahydrate were obtained from Tokyo Chemical Industry Co. Ltd. and Aldrich Chemical Company Inc. All other chemicals and solvents were reagent grade and were used as received.

3.2.2 Apparatus

Infrared spectra were recorded on a JASCO FT/IR-420 spectrometer. Powder X-ray diffraction patterns were collected on a RIGAKU RINT 2000 Ultima. Obtained patterns were calibrated by the signal of silicon powder at 28.4°. ^{1}H NMR (400 MHz) spectrum was recorded on a JEOL ECS400. Chemical shifts are reported in δ ppm, referenced to an internal tetramethylsilane standard. Mass spectrum was measured using a JEOL JMS-700TZ. Elemental analysis was performed using a Yanaco CHN corderMT-6. Inductively coupled plasma (ICP) emission spectroscopy was performed on a Shimadzu ICPE-9000.

3.2.3 Syntheses

Preparation of 4,4'-bis(diphenylphosphoryl)biphenyl (dpbp)[22]

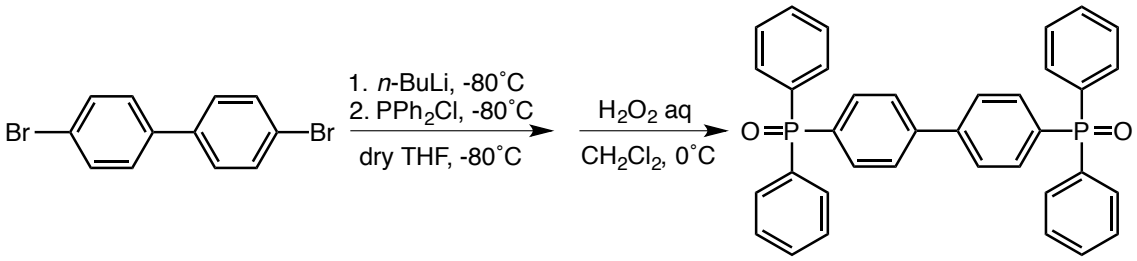

4,4'-Bis(diphenylphosphoryl)biphenyl was synthesized according to the published procedure. 4,4'-Dibromobiphenyl (11 g, 36 mmol) was dissolved in dry THF (140 mL). A solution of 1.6 M *n*-BuLi (56 mL, 90 mmol) was added dropwise to the solution at −80˚C. The mixture was allowed to stir for 3 h at −10˚C, after which a PPh_2Cl (17 mL, 90 mmol) was added dropwise at −80˚C. The mixture was gradually brought to room temperature, and stirred overnight. The product was extracted with ethyl acetate, concentrated, and resulting residue was washed with acetone and ethanol for several times. The obtained white solid was dissolved in dichloromethane (120 mL), followed by addition of a 30% H_2O_2 aqueous solution (30 mL). The reaction mixture was stirred for 3 h at 0˚C. The product was extracted with dichloromethane, washed with brine for three times and dried over anhydrous $MgSO_4$. The solvent was evaporated to afford a white powder of 4,4'-bis(diphenylphsphoryl)biphenyl (dpbp).

Yield: 12 g (60%). ^{1}H NMR (400 MHz, $CDCl_3$, 25˚C) δ 7.66-7.77 (m, 16H, -CH), δ 7.53-7.57 (m, 4H, -CH), δ 7.44-7.49 (m, 8H, -CH) ppm. ESI-Mass (*m*/*z*): calcd for $C_{36}H_{29}O_2P_2$ $[M+H]^+$, 555.2; found, 555.2. Anal. Calcd for $C_{36}H_{28}O_2P_2$: C, 77.97; H, 5.09%. Found: C, 77.49; H, 5.20%.

Preparation of Tb(III)/Eu(III) mixed coordination polymer $[Tb,Eu(hfa)_3(dpbp)]_n$ (Tb/Eu = 1).

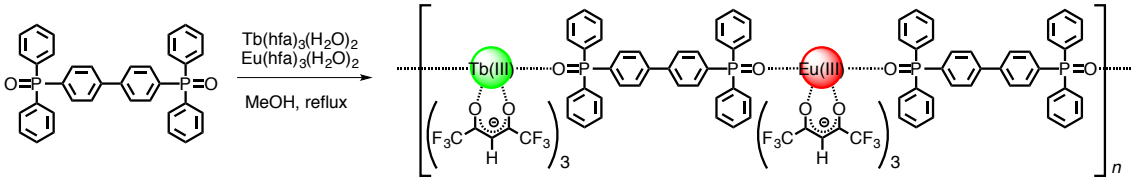

Phosphine oxide ligand (dpbp, 0.44 g), $Tb(hfa)_3(H_2O)_2$ (0.33 g) and $Eu(hfa)_3(H_2O)_2$ (0.32 g) were dissolved in methanol with mixture ratio as shown in the following Table 1. The solution was refluxed while stirring for 2 h to give white precipitates. The precipitates were filtered, washed with methanol and chloroform for several times, and dried in vacuo.

Tb(III)/Eu(III) mixed coordination polymers $[Tb,Eu(hfa)_3(dpbp)]_n$ (Tb/Eu = 10-1000) were similarly synthesized following the mixture ratios in Table 3-1.

IR (KBr): 1650 (st, C=O), 1253-1142 (st, C-F), 1125 (st, P=O) cm^{-1}.

Table 3-1. Tb/Eu mixture ratio for syntheses of $[Tb,Eu(hfa)_3(dpbp)]_n$ (Tb/Eu = X)

X	$Tb(hfa)_3(H_2O)_2$ / mg	$Eu(hfa)_3(H_2O)_2$ / mg
1	326	324
10	594	58.9
50	640	12.7
150	649	4.29
250	650	2.58
350	651	1.84
500	652	1.29
650	652	0.99
750	652	0.86
850	652	0.76
1000	652	0.65

To determine a Tb:Eu ratios of $[Tb,Eu(hfa)_3(dpbp)]_n$, ICP-AES was conducted. ICP samples were prepared by thoroughly drying $[Tb,Eu(hfa)_3(dpbp)]_n$, then digesting the samples to concentrated (60%) HNO_3 and diluting to 1.2% HNO_3. Calibration standards were made by diluting 1000 ppm standards of both Eu and Tb (purchased from Kanto Chemical) over the range of 0.1-1000 ppb for each. Concentrations were calculated from the emission intensities of Eu and Tb (λ_{obs} = 381.917 and 350.917 nm, respectively) for each sample using the appropriate calibration curves and averaged. These analyses revealed a ratio of Tb: Eu ions.

Table 3-2. Emission intensities of Tb(III) and Eu(III) ions and estimated Tb/Eu mixture ratios based on ICP measurements.

$(Tb/Eu)_{syn}$[a]	I_{Tb}	I_{Eu}	$(Tb/Eu)_{ICP}$[b]
1	9769	9856.7	0.99
10	9568	973.41	9.83
50	9687	194.68	49.76
150	9854	64.89	151.86
250	9867	38.94	253.39
350	9876	27.81	355.12
500	9513	19.47	488.60
650	9687	14.98	646.66
750	9986	12.98	769.34
850	9956	11.45	869.52
1000	9947	9.73	1022.30

[a] Tb/Eu ratio while synthesis. [b] Tb/Eu mixture ratio estimated from ICP analyses

3.2.4 Optical measurements

Emission spectra were recorded on a JASCO F-6300-H spectrometer and corrected for the response of the detector system. Emission lifetimes of Tb(III) ions in coordination polymers were measured using the third harmonics (355 nm) of a Q-switched Nd:YAG laser (Spectra Physics, INDI-50, fwhm = 5 ns, λ = 1064 nm), filter transmitting wavelength shorter than 550 nm, and photomultiplier (Hamamatsu photonics R5108, response time ≤ 1.1 ns). The Nd:YAG laser response was monitored with a digital oscilloscope (Sony Tektronix, TDS3052, 500 MHz) synchronized to the single-pulse excitation. Emission lifetimes were determined from the slope of logarithmic plots of the decay profiles. Emission lifetimes and emission spectra from the range between 100-400 K were measured with a cryostat (Thermal Block Company, SA-SB245T) and a temperature controller (Oxford, Instruments, ITC 502S). The emission quantum yields of coordination polymers excited at 380 nm were estimated using JASCO F-6300-H spectrometer attached with JASCO ILF-533 integrating sphere unit (φ = 100 mm). The wavelength dependences of the detector response and the beam intensity of Xe light source for each spectrum were calibrated using a standard light source.

3.3 Results and Discussion

3.3.1 Powder X-ray diffraction measurements

The structures of Ln(III) coordination polymers were identified using powder XRD analyses. All signals were calibrated by the signal of silicon powder at 28.4˚. Observed signals at 7.5˚, 8.8˚, 9.4˚, 10.3˚, 20.1˚ and 21.5˚ were attributed to the geometrical structures of $[Tb,Eu(hfa)_3(dpbp)]_n$ (Figure 3-3). The signals of $[Tb,Eu(hfa)_3(dpbp)]_n$ were found to agree with those of previously reported $[Eu(hfa)_3(dpbp)]_n$ or $[Tb(hfa)_3(dpbp)]_n$,[22] indicating that the mixture ratio of lanthanide ions had no effect on contraction or extension of the crystal lattice. These results indicate that the geometrical structures of $[Tb,Eu(hfa)_3(dpbp)]_n$ are the same as that of $[Eu(hfa)_3(dpbp)]_n$. According to our previous data obtained by using X-ray single crystal analysis of $[Eu(hfa)_3(dpbp)]_n$, distances between Eu(III) ions inter- and intra-polymer chains were 11.4 Å and 13.6 Å, respectively.

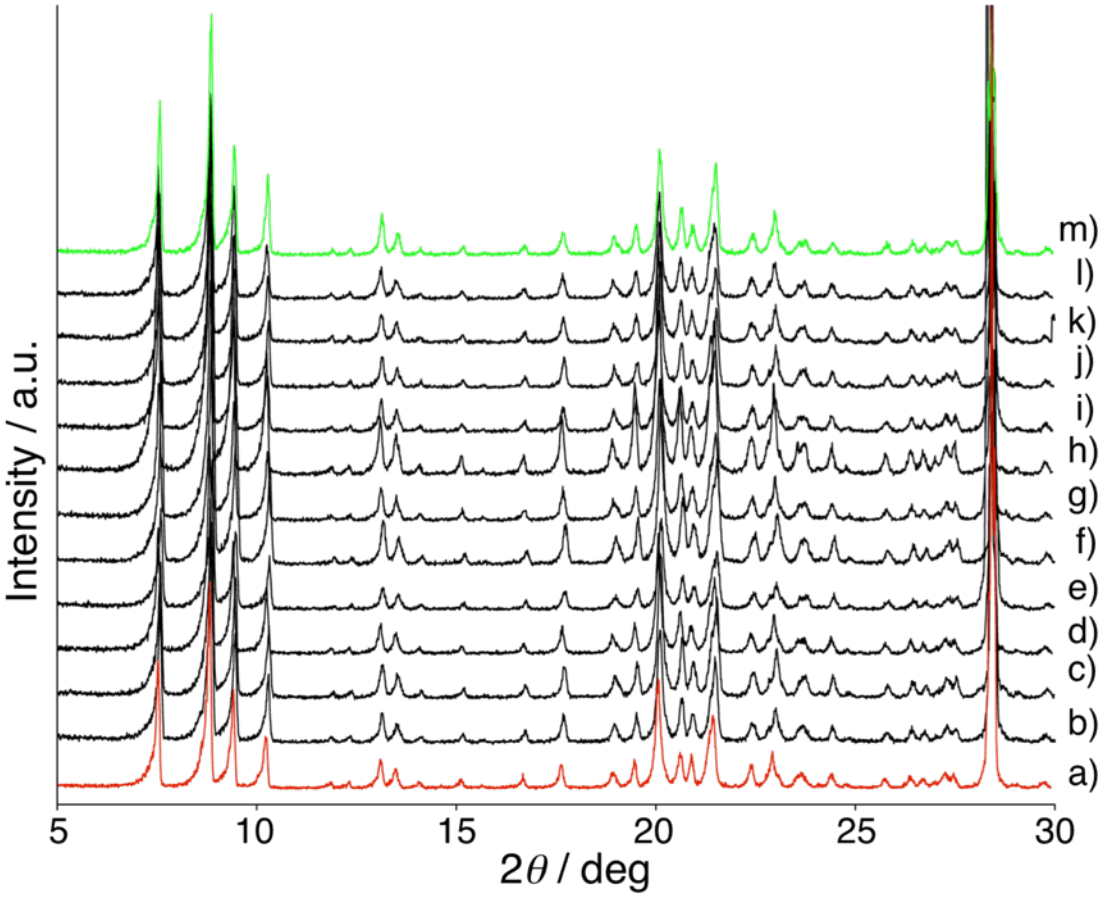

Figure 3-3. XRD patterns of a) $[Eu(hfa)_3(dpbp)]_n$, b-l) $[Tb,Eu(hfa)_3(dpbp)]_n$ (Tb/Eu = 1-1000), and m) $[Tb(hfa)_3(dpbp)]_n$.

3.3.2 Emission spectra

The photophysical properties of selected samples (Tb/Eu = 1, 10, 250, 500, 750) are discussed below. In order to estimate the energy transfer efficiency between Tb(III) and Eu(III) ions in the solid state, temperature-dependent photophysical properties of $[Tb,Eu(hfa)_3(dpbp)]_n$ were investigated. Temperature-dependent emission spectra of $[Tb,Eu(hfa)_3(dpbp)]_n$ (Tb/Eu = 10) in the solid state in the temperature range of 100 K to 400 K are presented in Figure 3-4, showing a gradual color change from green, yellow, orange, to red.

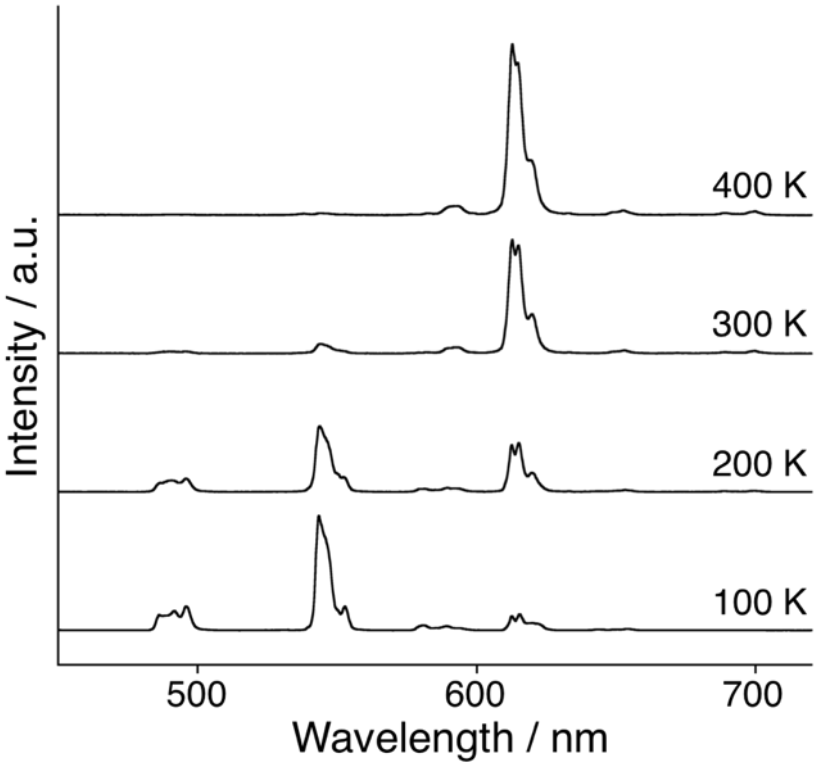

Figure 3-4. Temperature dependent emission spectra of $[Tb,Eu(hfa)_3(dpbp)]_n$ (λ_{ex} = 380 nm, Tb/Eu = 10).

The characteristic emission bands at 488, 543, and 613 nm are attributed to 4f-4f transitions of Tb(III) ($^5D_4 \rightarrow {}^7F_6$, $^5D_4 \rightarrow {}^7F_5$) and Eu(III) ($^5D_0 \rightarrow {}^7F_2$), respectively. The emission quantum yield and lifetime at 300 K (λ_{ex} = 380 nm) were 59.8% and 0.11 ms, respectively. The emission intensities of Tb(III) ions in $[Tb,Eu(hfa)_3(dpbp)]_n$ decreased with increasing temperature, particularly at temperatures above room temperature. The emission intensities of Eu(III) ions in $[Tb,Eu(hfa)_3(dpbp)]_n$ also increased with rise of temperature. The emission intensity ratio of Tb(III) and Eu(III) ions (I_{Eu}/I_{Tb}) therefore exhibited a dramatic change, and their values for $[Tb,Eu(hfa)_3(dpbp)]_n$ (Tb/Eu = 1, 10, 250, 500, 750) are shown in Figure 3-5a. The intensity ratio (I_{Eu}/I_{Tb}) depended on the concentrations of Tb(III) and Eu(III) ions.

3.3.3 Energy transfer efficiency

The temperature-dependent emission spectra of [Tb,Eu(hfa)$_3$(dpbp)]$_n$ are attributed to energy transfer between Tb(III) and Eu(III) ions. The energy transfer efficiency from Tb(III) to Eu(III) ions ($\eta_{Tb\text{-}Eu}$) are estimated by following equation (1),[33] when assuming that the energy-transfer process is dipolar-dipolar,

$$\eta_{Tb-Eu} = 1 - \left(\frac{\tau_{obs}}{\tau_{Tb}} \right) \qquad (1)$$

in which τ_{obs} is the Tb($^5D_4$) emission lifetime in a Tb/Eu mixed system ([Tb,Eu(hfa)$_3$(dpbp)]$_n$) and τ_{Tb} is the lifetime in a pure Tb(III) system ([Tb(hfa)$_3$(dpbp)]$_n$). The η_{sens} value of Tb/Eu = 99 compound was reported to be 38% at room temperature.[26] The author here considers that the equation (1) is similarly applicable to the compounds in this study. The emission lifetimes were estimated by monitoring the 4f-4f transition bands of Tb(III) ions, $^5D_4 \rightarrow {}^7F_6$ (545 nm) and $^5D_4 \rightarrow {}^7F_5$ (488 nm), using an optical filter (550 nm short pass filter). The obtained emission decay profiles were analyzed as single exponential and summarized in Table 3-3.

Table 3-3. Emission lifetimes of Tb(III) ions in chameleon polymers.

Temperature	[Tb,Eu(hfa)$_3$(dpbp)]$_n$ (Tb/Eu = X)					[Tb(hfa)$_3$(dpbp)]$_n$
/ K	X = 1	X = 10	X = 250	X = 500	X = 750	
100	0.85	0.87	0.89	0.90	0.92	0.95
150	0.65	0.82	0.87	0.90	0.93	0.94
200	0.12	0.58	0.79	0.79	0.85	0.83
250	0.24	0.26	0.62	0.60	0.69	0.63
300	0.34	0.11	0.30	0.28	0.40	0.30
350	0.27	0.54	0.11	0.12	0.17	0.12

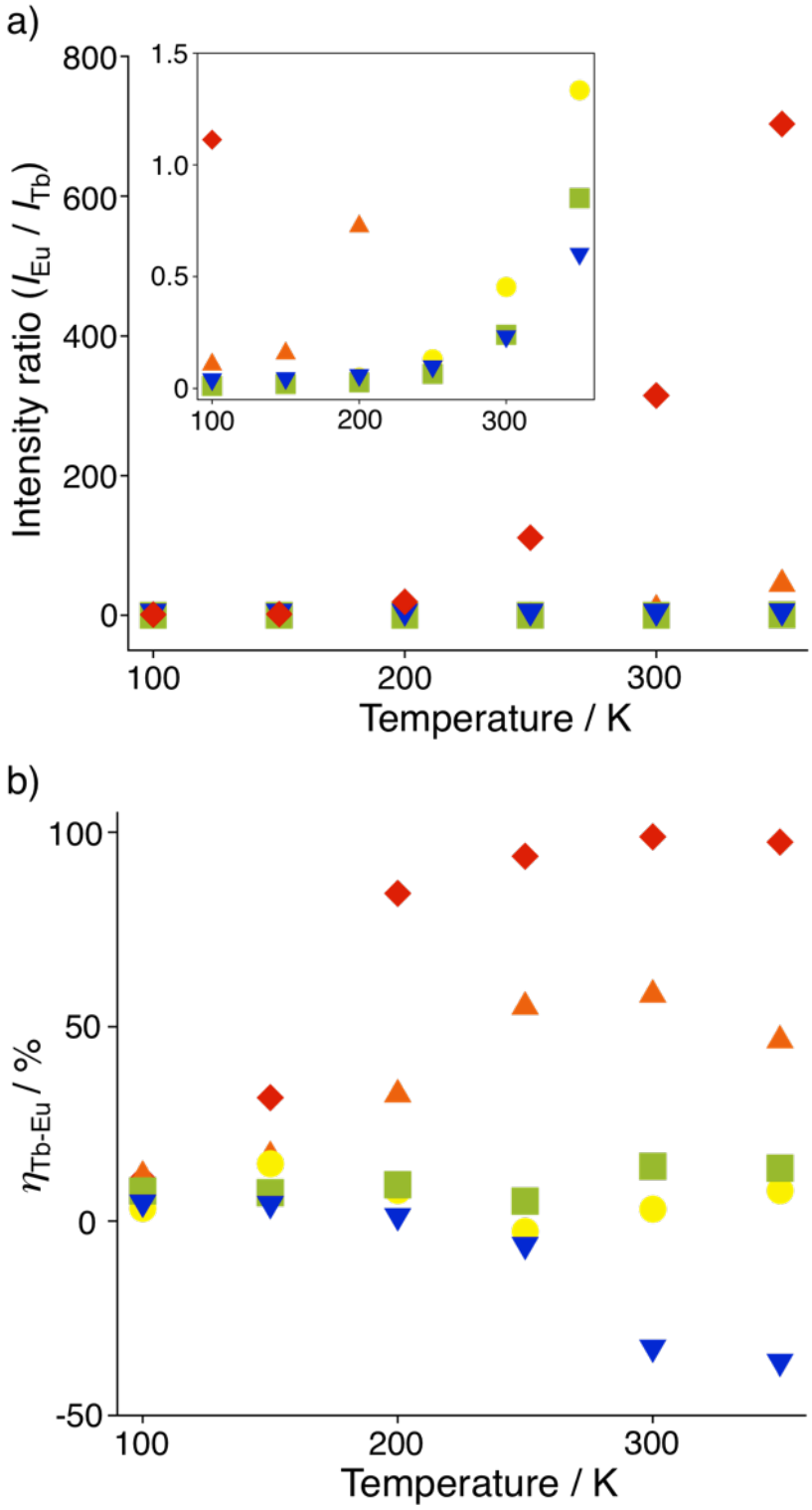

Figure 3-5. Temperature dependence of a) relative emission intensities (I_{Eu}/I_{Tb}) and b) energy transfer efficiencies of $[Tb,Eu(hfa)_3(dpbp)]_n$ (λ_{ex} = 380 nm, ♦: Tb/Eu = 1, ▲: Tb/Eu = 10, ●: Tb/Eu = 250, ■: Tb/Eu = 500 and ▼: Tb/Eu = 750).

The temperature dependence of the energy transfer efficiency $\eta_{Tb\text{-}Eu}$ of $[Tb,Eu(hfa)_3(dpbp)]_n$ is shown in Figure 3-5b. The value of $\eta_{Tb\text{-}Eu}$ at 100 K was approximately zero. According to the measurements at 300 K, the $\eta_{Tb\text{-}Eu}$ are found to be 99%, 65%, 7.4% and 8.2% for Tb/Eu = 1, 10, 250 and 500, respectively. These results indicate that $\eta_{Tb\text{-}Eu}$ depends on the concentration of the energy transfer acceptors, Eu(III) ions. The value of $\eta_{Tb\text{-}Eu}$ of $[Tb,Eu(hfa)_3(dpbp)]_n$ (Tb/Eu = 750) was also found to be negative (−33%), due to the longer emission lifetime of the Tb/Eu = 750 mixture than that of the Tb(III) pure one. The author considers this to be responsible for the different dominating concentration quenching mechanisms of Tb(III) and Eu(III) ions.

3.4 Conclusions

Lanthanide coordination polymers with various ionic ratios, $[Tb,Eu(hfa)_3(dpbp)]_n$ (Tb/Eu = 1, 10, 250, 500, 750), were synthesized and temperature-dependent photophysical properties were examined. The energy transfer efficiency between Ln(III) ions was depended on Tb(III)/Eu(III) mixture ratios, and emission color tuning was also demonstrated. Characteristic luminescent properties of lanthanide coordination polymers composed of Tb(III) and a small amount of Eu(III) ions (Tb/Eu = 750) were also observed. In the solid-state polymers, the bridging ligands also affect the thermo-sensing properties. These studies will provide information on novel aspects of the energy transfer mechanisms in solid-state lanthanide coordination polymers and lead to further development of ideal sensor materials.

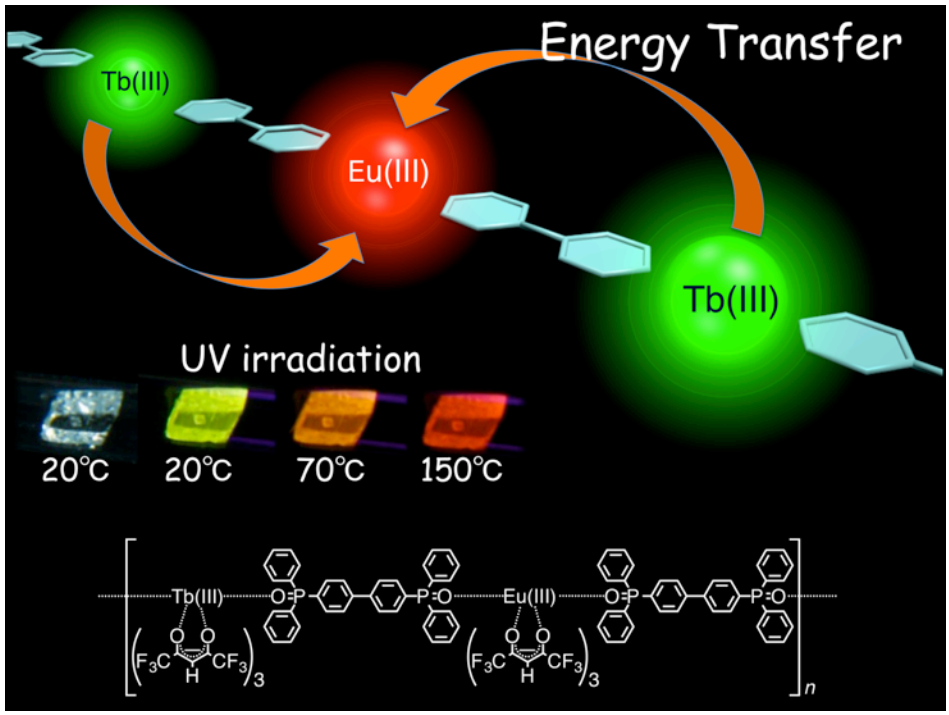

3.5 References

[1] R.J. Adrian, *Annu. Rev. Fluid Mech.* **1991**, *23*, 261-304.

[2] J.H. Bell, E.T. Schairer, L.A. Hand, R.D. Mehta, *Annu. Rev. Fluid Mech.* **2001**, *33*, 155-206.

[3] W.L. Barth, C.A. Burns, *Ieee Trans. Vis. Comput. Graph.* **2007**, *13*, 1751-1758.

[4] H. Sakaue, T. Hayashi, H. Ishikawa, *Sensors* **2013**, *13*, 7053-7064.

[5] M. Edmunds, R.S. Laramee, G.N. Chen, N. Max, E. Zhang, C. Ware, *Comput. Graph.-Uk* **2012**, *36*, 974-990.

[6] J.J. Lee, J.C. Dutton, A.M. Jacobi, *J. Mech. Sci. Technol.* **2007**, *21*, 1253-1262.

[7] L. Yang, H. Zare-Behtash, E. Erdem, K. Kontis, *Exp. Therm. Fluid Sci.* **2012**, *40*, 50-56.

[8] M. Schaferling, *Angew. Chem. Int. Ed.* **2012**, *51*, 3532-3554.

[9] X.D. Wang, O.S. Wolfbeis, R.J. Meier, *Chem. Soc. Rev.* **2013**, *42*, 7834-7869.

[10] Pratt Miller Computational Fluid Dynamics: http://prattmiller.com/veils /default/modeling/cfd

[11] Arnold Air Force Base Aerodynamic Wind Tunnel: http://www.arnold.af.mil /About-Us/Fact-Sheets/Display/Article/409295/aerodynamic-wind-tunnel-4t

[12] S. Fang, S.R. Long, K.J. Disotell, J.W. Gregory, F.C. Semmelmayer, R.W. Guyton, *Aiaa Journal*, **2012**, *50*, 109-122.

[13] K. Binnemans, *Chem. Rev.* **2009**, *109*, 4283-4374.

[14] S.V. Eliseeva, J.C.G. Bunzli, *Chem. Soc. Rev.* **2010**, *39*, 189-227.

[15] J.C.G. Bünzli, S. Comby, A.S. Chauvin, C.D.B. Vandevyver, *J. Rare Earths* **2007**, *25*, 257-274.

[16] L. Armelao, S. Quici, F. Barigelletti, G. Accorsi, G. Bottaro, M. Cavazzini, E. Tondello, *Coord. Chem. Rev.* **2010**, *254*, 487-505.

[17] S. Faulkner, S.J.A. Pope, *J. Am. Chem. Soc.* **2003**, *125*, 10526-10527.

[18] S.J. Butler, D. Parker, *Chem. Soc. Rev.* **2013**, *42*, 1652-1666.

[19] R.K. Mahajan, I. Kaur, R. Kaur, S. Uchida, A. Onimaru, S. Shinoda, H. Tsukube, *Chem. Commun.* **2003**, *17*, 2238-2239.

[20] T. Gunnlaugsson, J.P. Leonard, K. Sènèchal, A.J. Harte, *J. Am. Chem. Soc.* **2003**, *125*, 12062-12063.

[21] J.-F. Lemonnier, L. Guénée, C. Beuchat, T.A. Wesolowski, P. Mukherjee, D.H. Waldeck, K.A. Gogick, S. Petoud, C. Piguet, *J. Am. Chem. Soc.* **2011**, *133*, 16219-16234

[22] K. Miyata, T. Ohba, A. Kobayashi, M. Kato, T. Nakanishi, K. Fushimi, Y. Hasegawa, *Chempluschem* **2012**, *77*, 277-280.

[23] M. Mitsuishi, S. Kikuchi, T. Miyashita, Y. Amao, *J. Mater. Chem.* **2003**, *13*, 2875-2879.

[24] S.M. Borisov, O.S. Wolfbeis, *Anal. Chem.* **2006**, *78*, 5094-5101.

[25] S. Katagiri, Y. Hasegawa, Y. Wada, S. Yanagida, *Chem. Lett.* **2004**, *33*, 1438-1439.

[26] K. Miyata, Y. Konno, T. Nakanishi, A. Kobayashi, M. Kato, K. Fushimi, Y. Hasegawa, *Angew. Chem. Int. Ed.* **2013**, *52*, 6413-6416.

[27] J.F. Lemonnier, L. Guenee, C. Beuchat, T.A. Wesolowski, P. Mukherjee, D.H. Waldeck, K.A. Gogick, S. Petoud, C. Piguet, *J. Am. Chem. Soc.* **2011**, *133*, 16219-16234.

[28] A.M. Funk, P.H. Fries, P. Harvey, A.M. Kenwright, D. Parker, *J. Phys. Chem. A* **2013**, *117*, 905-917.

[29] Y. Cui, W. Zou, R. Song, J. Yu, W. Zhang, Y. Yang, G. Qian, *Chem Commun.* **2014**, *50*, 719-721.

[30] D. Zhao, X. Rao, J. Yu, Y. Cui, Y. Yang, G. Qian, *Inorg. Chem.* **2015**, *54*, 11193-11199.

[31] X. Liu, S. Akerboom, M. de Jong, I. Mutikainen, S. Tanase, A. Meijerink, E. Bouwman, *Inorg. Chem.* **2015**, *54*, 11323-11329.

[32] H. Wang, D. Zhao, Y. Cui, Y. Yang. G. Qian, *J. Solid State Chem.* **2017**, *246*, 341-345.

[33] C. Piguet, J.C.G. Bünzli, G. Bernardinelli, G. Hopfgartner, A.F. Williams, *J. Am. Chem. Soc.* **1993**, *115*, 8197-8206.

Appendices

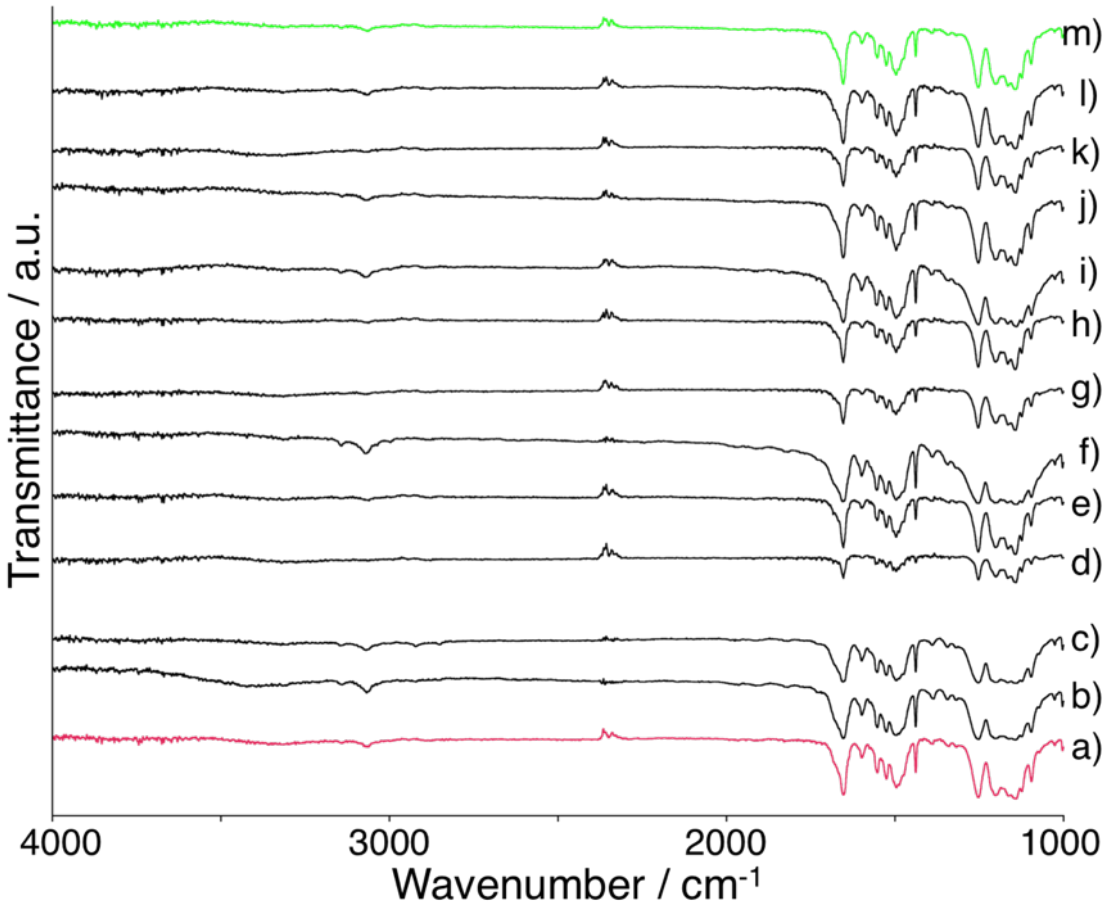

Figure A3-1. IR spectra of a) $[Eu(hfa)_3(dpbp)]_n$, b)-l) $[Tb,Eu(hfa)_3(dpbp)]_n$ (Tb/Eu = 1-1000), and m) $[Tb(hfa)_3(dpbp)]_n$ using KBr.

Hypersonic wind tunnel experiment

The temperature-sensitive property and durability of the compounds in hypersonic wind (Mach 10) were tested using 1.27 m Hypersonic Wind Tunnels in Japan Aerospace Exploring Agency (JAXA, Figure A3-2). It is generally known that the temperature on the surface of a material rises to 150˚C in 3 seconds in a Mach 10 wind. The sample powder $[Tb,Eu(hfa)_3(dpbp)]_n$ (Tb/Eu = 150) was painted on a hemi-sphered test model using a spray sticker. The test model was mounted on an arm in the wind tunnel. Although emission color change was observed by the naked eye during the hypersonic wind flow, temperature mapping was only obtained by IR thermography.

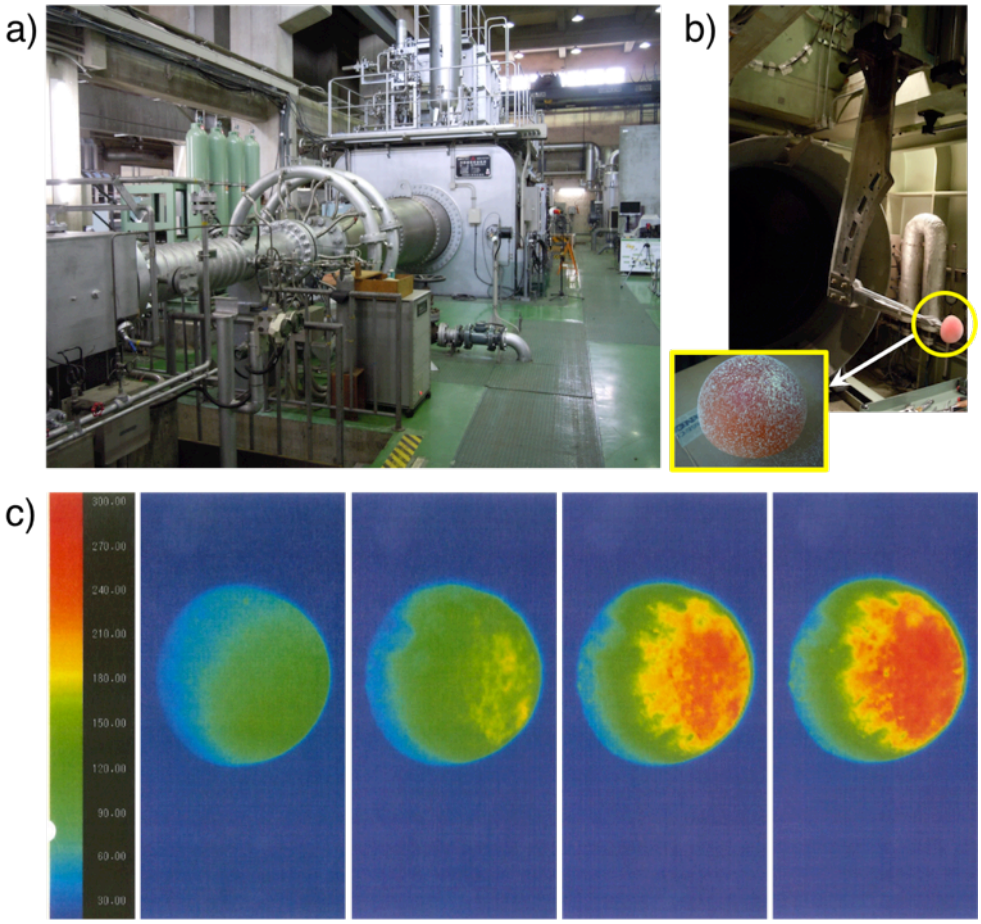

Figure A3-2. a) Hypersonic wind tunnel in JAXA, b) test model with $[Tb,Eu(hfa)_3(dpbp)]_n$ (Tb/Eu = 150) powder, and c) images of temperature elevation on the surface of a material obtained from infrared thermography.

Chapter 4

Construction of luminescent lanthanide(III) coordination glasses

Abstract

Construction of luminescent Eu(III) coordination glasses $[Eu(hfa)_3(o\text{-dpeb})]_2$, $[Eu(hfa)_3(m\text{-dpeb})]_3$, and $[Eu(hfa)_3(p\text{-dpeb})]_n$ (*o*-, *m*-, *p*-dpeb: 1,2-, 1,3-, 1,4-bis(diphenylphosphorylethynyl)benzene) are reported. The coordination structures and glass formability were dependent on the regiochemistry of substitution in regard to the internal phenylene core. Single-crystal X-ray analyses and DFT calculations revealed dimer, trimer, and polymer structures of Eu(III) coordination glasses. All of these compounds exhibited glass transition temperature in the range of 25˚C to 96˚C, and strong luminescence was also observed with intrinsic emission quantum yields above 70%.

Based on
Luminescent Coordination Glass: Remarkable Morphological Strategy for Assembled Eu(III) Complexes
Y. Hirai, T. Nakanishi, Y. Kitagawa, K. Fushimi, T. Seki, H. Ito, H. Fueno, K. Tanaka, T. Satoh, Y. Hasegawa, *Inorg. Chem.* **2015**, *54*, 4364-4370.

4.1 Introduction

Amorphous inorganic or organic compounds have attracted attention in the field of materials science.[1-4] In particular, small organic molecules with amorphous formability are referred to as “amorphous molecular materials,” and expected as promising candidates for optical applications due to their processability, transparency, isotropy, and homogeneous properties.[5,6] The π-conjugated organic molecules with stable amorphous state above room temperature have been developed for use in organic electroluminescent (EL) and field-effect transistor (FET) devices.[7,8] Shirota and co-workers reported that a series of organic molecules based on C_3-symmetrical starburst molecules such as triphenylamines and triarylbenzenes forms stable amorphous solid and exhibits charge transfer abilities (Figure 4-1a).[9,10] Tian *et al.* demonstrated the glass formability of small organic molecules with electron-accepting 2-pyran-4-ylidenemalononitrile.[11] Balcerzak recently developed thermally stable molecular glasses composed of thiophene rings, diimide, and imine groups (T_g > 300˚C).[12]

The author here focuses on luminescent glasses based on Ln(III) coordination compounds as a new class of amorphous molecular materials with characteristic 4f-4f transitions.[13-19] Control of molecular morphology, which dominates the molecular motions and packing structures, is thus required to construct amorphous lanthanide coordination compounds. Bazan and co-workers developed an amorphous Eu(III) complex by introducing hexyloxy groups in order to prevent easy crystal packing.[20] Long alkyl chains in Eu(III) complexes improve their solubility and amorphous formability; however, high-vibrational frequency of C-H bonds promote thermal decomposition and

non-radiative quenching process of Eu(III)-centered emission.[21,22] In order to construct an ideal amorphous lanthanide coordination compounds, novel molecular structures without long alkyl chains are designed based on Eu(III)-*β*-diketonates for their strong luminescence properties[23-27] (Figure 4-1b). Hasegawa and co-workers reported the crystalline Eu(III) coordination polymers with *meta*- and *para*-substituted phenylene bridging ligands (1,3- and 1,4-bis(diphenylphosphoryl)benzene).[28,29] They also developed the 4,4'-substituted biphenylene bridge (4,4'-bis(diphenylphosphoryl)biphenyl: dpbp) to form rigid coordination polymers with intermolecular CH/π interactions.[29,30] Introduction of ethynyl groups into these rigid aromatic moieties would be expected to suppress tight-binding interactions and crystallization of assembled Eu(III) complexes.

In this chapter, *o*-, *m*-, and *p*-substituted phenylene bridging ligands with ethynyl groups were prepared for systematic control of the coordination structures. The morphological properties were characterized using X-ray single crystal analyses, DFT calculations, and surface observations by scanning probe microscope (SPM). The thermal and photophysical properties were evaluated based on differential scanning calorimetry (DSC) and spectroscopy.

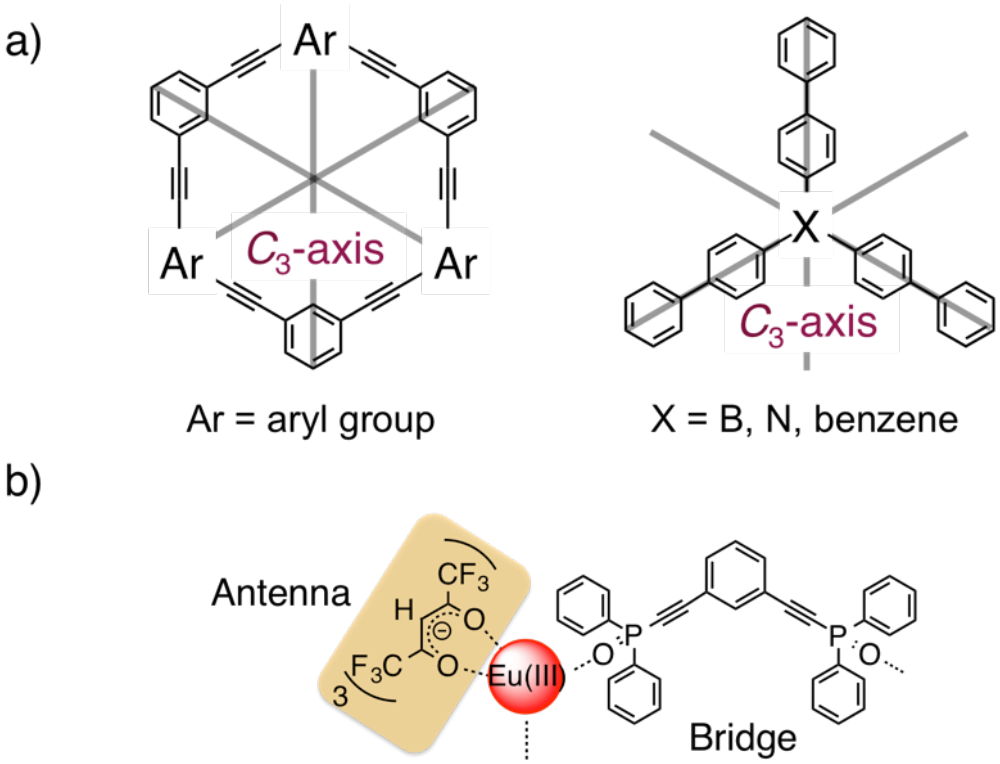

Figure 4-1. a) Chemical structures of small organic compounds with amorphous formability (Ar: aryl groups, X: boron, nitrogen, or benzene) and b) design of Eu(III) coordination glasses.

4.2 Experimental Section

4.2.1 Materials

Europium acetate *n*-hydrate (99.9%), *n*-BuLi (in *n*-hexane, 1.6 M), and hydrogen peroxide were purchased from Kanto Chemical Co., Inc. 1,2-Diiodobenzene, 1,3-diethynylbenzene, 1,4-diethynylbenzene, trimethylsilylacetylene, bis(triphenylphosphine)palladium dichloride, and chlorodiphenylphosphine were obtained from Tokyo Chemical Industry Co., Ltd. All other chemicals and solvents were reagent grade and were used without further purification.

4.2.2 Apparatus

^{1}H NMR (400 MHz) spectra were recorded on a JEOL ECS400. Chemical shifts were reported in δ ppm, referenced to an internal tetramethylsilane standard for ^{1}H NMR spectroscopy. Infrared spectra were recorded on a JASCO FTIR-420 spectrometer using KBr pellets. Elemental analyses were performed by an Exeter Analytical CE440. Mass spectrometry was performed by a Thermo Scientific Exactive (ESI-MS) and a JEOL JMS-700TZ (FAB-MS)

4.2.3 Syntheses

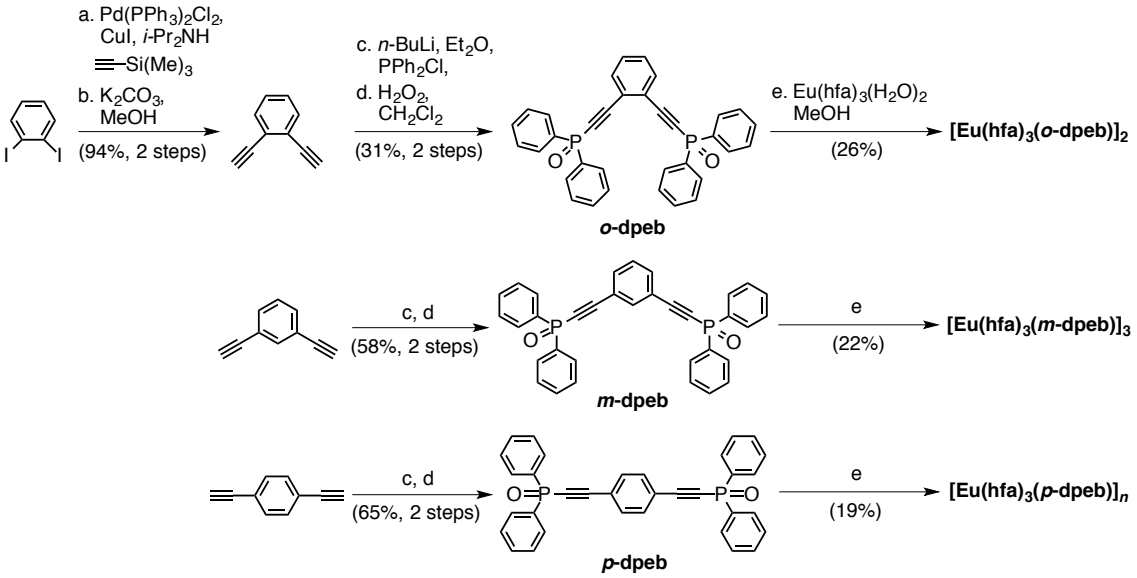

Scheme 4-1. Synthetic schemes of phosphine oxide ligands with ehtynyl groups and Eu(III) coordination compounds.

Preparation of 1,2-bis(trimethylsilylethynyl)benzene:[31]

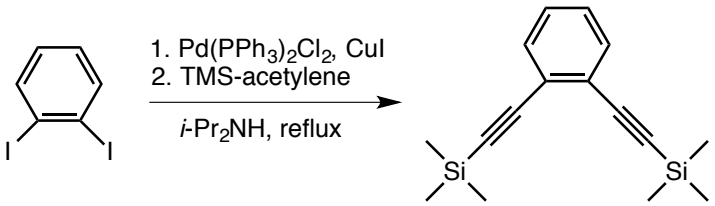

In a degassed 3-neck round-bottomed flask (300 mL vol.), 1,2-diiodobenzene (5.0 mL, 15 mmol), $PdCl_2(PPh_3)_2$ (0.5 g, 0.7 mmol), CuI (0.5 g, 2.5 mmol) were added and dissolved in diisopropylamine (100 mL) under argon atmosphere, then stirred until a homogeneous solution was formed at room temperature. The mixture was refluxed under argon for 4 h. The reaction mixture was allowed to cool to room temperature, ammonium salt was removed by filtration and the solvent was evaporated in vacuo. The residue was purified by column chromatography on SiO_2 using hexanes as an eluent to afford 1,2-bis(trimethylsilylethynyl)benzene (Yield: 3.8 g, 94%).

Preparation of 1,2-diethynylbenzene: [32]

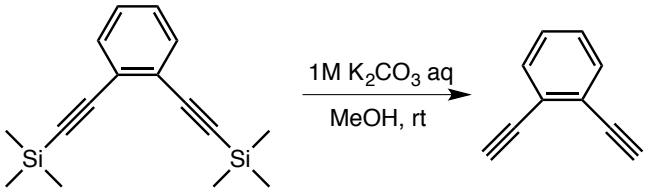

1,2-Bis(trimethylsilylethynyl)benzene (3.8 g, 14 mmol) was dissolved in methanol (40 mL) and 1 M K_2CO_3 aqueous solution (35 mL, 35 mmol) was added. The mixture was stirred for 3 h. The product was extracted with diethylether and dried over anhydrous $MgSO_4$. The solvent was evaporated to afford 1,2-diethynylbenzene as yellow oil (Yield: 1.8 g, 100%).

Preparation of 1,2-bis(diphenylphosphorylethynyl)benzene:

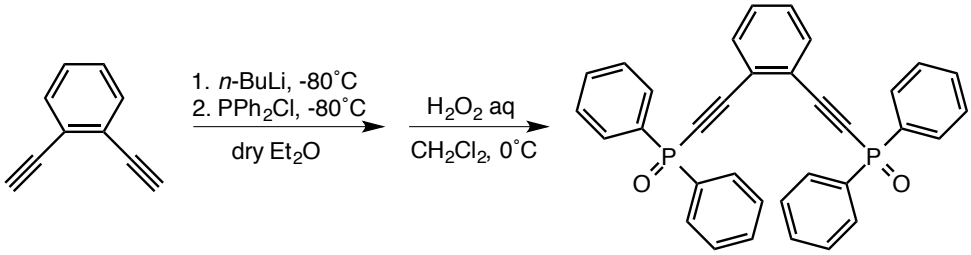

In a degassed 3-neck round-bottomed flask (300 mL vol.), 1,2-diethynylbenzene (1.8 g, 14 mmol) was added and dissolved in dry diethylether (60 mL) under argon atmosphere, then stirred until a homogeneous solution was formed at room temperature. A solution of *n*-BuLi (19 mL, 31 mmol) was added dropwise to the solution at −80˚C. The addition was completed in ca. 15 min during which time the solution color changed from orange, dark green, then black. The mixture was allowed to stir for 3 h at −10˚C, after which a PPh_2Cl (5.6 mL, 31 mmol) was added dropwise at −80˚C, then the solution color turned to red-brown. The mixture was gradually brought to room temperature, and stirred for 14 h to form clouded brown solution. The reaction mixture was extracted with dichloromethane and dried over anhydrous

$MgSO_4$. The solvent was evaporated, and the obtained pale yellow solid was placed with dichloromethane (50 mL) in a flask. The solution was cooled to 0˚C and then 30% H_2O_2 aqueous solution (34 mL) was added to it. The reaction mixture was stirred for 2 h. The product was extracted with dichloromethane, the extracts were purified by column chromatography on SiO_2 using ethyl acetate and hexanes as mixed eluent (ethyl acetate : hexane = 2 : 1).

Yield: 1.5 g (20%). ^{1}H NMR (400 MHz, $CDCl_3$, 25˚C) *δ* 7.79-7.86 (m, 8H, -CH), *δ* 7.64-7.67 (m, 2H, -CH), *δ* 7.43-7.49 (m, 6H, -CH), *δ* 7.35-7.41 (m, 8H, -CH) ppm. ESI-Mass (*m*/*z*): $[M+H]^+$ calcd for $C_{34}H_{25}O_2P_2$, 527.1; found, 527.1. Anal. Calcd for $C_{34}H_{24}O_2P_2$: C, 75.56; H, 4.59%. Found: C, 75.99; H, 4.58%.

Preparation of 1,3-bis(diphenylphosphorylethynyl)benzene (*m*-dpeb):

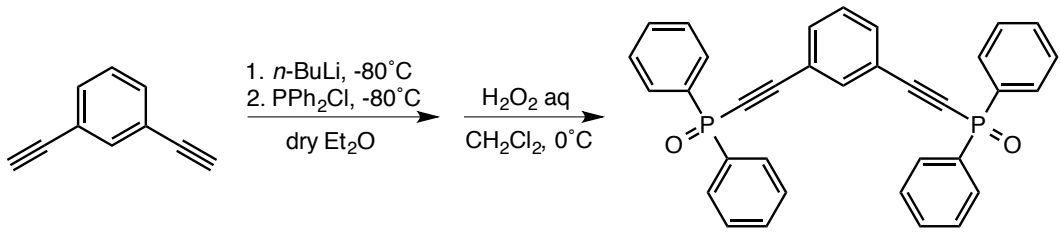

The 1,3-diethynylbenzene was dissolved in dry diethylether (50 mL) and the mixture degassed by argon bubbling for 20 min. A solution of *n*-BuLi (13 mL, 21 mmol) was added dropwise to the solution at −80˚C. The addition was completed in ca. 15 min during which time a yellow precipitate was formed. The mixture was allowed to stir for 3 h at −10˚C, after which a PPh_2Cl (3.8 mL, 21 mmol) was added dropwise at −80˚C. The mixture was gradually brought to room temperature, and stirred for 14 h. The product was extracted with dichloromethane, the extracts washed with brine for three times and dried over anhydrous $MgSO_4$. The solvent was evaporated, and the obtained pale yellow solid was placed with dichloromethane (50 mL) in a flask. The solution was

cooled to 0˚C and then 30% H_2O_2 aqueous solution (10 mL) was added to it. The reaction mixture was stirred for 2 h. The product was extracted with dichloromethane and purified by column chromatography on SiO_2 using ethyl acetate and hexanes as mixed eluent (ethyl acetate : hexane = 2 : 1).

Yield: 4.3 g (58%). ^{1}H-NMR (400 MHz, $CDCl_3$, 25 ˚C) *δ* 7.84-7.95 (m, 8H, -CH), *δ* 7.82 (s, 1H, -CH), *δ* 7.67-7.70 (d, 1H, -CH), *δ* 7.64-7.66 (d, 1H, -CH), *δ* 7.47-7.62 (m, 12H, -CH), *δ* 7.38-7.46 (t, 1H, -CH) ppm. ESI-Mass (*m*/*z*): $[M+H]^+$ calcd for $C_{34}H_{25}O_2P_2$, 527.1; found, 527.1. Anal. Calcd for $C_{34}H_{24}O_2P_2$: C, 77.56; H, 4.59%. Found: C, 77.70; H, 4.64%.

Preparation of 1,4-bis(diphenylphosphorylethynyl)benzene (*p*-dpeb):

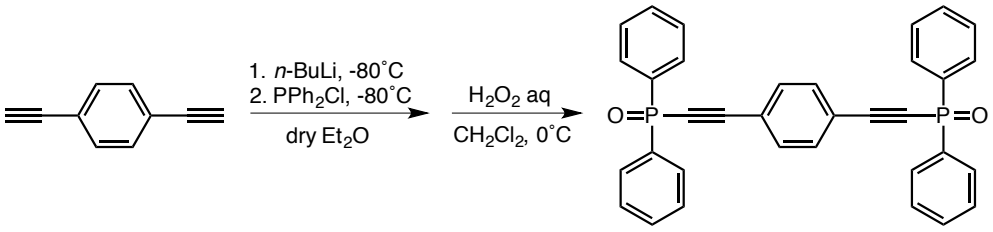

The 1,4-diethynylbenzene was dissolved in dry diethylether (50 mL) and the mixture degassed by Ar bubbling for 20 min. A solution of *n*-BuLi (13 mL, 21 mmol) was added dropwise to the solution at −80˚C. The addition was completed in ca. 15 min during which time a yellow precipitate was formed. The mixture was allowed to stir for 3 h at −10˚C, after which a PPh_2Cl (3.8 mL, 21 mmol) was added dropwise at −80˚C. The mixture was gradually brought to room temperature, and stirred for 14 h. The product was extracted with dichloromethane, the extracts washed with brine for three times and dried over anhydrous $MgSO_4$. The solvent was evaporated, and the obtained pale yellow solid was placed with dichloromethane (50 mL) in a flask. The solution was cooled to 0˚C and then 30% H_2O_2 aqueous solution (10 mL) was added to it.

The reaction mixture was stirred for 2 h. The product was extracted with dichloromethane and purified by column chromatography on SiO_2 using ethyl acetate and hexanes as mixed eluent (ethyl acetate : hexane = 2 : 1).
Yield: 4.3 g (58%). ^{1}H NMR (400 MHz, $CDCl_3$, 25 ˚C) *δ* 7.84-7.90 (m, 8H, -CH), *δ* 7.59 (s, 4H, -CH), *δ* 7.55-7.56 (d, 4H, -CH), *δ* 7.47-7.51 (m, 8H, -CH) ppm. ESI-Mass (*m*/*z*): $[M+H]^+$ calcd for $C_{34}H_{25}O_2P_2$, 527.1; found, 527.1. Anal. Calcd for $C_{34}H_{24}O_2P_2$: C, 77.56; H, 4.59%. Found: C, 77.52; H, 4.72%.

Preparation of Eu(III) complexes [Eu(hfa)$_3$(*o*-dpeb)]$_2$, [Eu(hfa)$_3$(*m*-dpeb)]$_3$, [Eu(hfa)$_3$(*p*-dpeb)]$_n$:

Phosphine oxide ligands (0.21 g, 0.40 mmol) and $Eu(hfa)_3(H_2O)_2$ (0.32 g, 0.40 mmol) were dissolved in methanol (20 mL), respectively. The solutions were mixed and stirred for 2 h. The solvent was evaporated, and the obtained white solid was washed with chloroform and hexanes.

[Eu(hfa)$_3$(*o*-dpeb)]$_2$: Yield 0.27 g (26%). IR (KBr) 1657 (st, C=O), 1132 (st, P=O), 1093-1249 (st, C-O-C and st, C-F) cm^{-1}. FAB-Mass (*m*/*z*): $[M-hfa]^+$ calcd for $C_{93}H_{53}Eu_2F_{30}O_{14}P_4$, 2392.2; found, 2392.0. Anal. Calcd for: C, 45.29; H, 2.09%. Found: C, 45.05; H, 2.21%.

[Eu(hfa)$_3$(*m*-dpeb)]$_3$: Yield 0.34 g (22%). IR (KBr) 1657 (st, C=O), 1142 (st, P=O), 1093-1258 (st, C-O-C and st, C-F) cm^{-1}. FAB-Mass (*m*/*z*): $[M-hfa]^+$ calcd for $C_{142}H_{80}Eu_3F_{48}O_{22}P_6$, 3691.8; found, 3691.8. Anal. Calcd for: C, 45.29; H, 2.09%. Found: C, 45.48; H, 2.51%.

[Eu(hfa)$_3$(*p*-dpeb)]$_n$: Yield 0.39 g (75% for monomer). IR (KBr) 1657 (st, C=O), 1141 (st, P=O), 1093-1249 (st, C-O-C and st, C-F) cm^{-1}. FAB-Mass (*m*/*z*): $[M-hfa]^+$ calcd for $C_{44}H_{26}EuF_{12}O_6P_2$, 1092.6; found, 1092.7. Anal. Calcd for: C, 45.29; H, 2.09%. Found: C, 44.98; H, 2.18%.

4.2.4 Crystallography

The X-ray crystal structures and crystallographic data for $[Eu(hfa)_3(o\text{-dpeb})]_2$ and $[Eu(hfa)_3(p\text{-dpeb})]_n$, recrystallized from methanol, are shown in Figure 4-2, 4-3, and Table 4-1. Colorless single crystals of the complexes were mounted on a glass fiber using paraffin oil. All measurements were made on a Rigaku RAXIS RAPID imaging plate area detector with graphite monochromated MoKa radiation. Correction for decay and Lorentz-polarization effects were made using empirical absorption correction, solved by direct methods and expanded using Fourier techniques. Non-hydrogen atoms were refined anisotropically. Hydrogen atoms were refined using the riding model. The final cycle of full-matrix least-squares refinement was based on observed reflections and variable parameters. All calculations were performed using the crystal structure crystallographic software package. The CIF data was confirmed by the checkCIF/PLATON service. CCDC-1037529 (for $[Eu(hfa)_3(o\text{-dpeb})]_2$), and CCDC 1037531 (for $[Eu(hfa)_3(p\text{-dpeb})]_n$) contain the supplementary crystallographic data for this paper. These data can be obtained free of charge from The Cambridge Crystallographic Data Centre via www.ccdc.cam.ac.uk/data_request/cif.

4.2.5 Optical measurements

UV-Vis absorption spectra were recorded on a JASCO V-670 spectrometer. Emission and excitation spectra were recorded on a HORIBA Fluorolog-3 spectrofluorometer and corrected for the response of the detector system. Emission lifetimes (τ_{obs}) were measured using the third harmonics (355 nm) of a Q-switched Nd:YAG laser (Spectra Physiscs, INDI-50, fwhm = 5 ns, λ = 1064 nm) and a photomultiplier (Hamamatsu photonics, R5108, response time ≤ 1.1 ns). The Nd:YAG laser response was monitored with a digital oscilloscope (Sony Tektronix, TDS3052, 500 MHz) synchronized to the single-pulse excitation. Emission lifetimes were determined from the slope of logarithmic plots of the decay profiles. The emission quantum yields excited at 380 nm (Φ_{tot}) were estimated using JASCO F-6300-H spectrometer attached with JASCO ILF-533 integrating sphere unit (φ = 100 mm). The wavelength dependence of the detector response and the beam intensity of Xe light source for each spectrum were calibrated using a standard light source.

4.2.6 DFT calculations

Due to lack in the structural data of [Eu(hfa)(*m*-dpeb)]$_3$, the DFT calculation was carried out at B3LYP level with the basis sets SDD for Eu and 6-31G** for other atoms using the Gaussian 09 program package.[33-36] The ultrafine grid was used for numerical integrations. A trimer structure was plausibly assumed for this complex.

4.3 Results and Discussion

4.3.1 Structural characterization

In order to investigate the coordination geometry around Eu(III) ions and assembled structures, single crystals were prepared for $[Eu(hfa)_3(o\text{-dpeb})]_2$ and $[Eu(hfa)_3(p\text{-dpeb})]_n$. Crystallographic data of these compounds were summarized in Table 4-1. The Eu(III) ions for both compounds formed typical 8-coordination with three hfa and two bridging ligands (Figure 4-2a, 4-3a).

The coordination geometry around Eu(III) ions was examined on the basis of shape factor *S* as described in Chapter 2. The observed dihedral angles (δ_i), ideal dihedral angles for square antiprism (θ_{SAP}) and trigonal dodecahedron (θ_{TDH}), calculated measure shape criteria, S_{SAP} and S_{TDH} were summarized (see Figure A4-1, 4-2, Table A4-1, 4-2 in appendices). When assuming 8-SAP structures, the *S* values for $[Eu(hfa)_3(o\text{-dpeb})]_2$ and $[Eu(hfa)_3(p\text{-dpeb})]_n$ (S_{SAP} = 6.90 and 5.17, respectively) are smaller than those for 8-TDH (S_{TDH} = 11.1 and 13.5, respectively), suggesting that 8-SAP structure is less distorted than the 8-TDH structure. The coordination geometry of these compounds is therefore determined to be 8-SAP.

The author also focused on assembled structures of these compounds. $[Eu(hfa)_3(o\text{-dpeb})]_2$ formed a C_2-symmetrical dimer structure composed of two Eu(III) ions, six hfa, and two phosphine oxide bridging ligands, which was highly fixed with multiple intra and intermolecular CH/F ($d_{CH/F}$ = 2.63 Å (H39/F6), 3.00 Å (H44/F4), and 2.79 Å (H56/F9)) and π/π ($d_{\pi/\pi}$ = 3.19 Å and 3.43 Å) interactions. A large crystal density (1.754 g cm^{-3}) was responsible for the highly-ordered packing structure.

$[Eu(hfa)_3(p\text{-dpeb})]_n$ formed a polymer chain (Figure 4-3) with intra and

intermolecular CH/F interactions ($d_{CH/F}$ = 3.03 Å (H25/F73), 2.63 Å (H46/F38), and 2.69 Å (H22/F38)). $[Eu(hfa)_3(p\text{-dpeb})]_n$ showed relatively loose-packed structure due to the absence of intermolecular CH/π interactions between single polymer chains, unlike reported rigid Eu(III) coordination polymer, $[Eu(hfa)_3(dpbp)]_n$.[29] The author considered this to be responsible for ethynyl groups in *p*-dpeb that provided a large crystal volume with small availability of aromatic surfaces for intermolecular CH/π interactions.

On the other hand, $[Eu(hfa)_3(m\text{-dpeb})]_3$ formed amorphous state. A trimer structure was assumed based on the fragments of $Eu_3(hfa)_8(m\text{-dpeb})^{3+}$ in FAB-MS spectrum (Figure 4-4a). The X-ray diffraction image and patterns also indicated the lack of crystallinity and the obtained signals were similar to those of glass ceramics (Figure 4-4b, c).[37]

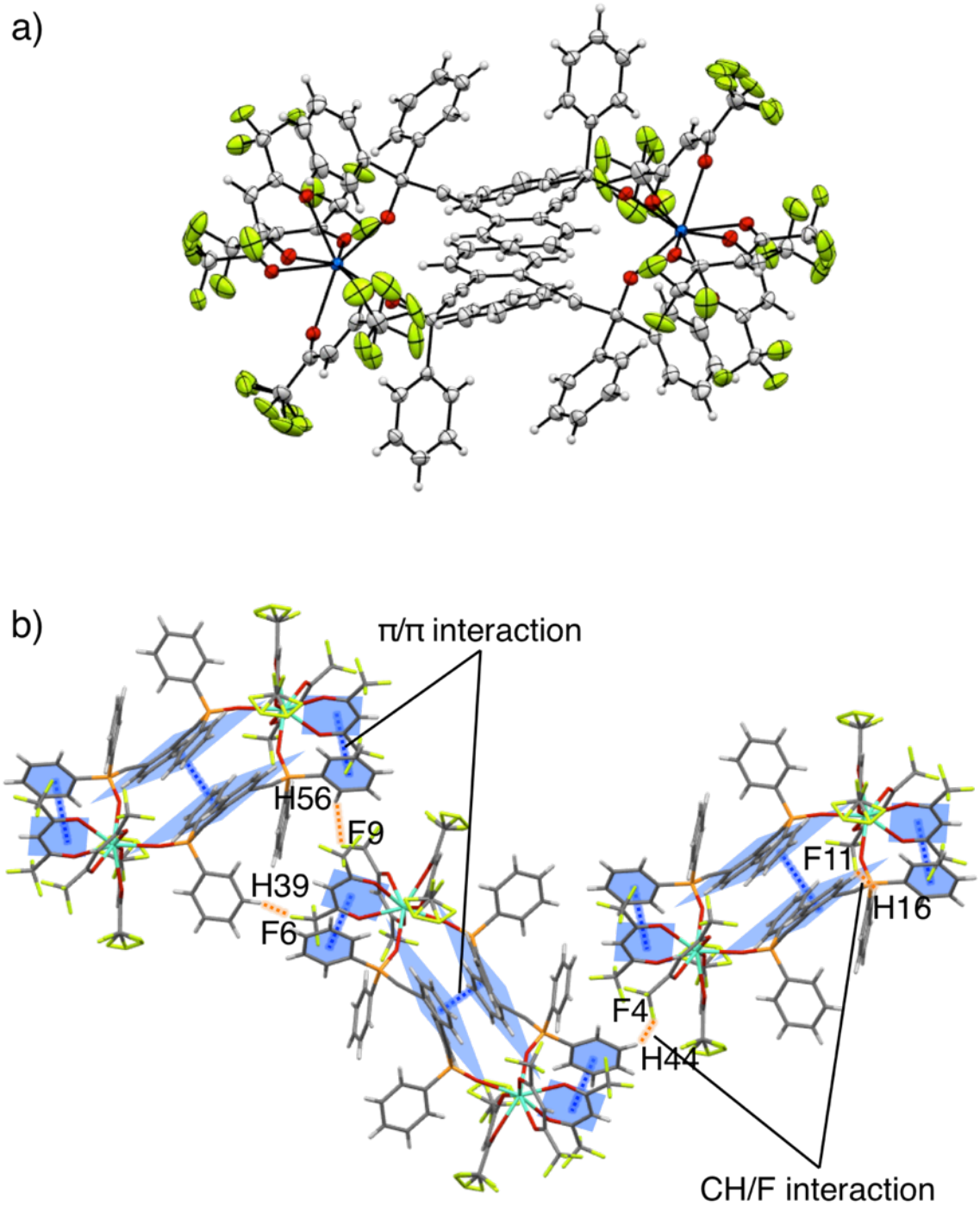

Figure 4-2 a) ORTEP drawings of a single crystal of $[Eu(hfa)_3(o\text{-dpeb})]_2$ from methanol solution. Thermal ellipsoids are shown at 50% probability level. b) Capped sticks model of $[Eu(hfa)_3(o\text{-dpeb})]_2$ focused on the selected intra and intermolecular interactions. Dashed lines denote CH/F and π/π interactions.

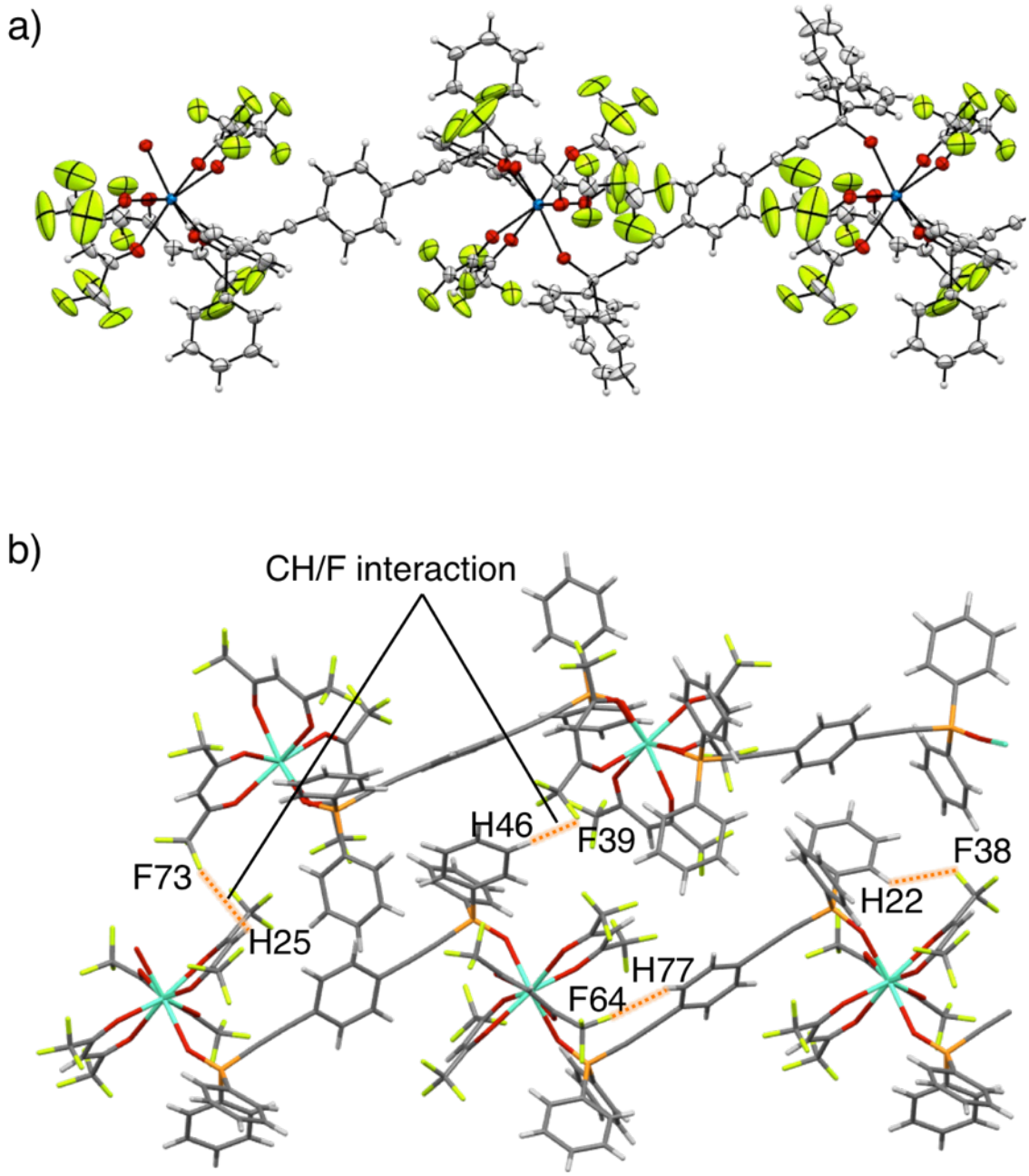

Figure 4-3 a) ORTEP drawings of a single crystal of $[Eu(hfa)_3(p\text{-dpeb})]_n$ from methanol solution. Thermal ellipsoids are shown at 50% probability level. b) Capped sticks model of $[Eu(hfa)_3(p\text{-dpeb})]_n$ focused on the selected intra and intermolecular interactions. Dashed lines denote CH/F interactions.

Table 4-1. Crystallographic data of Eu(III) coordination compounds.

	$[Eu(hfa)_3(o\text{-dpeb})]_2$	$[Eu(hfa)_3(p\text{-dpeb})]_n$
Chemical formula	$C_{98}H_{54}Eu_2F_{36}O_{16}P_4$	$C_{49}H_{27}EuF_{18}O_8P_2$
Formula weight	2599.25	1299.63
Crystal system	Monoclinic	Monoclinic
Space group	$P2_1/n$ (#14)	$P2_1/c$ (#14)
a / Å	12.5432(9)	23.1941(10)
b / Å	30.3644(15)	13.4114(5)
c / Å	12.9212(9)	16.7226(6)
a / deg	90.000	90.000
b / deg	90.378(6)	91.6148(10)
g / deg	90.000	90.000
Volume / $Å^3$	4921.1(5)	5199.8(4)
Z	2	4
d_{calc} / g cm^{-3}	1.754	1.660
Temperature / °C	23.0	−150
m (Mo Kα) / cm^{-1}	14.590	13.809
max $2q$ / deg	55.0	55.00
Reflections collected	48310	49124
Independent	11257	11871
R_1	0.0439	0.0420
wR_2	0.0728	0.0998

[a] $R_1 = \sum ||F_o| - |F_c|| / \sum |F_o|$. [b] $wR_2 = [\sum w (F_o^2 - F_c^2)^2 / \sum w (F_o^2)^2]^{1/2}$.

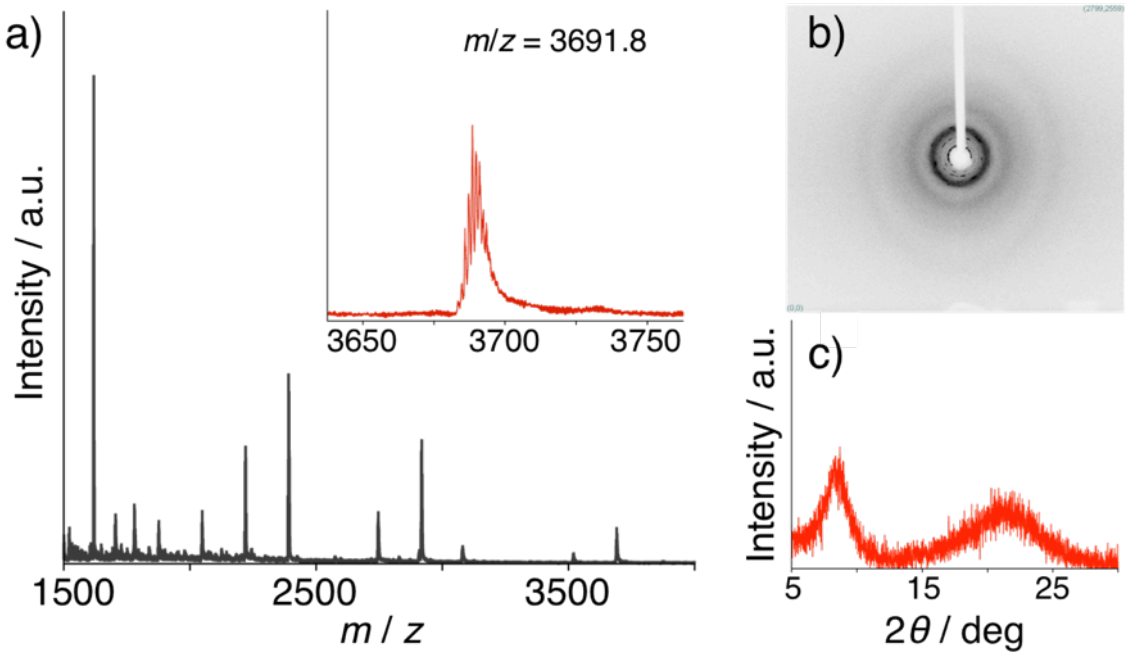

Figure 4-4. a) FAB-MS spectrum, b) X-ray diffraction image and c) powder X-ray diffraction patterns of $[Eu(hfa)_3(m\text{-dpeb})]_3$.

4.3.2 DFT optimization

Optimization of $[Eu(hfa)_3(o\text{-dpeb})]_2$ was first carried out. The dimer structure determined by single crystal X-ray analysis was used as the initial structure for DFT calculation. The optimized structure almost completely matched that of the X-ray analysis with C_2 symmetry (Figure 4-5a). The unit cell of $[Eu(hfa)_3(p\text{-dpeb})]_n$ was also calculated as a closed-shell singlet configuration since it was composed of an Eu(III) ion and three anionic hfa ligands. The optimized structure was the same as that of the X-ray analysis (Figure 4-5b). According to the band structure of $[Eu(hfa)_3(p\text{-dpeb})]_n$, conjugation was not extended over the whole polymer chains. The band gap was also estimated for the orbital phase on Γ point. The estimated band gap energy (≈ 4.0 eV) for $[Eu(hfa)_3(o\text{-dpeb})]_2$ and $[Eu(hfa)_3(p\text{-dpeb})]_n$ corresponded to the S_0-S_1 gap of hfa ligands (see appendices for precise data of DFT calculations).

Based on these results, optimization for $[Eu(hfa)_3(m\text{-dpeb})]_3$ was carried out using the same basis sets as those for the other two compounds. The initial structure was determined to be the assumed trimer structure, and the *pseudo*-C_3 symmetrical moiety was optimized (Figure 4-5c). The $[Eu(hfa)_3(m\text{-dpeb})]_3$ has highly broken symmetry compared to that of the C_2-symmetrical $[Eu(hfa)_3(o\text{-dpeb})]_2$. Multiple meta-stable states observed during calculations are probably related to the broken symmetry of $[Eu(hfa)_3(m\text{-dpeb})]_3$ and lead to the formation of an amorphous state instead of crystal packing.

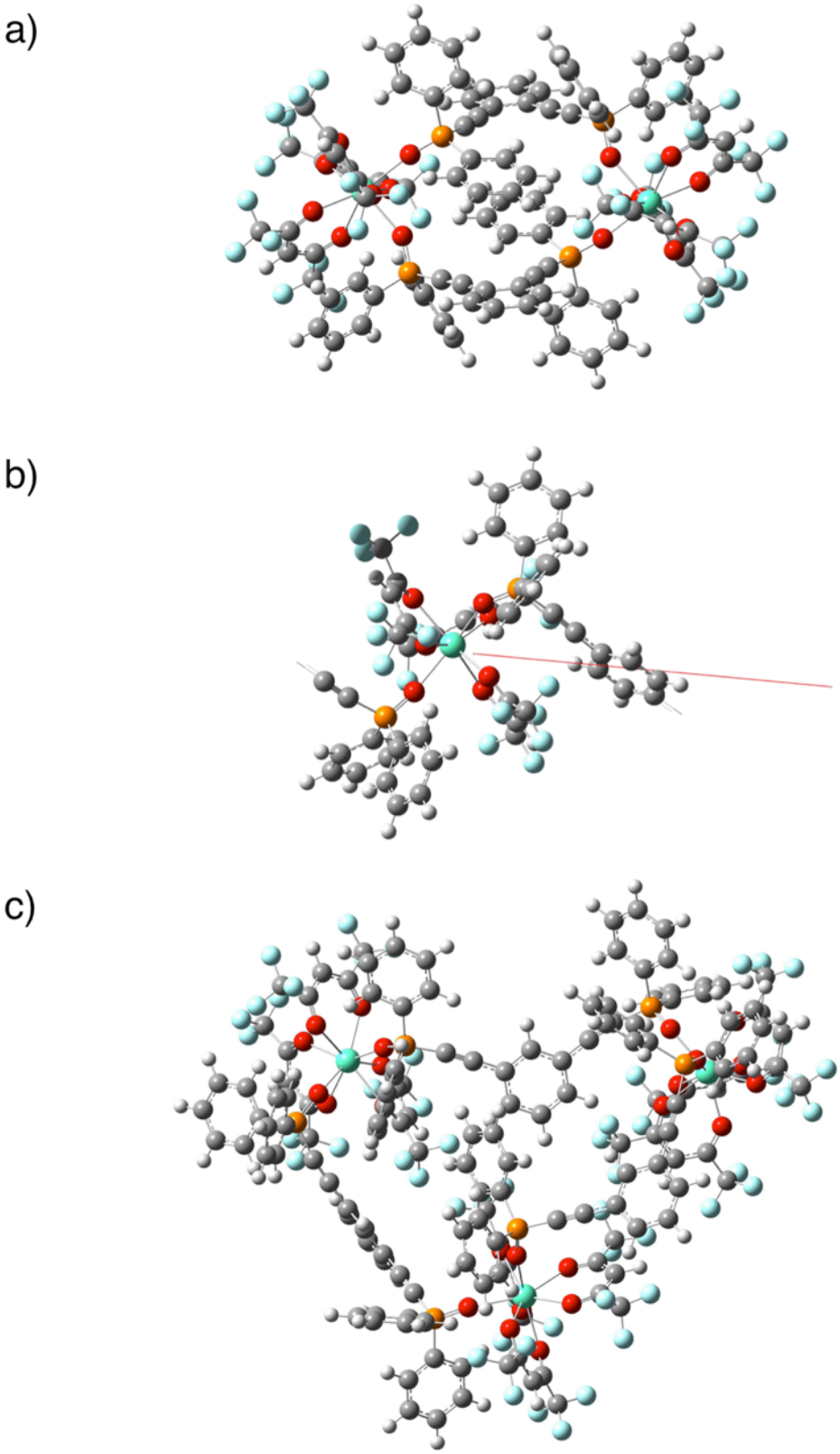

Figure 4-5. DFT optimized structures of a) $[Eu(hfa)_3(o\text{-dpeb})]_2$, b) $[Eu(hfa)_3(p\text{-dpeb})]_n$, and c) $[Eu(hfa)_3(m\text{-dpeb})]_3$.

4.3.2 Thermal properties

DSC measurements were conducted to evaluate the thermophysical properties of the Eu(III) complexes (Figure 4-6). $[Eu(hfa)_3(o\text{-dpeb})]_2$ exhibited a glass transition point (T_g) at 25˚C by cooling the supercooled liquid, which is a characteristic of amorphous molecular materials. Structural relaxation of amorphous molecular materials generally occurs from glass to crystal via a meta-stable supercooled liquid state. In the presence of a polymorph, these compounds finally form a crystal with the highest melting point based on the solid-solid phase transitions or melt-crystallization.[38,39] Here the structural rearrangement of dimer compounds were frozen below T_g to form a glassy state. $[Eu(hfa)_3(p\text{-dpeb})]_n$ also showed T_g at 46˚C, corresponding to the relaxation of segmental movements of polymer chains. The author considered a broad endothermic peak at 96˚C to be responsible for the melting point of various-sized crystals.

The T_g of $[Eu(hfa)_3(m\text{-dpeb})]_3$ was confirmed to be 65˚C. In the case of $[Eu(hfa)_3(m\text{-dpeb})]_3$, crystals are not formed above T_g, since the most thermodynamically stable structure has highly broken symmetry as shown in the DFT optimization and crystallization speed is expected to be quite slow. A sharp endothermic peak was observed at around T_g in first heating process, and a viscous liquid was formed above this temperature. These thermodynamic behaviors are similar to that of complete amorphous polymer.[40] Thus the sharp endothermic peak around T_g in the first run is probably responsible for the enthalpy relaxation of $[Eu(hfa)_3(m\text{-dpeb})]_3$ due to the stable-glass formation.

These results indicate that the bent angles of the dpeb ligands (60, 120, 180˚) have an influence on the molecular morphologies and the glass-transition properties. The author also considers that these glass-transition phenomena

are caused by the presence of ethynyl groups in the bent-angled dpeb ligands, although phenylene-bridged Eu(III) coordination polymers with tight-packing structures have no glass-transition points.[28,29]

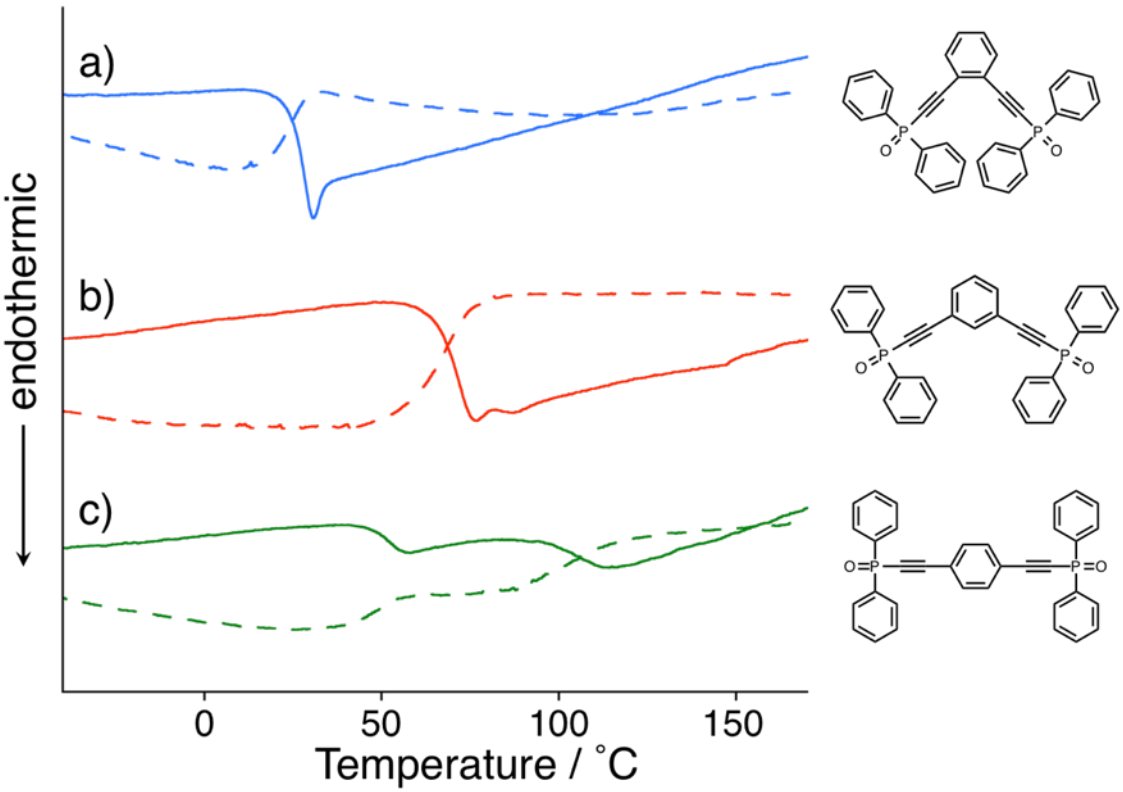

Figure 4-6. DSC thermograms of a) $[Eu(hfa)_3(o\text{-dpeb})]_2$, b) $[Eu(hfa)_3(m\text{-dpeb})]_3$, c) $[Eu(hfa)_3(p\text{-dpeb})]_n$ and chemical structures of bridging ligands (argon atmosphere, heating/cooling rate =5°C min^{-1}, dashed line: cooling process, solid line: heating process).

4.3.3 Surface observations by scanning probe microscope (SPM)

The crystal surfaces of obtained compounds were observed using a scanning probe microscope (see Figure 4-7 and appendices for precise information). A step-like surface was observed for $[Eu(hfa)_3(o\text{-dpeb})]_2$. The heights of the steps were estimated to be 1.56 or 3.13 nm, corresponding to the size of one or two $[Eu(hfa)_3(o\text{-dpeb})]_2$ molecules (1.52 and 3.05 nm, respectively) analyzed from single crystal X-ray data. The $[Eu(hfa)_3(p\text{-dpeb})]_n$ exhibited a fibrous surface structure due to the polymer chains in the crystal packing system. The height profile was also analyzed, and obtained values (0.99 and 1.00 nm) matched the width of a single polymer chain (1.08 nm). Thus, the crystal structures and molecular shapes are highly reflected on the SPM images, and surface moiety is successfully observed by these observations.

Compared to the two compounds above, a flat and smooth surface was observed for $[Eu(hfa)_3(m\text{-dpeb})]_3$. Step- or fiber-like terrace steps were not found, and the height profiles indicated that no regularity is identified due to the amorphous property.

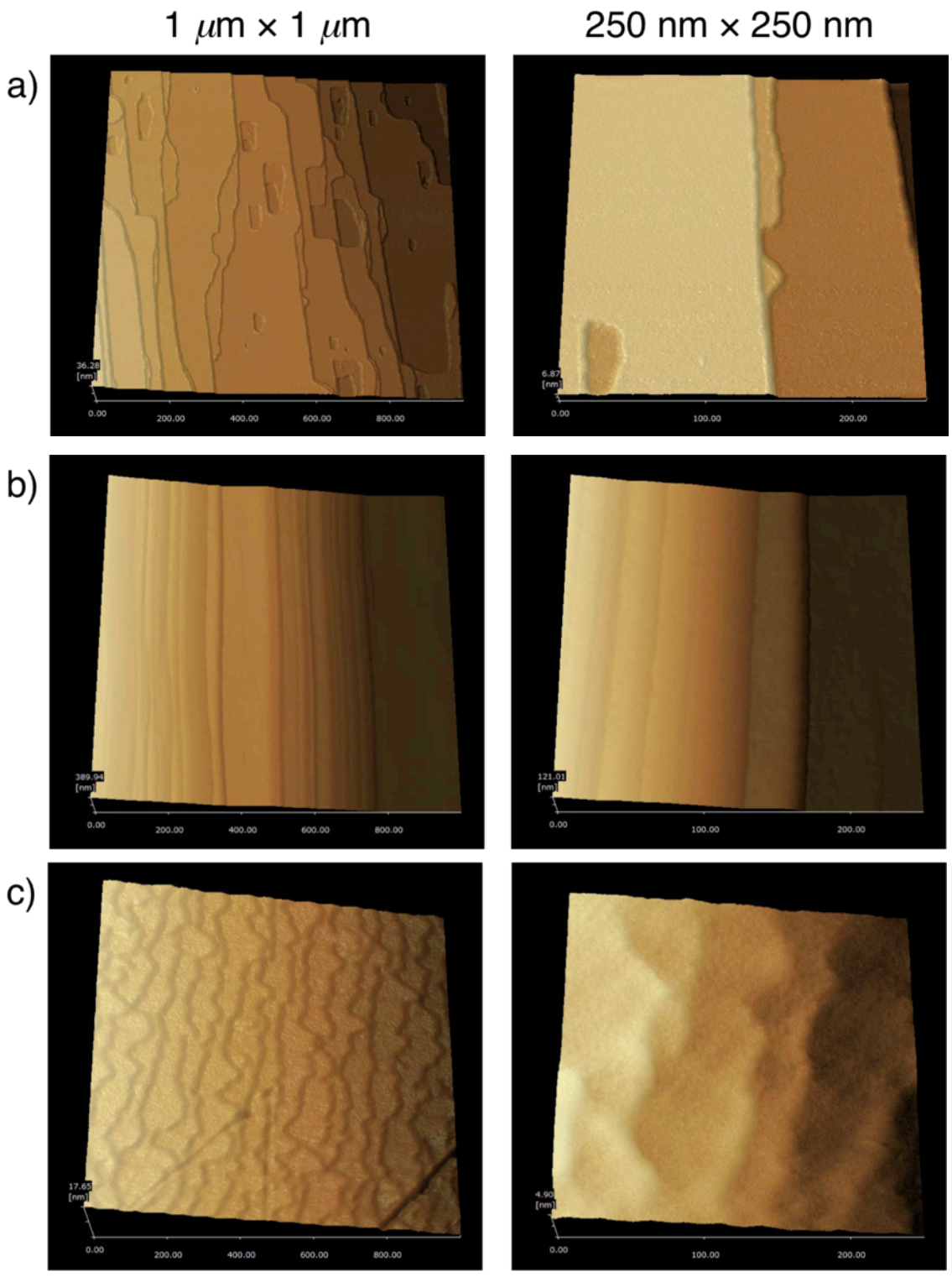

Figure 4-7. SPM images (left 1μm × 1μm, right 250 nm × 250 nm) of a) $[Eu(hfa)_3(o\text{-dpeb})]_2$, b) $[Eu(hfa)_3(m\text{-dpeb})]_3$, and c) $[Eu(hfa)_3(p\text{-dpeb})]_n$.

4.3.4 Photophysical properties

The emission spectra in the solid state are shown in Figure 4-8a. Emission bands observed at 578, 591, 613, 650, and 698 nm are attributed to the 4f-4f transitions of Eu(III) ions ($^5D_0 \rightarrow {}^7F_J$: J = 0, 1, 2, 3, 4). The stark splitting energy of $^5D_0 \rightarrow {}^7F_2$ is generally depended on the coordination geometry.[28,41] The stark splittings were not clearly observed for [Eu(hfa)$_3$(*m*-dpeb)]$_3$, compared to other two compounds (Figure 4-9a, inset). This can be explained by the isotropy and low crystallinity of amorphous compounds. The time-resolved emission profiles for all the three compounds revealed single-exponential decay with millisecond scale lifetimes (Figure 4-9c). The photophysical parameters such as intrinsic emission quantum yields (Φ_{ff}), radiative (k_r) and nonradiative (k_{nr}) rate constants were estimated (Table 4-2) using the equations (3)-(5) in Chapter 2.

The [Eu(hfa)$_3$(*o*-dpeb)]$_2$ showed large intrinsic emission quantum yield (Φ_{ff} = 94%) due to the large k_r and small k_{nr} values. The large k_r constants for [Eu(hfa)$_3$(*o*-dpeb)]$_2$ (9.1 × 10^2 s^{-1}) and [Eu(hfa)$_3$(*p*-dpeb)]$_n$ (9.2 × 10^2 s^{-1}) reflect the enhancement of electric dipole transition probability under the asymmetrical coordination geometries. The significantly small k_{nr} for [Eu(hfa)$_3$(*o*-dpeb)]$_2$ is induced by the multiple intramolecular CH/F and π/π interactions in the dimer structures. The relatively small k_r (7.2 × 10^2 s^{-1}) and large k_{nr} (2.8 × 10^2 s^{-1}) of [Eu(hfa)$_3$(*m*-dpeb)]$_3$ were due to the isotropic and loose-packed character of amorphous solid. By utilizing the advantage of hard-to-crystallize property, the notable amorphous form of luminescent [Eu(hfa)$_3$(*m*-dpeb)]$_3$ without polymer matrices was demonstrated in Figure 4-8b.

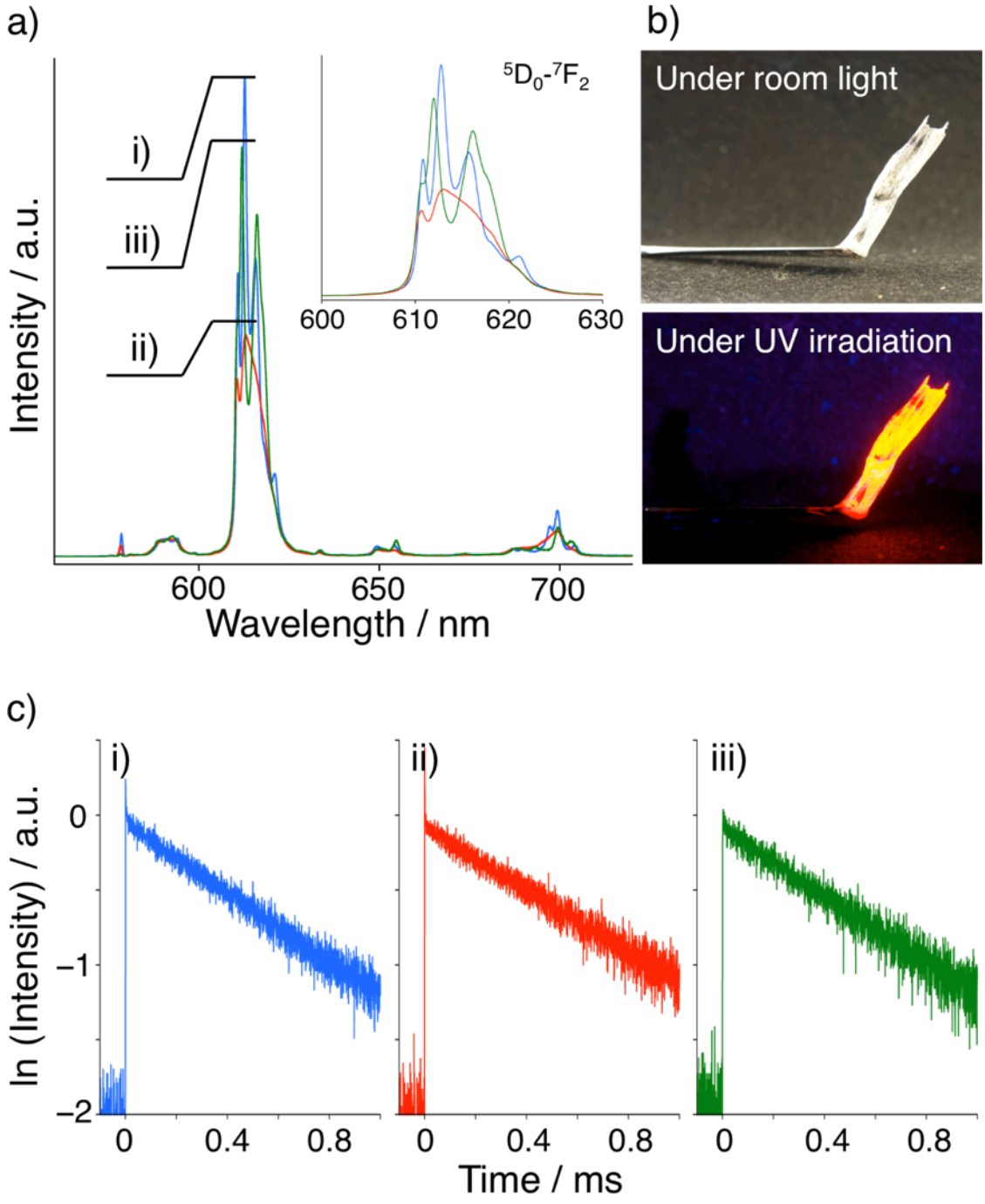

Figure 4-8. a) Emission spectra in solid state (λ_{ex} = 465 nm, inset shows $^5D_0 \rightarrow {}^7F_2$ transition), b) pictures of amorphous solid under room light and under UV-irradiation, and c) emission decay profiles of i) $[Eu(hfa)_3(o\text{-dpeb})]_2$, ii) $[Eu(hfa)_3(m\text{-dpeb})]_3$, and iii) $[Eu(hfa)_3(p\text{-dpeb})]_n$.

Table 4-2. Photophysical parameters of Eu(III) coordination glasses in solid state.

Compounds	Φ_{tot}[a] / %	Φ_{ff}[b] / %	τ_{obs}[c] / ms	k_r[b] / s^{-1}	k_{nr}[b] / s^{-1}
$[Eu(hfa)_3(o\text{-dpeb})]_2$	52	94	1.0	9.1×10^2	6.1×10
$[Eu(hfa)_3(m\text{-dpeb})]_3$	44	72	1.0	7.2×10^2	2.8×10^2
$[Eu(hfa)_3(p\text{-dpeb})]_n$	54	86	0.93	9.2×10^2	1.5×10^2

[a] λ_{ex} = 380 nm. [b] Equation 3-5 in Chapter 2. [c] λ_{ex} = 355 nm.

The transmittance spectrum of the glassy-state $[Eu(hfa)_3(m\text{-dpeb})]_3$ in a laminate film also supports the transparency (≈ 70%) in visible region (Figure 4-9a). The small spike observed at 465 nm is 4f-4f absorption of Eu(III) ions. The bright red luminescence was observed under UV irradiation. When conventional Eu(III) complexes with *β*-diketonates (absorption coefficient > 30, 000 L mol^{-1} cm^{-1}) are embedded in polymer thin films (thickness: 0.1 μm, dopant concentration: 1 wt%), the absorbance of the films are estimated to be approximately 0.003. On the other hand, absorbance of thin films prepared from Eu(III) coordination glasses is estimated to be 0.3. These simple estimations for absorbance indicate that the latter film would be much brighter than those of former films. The transparent films without scattering from crystal grain boundaries on glass substrate (Figure 4-9b, c) also indicate the dramatically improved coating ability of luminescent Eu(III) coordination glass.

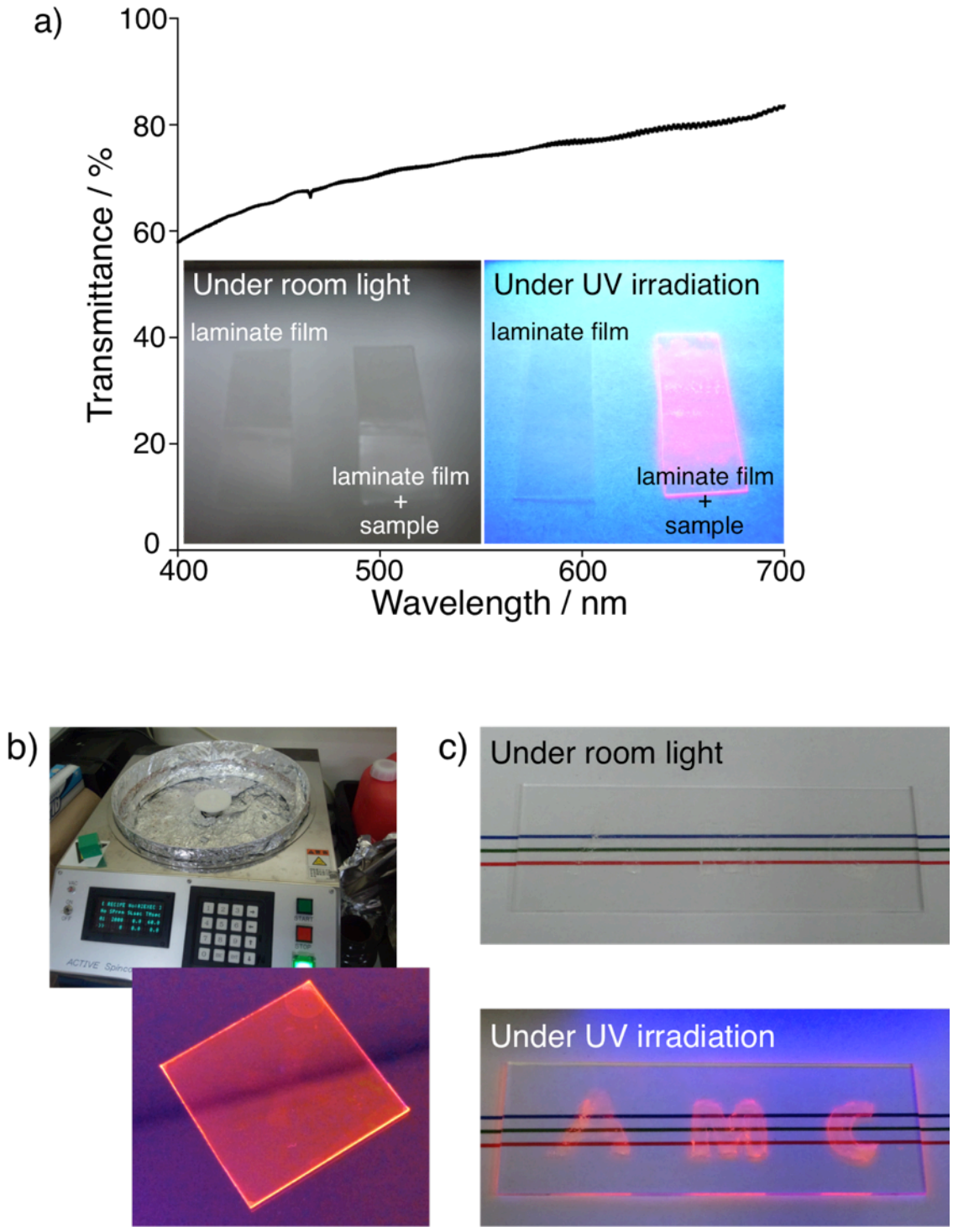

Figure 4-9. a) Transmittance spectrum of glassy-state $[Eu(hfa)_3(m\text{-dpeb})]_3$ in a laminate film (pictures below show the laminate films with and without samples under room light and UV). b) Spin coated film and c) amorphous painting on glass substrate.

4.4 Conclusions

In conclusion, the author successfully controlled the morphological properties of novel luminescent Eu(III) coordination compounds by introducing *ortho*-, *meta*-, and *para*-substituted phenylene bridges with ethynyl groups. The coordination structures were determined to be dimer, trimer, and polymer structures, respectively. All of these compounds exhibited glass transition points, and the trimer compound with 120˚-angled *meta*-substituted bridges in particular, formed stable amorphous state. The glass transition properties were dependent on the regiochemistry of substitution in regard to the internal phenylene core. They exhibited relatively strong emission as well.

These results would provide a guideline on molecular designs to control the entire structures and thermal properties of assembled Ln(III) complexes via small organic bridging ligands. Ln(III) complexes with amorphous-forming and strong-luminescence properties that can be processed at ambient temperatures are also expected as paintable luminescent materials without polymer matrices.

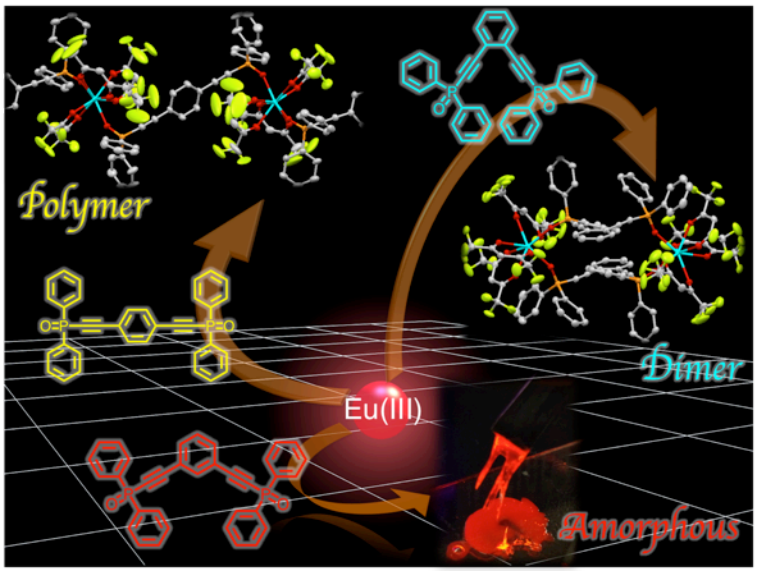

4.5 References

[1] S.J. Wang, W.J. Oldham, R.A. Hudack, G.C. Bazan, *J. Am. Chem. Soc.* **2000**, *122*, 5695-5709.

[2] S.Y. Reece, J.A. Hamel, K. Sung, T.D. Jarvi, A.J. Esswein, J.J.H. Pijpers, D.G. Nocera, *Science* **2011**, *334*, 645-648.

[3] R.D.L. Smith, M.S. Prevot, R.D. Fagan, Z.P. Zhang, P.A. Sedach, M.K.J. Siu, S. Trudel, C.P. Berlinguette, *Science* **2013**, *340*, 60-63.

[4] V.L. Deringer, W. Zhang, M. Lumeij, S. Maintz, M. Wuttig, R. Mazzarello, R. Dronskowski, *Angew. Chem. Int. Ed.* **2014**, *53*, 10817-10820.

[5] Y. Shirota, *J. Mater. Chem.* **2000**, *10*, 1-25.

[6] Y. Shirota, *J. Mater. Chem.* **2005**, *15*, 75-93.

[7] A. Mishra, P. Bäuerle, *Angew. Chem. Int. Ed.* **2012**, *51*, 2020-2067.

[8] J.C.S. Costa, L.J. Santos, *Phys. Chem. C* **2013**, *117*, 10919-10928.

[9] H. Nakano, T. Tanino, T. Takahashi, H. Ando, Y. Shirota, *J. Mater. Chem.* **2008**, *18*, 242-246.

[10] H. Nakano, S. Seki, H. Kageyama, *Phys. Chem. Chem. Phys.* **2010**, *12*, 7772-7774.

[11] Z. Li, Q. Dong, Y. Li, B. Xu, M. Deng, J. Pei, J. Zhang, F. Chen, S. Wen, Y. Gao, W. Tian, *J. Mater. Chem.* **2011**, *21*, 2159-2168.

[12] M. Grucela-Zajac, K. Bijak, S. Kula, M. Filapek, M. Wiacek, H. Janeczek, L. Skorka, J. Gasiorowski, K. Hingerl, N.S. Sariciftci, N. Nosidlak, G. Lewinska, J. Sanetra, E. Schab-Balcerzak, *J. Phys. Chem. C* **2014**, *118*, 13070-13086.

[13] J.-C.G. Bünzli, *Chem. Rev.* **2010**, *110*, 2729-2755.

[14] S.V. Eliseeva, J.-C.G. Bünzli, *Chem. Soc. Rev.* **2010**, *39*, 189-227.

[15] P. Nockemann, E. Beurer, K. Driesen, R. Van Deun, K. Van Hecke, L. Van Meervelt, K. Binnemans, *Chem. Commun.* **2005**, 4354-4356.

[16] S. Petoud, G. Muller, E.G. Moore, J.D. Xu, J. Sokolnicki, J.P. Riehl, U.N. Le, S.M. Cohen, K.N. Raymond, *J. Am. Chem. Soc.* **2007**, *129*, 77-83.

[17] S.J. Butler, D. Parker, *Chem. Soc. Rev.* **2013**, *42*, 1652-1666.

[18] A.P. Bassett, S.W. Magennis, P.B. Glover, D.J. Lewis, N. Spencer, S. Parsons, R.M. Williams, L. De Cola, Z. Pikramenou, *J. Am. Chem. Soc.* **2004**, *126*, 9413-9424.

[19] L. Armelao, S. Quici, F. Barigelletti, G. Accorsi, G. Bottaro, M. Cavazzini, E. Tondello, *Coord. Chem. Rev.* **2010**, *254*, 487-505.

[20] M.R. Robinson, M.B. O'Regan, G.C. Bazan, *Chem. Commun.* **2000**, 1645-1646.

[21] Y. Hasegawa, K. Murakoshi, Y. Wada, S. Yanagida, J.H. Kim, N. Nakashima, T. Yamanaka, *Chem. Phys. Lett.* **1996**, *248*, 8-12.

[22] Y. Hasegawa, K. Sogabe, Y. Wada, T. Kitamura, N. Nakashima, S. Yanagida, *Chem. Lett.* **1999**, *1*, 35-36.

[23] H.F. Brito, O.M.L. Malta, M.C.F.C. Felinto, E.E.S. Teotonio, *The Chemistry of Metal Enolates*, **2009**, chapter 3, 131.

[24] N.B.D. Lima, S.M.C. Gonçalves, S.A. Junior, A.M. Simas, *Sci. Rep.* **2013**, *3*, 1-8.

[25] S.M. Borisov, O.S. Wolfbeis, *Anal. Chem.* **2006**, *78*, 5094-5101.

[26] G.E. Khalil, K. Lau, G.D. Phelan, B. Carlson, M. Gouterman, J.B. Callis, L.R. Dalton, *Rev. Sci. Instrum.* **2004**, *75*, 192-206.

[27] S.V. Eliseeva, D.N. Pleshkov, K.A. Lyssenko, L.S. Lepnev, J.-C.G. Bünzli, N.P. Kuzmina, *Inorg. Chem.* **2010**, *49*, 9300-9311.

[28] K. Nakamura, Y. Hasegawa, H. Kawai, N. Yasuda, Y. Wada, S. Yanagida,

J. Alloys. Compd. **2006**, *408*, 771-775.

[29] K. Miyata, T. Ohba, A. Kobayashi, M. Kato, T. Nakanishi, K. Fushimi, Y. Hasegawa, *ChemPlusChem* **2012**, *77*, 277-280.

[30] K. Miyata, Y. Konno, T. Nakanishi, A. Kobayashi, M. Kato, K. Fushimi, Y. Hasegawa, *Angew. Chem. Int. Ed.* **2013**, *52*, 6413-6416.

[31] I.V. Alabugin, S.V. Kovalenko, *J. Am. Chem. Soc.* **2002**, *124*, 9052-9053.

[32] P. Suresh, S. Srimurugan, B. Babu, H.N. Pati, *Acta Chim. Slov.* **2008**, *55*, 453-457.

[33] J. Tirado-Rives, W.L. Jorgensen, *J. Chem. Theory Comput.* **2008**, *4*, 297-306.

[34] M. Dolg, H. Stoll, A. Savin, H. Preuss, *Theor. Chim. Acta* **1989**, *75*, 173-194.

[35] L. Maron, O. Einstein, *J. Phys. Chem. A* **2000**, *104*, 7140-7143.

[36] M.J. Frisch et al. *Gaussian 09*, Revision D.01, Gaussian, Inc., Wallingford CT, **2009**.

[37] J. Ueda, S. Tanabe, *J. Am. Ceram. Soc.* **2010**, *93*, 3084-3087.

[38] E. Ueta, H. Nakano, Y. Shirota, *Chem. Lett.* **1994**, *23*, 2397-2400

[39] M.D. Ediger, C.A. Angell, S.R. Nagel, *J. Phys. Chem.* **1996**, *100*, 13200-13212.

[40] M. Todoki, *SEN'I GAKKAISHI*, **2009**, *65*, 385-393.

[41] K. Nakamura, Y. Hasegawa, Y. Wada, S. Yanagida, *Chem. Phys. Lett.* **2004**, *398*, 500-504.

Appendices

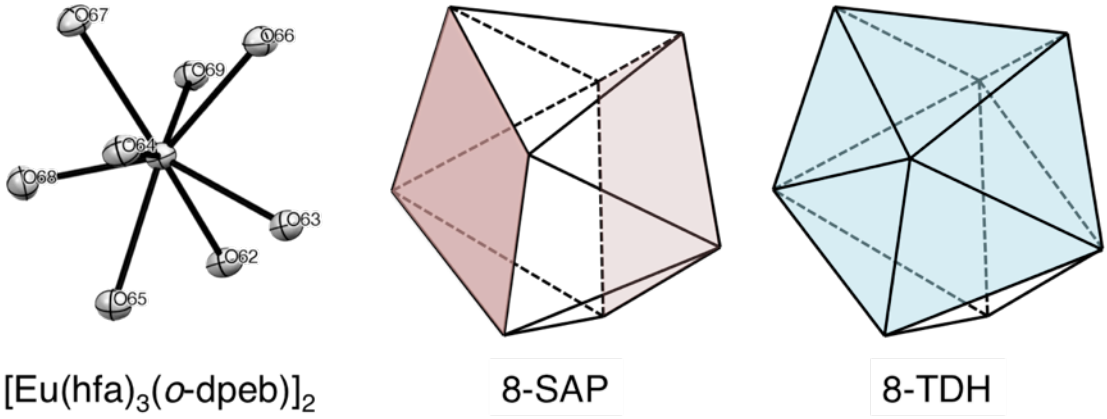

Figure A4-1. Coordination environments around an Eu(III) ion of $[Eu(hfa)_3(o\text{-dpeb})]_2$.

Table A4-1. The observed (δ_i), idealized dihedral angles (θ_{SAP}, θ_{TDH}), and calculated S values ($S_{8\text{-SAP}}$, $S_{8\text{-TDH}}$) for $[Eu(hfa)_3(o\text{-dpeb})]_2$.

		SAP			TDH		
	δ_i	θ_{SAP}	$\delta_i - \theta_{SAP}$	$(\delta_i - \theta_{SAP})^2$	θ_{TDH}	$\delta_i - \theta_{TDH}$	$(\delta_i - \theta_{TDH})^2$
O64-O68	17.52	0	17.52	306.95	29.86	−12.34	152.28
O64-O67	69.82	77.1	−7.28	53.00	61.48	8.34	69.56
O64-O65	69.04	77.1	−8.06	64.96	74.29	−5.25	27.56
O68-O67	71.43	77.1	−5.67	32.15	74.29	−2.86	8.18
O68-O65	71.85	77.1	−5.25	27.56	61.48	10.37	107.54
O63-O69	0.88	0	0.88	0.77	29.86	−28.98	839.84
O63-O62	74.61	77.1	−2.49	6.20	61.48	13.13	172.40
O63-O66	80.38	77.1	3.28	10.76	74.29	6.09	37.09
O69-O66	72.54	77.1	−4.56	20.79	76.62	−4.08	16.65
O69-O62	84.73	77.1	7.63	58.22	74.84	9.89	97.81
O62-O68	43.07	51.6	−8.53	72.76	54.51	−11.44	130.87
O62-O65	58.75	51.6	7.15	51.12	48.09	10.66	113.64
O63-O64	47.73	51.6	−3.87	14.98	47.76	−0.03	0.0009
O63-O65	51.74	51.6	0.14	0.02	54.48	−2.74	7.51
O66-O64	44.26	51.6	−7.34	53.88	52.57	−8.31	69.06
O66-O67	60.19	51.6	8.59	73.79	52.85	7.34	53.88
O69-O68	53.04	51.6	1.44	2.07	47.34	5.70	32.49
O69-O67	54.25	51.6	2.65	7.02	52.63	1.62	2.62
			$S_{8\text{-SAP}}$ = 6.90			$S_{8\text{-TDH}}$ = 10.38	

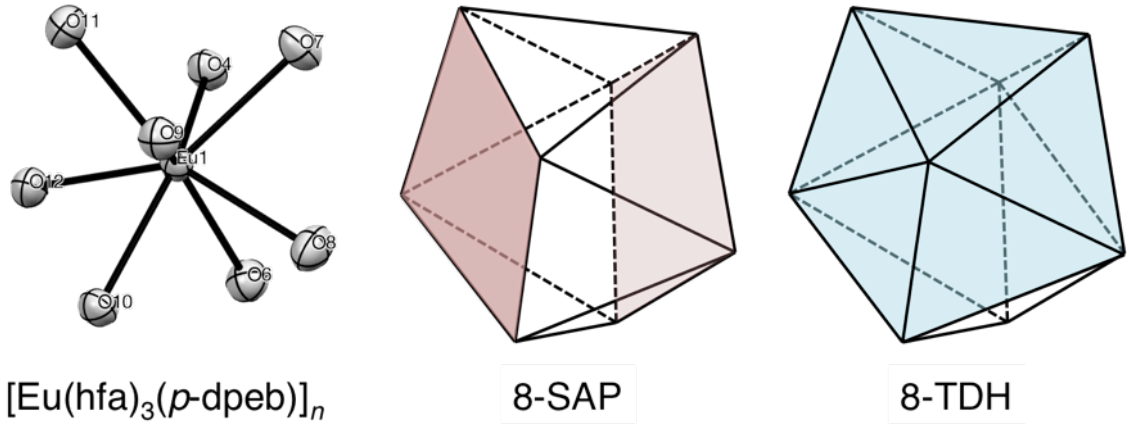

Figure A4-2. Coordination environments around an Eu(III) ion of $[Eu(hfa)_3(p\text{-dpeb})]_n$.

Table A4-2. The observed (δ_i), idealized dihedral angles (θ_{SAP}, θ_{TDH}), and calculated S values ($S_{8\text{-SAP}}$, $S_{8\text{-TDH}}$) for $[Eu(hfa)_3(p\text{-dpeb})]_n$.

		SAP			TDH		
	δ_i	θ_{SAP}	$\delta_i - \theta_{SAP}$	$(\delta_i - \theta_{SAP})^2$	θ_{TDH}	$\delta_i - \theta_{TDH}$	$(\delta_i - \theta_{TDH})^2$
O9-O12	10.03	0	10.03	100.60	29.86	−19.83	393.23
O9-O11	82.39	77.1	5.29	27.98	61.48	20.91	437.23
O9-O10	75.35	77.1	−1.75	3.06	74.29	1.06	1.12
O12-O11	83.53	77.1	6.43	41.34	74.29	9.24	85.38
O12-O10	83.40	77.1	6.3	39.69	61.48	21.92	480.49
O8-O4	10.15	0	10.15	103.02	29.86	−19.71	388.48
O8-O6	84.85	77.1	7.75	60.06	61.48	23.37	546.16
O8-O7	78.25	77.1	1.15	1.32	74.29	3.96	15.68
O4-O7	81.15	77.1	4.05	16.40	76.62	4.53	20.52
O4-O6	78.17	77.1	1.07	1.14	74.84	3.33	11.09
O6-O12	51.51	51.6	−0.09	0.0081	54.51	−3.00	9.00
O6-O10	49.56	51.6	−2.04	4.16	48.09	1.47	2.16
O8-O9	55.22	51.6	3.62	13.10	47.76	7.46	55.65
O8-O10	48.86	51.6	−2.74	7.51	54.48	−5.62	31.58
O7-O9	53.79	51.6	2.19	4.80	52.57	1.22	1.49
O7-O11	45.69	51.6	−5.91	34.93	52.85	−7.16	51.27
O4-O12	55.93	51.6	4.33	18.75	47.34	8.59	73.79
O4-O11	51.08	51.6	−0.52	0.27	52.63	−1.55	2.40
			$S_{8\text{-SAP}}$ = 5.15			$S_{8\text{-TDH}}$ = 12.03	

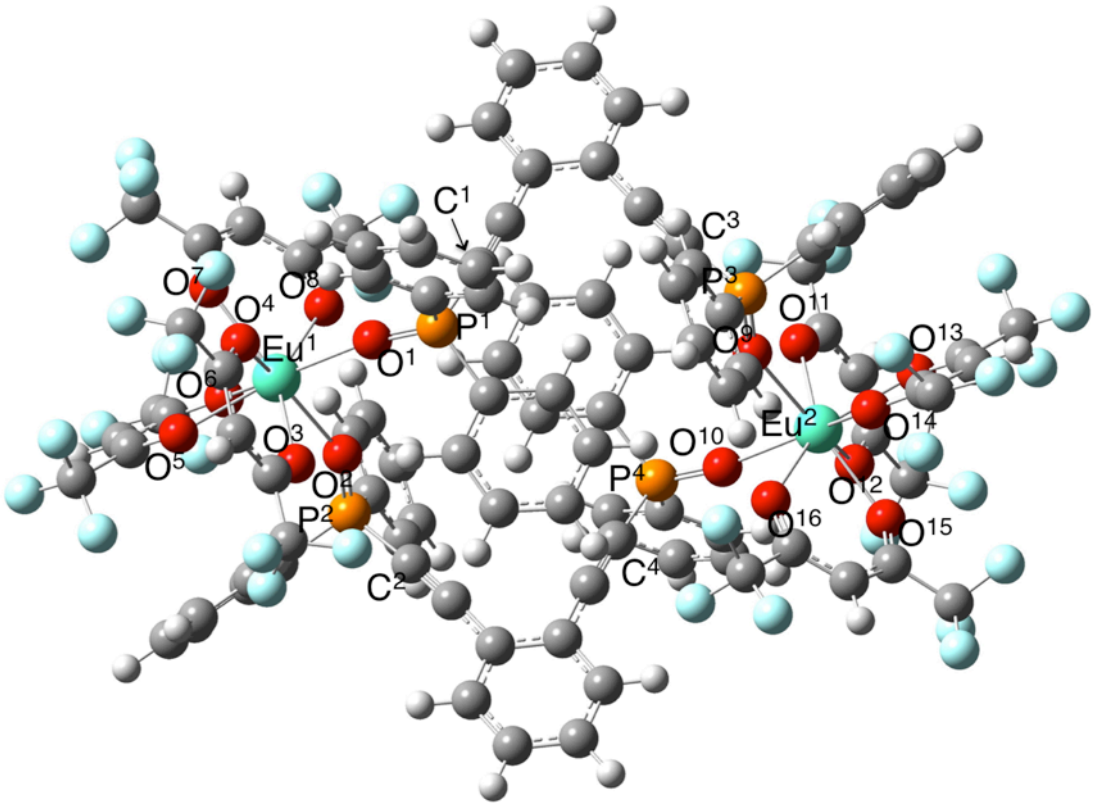

Figure A4-3. DFT optimized structure of $[Eu(hfa)_3(o\text{-dpeb})]_2$.

Table A4-3. Selected bond length of $[Eu(hfa)_3(o\text{-dpeb})]_2$.

Bond	Length / Å	Bond	Length / Å
Eu^1-O^1	2.3717	Eu^2-O^9	2.4001
O^1-P^1	1.5180	O^9-P^3	1.5200
P^1-C^1	1.7616	P^3-C^3	1.7616
Eu^1-O^2	2.4003	Eu^2-O^{10}	2.3718
O^2-P^2	1.5201	O^{10}-P^4	1.5180
P^2-C^2	1.7616	P^4-C^4	1.7616
Eu^1-O^3	2.4681	Eu^2-O^{11}	2.4681
Eu^1-O^4	2.4025	Eu^2-O^{12}	2.4024
Eu^1-O^5	2.3844	Eu^2-O^{13}	2.3843
Eu^1-O^6	2.4367	Eu^2-O^{14}	2.4367
Eu^1-O^7	2.3682	Eu^2-O^{15}	2.3679
Eu^1-O^8	2.4436	Eu^2-O^{16}	2.4444

Table A4-4. The atomic net charge (natural population analysis: NPA) and interatomic bond-order (wiberg bond index: WBI).

Atom	NPA	Atom	NPA	Bond	WBI	Bond	WBI
Eu^1	1.6310	Eu^2	1.6310	Eu^1-O^1	0.3426	Eu^2-O^9	0.3263
O^1	−1.0619	O^9	−1.0550	O^1-P^1	1.0102	O^9-P^3	1.0212
P^1	2.0493	P^3	2.0400	P^1-C^1	0.8648	P^3-C^3	0.8650
C^1	−0.4185	C^3	−0.4292	Eu^1-O^2	0.3264	Eu^2-O^{10}	0.3426
O^2	−1.0550	O^{10}	−1.0619	O^2-P^2	1.0212	O^{10}-P^4	1.0103
P^2	2.0399	P^4	2.0493	P^2-C^2	0.8650	P^4-C^4	0.8648
C^2	−0.4292	C^4	−0.4186	Eu^1-O^3	0.2885	Eu^2-O^{11}	0.2885
O^3	−0.6419	O^{11}	−0.6418	Eu^1-O^4	0.3021	Eu^2-O^{12}	0.3021
O^4	−0.6308	O^{12}	−0.6308	Eu^1-O^5	0.3198	Eu^2-O^{13}	0.3199
O^5	−0.6444	O^{13}	−0.6445	Eu^1-O^6	0.3027	Eu^2-O^{14}	0.3027
O^6	−0.6407	O^{14}	−0.6405	Eu^1-O^7	0.3231	Eu^2-O^{15}	0.3233
O^7	−0.6363	O^{15}	−0.6365	Eu^1-O^8	0.2994	Eu^2-O^{16}	0.2991
O^8	−0.6265	O^{16}	−0.6263				

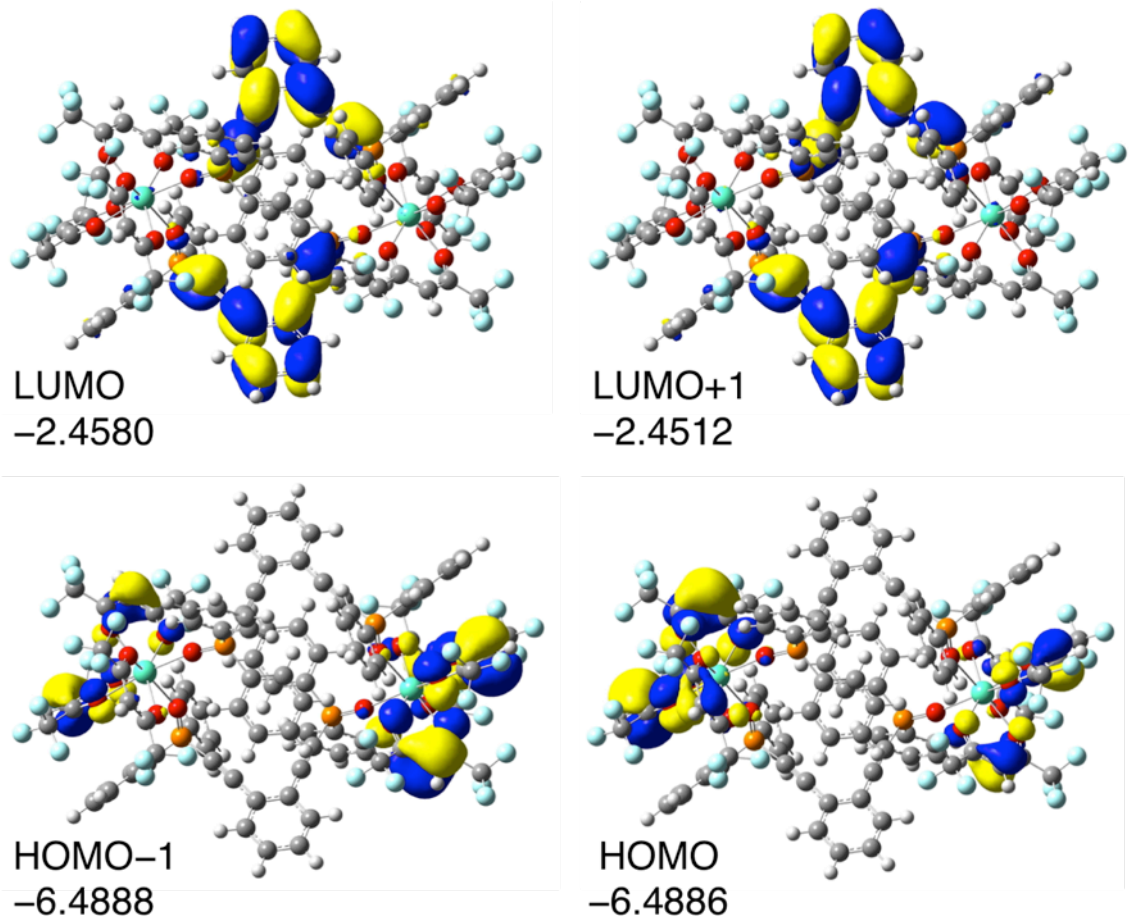

Figure A4-4. HOMO-LUMO frontier orbitals of $[Eu(hfa)_3(o\text{-dpeb})]_2$.

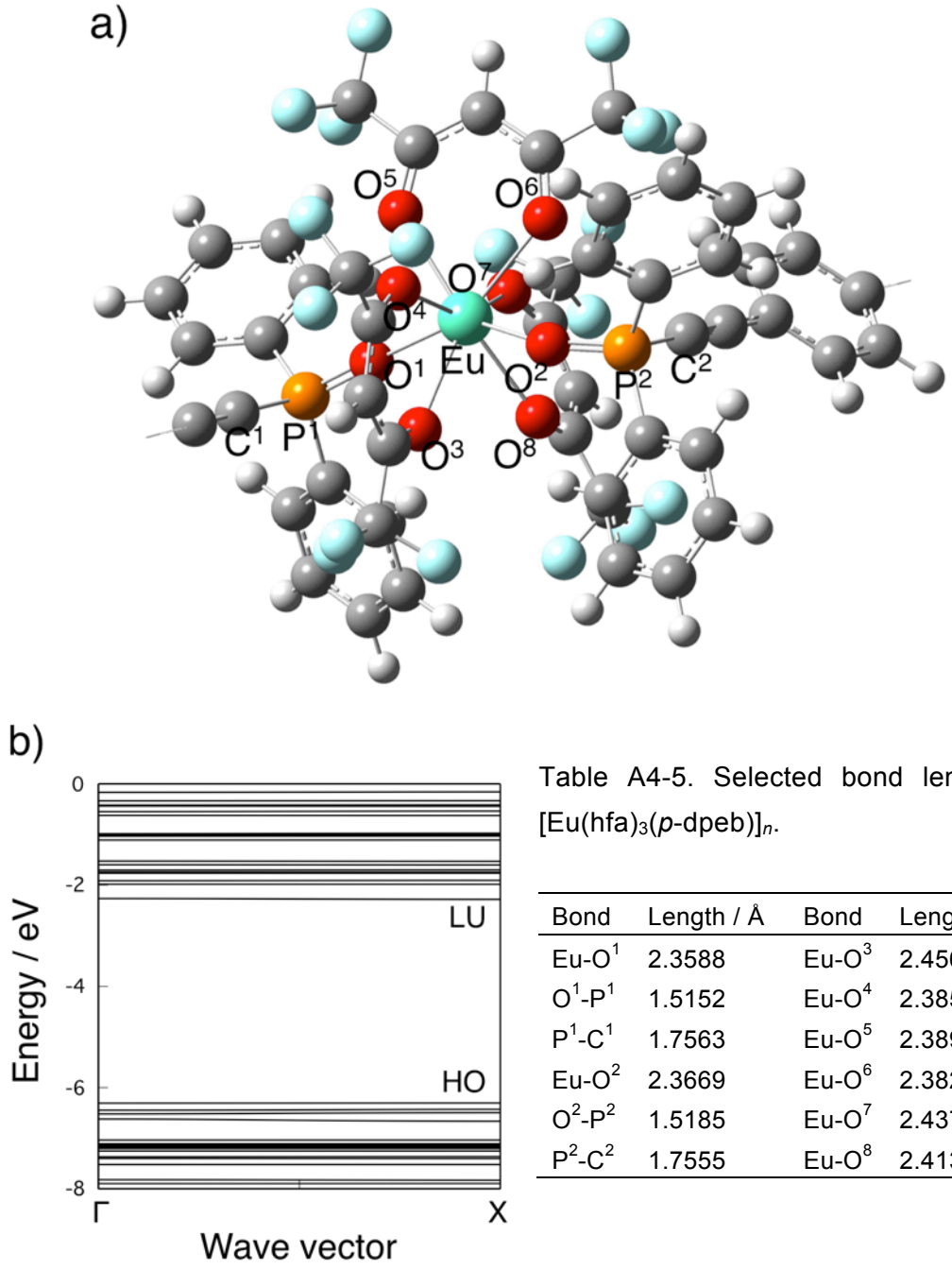

Table A4-5. Selected bond length of $[Eu(hfa)_3(p\text{-dpeb})]_n$.

Bond	Length / Å	Bond	Length / Å
Eu-O^1	2.3588	Eu-O^3	2.4563
O^1-P^1	1.5152	Eu-O^4	2.3856
P^1-C^1	1.7563	Eu-O^5	2.3895
Eu-O^2	2.3669	Eu-O^6	2.3821
O^2-P^2	1.5185	Eu-O^7	2.4378
P^2-C^2	1.7555	Eu-O^8	2.4131

Figure A4-5. a) DFT optimized unit cell and b) band structure of $[Eu(hfa)_3(p\text{-dpeb})]_n$ (band gap at Γ and X are estimated to be 4.0420 and 4.0231 eV, respectively).

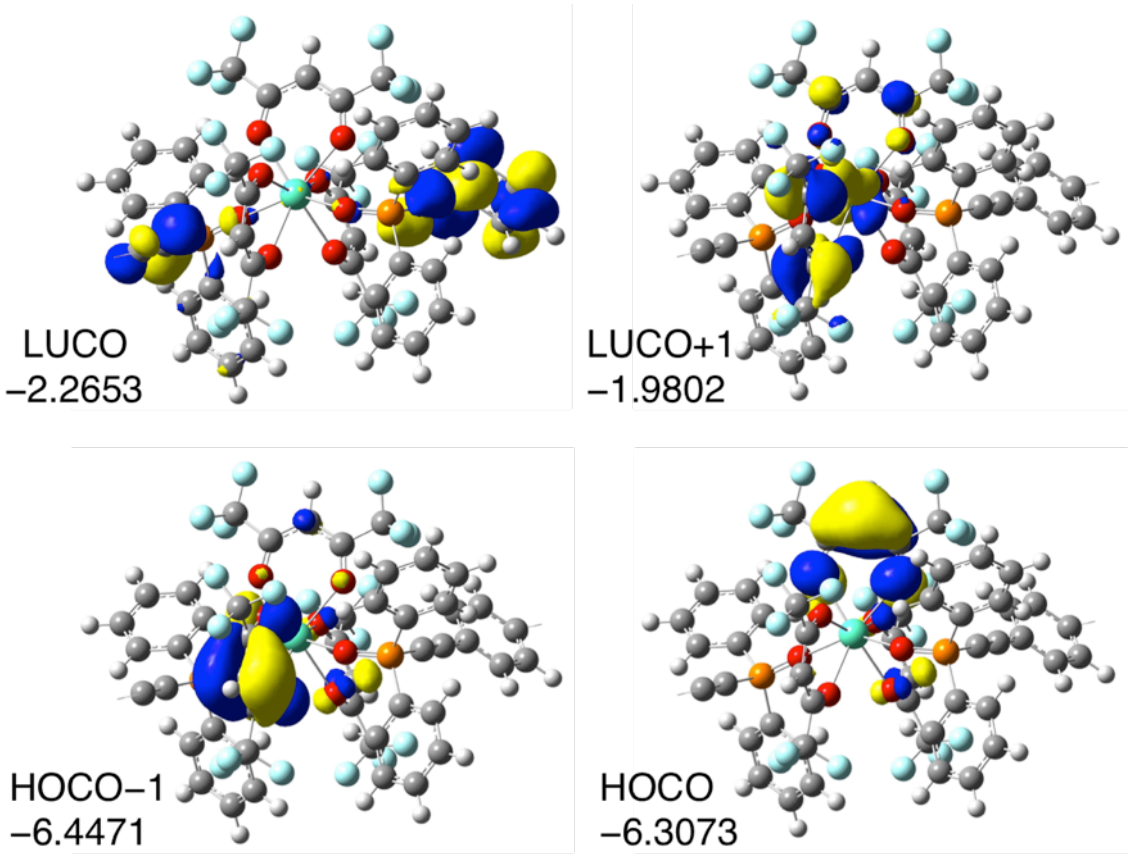

Figure A4-6. HOCO-LUCO structure of $[Eu(hfa)_3(p\text{-dpeb})]_n$ (HOCO: highest occupied crystal orbital, LUCO: lowest unoccupied crystal orbital).

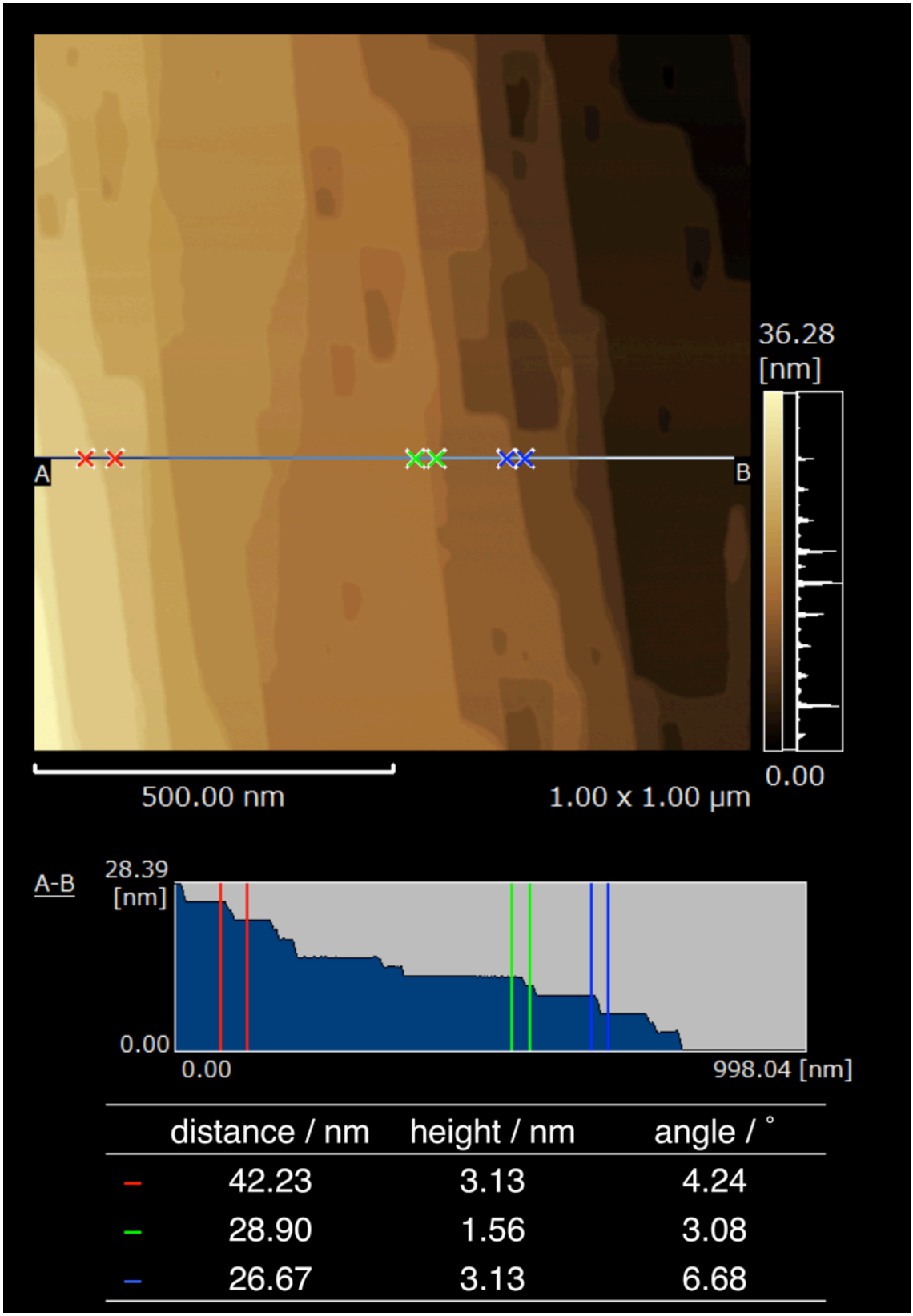

Figure A4-7. SPM image and height analyses of $[Eu(hfa)_3(o\text{-dpeb})]_2$.

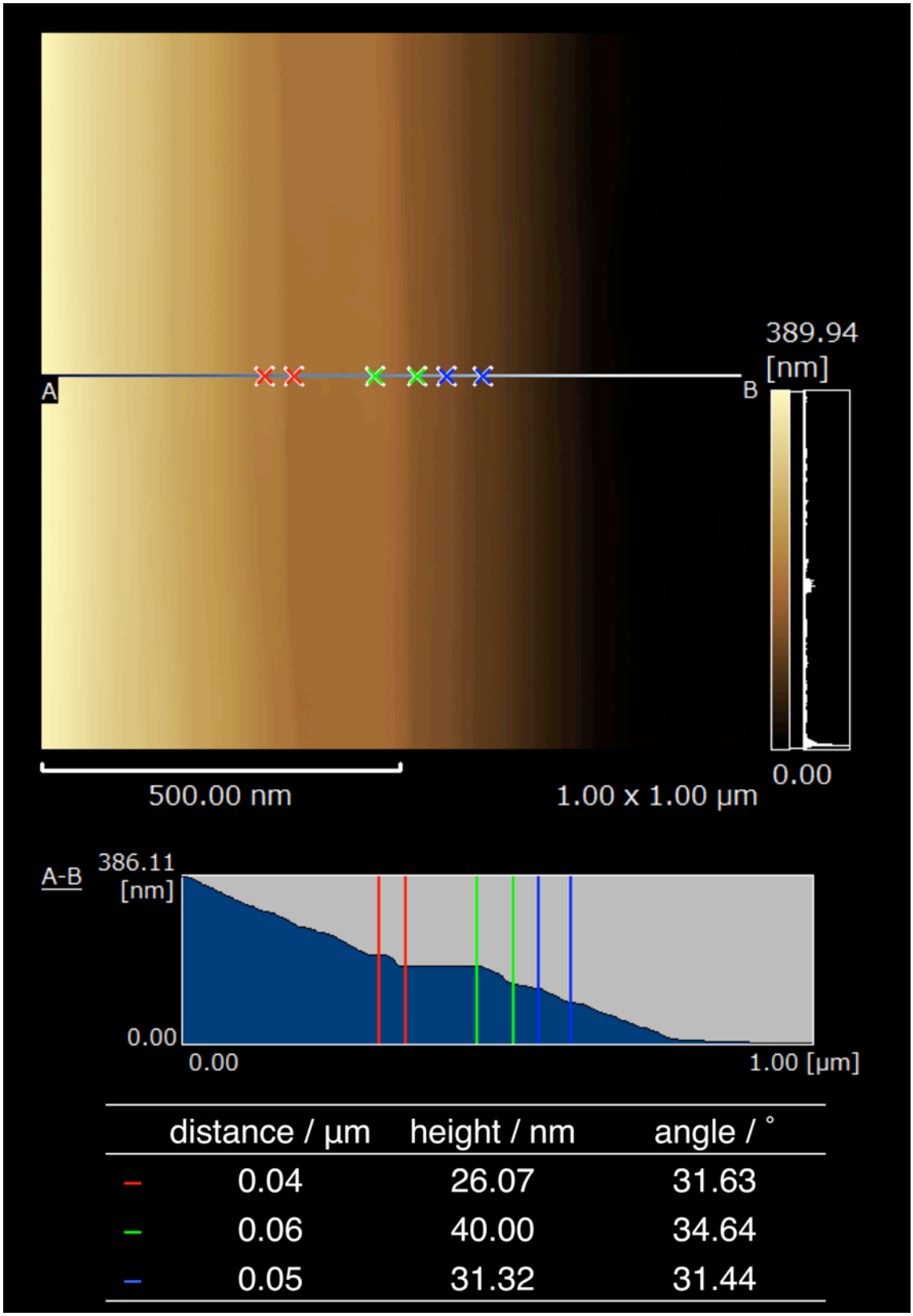

	distance / µm	height / nm	angle / °
–	0.04	26.07	31.63
–	0.06	40.00	34.64
–	0.05	31.32	31.44

Figure A4-8. SPM image and height analyses of $[Eu(hfa)_3(m\text{-dpeb})]_3$.

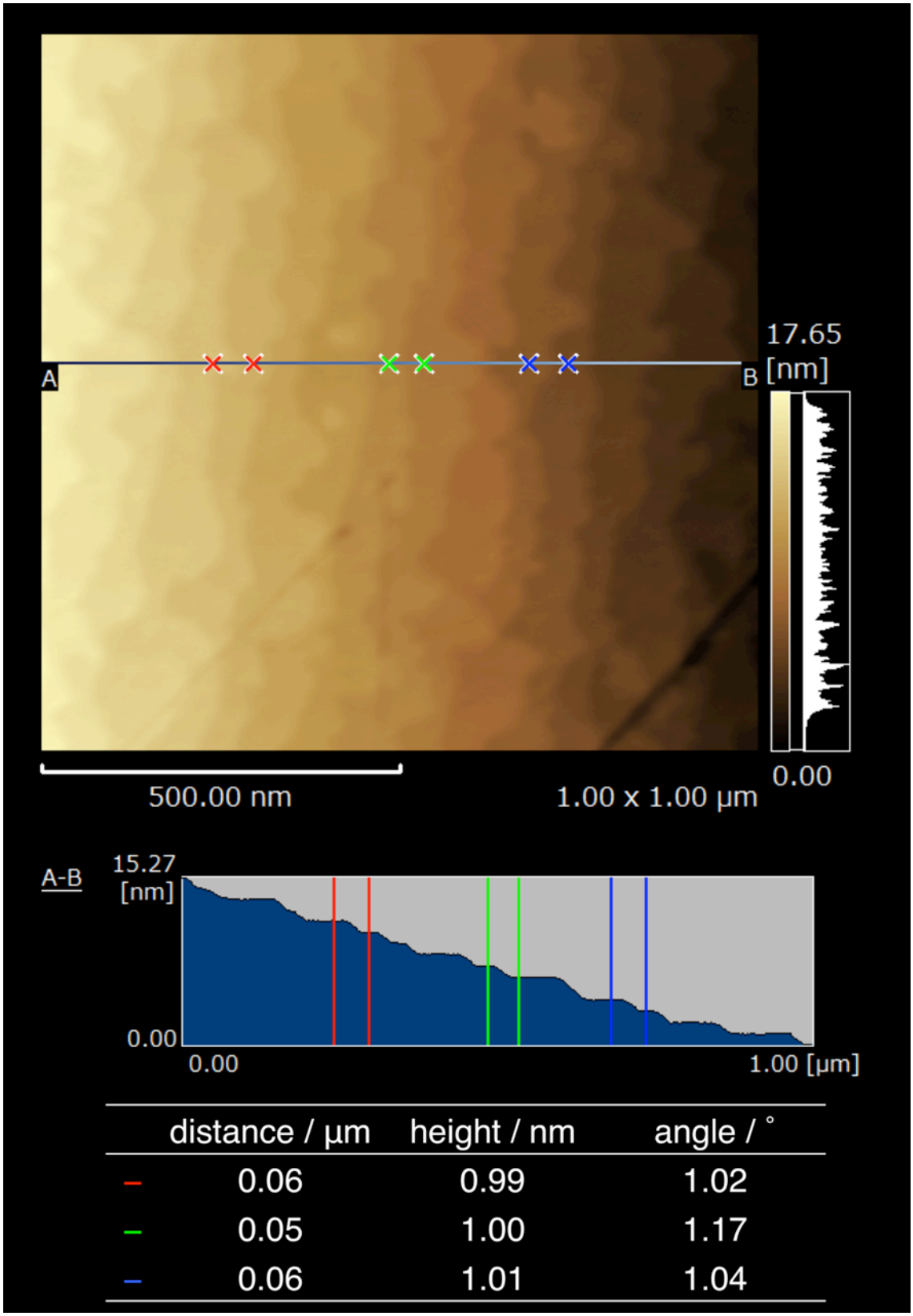

	distance / µm	height / nm	angle / °
–	0.06	0.99	1.02
–	0.05	1.00	1.17
–	0.06	1.01	1.04

Figure A4-9. SPM image and height analyses of $[Eu(hfa)_3(p\text{-dpeb})]_n$.

Chapter 5

Amorphous formability and temperature-sensitive luminescence of lanthanide(III) coordination glasses

Abstract

Glass-transition properties and temperature-sensitive luminescence of lanthanide (Ln(III)) coordination compounds are demonstrated. The amorphous formability was systematically provided by introducing bent-angled phosphine oxide ligands based on thienyl, naphthyl, and phenyl cores with ethynyl groups. Glass transition points were clearly identified for all Ln(III) coordination compounds from 65˚C to 87˚C. The Tb(III)/Eu(III) coordination glass also exhibited temperature-responsive emission from green, yellow, orange, to red in the range of 100 to 400 K.

Based on

Amorphous Formability and Temperature-Sensitive Luminescence of Lanthanide Coordination Glasses Linked by Thienyl, Naphthyl, and Phenyl Bridges with Ethynyl Groups

Y. Hirai, P.P. Ferreira da Rosa, T. Nakanishi, Y. Kitagawa, K. Fushimi, Y. Hasegawa, *Bull. Chem. Soc. Jpn.* **2017**, *90*, 322-326.

5.1 Introduction

Amorphous molecular materials or molecular glasses composed of low molecular-weight organic compounds are promising candidates for optical devices such as displays, lighting devices and LEDs because of their isotropy, transparency, and high processability as mentioned in Chapter 4.[1-3] Nakano and Shirota provided a series of C_3 starburst organic compounds with glass transition and electrical conductivity.[3,4] Bhowmik and co-workers demonstrated fluorescence and amorphous properties of molecular materials based on quinoline amines.[5] Molecular glasses are expected to have applications as electro- and photo-active materials.

Luminescent Ln(III) coordination compounds are attractive candidates for optical applications such as displays and sensors.[6-9] They are usually dispersed in polymer matrices such as polymethyl methacrylate for transparent luminescent materials.[10,11] As described in Chapter 4, the author succeeded in synthesizing luminescent and amorphous Ln(III) coordination compounds with Eu(III) ions, light-harvesting hexafluoroacetylacetonate (hfa) ligands, and 120˚-angled bridging ligands with ethynyl groups (Figure 5-1, *m*-dpeb).[12] Quantum calculations and mass spectrometry revealed the formation of a trimer structure with a *pseudo*-C_3 axis (Figure 5-1, $[Eu(hfa)_3(m\text{-dpeb})]_3$). The amorphous formability should be caused by the multiple quasi-stable states, leading to thermodynamically non-equilibrium states, which result in suppression of crystal packing to form an amorphous solid.

In this chapter, the author focuses on systematic construction of Ln(III) coordination compounds with amorphous-forming ability by simply altering the aryl cores of organic bridging ligands to broaden the range of molecular designs.

Ln(III)-mixed coordination glasses would also provide transparent and temperature-dependent luminescent materials. Hasegawa and co-workers reported that Tb(III)/Eu(III) mixed rigid coordination polymers, “chameleon luminophores,” show brilliant green, yellow, orange, and red photoluminescence depending on the temperature.[13] The emission colors and temperature-responsive regions were also tuned by Tb(III)/Eu(III) mixture ratios in Chapter 3.[14] These compounds are expected to be temperature/pressure sensitive paints (TSPs/PSPs) in the field of fluid dynamics and aeronautical engineering to visualize fluid phenomena such as aerodynamic heating.[15-18] The Ln(III)-mixed coordination glasses would provide a dramatically improved coating properties on the surface of materials for high-concentration TSPs/PSPs without polymer matrices.

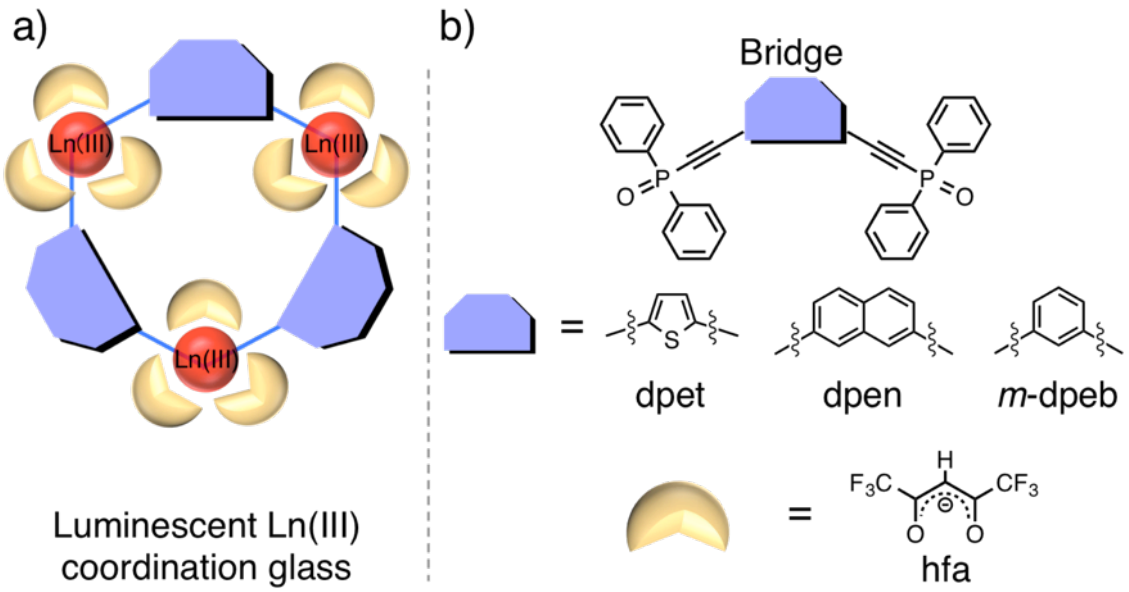

Figure 5-1. a) The molecular design of Ln(III) coordination glasses and b) chemical structures of organic ligands.

In this chapter, the construction of Ln(III) coordination glasses and control of the physical properties are described. Three bidentate phosphine oxide ligands based on thienyl, naphthyl, and phenyl cores with ethynyl groups (2,5-bis(diphenylphosphorylethynyl)thiophene: dpet, 2,7-bis(diphenylphosphorylethynyl)naphthalene: dpen, and 1,3-bis(diphenylphosphorylethynyl)benzene: *m*-dpeb, Figure 5-1b) were prepared. The corresponding Eu(III) coordination glasses were successfully synthesized, and their thermal properties were characterized by DSC and TG-DTA measurements. The emission properties were evaluated on the basis of photophysical parameters such as emission quantum yields and lifetimes. The temperature-sensitive luminescence of a Tb(III)/Eu(III) mixed coordination glass is also demonstrated.

5.2 Experimental Section

5.2.1 Materials

Europium acetate *n*-hydrate (99.9%), terbium(III) acetate tetrahydrate (99.9 %), *n*-BuLi (in *n*-hexane, 1.6 M), and hydrogen peroxide were purchased from Kanto Chemical Co., Inc. 2,5-Dibromothiophene, 3,4-ethylenedioxythiophene, and chlorodiphenylphosphine were obtained from Tokyo Chemical Industry Co., Ltd. All other chemicals and solvents were reagent grade and were used without further purification.

5.2.2 Apparatus

All chemicals are reagent grade and used without further purification. ^{1}H NMR (400 MHz) spectra were recorded on a JEOL ECS400. Chemical shifts were reported in δ ppm, referenced to an internal tetramethylsilane standard for ^{1}H NMR spectroscopy. Infrared spectra were recorded on a JASCO FTIR-420 spectrometer using KBr pellets. Elemental analyses were performed by an Exeter Analytical CE440. Mass spectrometry was performed by a Thermo Scientific Exactive (ESI-MS) and a JEOL JMS-700TZ (FAB-MS). Differential thermal analysis was performed on a Shimadzu DSC-60 Plus under a nitrogen atmosphere at a heating/cooling rate of 5˚C min^{-1}. Thermogravimetric analyses were conducted on a Shimadzu DTG-60 under a nitrogen atmosphere at a heating/cooling rate of 5˚C min^{-1}.

5.2.3 Syntheses

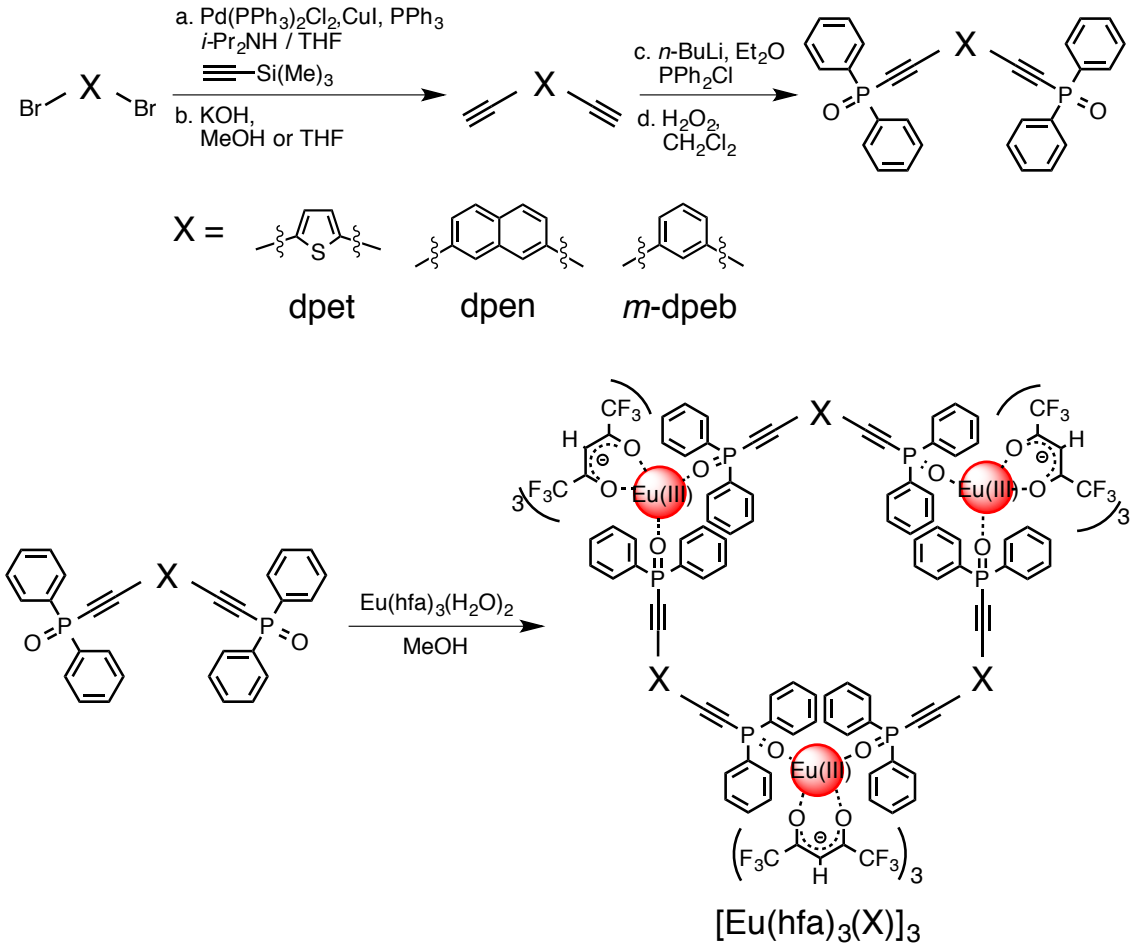

Scheme 5-1. Synthetic schemes of phosphine oxide ligands with ethynyl groups and Eu(III) coordination glasses.

Preparation of 2,5-bis(trimethylsilylethynyl)thiophene:

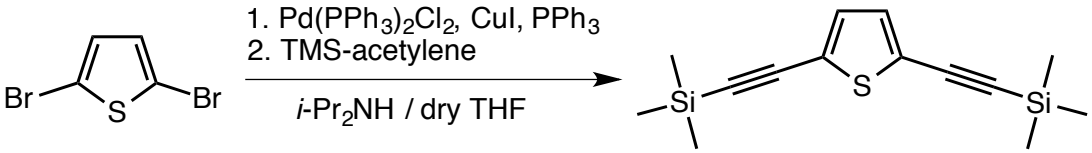

Trimethylsilylacetylene (9.5 mL, 69 mmol) was added in one portion to a solution of 2,5-dibromothiophene (3.0 mL, 27 mmol), $PdCl_2(PPh_3)_2$ (0.98 g), CuI (0.34 g), PPh_3 (0.94 g) in diisopropylamine/dry THF (80 mL / 80 mL) under argon atmosphere and stirred at room temperature for 20 min. The mixture was

stirred at 50˚C for 9 h, and then allowed to cool to room temperature. The ammonium salt was removed by filtration and the mixture was extracted with hexane and concentrated. The obtained crude oil was purified by column chromatography on SiO_2 using hexane as an eluent to afford 2,5-bis(trimethylsilylethynyl)thiophene (Yield: 6.5 g, 89%).

Preparation of 2,5- diethynylthiophene:

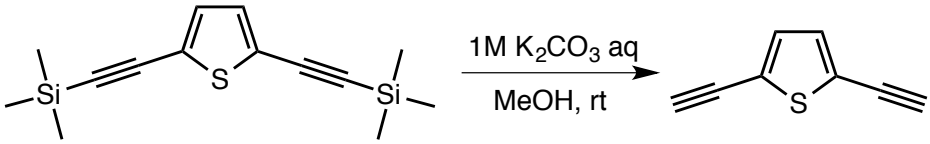

The resulting 2,5-bis(trimethylsilylethynyl)thiophene (6.5 g, 24 mmol) was dissolved in methanol (100 mL) and 1 M KOH aqueous solution (60 mL, 60 mmol) was added. The mixture was stirred for 3 h. The product was extracted with hexane, concentrated, and purified by column chromatography on SiO_2 using hexane as an eluent to afford 2,5-diethynylthiopehene (Yield: 2.1 g, 67%).

Preparation of 2,5-bis(diphenylphosphorylethynyl)thiophene (dpet):

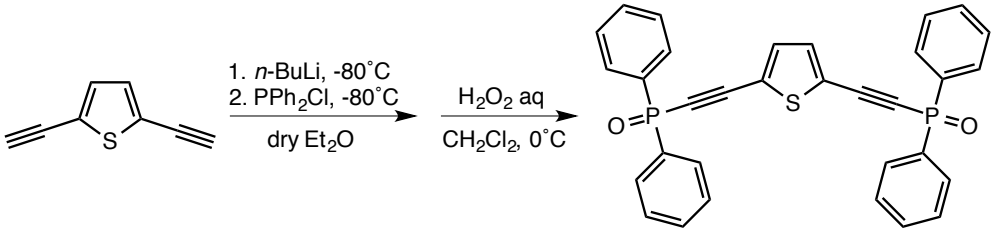

The 2,5-diethynylthiophene (2.1 g, 16 mmol) was dissolved in dry Et_2O (80 mL) under argon atmosphere. A solution of 1.6 M *n*-BuLi (23 mL, 35 mmol) was added dropwise to the solution at −80˚C. The mixture was allowed to stir for 3 h at −10˚C, after which a PPh_2Cl (6.2 mL, 34 mmol) was added dropwise at −80˚C. The mixture was gradually brought to room temperature, and stirred

overnight. The product was extracted with dichloromethane, concentrated, and re-dissolved in dichloromethane (60 mL), followed by addition of a 30% H_2O_2 aqueous solution (11 mL). The reaction mixture was stirred for 3 h at 0˚C. The product was extracted with dichloromethane and purified by column chromatography on SiO_2 using ethyl acetate and hexane as mixed eluent (ethyl acetate : hexane = 2 : 1). The residue was concentrated and recrystallized in ethyl acetate. The obtained powder was washed with ethyl acetate.

Yield: 3.6 g (26%). ^{1}H NMR (400 MHz, $CDCl_3$, 25 ˚C) δ 7.83-7.89 (m, 8H, -CH), δ 7.49-7.62 (m, 12H, -CH), δ 7.35 (s, 2H, -CH) ppm. ESI-Mass (*m*/*z*): calcd for $C_{32}H_{23}O_2P_2S$ $[M+H]^+$, 533.09; found, 533.09. Anal. Calcd for $C_{32}H_{22}O_2P_2S$: C, 72.17; H, 4.16%. Found: C, 72.31; H, 4.37%.

Preparation of 2,7-bis(trimethylsilylethynyl)naphthalene:

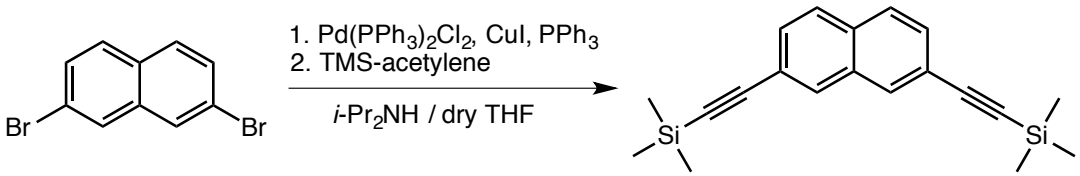

Trimethylsilylacetylene (5.5 mL, 40 mmol) was added in one portion to a solution of 2,7-dibromonaphthalene (5.3 g, 19 mmol), $PdCl_2(PPh_3)_2$ (0.55 g), CuI (0.19 g), PPh_3 (0.53 g) in diisopropylamine / dry THF (40 mL / 100 mL) under argon atmosphere and stirred at room temperature for 20 min. The mixture was stirred at 50˚C overnight, and then allowed to cool to room temperature. The ammonium salt was removed by filtration and the mixture was extracted with ethyl acetate and concentrated. The obtained crude oil was purified by column chromatography on SiO_2 using hexane and ethyl acetate as mixed eluent (hexane : ethyl acetate = 5 : 1) to afford 2,7-bis(trimethylsilylethynyl)naphthalene (Yield: 5.1 g, 84%).

Preparation of 2,7-diethynylnaphthalene:

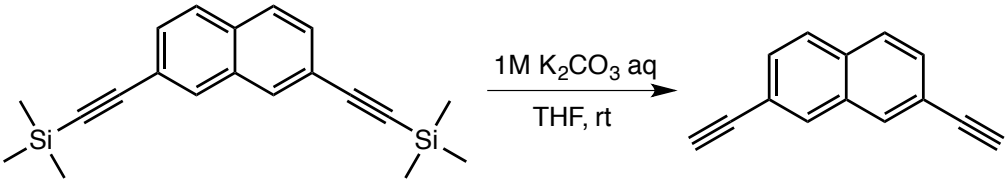

2,7-Bis(trimethylsilylethynyl)naphthalene (5.1 g, 16 mmol) was dissolved in THF (100 mL) and 1 M KOH aqueous solution (45 mL, 45 mmol) was added. The mixture was stirred overnight. The product was extracted with hexane and concentrated to afford 2,7-diethynylnaphthalene (Yield: 2.5 g, 88%).

Preparation of 2,7-bis(diphenylphosphorylethynyl)naphthalene:

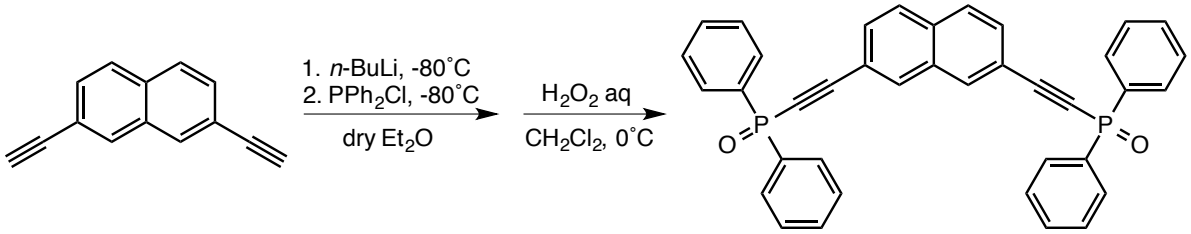

The 2,7-diethynylnaphthalene (2.5 g, 14 mmol) was dissolved in dry Et_2O (80 mL) under argon atmosphere. A solution of 1.6 M *n*-BuLi (20 mL, 31 mmol) was added dropwise at −80˚C. The mixture was allowed to stir for 3 h at −10˚C, after which a PPh_2Cl (5.6 mL, 31 mmol) was added dropwise at −80˚C. The mixture was gradually brought to room temperature and stirred overnight. The product was extracted with dichloromethane, concentrated, and re-dissolved in dichloromethane (60 mL), followed by addition of a 30% H_2O_2 aqueous solution (10 mL). The reaction mixture was stirred for 3 h at 0˚C. The product was extracted with dichloromethane and recrystallized. The obtained crude powder was washed with ethyl acetate.

Yield: 3.6 g (34 %). ^{1}H NMR (400 MHz, $CDCl_3$, 25 ˚C) *δ* 8.12 (s, 2H, -CH), *δ* 7.89-7.95 (m, 8H, -CH), *δ* 7.82-7.84 (d, 2H, -CH), *δ* 7.64-7.66 (dd, 2H, -CH), *δ*

7.48-7.59 (m, 12H, -CH) ppm. ESI-Mass (*m*/*z*): calcd for $C_{38}H_{27}O_2P_2$ $[M+H]^+$, 577.15; found, 577.15. Anal. Calcd for $C_{38}H_{26}O_2P_2$: C, 79.16; H, 4.55%. Found: C, 79.05; H, 4.70%.

Preparation of 1,3-bis(diphenylphosphorylethynyl)benzene (*m*-dpeb):[12]

The *m*-dpeb ligand was synthesized as described in Chapter 4.

Preparation of Eu(III) coordination glasses $[Eu(hfa)_3(X)]_3$ (X = dpet, dpen, *m*-dpeb):

The phosphine oxide ligand (0.8 mmoL) and $Eu(hfa)_3(H_2O)_2$ (0.8 mmoL) was dissolved in methanol (40 mL), respectively. The solutions were mixed and stirred for 3 h at 50˚C. The reaction mixture was concentrated, re-dissolved in methanol (5 mL), and then hexane (15 mL) was added. The organic solvents were removed by decompression to form amorphous solids.

$[Eu(hfa)_3(dpet)]_3$: Yield 0.62 g (20%). IR (KBr) 1656 (st, C=O), 1144 (st, P=O), 1100-1253 (st, C-O-C and st, C-F) cm^{-1}. FAB-Mass (*m*/*z*): $[M\text{-hfa}]^+$ calcd for $C_{136}H_{74}Eu_3F_{48}O_{22}P_6S_3$, 3710.9; found, 3709.9. Anal. Calcd for $C_{141}H_{75}Eu_3F_{54}O_{24}P_6S_3$: C, 43.24; H, 1.93 %. Found: C, 44.02; H, 2.24%.

$[Eu(hfa)_3(dpen)]_3$: Yield 0.52 g (16%). IR (KBr) 1656 (st, C=O), 1144 (st, P=O), 1100-1256 (st, C-O-C and st, C-F) cm^{-1}. FAB-Mass (*m*/*z*): $[M\text{-hfa}]^+$ calcd for $C_{154}H_{86}Eu_3F_{48}O_{22}P_6$, 3843.1; found, 3842.0. Anal. Calcd for $C_{159}H_{87}Eu_3F_{54}O_{24}P_6$: C, 47.17; H, 2.17%. Found: C, 46.85; H, 2.39%.

5.2.5 Optical measurements

UV-Vis absorption spectra were recorded on a JASCO V-670 spectrometer. Emission and excitation spectra were recorded on a HORIBA Fluorolog-3 spectrofluorometer and corrected for the response of the detector system. The temperature-dependent emission spectra were measured with a nitrogen bath cryostat (Oxford Instruments, Optistat DN) and a temperature controller (Oxford, Instruments, ITC 502S). Emission lifetimes (τ_{obs}) were measured using the third harmonics (355 nm) of a Q-switched Nd:YAG laser (Spectra Physiscs, INDI-50, fwhm = 5 ns, λ = 1064 nm) and a photomultiplier (Hamamatsu photonics, R5108, response time ≤ 1.1 ns). The Nd:YAG laser response was monitored with a digital oscilloscope (Sony Tektronix, TDS3052, 500 MHz) synchronized to the single-pulse excitation. Emission lifetimes were determined from the slope of logarithmic plots of the decay profiles. The emission quantum yields excited at 380 nm (Φ_{tot}) were estimated using JASCO F-6300-H spectrometer attached with a JASCO ILF-533 integrating sphere unit (φ = 100 mm). The wavelength dependence of the detector response and the beam intensity of Xe light source for each spectrum were calibrated using a standard light source.

5.3 Results and Discussion

5.3.1 Structural characterizations

Fragments of trimer structures $[Eu_3(hfa)_8(X)_3]^+$ (X = dpet, dpen, *m*-dpeb) in the mass spectra were confirmed for all compounds. The peaks for larger *m*/*z* values also indicate the presence of a wide range of other cyclic or linear oligomers. Considering the results of mass spectrometry and the DFT optimized structure as reported for $[Eu(hfa)_3(m\text{-dpeb})]_3$,[12] the author assumes that all of these compounds form trimer structures with a *pseudo*-C_3 axis in an amorphous solid state. The glassy states of these compounds were also demonstrated by halo signals of XRD patterns (Figure A5-1).

5.3.2 Thermal properties

DSC measurements were performed to determine the glass transition temperatures. All of the compounds clearly showed glass-transition temperatures, which were characteristic of amorphous molecular materials. These compounds formed transparent viscous fluids above T_g, and the intermolecular rearrangements of broken C_3-symmetrical units were probably frozen below T_g in a cooling process. The author considers the highest T_g of $[Eu(hfa)_3(dpen)]_3$ (T_g = 87°C) to be responsible for the largest molecular weight, planarity, and availability of aromatic surfaces for intermolecular interactions of the bridging ligand, dpen. The ethynyl groups in bridging ligands also play an important role in amorphous formation by suppressing tight-binding interaction and crystallization of assembled Eu(III) coordination compounds.

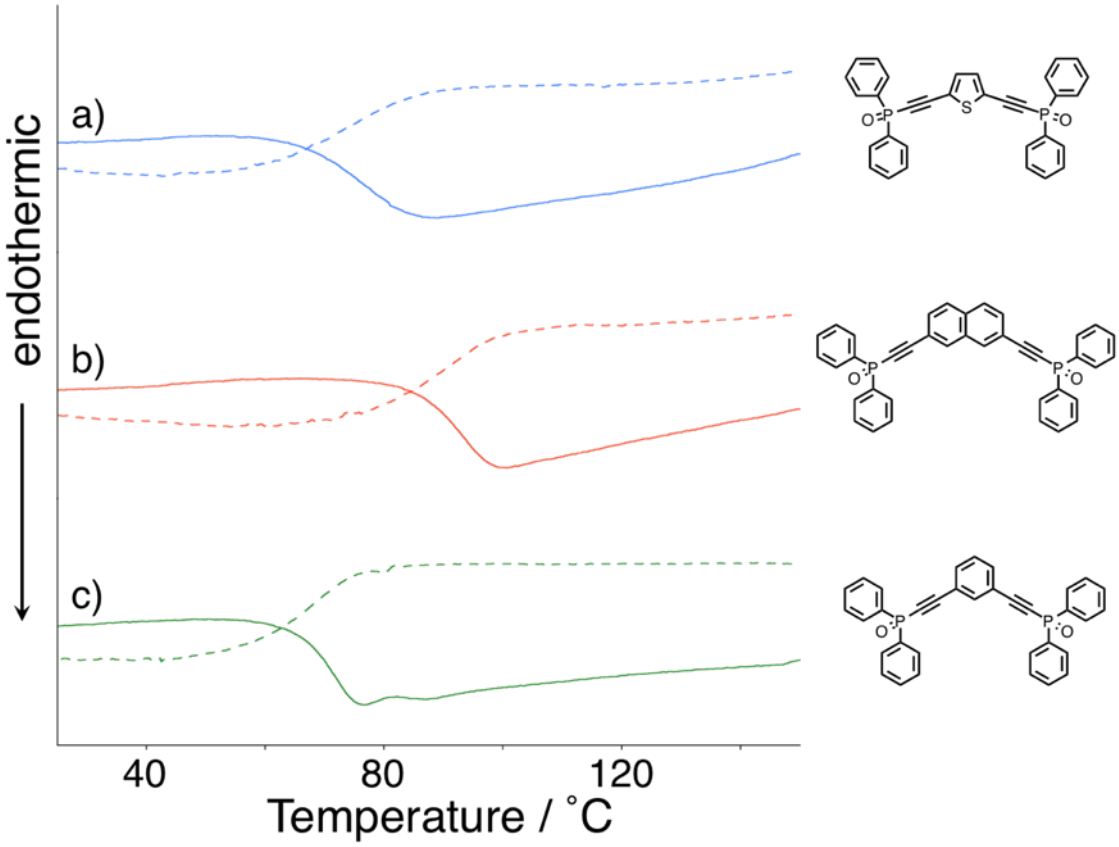

Figure 5-3. DSC thermograms of Eu(III) coordination glasses a) $[Eu(hfa)_3(dpet)]_3$, b) $[Eu(hfa)_3(dpen)]_3$, and c) $[Eu(hfa)_3(m\text{-}dpeb)]_3$ (dashed line: cooling process, solid line: heating process), the chemical structures on right shows the bridging ligands.

Table 5-1. Thermal properties of an Eu(III) coordination polymer $[Eu(hfa)_3(dpt)]_n$ and coordination glasses $[Eu(hfa)_3(X)]_3$.

Compounds	M_w of bridging ligand / g mol^{-1}	Glass transition temperature / ˚C	Decomposition temperature[a] / ˚C
$[Eu(hfa)_3(dpt)]_n$[b]	484.08	-	322[b]
$[Eu(hfa)_3(dpet)]_3$	532.08	73	242
$[Eu(hfa)_3(dpen)]_3$	576.14	87	260
$[Eu(hfa)_3(m\text{-}dpeb)]_3$[c]	526.13	65	249

[a] Decomposition temperatures were estimated from thermogravimetric curves (Figure A5-3). [b] Reference [19]. [c] Reference [12].

The reported thiophene-linked Eu(III) coordination compound without ethynyl groups, $[Eu(hfa)_3(dpt)]_n$ (dpt: 2,5-bis(diphenylphosphoryl)thiophene),[19] exhibited no glass-transition point (Figure A5-2). Thus, glass-forming ability can be systematically introduced by bent-angled bridging ligands with ethynyl groups that make more irregularly shaped molecules, which are more difficult to crystallize and more likely to form amorphous state.

5.3.3 Photophysical properties

Diffuse-reflectance absorption spectra and emission spectra were measured to evaluate the photophysical properties of Eu(III) coordination glasses (Figure 5-3). The absorption bands at around 350 nm were assigned to the π-π* transitions of antenna ligands. Absorption shoulder bands of the bridging ligands were also observed at around 500 nm for $[Eu(hfa)_3(dpet)]_3$ and $[Eu(hfa)_3(dpen)]_3$. Sharp and small absorption bands at 465 nm were due to the $^7F_0 \rightarrow {}^5D_2$ transitions of Eu(III) ions. The emission bands at 578, 591, 613, 650, and 698 nm are attributed to the 4f-4f transitions of $^5D_0 \rightarrow {}^7F_J$ (J = 0, 1, 2, 3, 4). The emission lifetimes (τ_{obs}) were measured and analyzed as single-exponential decay with a millisecond-scale lifetime for each Eu(III) coordination glass. Their intrinsic emission quantum yields (Φ_{ff}), radiative (k_r), and non-radiative constants (k_{nr}) were estimated using equations (3)-(5) as shown in Chapter 2. The estimated photophysical parameters are summarized in Table 5-2.

The Φ_{ff} values of $[Eu(hfa)_3(dpen)]_3$ and $[Eu(hfa)_3(m\text{-dpeb})]_3$ were estimated to be 46% and 72%, respectively. Unfortunately, $[Eu(hfa)_3(dpet)]_3$ exhibits weak red luminescence along with the luminescence from bridging ligands in the visible region (Figure A5-4), and thus the photophysical parameters were not

available. The k_r value of $[Eu(hfa)_3(dpen)]_3$ was the same as that of $[Eu(hfa)_3(m\text{-dpeb})]_3$, indicating that the coordination geometries around Eu(III) ions in the trimer structures were similar. The k_{nr} value of $[Eu(hfa)_3(dpen)]_3$ was much larger than that of $[Eu(hfa)_3(m\text{-dpeb})]_3$. The low-lying absorption edges of $[Eu(hfa)_3(dpen)]_3$ and $[Eu(hfa)_3(dpet)]_3$ at around 500 nm indicated the low excited triplet (T_1) states. The relatively lower T_1 states of dpen and dpet would promote the quenching of Eu(III)-centered emission through ligand-centered emission.[23] Thus, the electronic structures of organic cores in the bridging ligands affect the Eu(III)-centered emission properties of coordination glasses.

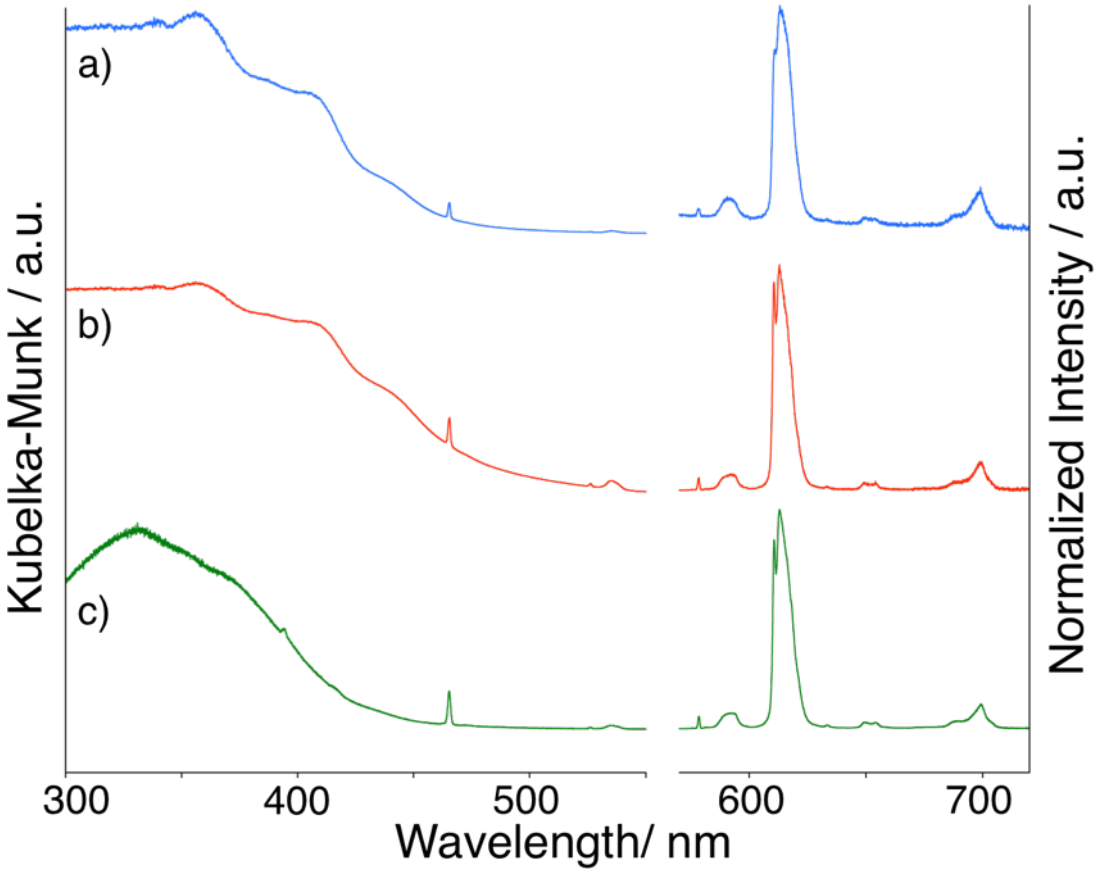

Figure 5-4. Diffuse-reflectance absorption spectra (left) and emission spectra excited at 380 nm (right) of Eu(III) coordination glasses a) $[Eu(hfa)_3(dpet)]_3$, b) $[Eu(hfa)_3(dpen)]_3$, and c) $[Eu(hfa)_3(m\text{-dpeb})]_3$.

Table 5-2. Photophysical parameters of Eu(III) coordination glasses $[Eu(hfa)_3(X)]_3$ in solid state.

X	Φ_{tot}[a] / %	Φ_{ff}[b] / %	η_{sens}[a] / %	τ_{obs}[c] / ms	k_r[b] / s^{-1}	k_{nr}[b] / s^{-1}
dpet[d]	n.a.	n.a.	n.a.	0.06	n.a.	n.a.
dpen	15	46	33	0.63	7.2×10^2	8.6×10^2
m-dpeb[e]	44	72	61	1.0	7.2×10^2	2.8×10^2

[a] λ_{ex} = 380 nm. [b] Equation 3-5. [c] λ_{ex} = 355 nm. [d] Photophysical parameters were not available because of the weak luminescence. [e] Reference [12].

A Tb(III)/Eu(III)-mixed coordination glass, $[Tb,Eu(hfa)_3(m\text{-dpeb})]_3$ (Tb/Eu = 50), was also prepared to introduce a temperature-responsive emission property in a glassy state. The emission spectra were recorded in the range of 100 K to 400 K, and corresponding green to red photoluminescence in glassy state was observed for the first time (Figure 5-5a, A5-5). According to the emission intensity ratio (Figure 5-5b), the Tb(III)/Eu(III)-mixed coordination glass was found to show as high temperature sensitivity (0.92% K^{-1}) as that of the reported chameleon luminophore, $[Tb,Eu(hfa)_3(dpbp)]_3$ (Tb/Eu = 99, 0.83% K^{-1}).[13] These results indicate that energy transfer between Tb(III) and Eu(III) ions can effectively occur in the amorphous state.

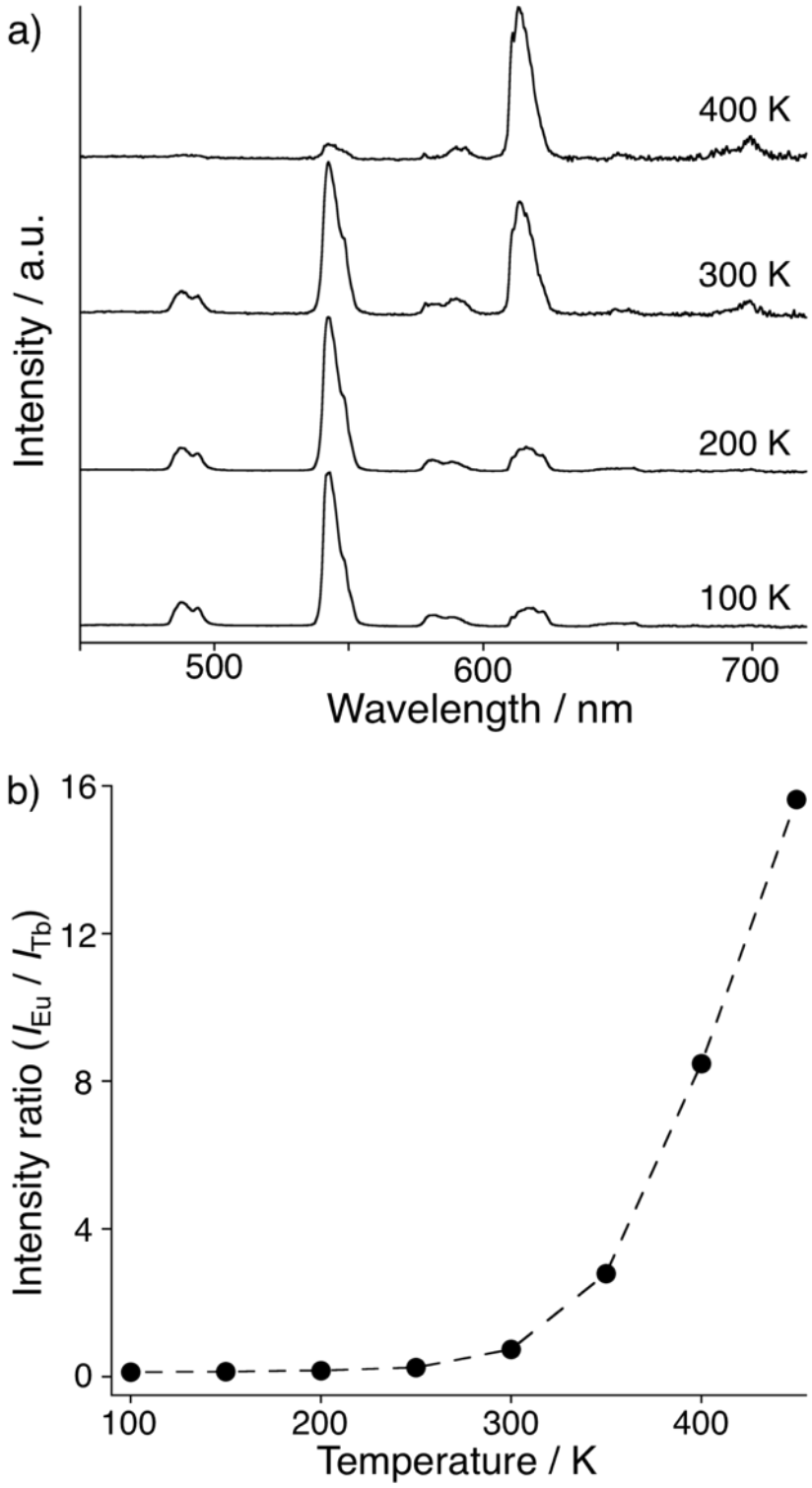

Figure 5-5. Temperature-dependent a) emission spectra and b) emission intensity ratio of $[Tb,Eu(hfa)_3(m\text{-dpeb})]_3$ (Tb/Eu = 50) in amorphous state (λ_{ex} = 380 nm).

5.4 Conclusion

A series of Ln(III) coordination glasses was successfully prepared, and temperature-sensitive luminescence in a glassy state was reported for the first time. The glass transition properties were dominated by molecular weight, geometry of the bridging ligands, and availability of aromatic surface for π-stacking. The trimer structures of Ln(III) coordination compounds were found to be suitable for thermodynamically non-equilibrium states, which makes them more difficult to crystallize and more likely to form an amorphous solid. The Tb(III)/Eu(III) mixed coordination glass also showed green, yellow, orange and red photoluminescence depending on temperature.

The idea of coordination glass enables the reported emissive Ln(III) coordination compounds to achieve dramatically improved painting properties on the surface of materials. These molecular designs also have the potential for providing thermo-stable Ln(III) coordination glasses for industrial applications. There is a global demand for these compounds as highly processable emissive dyes for fluidics, aeronautics, and chemical engineering.

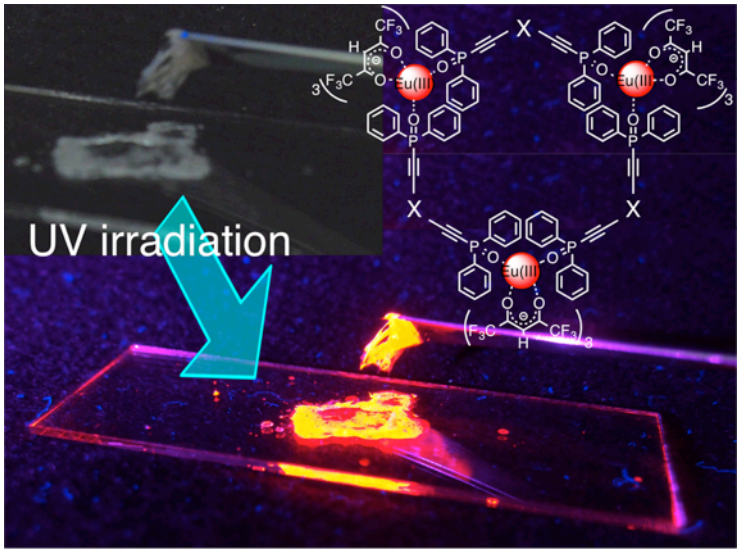

5.5 References

[1] A. Mishra, P. Bauerle, *Angew. Chem. Int. Ed.* **2012**, *51*, 2020-2067.

[2] J.C.S. Costa, L. Santos, *J. Phys. Chem. C* **2013**, *117*, 10919-10928.

[3] Y. Shirota, *J. Mater. Chem.* **2000**, *10*, 1-25.

[4] H. Nakano, S. Seki, H. Kageyama, *Phys. Chem. Chem. Phys.* **2010**, *12*, 7772-7774.

[5] A.K. Nedeltchev, H. Han, P.K. Bhowmik, *Tetrahedron* **2010**, *66*, 9319-9326.

[6] J. Kido, Y. Okamoto, *Chem. Rev.* **2002**, *102*, 2357-2368.

[7] J.-C.G. Bünzli, *Chem. Rev.* **2010**, *110*, 27292755.

[8] A. de Bettencourt-Dias, *Dalton Trans.* **2007**, 2229-2241.

[9] S.J. Butler, D. Parker, *Chem. Soc. Rev.* **2013**, *42*, 1652-1666.

[10] O. Moudam, B.C. Rowan, M. Alamiry, P. Richardson, B.S. Richards, A.C. Jones, N. Robertson, *Chem. Commun.* **2009**, 6649-6651.

[11] G. Zucchi, V. Murugesan, D. Tondelier, D. Aldakov, T. Jeon, F. Yang, P. Thuery, M. Ephritikhine, B. Geffroy, *Inorg. Chem.* **2011**, *50*, 4851-4856.

[12] Y. Hirai, T. Nakanishi, Y. Kitagawa, K. Fushimi, T. Seki, H. Ito, H. Fueno, K. Tanaka, T. Satoh, Y. Hasegawa, *Inorg. Chem.* **2015**, *54*, 4364-4370.

[13] K. Miyata, Y. Konno, T. Nakanishi, A. Kobayashi, M. Kato, K. Fushimi, Y. Hasegawa, *Angew. Chem. Int. Ed.* **2013**, *52*, 6413-6416.

[14] Y. Hirai, T. Nakanishi, K. Miyata, K. Fushimi, Y. Hasegawa, *Mater. Lett.* **2014**, *130*, 91-93.

[15] S.M. Borisov, O.S. Wolfbeis, *Anal. Chem.* **2006**, *78*, 5094-5101.

[16] M. Schaferling, *Angew. Chem. Int. Ed.* **2012**, *51*, 3532-3554.

[17] M.I.J. Stich, S. Nagl, O.S. Wolfbeis, U. Henne, M. Schaeferling, *Adv. Funct.*

Mater. **2008**, *18*, 1399-1406.

[18] K. Nakakita, M. Kurita, K. Mitsuo, S. Watanabe, *Meas. Sci. Technol.* **2008**, *17*, 359-366.

[19] Y. Hirai, T. Nakanishi, Y. Kitagawa, K. Fushimi, T. Seki, H. Ito, Y. Hasegawa, *Angew. Chem. Int. Ed.* **2016**, *55*, 12059-12062.

[20] M.H.V. Werts, R.T.F. Jukes, J.W. Verhoeven, *Phys. Chem. Chem. Phys.* **2002**, *4*, 1542-1548.

[21] A. Aebischer, F. Gumy, J.-C.G. Bünzli, *Phys. Chem. Chem. Phys.* **2009**, *11*, 1346-1353.

[22] R. Pavithran, N.S.S. Kumar, S. Biju, M.L.P. Reddy, S.A. Junior, R.O. Freire, *Inorg. Chem.* **2006**, *45*, 2184-2192.

[23] M. Hatanaka, Y. Hirai, Y. Kitagawa, T. Nakanishi, Y. Hasegawa, K. Morokuma, *Chem. Sci.* **2017**, *8*, 423-429.

Appendices

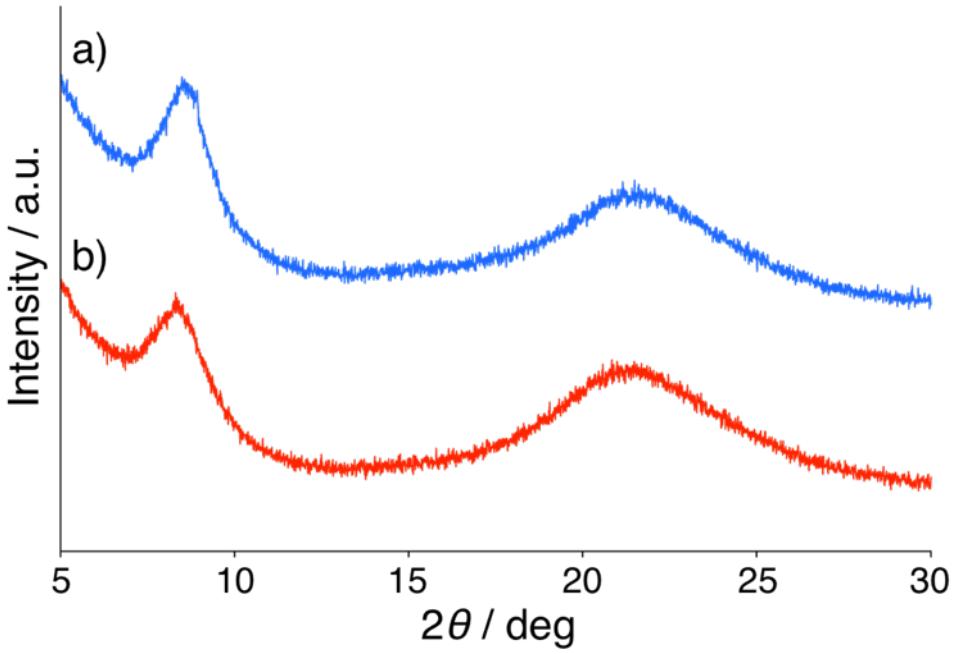

Figure A5-1. X-ray diffraction patterns of Eu(III) coordination glasses a) $[Eu(hfa)_3(dpet)]_3$ and b) $[Eu(hfa)_3(dpen)]_3$.

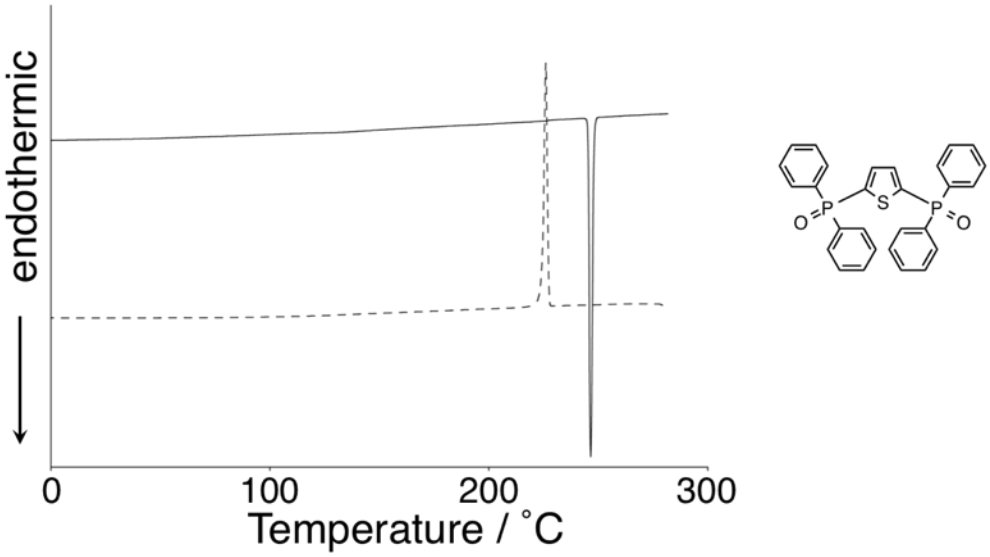

Figure A5-2. A DSC curve of $[Eu(hfa)_3(dpt)]_n$ (dashed line: cooling process, solid line: 2nd heating process), the chemical structure on right shows the bridging ligands.

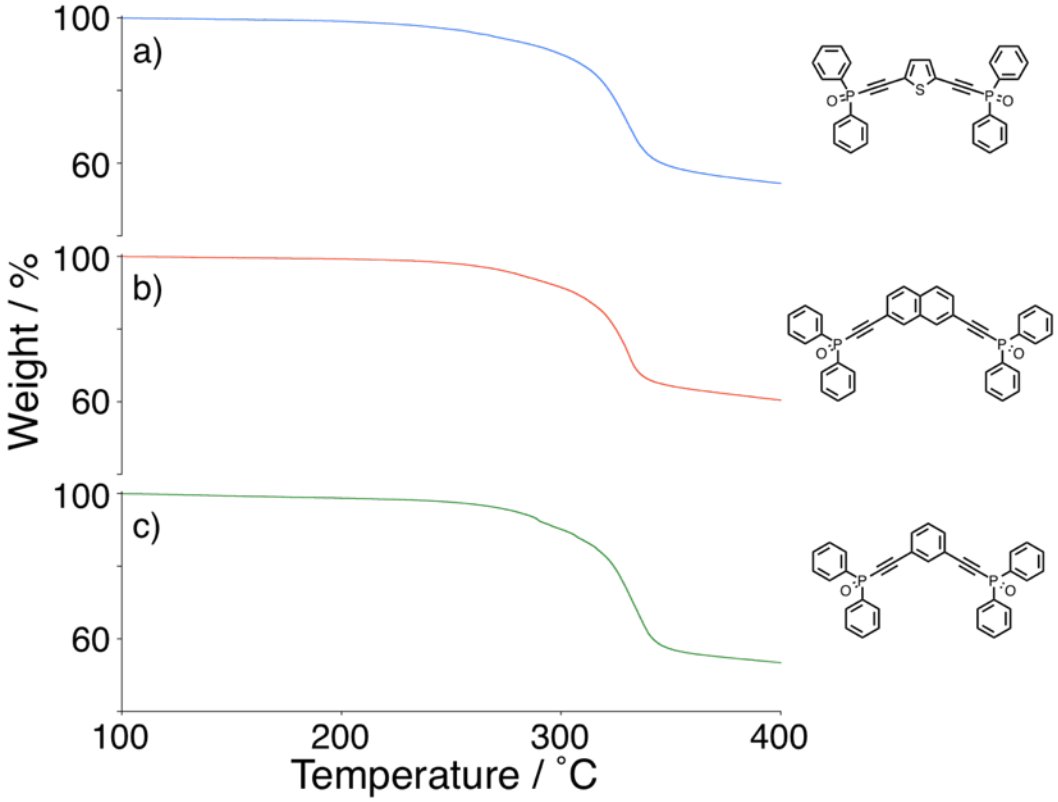

Figure A5-3. TG curves of Eu(III) coordination glasses a) $Eu(hfa)_3(dpet)]_3$, b) $[Eu(hfa)_3(dpen)]_3$, and c) $[Eu(hfa)_3(m\text{-}dpeb)]_3$ (5˚C min^{-1}, N_2 atmosphere), the chemical structures on right show the bridging ligands.

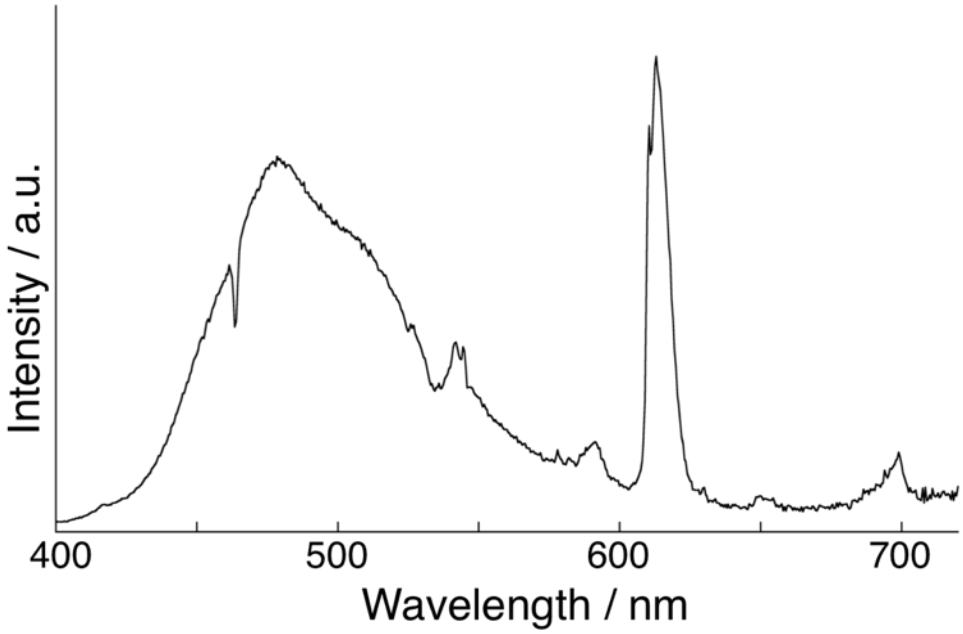

Figure A5-4. Emission spectrum of $[Eu(hfa)_3(dpet)]_3$ that shows the luminescence from bridging ligands and Eu(III) ions (λ_{ex} = 380 nm).

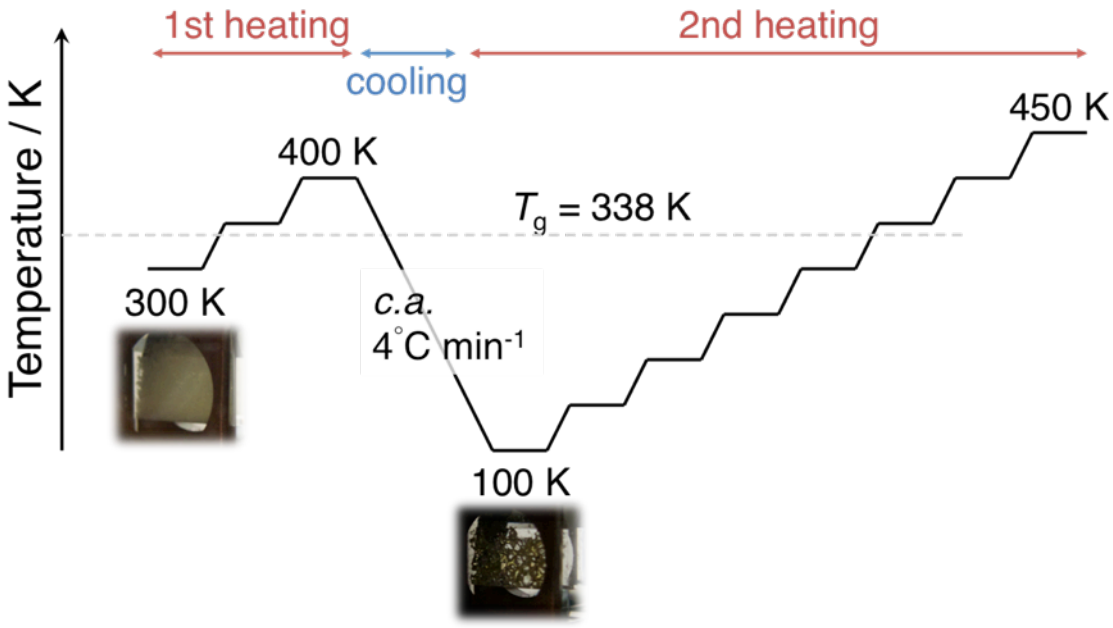

Figure A5-5. A sequence of temperature-dependent emission spectra in glassy state (the pictures show the sample in a quartz cell before and after glass transition).

Chapter 6

Triboluminescence of lanthanide(III) coordination polymers

Abstract

Triboluminescence (TL) and photoluminescence (PL) of novel Ln(III) coordination polymers $[Ln(hfa)_3(dpf)]_n$ (Ln = Tb, Gd, Eu, dpf: 2,5-bis(diphenylphosphoryl)furan) are reported. The coordination polymers exhibited bright TL due to the face-to-face arrangement of substituents between single polymer chains. The observation of TL in a series of Eu(III) coordination polymers and a Gd(III) compound indicated that both hfa ligands and Ln(III) ions were excited under grinding. Significant PL/TL spectral differences in $[Tb,Eu(hfa)_3(dpf)]_n$ due to distinct excitation processes upon grinding and UV irradiation were observed for the first time.

Based on

Cracking the Code of Triboluminescence Using Lanthanide Coordination Polymers with Face-to-Face Arranged Substituents

Y. Hirai, T. Nakanishi, Y. Kitagawa, K. Fushimi, T. Seki, H. Ito, Y. Hasegawa, **2017**, *in contribution*.

6.1 Introduction

Luminescence upon grinding solid materials is called triboluminescence (TL). In 17th century, it was first noted by Francis Bacon that: “It is well known that all sugar, whether candied or plain, if it be hard, will sparkle when broken or scraped in the dark.” TL phenomena, unlike well-known photoluminescence (PL), have advantages that they are generated without photo-irradiation. The fracture-induced luminescence properties of TL materials make them attractive for application as structural damage sensors and security marking techniques.[1-4]

TL phenomena have been widely found in inorganic and organic compounds, [5-9] and about half of all crystalline materials are predicted to show TL.[10] Wang demonstrated yellow-to-red TL of CaZnOS: Mn(II) depending on the concentration of Mn(II) ions.[11] Yamashita and co-workers reported blue TL of trifluoromethyl and pentafluoromethyl substituted imide derivatives under daylight.[12,13] Coordination compounds including Cu(I), Pt(II), Mn(II), and Ln(III) ions have also been reported for their TL properties.[14-18]

These TL-active compounds are known to show PL as well. TL and PL occur from distinct stimuli such as grinding and photo-irradiation; however, their spectra usually exhibit similar profiles.[19,20] Relationships between TL and PL are still being discussed form a scientific point of view. In order to provide new insights into TL phenomena, the author focuses on Ln(III) complexes with efficient TL and PL properties because of their high spectral resolution arising from intraconfigurational 4f-4f transitions.[21-26]

In Chapter 6, the author focused on the specific arrangement of substituents in solid-state Ln(III) complexes. Sweeting and Rheingold reported that the

disorder of phenyl rings and cations in $[Eu(dbm)_4]^-[Et_3NH]^+$ (dbm: dibenzoylmethanato) provided a sufficient source of localized polarity to induce TL activity.[27] Chen reported that the disorder of thienyl and trifluoromethyl (CF_3) groups in Eu(III) complexes played an important role in providing charge separation by creating randomly distributed sites of electron affinities at the faces of fractures.[17] There have also been some reports on TL-active Ln(III) coordination polymers based on *β*-diketonato and aromatic bridging ligands.[28,29]

The author considers that strong TL Ln(III) coordination polymers can be constructed by introducing disordered arrangement of substituents between single polymer chains in the solid state. A novel furan-based bridging ligand (2,5-bis(diphenylphosphoryl)furan: dpf) is designed to provide the disordered face-to-face arrangement of CF_3 substituents in Ln(III)-hfa coordination polymers (Figure 6-1a). The polar character and small aromatic ring of the furyl-bridging ligand are expected to prevent the polymer chains from forming highly ordered alternate packing structures (Figure 6-1b). The reported coordination polymers with thiophene-based bridges, $[Eu(hfa)_3(dpt)]_n$ and $[Eu(hfa)_3(dpedot)]_n$ are also prepared for comparison of TL and PL properties.[30] The relationships between coordination structures and TL activities are evaluated using single crystal X-ray analyses and TL observations. A large spectral difference between TL and PL is confirmed in Tb(III)/Eu(III) mixed polymers using a charge coupled detector (CCD) system. The excitation processes in TL and PL are proposed on the basis of photo science.

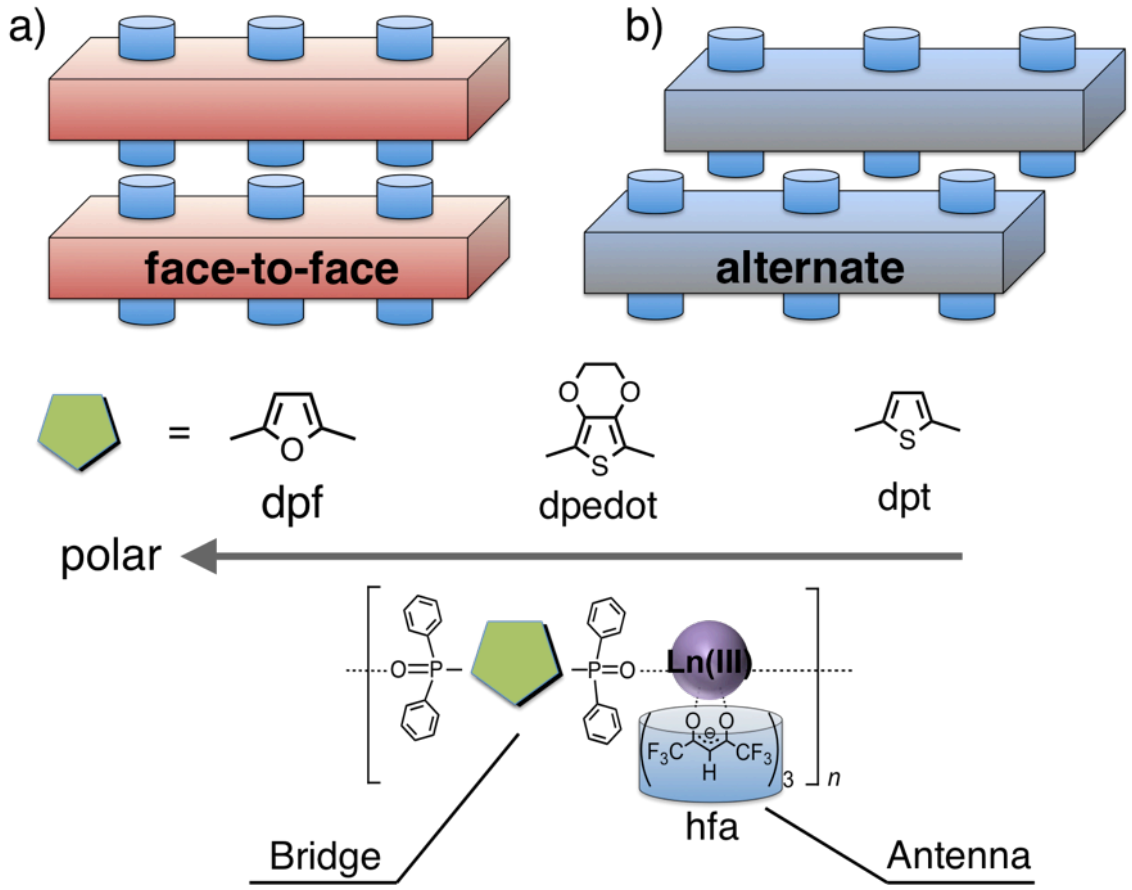

Figure 6-1. Schematic representation of Ln(III) coordination polymers with a) face-to-face and b) alternate intermolecular packing structures.

6.2 Experimental Section

6.2.1 Materials

Europium acetate *n*-hydrate (99.9%), terbium(III) acetate tetrahydrate (99.9 %), gadolinium(III) acetate tetrahydrate (99.9 %), *n*-BuLi (in *n*-hexane, 1.6 M), and hydrogen peroxide were purchased from Kanto Chemical Co., Inc. 2,5-Dibromofuran, 3,4-ethylenedioxythiophene, 2,5-dibromothiophene, and chlorodiphenylphosphine were obtained from Tokyo Chemical Industry Co., Ltd. All other chemicals and solvents were reagent grade and were used without further purification.

6.2.2 Apparatus

^{1}H NMR (400 MHz) spectra were recorded on a JEOL ECS400. Chemical shifts were reported in δ ppm, referenced to an internal tetramethylsilane standard for ^{1}H NMR spectroscopy. Infrared spectra were recorded on a JASCO FTIR-420 spectrometer using KBr pellets. Elemental analyses were performed by an Exeter Analytical CE440. Mass spectrometry was performed by a Thermo Scientific Exactive (ESI-MS) and a JEOL JMS-700TZ (FAB-MS).

6.2.3 Syntheses

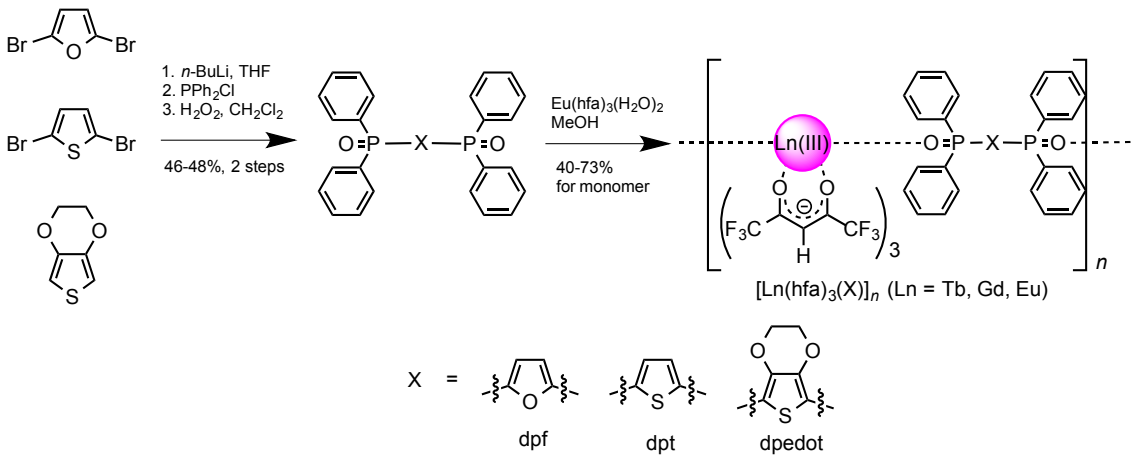

Scheme 6-1. Synthetic schemes of phosphine oxide ligands and Ln(III) coordination polymers.

Preparation of 2,5-bis(diphenylphosphoryl)furan (dpf):

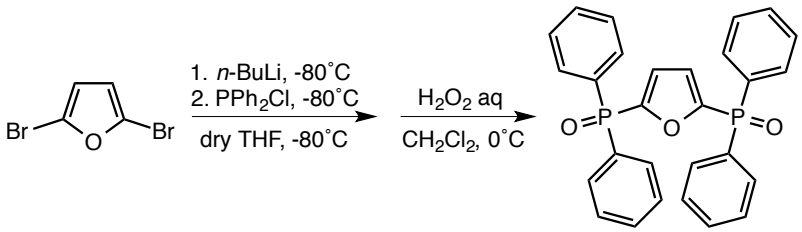

In a degassed 3-neck round-bottomed flask (300 mL vol.), 2,5-dibromofuran (2.6 mL, 24 mmol) was dissolved in dry THF (130 mL) under argon atmosphere, then stirred until a homogeneous solution was formed at room temperature. A solution of *n*-BuLi (40 mL, 62 mmol) was added dropwise to the solution at −80˚C. The addition was completed in ca. 15 min. The mixture was allowed to stir for 3 h, after which a PPh_2Cl (12 mL, 67 mmol) was added dropwise at −80˚C, then the solution became cloudy. The mixture was gradually brought to room temperature, and stirred for 14 h to form clouded yellow solution. The product was extracted with dichloromethane and dried over anhydrous $MgSO_4$. The solvent was concentrated and dissolved in dichloromethane (100 mL) in a

flask. The solution was cooled to 0˚C and then 30% H_2O_2 aqueous solution (21 mL) was added to it. The reaction mixture was stirred for 3 h. The product was extracted with dichloromethane and the obtained crude powder was washed with ethyl acetate for several times to afford white powder.

Yield: 5.5 g (48%). ^{1}H NMR (400 MHz, CD_3OD, 25˚C) *δ* 7.61-7.67 (m, 12H, -CH), *δ* 7.51-7.55 (m, 8H, -CH), *δ* 7.27 (t, 2H, -CH) ppm. ESI-Mass (*m*/*z*): calcd for $C_{28}H_{23}O_3P_2$ $[M+H]^+$, 469.11; found, 469.11. Anal. Calcd for $C_{28}H_{22}O_3P_2$: C, 71.79; H, 4.73%. Found: C, 71.51; H, 4.67%.

Preparation of 3,4-bis(diphenylphosphoryl)ethylenedioxythiophene (dpedot) and 2,5-bis(diphenylphosphoryl)thiophene (dpt):[30]

The dpedot and dpt ligands were synthesized as described in Chapter 2.

Preparation of Ln(III) coordination polymers $[Ln(hfa)_3(dpf)]_n$ (Ln = Tb, Gd, Eu):

Phosphine oxide ligand, dpf (0.37 g, 0.80 mmol) and $Ln(hfa)_3(H_2O)_2$ (Ln = Tb, Gd, Eu, 0.80 mmol) were dissolved in methanol (40 mL), respectively. The solutions were mixed and refluxed for 3 h. The reaction mixture was concentrated and washed with chloroform. The solvent was evaporated and re-dissolved in 50˚C methanol for recrystallization. The obtained crystals were washed with −20˚C methanol.

$[Tb(hfa)_3(dpf)]_n$. Yield: 0.65 g (65% for monomer). IR (KBr): 1657 (st, C=O), 1145 (st, P=O) cm^{-1}. ESI-Mass (*m*/*z*): calcd for $C_{38}H_{24}TbF_{12}O_7P_2$ $[M\text{-}hfa]^+$: 1041.0, found, 1041.0. Anal. Calcd for $C_{43}H_{25}TbF_{18}O_9P_2$: C, 41.37; H, 2.02%. Found: C, 41.32; H, 1.88%.

$[Gd(hfa)_3(dpf)]_n$. Yield: 0.57 g (57% for monomer). IR (KBr): 1657 (st, C=O), 1145 (st, P=O) cm^{-1}. ESI-Mass (*m*/*z*): calcd for $C_{38}H_{24}GdF_{12}O_7P_2$ $[M\text{-}hfa]^+$: 1040.0, found, 1040.0. Anal. Calcd for $C_{43}H_{25}GdF_{18}O_9P_2$: C, 41.42; H, 2.02%. Found: C, 41.30; H, 1.87%.

$[Eu(hfa)_3(dpf)]_n$. Yield: 0.73 g (73% for monomer). IR (KBr): 1657 (st, C=O), 1145 (st, P=O) cm^{-1}. ESI-Mass (*m*/*z*): calcd for $C_{38}H_{24}EuF_{12}O_7P_2$ $[M\text{-}hfa]^+$: 1035.0, found, 1034.7. Anal. Calcd for $C_{43}H_{25}EuF_{18}O_9P_2$: C, 41.60; H, 2.03%. Found: C, 41.62; H, 2.32%.

Preparation of Eu(III) coordination polymers $[Eu(hfa)_3(dpedot)]_n$, and $[Eu(hfa)_3(dpt)]_n$:[30]

The $[Eu(hfa)_3(dpedot)]_n$ and $[Eu(hfa)_3(dpt)]_n$ were synthesized following the method in Chapter 2.

6.2.4 Crystallography

Single crystals of $[Ln(hfa)_3(dpf)]_n$ (Ln = Tb, Gd, Eu) were prepared by slow evaporation of $[Ln(hfa)_3(dpf)]_n$/methanol solution. A colorless block-shaped single crystal of $[Ln(hfa)_3(dpf)]_n$ was mounted on a MiTiGen micromesh using Paratone-N. The measurement was performed on a Rigaku R-AXIS RAPID diffractometer using graphite monochromated Mo-Kα radiation. Non-hydrogen atoms were refined anisotropically. Hydrogen atoms were refined using the riding model. All calculations were performed using the CrystalStructure crystallographic software package. CIF data was confirmed by using the checkCIF/PLATON service.

6.2.5 Optical measurements

UV-Vis absorption spectra were recorded on a JASCO V-670 spectrometer. Emission and excitation spectra were recorded on a HORIBA Fluorolog-3 spectrofluorometer and corrected for the response of the detector system. Emission lifetimes (τ_{obs}) were measured using the third harmonics (355 nm) of a Q-switched Nd:YAG laser (Spectra Physiscs, INDI-50, fwhm = 5 ns, λ = 1064 nm) and a photomultiplier (Hamamatsu photonics, R5108, response time ≤ 1.1 ns). The Nd:YAG laser response was monitored with a digital oscilloscope (Sony Tektronix, TDS3052, 500 MHz) synchronized to the single-pulse excitation. Emission lifetimes were determined from the slope of logarithmic plots of the decay profiles. Emission lifetimes and emission spectra from the range between 100-350 K were measured with a cryostat (Thermal Block Company, SA-SB245T) and a temperature controller (Oxford, Instruments, ITC 502S). The emission quantum yields excited at 380 nm (Φ_{tot}) were estimated using JASCO F-6300-H spectrometer attached with JASCO ILF-533 integrating

sphere unit (φ = 100 mm). The wavelength dependence of the detector response and the beam intensity of Xe light source for each spectrum were calibrated using a standard light source. The TL spectra were recorded on a Photonic Hamamatsu PMA-12 Multichannel Analyzer.

6.3 Results and Discussion

6.3.1 Coordination structures

The crystal structure of $[Eu(hfa)_3(dpf)]_n$ is shown in Figure 6.2. The Eu(III) ions are coordinated to eight oxygen atoms from three hfa ligands and two bridging ligands. The space group is categorized as non-centrosymmetric *C*-centered. In order to investigate the geometrical symmetry around Eu(III) ions, the degree of distortion against an 8-coordinated square-antiprismatic structure (8-SAP, point group: D_{4d}) and an 8-coordinated trigonal-dodecahedral structure (8-TDH, point group: D_{2d}) was evaluated on the basis of shape factor *S* (Figure A6-1). The observed dihedral angles (δ_i), idealized dihedral angles for square antiprism (θ_{SAP}) and trigonal dodecahedron (θ_{TDH}), calculated measure shape criteria, S_{SAP} and S_{TDH} are summarized in Table A6-1. The S_{SAP} value is much smaller than that of S_{TDH} (S_{SAP} = 4.98 < S_{TDH} = 12.1), indicating that the coordination geometry is categorized to be an 8-SAP. Multiple intermolecular CH/F ($d_{CH/F}$ = 2.66 Å (H5/F66), 2.75 Å (H11/F40), 2.93 Å (H55/F46)) and intramolecular CH/π ($d_{CH/\pi}$ = 2.44 Å (H12/π), 2.99 Å (H32/π)) interactions were observed. On the other hand, intermolecular CH/π interactions, which usually contribute to tight packing structures, were not identified.[31] The relatively weak intermolecular interactions of $[Eu(hfa)_3(dpf)]_n$ were attributed to the twisted structure of single polymer chains.

According to the crystal structures observed above and in Chapter 2, Ln(III) coordination polymers linked with polar bridges tend to cancel out the dipole moment by giving a twist to single polymer chains. Coordination polymers with relatively small polar bridges balance the dipoles by intermolecular alternate arrangement. The twisted polymer backbones with disorderly-arranged CF_3

substituents in $[Eu(hfa)_3(dpf)]_n$ were probably due to the largest ground state dipole moment of dpf among the three bridging ligands (D_{dpf}: 5.80 > D_{dpedot}: 4.30 > D_{dpt}: 1.17 D). The small furyl core also prevented the polymer chains from forming highly ordered packing structures, resulting in the absence of intermolecular CH/π interactions. Therefore, the novel furan-based bridging ligand with a large D value and a small aromatic core well contribute to the formation of a disordered face-to-face arrangement of CF_3 substituents in the crystal packing system, leading to a mechanically or a thermodynamically unstable structure.

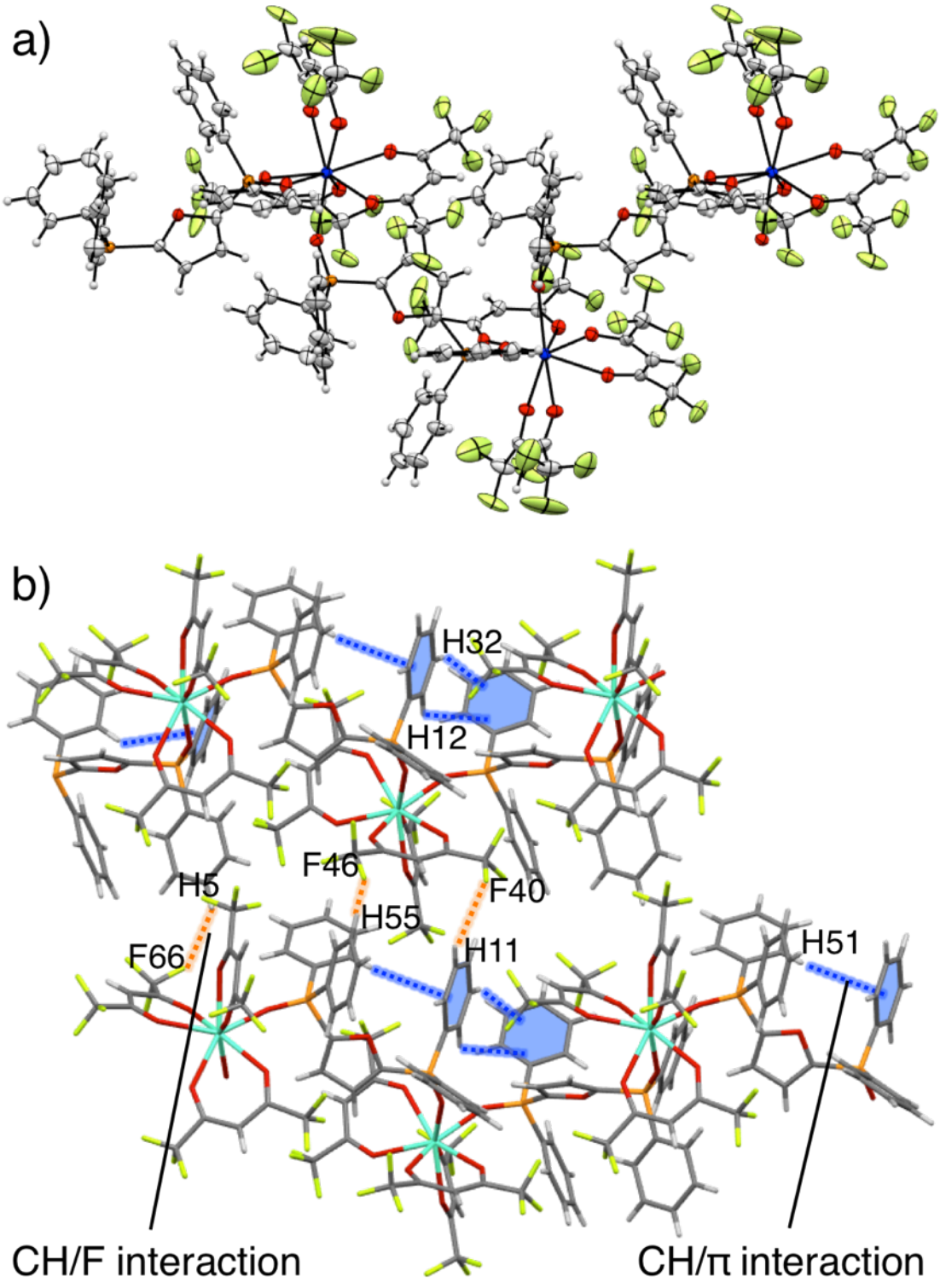

Figure 6-2. a) ORTEP drawing (showing 50% probability displacement ellipsoids) and b) crystal packing structure focused on intra- and inter-molecular interactions between single polymer chains of $[Eu(hfa)_3(dpf)]_n$.

6.3.2 TL activity of Eu(III) coordination polymers

The ability for generation of TL was ascertained by observing Eu(III)-characteristic red emission upon grinding of solid Eu(III) coordination polymers. Pictures of red TL and corresponding space-fill models focused on crystal packing structures are shown in Figure 6-3. The author observed quite weak TL for $[Eu(hfa)_3(dpt)]_n$ which exhibited highly ordered arrangement to form a thermodynamically stable structure. The TL activity was clearly high in $[Eu(hfa)_3(dpedot)]_n$ and $[Eu(hfa)_3(dpf)]_n$, qualitatively. These observations indicate that the ability to generate TL strongly depends on the proportion of face-to-face arrangement of bulky CF_3 groups in crystal packing structures. Eliseeva and co-workers also demonstrated strong TL of an Eu(III) coordination polymer $[Eu(hfa)_3(acetbz)]_n$ (acetbz: 1,4-diacetoxybenzene) with similar arrangement of CF_3 groups between single polymer chains.[28] Therefore, the author also suggests that the mechanical stimuli under grinding generates intermolecular cracking of Ln(III) coordination polymers, resulting in fracture-induced TL.

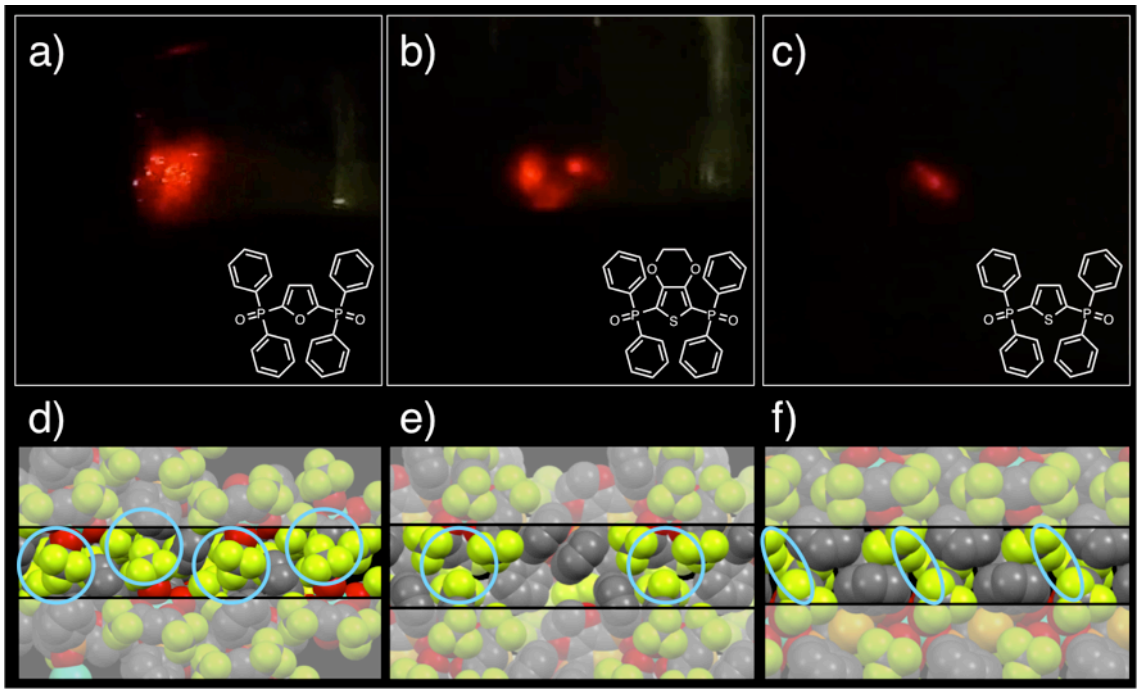

Figure 6-3. a-c) Pictures of TL and chemical structures of bridging ligands, and d-f) corresponding space filling models focused on intermolecular CF_3 arrangement in $[Eu(hfa)_3(dpf)]_n$, $[Eu(hfa)_3(dpedot)]_n$, and $[Eu(hfa)_3(dpt)]_n$.

6.3.3 Photoluminescence (PL) properties

$[Eu(hfa)_3(dpf)]_n$ also exhibited strong red PL under UV irradiation in solid state (Figure 6-4a, λ_{ex} = 380 nm). In order to evaluate the PL performance of $[Eu(hfa)_3(dpf)]_n$, PL measurements and calculations of photophysical parameters were carried out. The emission bands observed at 578, 591, 613, 650, and 698 nm were assigned to be 4f-4f transitions of $^5D_0 \rightarrow {}^7F_J$ (J = 0, 1, 2, 3, 4) in Eu(III) ions. Based on the emission lifetime measurements and calculations, photophysical parameters were compared with those of $[Eu(hfa)_3(dpt)]_n$ and $[Eu(hfa)_3(dpedot)]_n$ in Chapter 2 (Table 6-1). The emission quantum yield (Φ_{tot} = 64%) and energy transfer efficiency (η_{sens} = 88%) of $[Eu(hfa)_3(dpf)]_n$ were higher than those of $[Eu(hfa)_3(dpt)]_n$ and $[Eu(hfa)_3(dpedot)]_n$. The enhanced radiative rate constant (k_r = 1.0 × 10^3 s^{-1}) in

$[Eu(hfa)_3(dpf)]_n$ was due to the polar character of bridging ligands and asymmetric coordination geometry without an inversion center around Eu(III) ions. The low-lying ILCT band generated by the stabilized energy level of hfa ligands were responsible for the large Φ_{tot} and η_{sens} values as mentioned for $[Eu(hfa)_3(dpt)]_n$ in Chapter 2. $[Tb(hfa)_3(dpf)]_n$ also exhibited strong green PL with emission bands at 490, 540, 580, 620, and 650 nm, corresponding to 4f-4f transition of $^5D_4 \rightarrow {}^7F_J$ (J = 6, 5, 4, 3, 2) in Tb(III) ions (Figure 6-4b, λ_{ex} = 380 nm). The intrinsic emission quantum yield (Φ_{ff}) and η_{sens} values were determined to be 88% and 45%, respectively. The relatively low η_{sens} value was due to the energy back transfer (BET) from the emissive level of Tb(III) ions to the excited triplet state of hfa ligands.[32] The author also considers that the ILCT state which boost energy forward transfer to Eu(III) ions negatively affect Tb(III)-centered emission. Kuzmina and co-workers indicated that appearance of long-wavelength band resulted in an improved energy transfer efficiency for an Eu(III) compound, although for a Tb(III) compound it increased the probability of energy back transfer.[33]

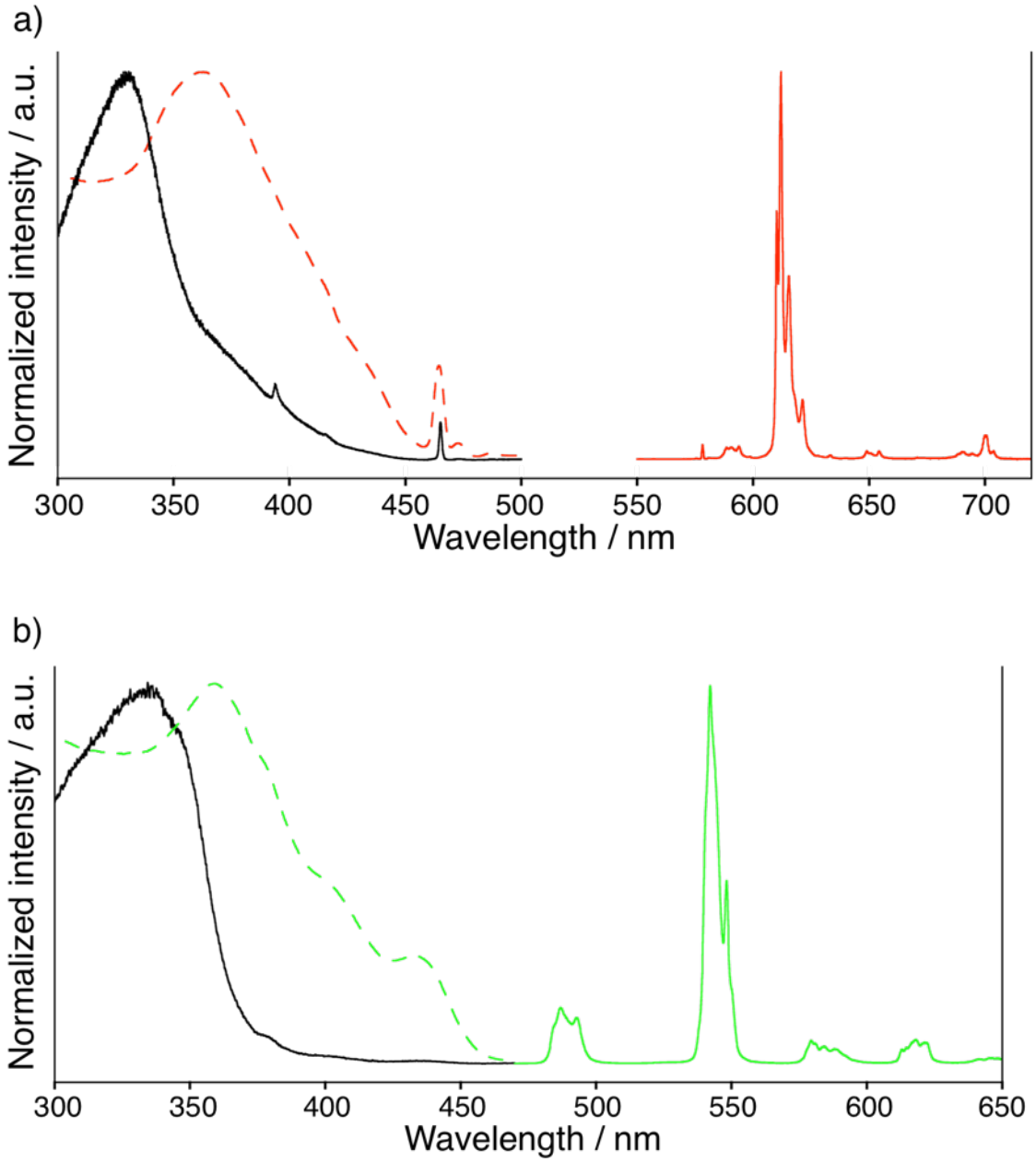

Figure 6-4. Diffuse reflectance (solid black line), excitation (dotted line, monitored at 613 nm for Eu(III) ions, 545 nm for Tb(III) ions), and emission (λ_{ex} = 380 nm) spectra of a) $[Eu(hfa)_3(dpf)]_n$ and b) $[Tb(hfa)_3(dpf)]_n$ in solid state.

Table 6-1. Photophysical parameters of Eu(III) coordination polymers $[Eu(hfa)_3(X)]_n$ in solid state.

Sample	Φ_{tot}[a] / %	Φ_{ff}[b] / %	η_{sens}[a] / %	τ_{obs}[d] / ms	k_r[b] / s^{-1}	k_{nr}[b] / s^{-1}
$[Eu(hfa)_3(dpf)]_n$	64	73	88	0.72	1.0×10^3	3.8×10^2
$[Eu(hfa)_3(dpt)]_n$	60	75	80	0.75	1.0×10^3	3.3×10^2
$[Eu(hfa)_3(dpedot)]_n$	56	85	66	0.93	9.1×10^2	1.6×10^2

[a] λ_{ex} = 380 nm. [b] Equation 3-5 in Chapter 2. [c] λ_{ex} = 355 nm.

6.3.4 PL and TL properties in Tb(III)/Eu(III) mixed systems

$[Eu(hfa)_3(dpf)]_n$ and $[Tb(hfa)_3(dpf)]_n$ exhibited strong red and green TL under grinding, respectively. When the same excitation process in TL and PL is assumed, the emission colors of Tb(III)/Eu(III) mixed coordination polymers should be the same under grinding and under UV irradiation. Thus, Tb(III)/Eu(III) mixed coordination polymers were prepared for understanding the relationships between TL and PL properties. The author here considered that the dpf ligand is suitable for Tb(III)/Eu(III) mixed systems, since both $[Tb(hfa)_3(dpf)]_n$ and $[Eu(hfa)_3(dpf)]_n$ exhibited strong TL and PL with isomorphic crystal structures (Table A6-2).

The coordination polymers $[Tb,Eu(hfa)_3(dpf)]_n$ (Tb/Eu = 1, 10) were successfully prepared, and the obtained compounds exhibited strong TL and PL under UV irradiation and grinding. The TL and PL spectra were independently recorded using CCD system (Figure 6-5). The emission intensity of Eu(III) ions is larger than that of Tb(III) ions in the Tb/Eu = 1 compound under UV irradiation, resulting in reddish-orange PL. The PL colors of Tb(III)/Eu(III) mixed coordination polymers are dominated by Eu(III)-centered emission, since the Tb(III)-centered emission is affected by both the BET process and excitation energy transfer from Tb(III) to Eu(III) ions at room temperature.[34-36]

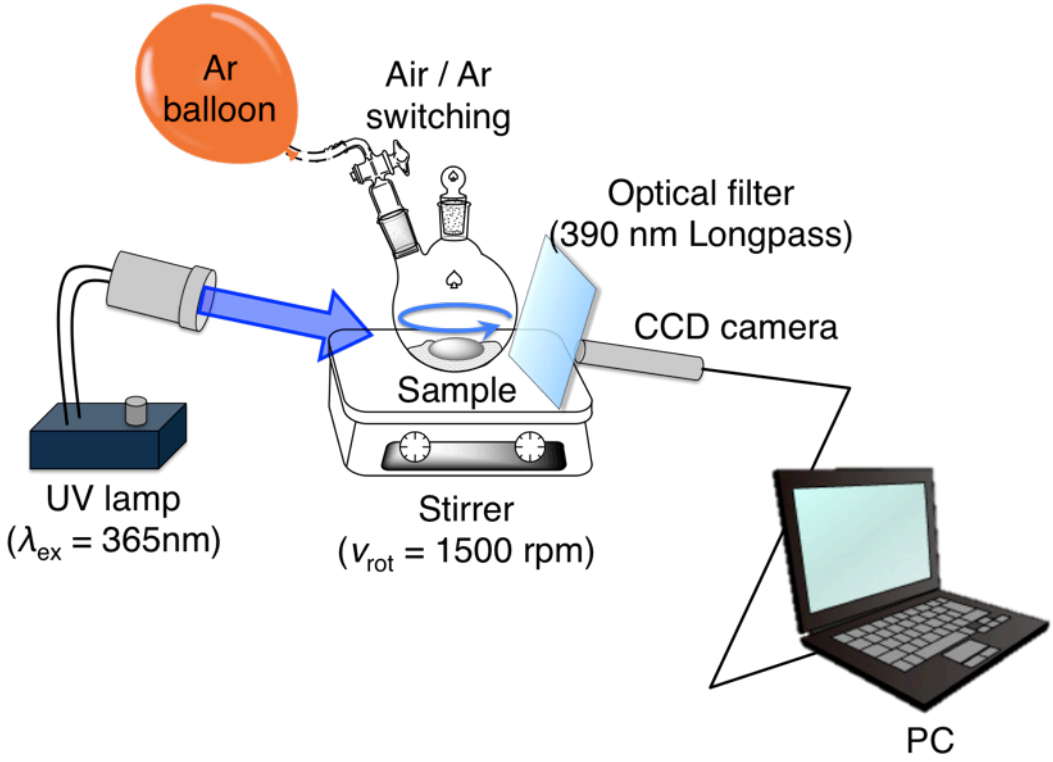

Figure 6-5. Experimental setups for TL/PL measurements using CCD detecting systems (exposure time: 1000 ms, averaging: 2 times)

Interestingly, the observed TL colors were clearly different from those of PL. The Tb/Eu = 1 compound exhibited yellow TL and reddish-orange PL (Figure 6-6a), while the Tb/Eu = 10 compound exhibited green TL and greenish-yellow PL (Figure 6-6b). These spectral differences between TL and PL were the most remarkable among previously reported organic, inorganic, and coordination compounds with TL and PL properties. The TL colors of these coordination polymers might not be explained by the simple excitation mechanisms in PL. Since the TL colors correspond to the Tb/Eu mixture ratios, TL would be dominated by direct excitation of Ln(III) ions; though, the possibility of antenna ligand (hfa)-mediated emission cannot be ruled out.

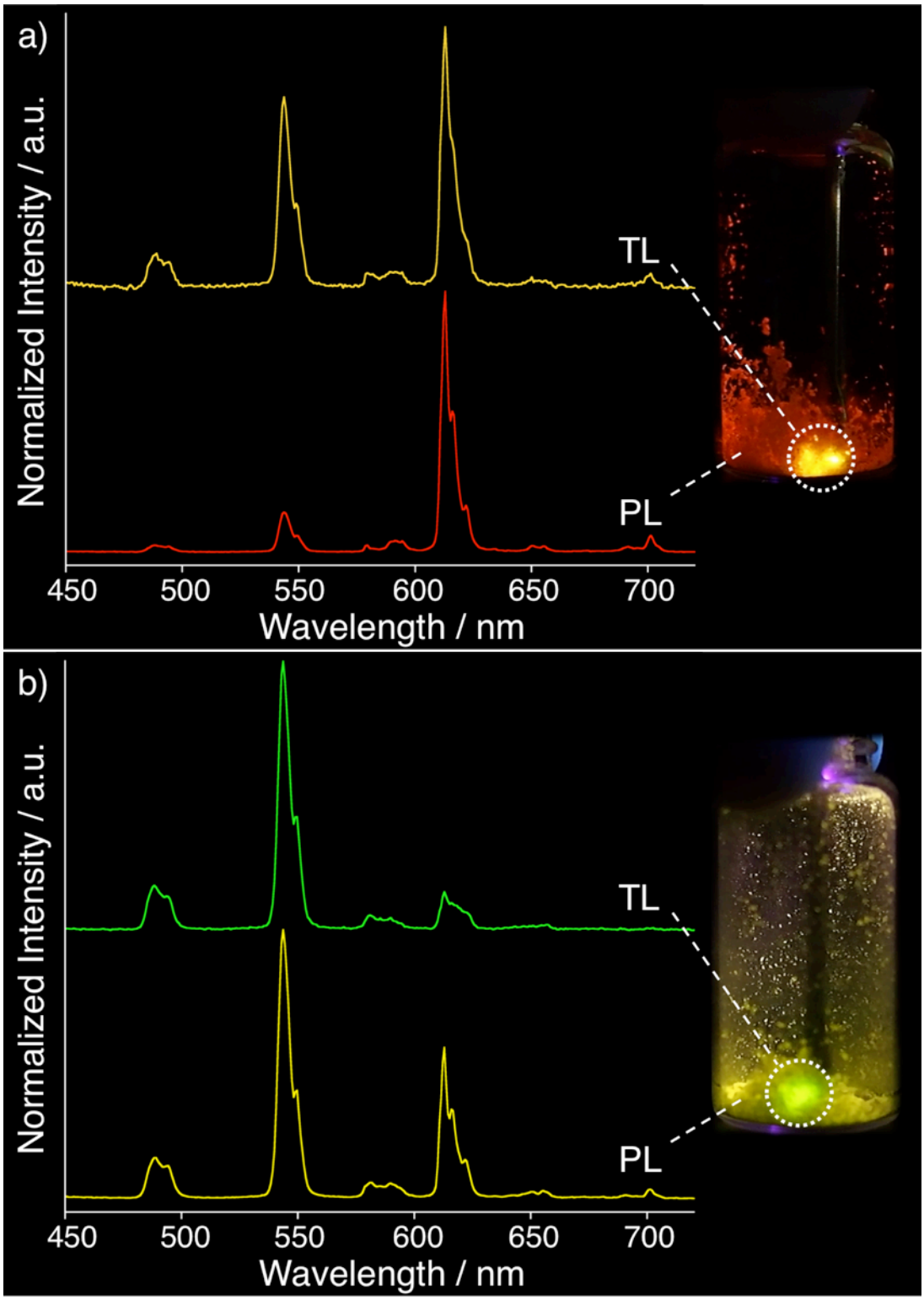

Figure 6-6. TL and PL spectra of a) $[Tb,Eu(hfa)_3(dpf)]_n$ (Tb/Eu = 1), b) $[Tb,Eu(hfa)_3(dpf)]_n$ (Tb/Eu = 10) measured on a Photonic Hamamatsu PMA-12 Multichannel Analyzer ($\lambda_{ex,PL}$ = 365 nm). The pictures inset were taken while irradiating UV light and grinding at the same time.

6.3.5 PL and TL properties of Gd(III) coordination polymers

With the view of the possibility of triplet excited state mediated TL, the PL/TL measurements were performed for $[Gd(hfa)_3(dpf)]_n$ (Figure 6-7). It is generally known that the Gd(III) $^6P_{7/2}$ level (at 32 100 cm^{-1}) is too high to transfer the energy from the triplet excited states of hfa ligands (at 22 000 cm^{-1}), resulting in hfa-centered emission. The characteristic blue PL and TL of hfa were observed under UV irradiation and grinding, respectively. These spectra exhibited equally spaced three emission bands with around 1320 cm^{-1} energy gaps, which were assigned to be the vibronic bands of hfa ligands. These results therefore indicate the generation of excited triplet states of hfa ligands under the condition of grinding.

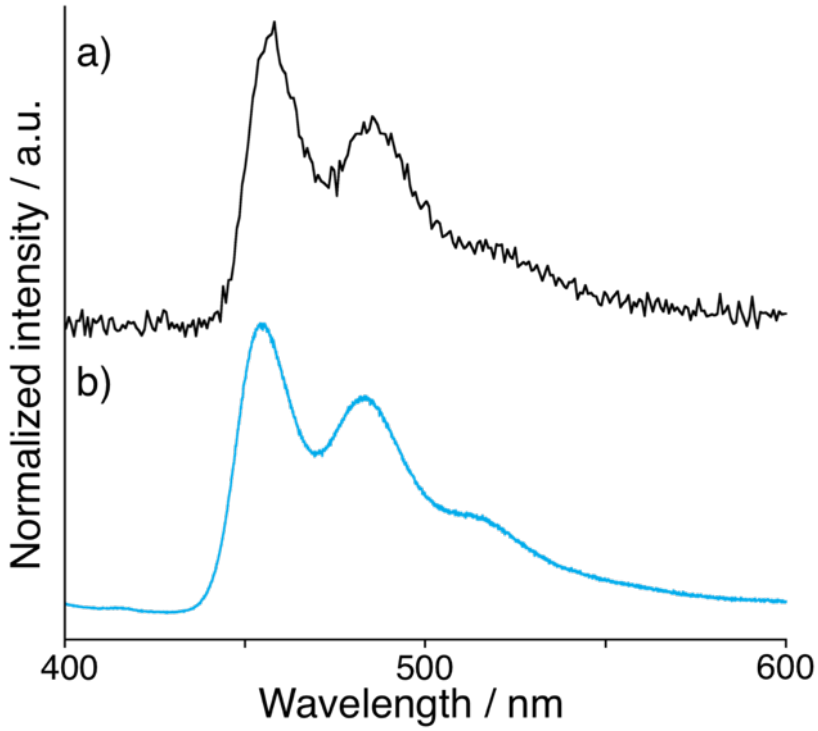

Figure 6-7. a) TL and b) PL spectra of $[Gd(hfa)_3(dpf)]_n$ using a CCD system and a spectrometer, respectively. The PL spectrum was measured at 100 K (λ_{ex} = 380 nm).

6.3.6 Atmospheric dependence of TL and PL

In order to lastly confirm the possibility of TL generated by excited N_2 gas in an air, the author also measured the PL and TL spectra of $[Tb,Eu(hfa)_3(dpf)]_n$ (Tb/Eu = 1) under an argon atmosphere and an air. The spectral difference depending on atmosphere was not observed for both TL and PL (Figure 6-8). The characteristic blue emission of excited nitrogen gas in the air at around 400 nm was not observed while grinding, too. In addition, the compound exhibited TL even under vacuum. Thus, the TL of $[Ln(hfa)_3(dpf)]_n$ occur through neither i) ligand excitation by absorbing the blue emission of excited N_2 gas nor ii) energy transfer from excited N_2 gas to Ln(III) excited state.

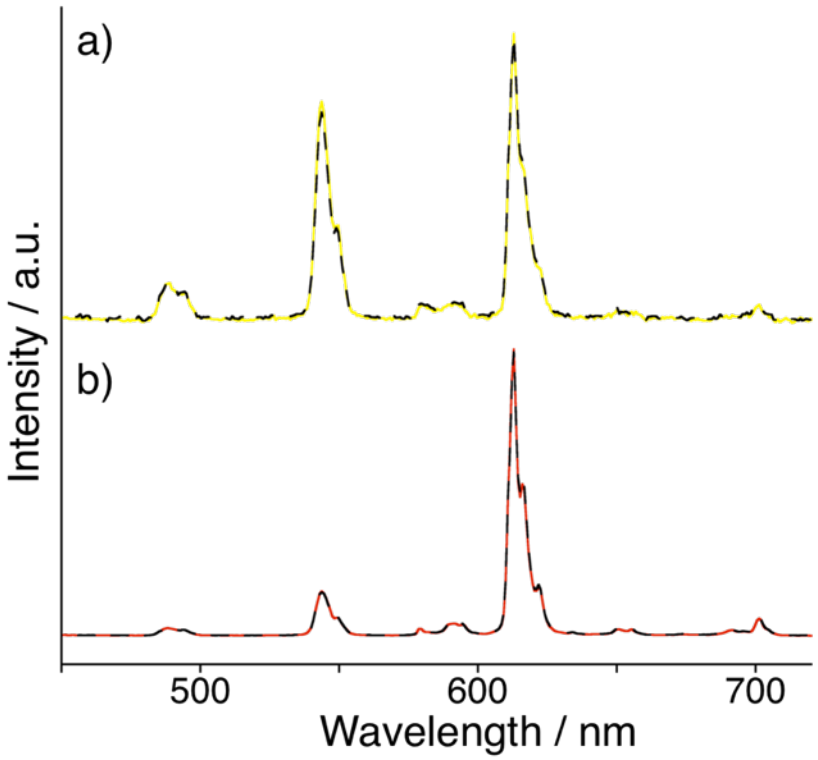

Figure 6-8. a) TL and b) PL spectra spectra of $[Tb,Eu(hfa)_3(dpf)]_n$ (Tb/Eu = 1) under an argon atmosphere (solid line) and an air (dashed line).

6.3.7 Summary of observed properties and further assumptions

The excitation process of TL in Ln(III) complexes has been basically discussed by ligand-excitation or direct Ln(III)-excitation. Sweeting and Rheingold reported that the charge separation upon cleavage excited the antenna ligands, followed by the formation of Ln(III) excited states via intramolecular energy transfer (ligand-excitation).[27] Bourhill and co-workers also described Ln(III) excitation by electron bombardment (direct Ln(III)-excitation).[37] In this study, we observed a large spectral difference between TL and PL. The contribution of Tb(III)-centered emission is larger than that of Eu(III)-centered emission in TL, in contrast to PL. According to the results, the author considers the TL of Ln(III) coordination compounds to be responsible for both the ligand-excitation and direct Ln(III)-excitation (Figure 6-9), unlike the selective excitation with a specific wavelength (e.g., λ_{ex} = 380 nm) in PL. The photophysical parameters in Table 6-2 also indicate that the efficiency of direct Ln(III)-excitation is higher than that of ligand-excitation under the condition of mechanical grinding. Thus, the reddish-orange PL and yellow TL of $[Tb,Eu(hfa)_3(dpf)]_n$ (Tb/Eu = 1) can be explained by the higher Φ_{ff} of Tb(III) ions ($\Phi_{ff,Tb}$ = 88%) than that of Eu(III) ions ($\Phi_{ff,Eu}$ = 73%). The greenish-yellow PL and green TL in the Tb/Eu = 10 polymer can also be explained by this difference. When considered in the same manner, the Tb(III)/Eu(III) mixed coordination polymers $[Tb,Eu(hfa)_3(X)]_n$ (Tb/Eu = 1, $\Phi_{ff,Tb} < \Phi_{ff,Eu}$) with yellow PL would exhibit orange or red TL.

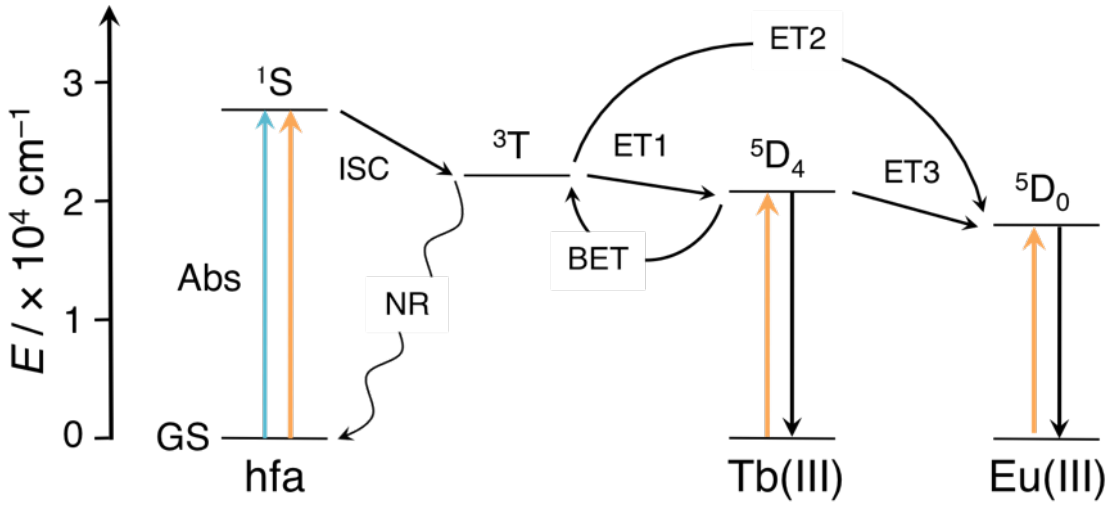

Figure 6-9. A simplified diagram of excitation processes of TL (orange line) and PL (blue line) in Tb(III)/Eu(III) mixed coordination polymers (Abs: absorption, ET: energy transfer, GS, ground state, ^{1}S: singlet excited state, ^{3}T: triplet excited state, ISC: intersystem crossing, NR: non-radiative relaxation).

Table 6-2. Summary of TL and PL properties of furan-bridged polymers $[Ln(hfa)_3(dpf)]_n$.

Sample	Φ_{tot}[a] / %	Φ_{ff}[b] / %	η_{sens}[a] / %	τ_{obs}[c] / ms	PL color	TL color
$[Eu(hfa)_3(dpf)]_n$	64	73	88	0.72	Red	Red
$[Tb(hfa)_3(dpf)]_n$	40	88[d]	45	0.60	Green	Green
$[Tb,Eu(hfa)_3(dpf)]_n$ (Tb/Eu = 1)	-	-	-	0.32 (τ_{Tb})	Reddish-orange	Yellow
$[Tb,Eu(hfa)_3(dpf)]_n$ (Tb/Eu = 10)	-	-	-	0.36 (τ_{Tb})	Greenish-yellow	Green

[a] λ_{ex} = 380 nm. [b] Equation 3-5 in Chapter 2. [c] λ_{ex} = 355 nm. [d] Φ_{ff} for Tb(III) complex was estimated by $\Phi_{ff,Tb} = (\tau_{obs,RT} / \tau_{obs,100K}) \times 100$, assuming that the τ_{obs} at 100 K is a lifetime without non-radiative process.

6.4 Conclusion

Highly TL-active and strong PL Ln(III) coordination polymers were successfully prepared by introducing a furan-based polar bridging ligand. The relationships between crystal structures and TL activity were systematically studied using Eu(III) coordination polymers with face-to-face/alternate intermolecular packing structures. The face-to-face arrangement of bulky substituents plays an important role in providing strong TL activity. The potential differences between TL and PL were clearly demonstrated by the TL and PL spectra of Tb(III)/Eu(III) mixed coordination polymers. Based on the results, the author suggested the existence of discrete excitation mechanisms for TL and PL phenomena.

The strategy for constructing strong TL-active compounds would be a key to reveal the ambiguous relationships between luminescence and mechanical stress. These compounds are also expected to be useful as optical sensors, being sensitive to impact and pressure. In addition, compounds with varied emission colors depending on the excitation methods are highly attractive for advanced security materials.

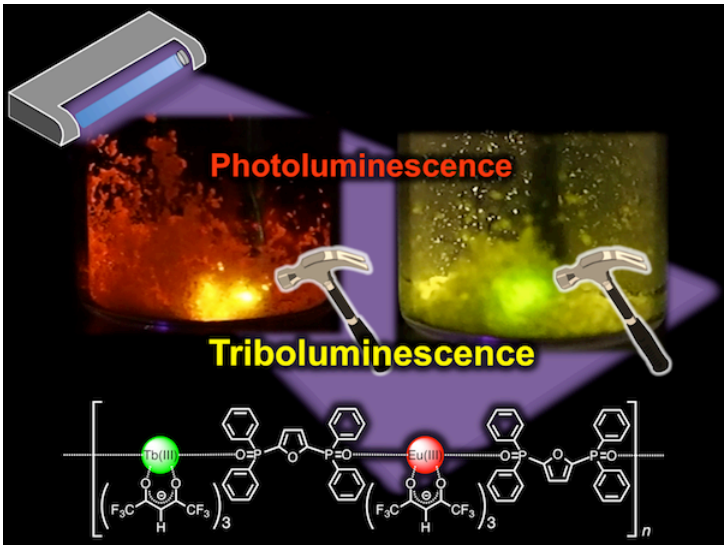

6.5 References

[1] D.O. Olawale, T. Dickens, W.G. Sullivan, O.I. Okoli, J.O. Sobanjo, B. Wang, *J. Lumin.* **2011**, *131*, 1407-1418.

[2] X.D. Wang, H.L. Zhang, R.M. Yu, L. Dong, D.F. Peng, A.H. Zhang, Y. Zhang, H. Liu, C.F. Pan, Z.L. Wang, *Adv. Mater.* **2015**, *27*, 2324-2331.

[3] D.O. Olawale, K. Kliewer, A. Okoye, T.J. Dickens, M.J. Uddin, O.I. Okoli, *J. Lumin.* **2014**, *147*, 235-241.

[4] R.S. Fontenot, W.A. Hollerman, K.N. Bhat, M.D. Aggarwal, B.G. Penn, *Poly. J.* **2014**, *46*, 111-116.

[5] G.P. Williams, T.J. Turner, *Solid State Commun.* **1979**, *29*, 201-203.

[6] J.I. Zink, *Inorg. Chem.* **1975**, *14*, 555-558.

[7] J.I. Zink, G.E. Hardy, J.E. Sutton, *J. Phys. Chem.* **1976**, *80*, 248-249.

[8] G.E. Hardy, J.C. Baldwin, J.I. Zink, W.C. Kaska, P.H. Liu, L. Dubois, *J. Am. Chem. Soc.* **1977**, *99*, 3552-3558.

[9] K.F. Wang, L.R. Ma, X.F. Xu, S.Z. Wen, J.B. Luo, *Sci. Rep.* **2016**, *6*, 1-9.

[10] A.J. Walton, *Adv. Phys.* **1977**, *26*, 887-948.

[11] J.C. Zhang, L.Z. Zhao, Y.Z. Long, H.D. Zhang, B. Sun, W.P. Han, X. Yan, X.S. Wang, *Chem. Mater.* **2015**, *27*, 7481-7489.

[12] H. Nakayama, J. Nishida, N. Takada, H. Sato, Y. Yamashita, *Chem. Mater.* **2012**, *24*, 671-676.

[13] J. Nishida, H. Ohura, Y. Kita, H. Hasegawa, T. Kawase, N. Takada, H. Sato, Y. Sei, Y. Yamashita, *J. Org. Chem.* **2016**, *81*, 433-441.

[14] F. Marchetti, C. Di Nicola, R. Pettinari, I. Timokhin, C. Pettinari, *J. Chem. Educ.* **2012**, *89*, 652-655.

[15] C.-W. Hsu, K. T. Ly, W.-K. Lee, C.-C. Wu, L.-C. Wu, J.-J. Lee, T.-C. Lin,

S.-H. Liu, P.-T. Chou, G.-H. Lee, Y. Chi, *ACS Appl. Mater. Inter.* **2016**, *8*, 33888-33898.

[16] J. Chen, Q. Zhang, F.-K. Zheng, Z.-F. Liu, S.-H. Wang, A. Q. Wu, G.-C. Guo, *Dalton Trans.* **2015**, *44*, 3289-3294.

[17] X.-F. Chen, X.-H. Zhu, Y.-H. Xu, S. Shanmuga Sundara Raj, S. Ozturk, H.-K. Fun, J. Ma, X.-Z. You, *J. Mater. Chem.* **1999**, *9*, 2919-2922.

[18] J. P. Duignan, I. D. H. Oswald, I. C. Sage, L. M. Sweeting, K. Tanaka, T. Ishihara, K. Hirao, G. Bourhill, *J. Lumin.* **2002**, *97*, 115-126.

[19] K.A. Gschneidner, Jr., J.-C.G. Bünzli, V.K. Pecharsky, *Handbook on the Physics and Chemistry of Rare Earths*; Elsevier: Amsterdam, **2005**.

[20] D.O. Olawale, O.O.I. Okoli, R.S. Fontenot, W.W. Hollerman, *Triboluminescence: Theory, Synthesis, and Application*; Springer Nature: Switzerland, **2016**.

[21] S.V. Eliseeva, J.-C.G. Bünzli, *Chem. Soc. Rev.* **2010**, *39*, 189-227.

[22] J.-C.G. Bünzli, C. Piguet, *Chem. Soc. Rev.* **2005**, *34*, 1048-1077.

[23] K. Binnemans, *Chem. Rev.* **2009**, *109*, 4283-4374.

[24] S.J. Butler, D. Parker, *Chem. Soc. Rev.* **2013**, *42*, 1652-1666.

[25] S. Petoud, G. Muller, E.G. Moore, J. Xu, J. Sokolnicki, J.P. Riehl, U.N. Le, S.M. Cohen, K.N. Raymond, *J. Am. Chem. Soc.* **2007**, *129*, 77-83.

[26] S. Petoud, S.M. Cohen, J.-C.G. Bünzli, K.N. Raymond, *J. Am. Chem. Soc.* **2003**, *125*, 13324-13325.

[27] L.M. Sweeting, A.L. Rheingold, *J. Am. Chem. Soc.* **1987**, *109*, 2652-2658.

[28] S.V. Eliseeva, D.N. Pleshkov, K.A. Lyssenko, L.S. Lepnev, J.-C.G. Bünzli, N.P. Kuzmina, *Inorg. Chem.* **2010**, *49*, 9300-9311.

[29] Y. Hasegawa, R. Hieda, K. Miyata, T. Nakagawa, T. Kawai, *Eur. J. Inorg. Chem.* **2011**, 4978-4984.

[30] Y. Hirai, T. Nakanishi, Y. Kitagawa, K. Fushimi, T. Seki, H. Ito, Y. Hasegawa, *Angew. Chem. Int. Ed.* **2016**, *55*, 12059-12062.

[31] K. Miyata, T. Ohba, A. Kobayashi, M. Kato, T. Nakanishi, K. Fushimi, Y. Hasegawa, *ChemPlusChem* **2012**, *77*, 277-280.

[32] S. Katagiri, Y. Hasegawa, Y. Wada, S. Yanagida, *Chem. Lett.* **2004**, *33*, 1438-1439.

[33] S.V. Eliseeva, O.V. Kotova, F. Gumy, S.N. Semenov, V.G. Kessler, L.S. Lepnev, J.-C.G. Bünzli, N.P. Kuzmina, *J. Phys. Chem. A* **2008**, *112*, 3614-3626.

[34] K. Miyata, Y. Konno, T. Nakanishi, A. Kobayashi, M. Kato, K. Fushimi, Y. Hasegawa, *Angew. Chem. Int. Ed.* **2013**, *52*, 6413-6416.

[35] Y. Hirai, T. Nakanishi, K. Miyata, K. Fushimi, Y. Hasegawa, *Mater. Lett.* **2014**, *130*, 91-93.

[36] M. Hatanaka, Y. Hirai, Y. Kitagawa, T. Nakanishi, Y. Hasegawa, K. Morokuma, *Chem. Sci.* **2017**, *8*, 423-429.

[37] I. Sage, G. Bourhill, *J. Mater. Chem.* **2001**, *11*, 231-245.

Appendices

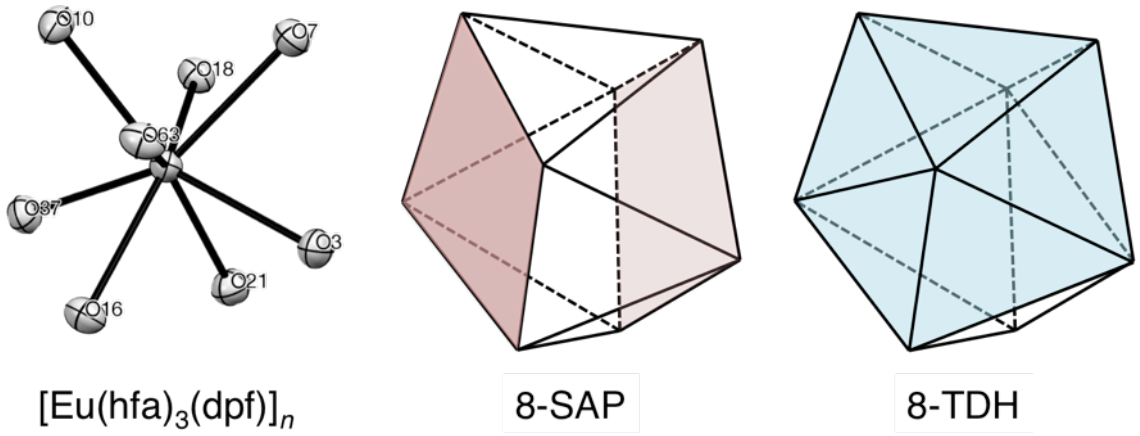

Figure A6-1. Coordination environments around an Eu(III) ion of $[Eu(hfa)_3(dpf)]_n$.

Table A6-1. The observed (δ_i), idealized dihedral angles (θ_{SAP}, θ_{TDH}), and calculated S values ($S_{8\text{-}SAP}$, $S_{8\text{-}TDH}$) for $[Eu(hfa)_3(dpf)]_n$.

		SAP			TDH		
	δ_i	θ_{SAP}	$\delta_i - \theta_{SAP}$	$(\delta_i - \theta_{SAP})^2$	θ_{TDH}	$\delta_i - \theta_{TDH}$	$(\delta_i - \theta_{TDH})^2$
O63-O37	12.23	0	12.23	149.57	29.86	−17.63	310.82
O63-O10	82.10	77.1	5.00	25.00	61.48	20.62	425.18
O63-O16	85.48	77.1	8.38	70.22	74.29	11.19	125.22
O37-O10	77.12	77.1	0.02	0.0004	74.29	2.83	8.01
O37-O16	84.09	77.1	6.99	48.86	61.48	22.61	511.21
O3-O18	3.13	0	3.13	9.80	29.86	−26.73	714.49
O3-O21	81.86	77.1	4.76	22.66	61.48	20.38	415.34
O3-O7	77.71	77.1	0.61	0.37	74.29	3.42	11.70
O18-O7	78.33	77.1	1.23	1.51	76.62	1.71	2.92
O18-O21	73.55	77.1	−3.55	12.60	74.84	−1.29	1.66
O21-O37	56.92	51.6	5.32	28.30	54.51	2.41	5.81
O21-O16	44.33	51.6	−7.27	52.85	48.09	−3.76	14.14
O3-O63	51.09	51.6	−0.51	0.26	47.76	3.33	11.09
O3-O16	49.83	51.6	−1.77	3.13	54.48	−4.65	21.62
O7-O63	53.72	51.6	2.12	4.49	52.57	1.15	1.32
O7-O10	48.83	51.6	−2.77	7.67	52.85	−4.02	16.16
O18-O37	54.33	51.6	2.73	7.45	47.34	6.99	48.86
O18-O10	52.63	51.6	1.03	1.06	52.63	0	0
			S_{SAP} = 4.98			S_{TDH} = 12.12	

Table A6-2. Crystal data of the $[Ln(hfa)_3(dpf)]_n$ (Ln = Tb, Gd, Eu).

	$[Tb(hfa)_3(dpf)]_n$	$[Gd(hfa)_3(dpf)]_n$	$[Eu(hfa)_3(dpf)]_n$
Chemical formula	$C_{43}H_{25}F_{18}O_9P_2Tb$	$C_{43}H_{25}F_{18}GdO_9P_2$	$C_{43}H_{25}EuF_{18}O_9P_2$
Formula weight	1248.51	1246.83	1241.54
Crystal system	Monoclinic	Monoclinic	Monoclinic
Space group	Cc(#9)	Cc(#9)	Cc(#9)
a / Å	19.9974(8)	19.9832(7)	19.9767(6)
b / Å	14.8560(4)	14.8898(5)	14.9113(4)
c / Å	16.0129(6)	16.0514(5)	16.0652(5)
α / deg	90.000	90.000	90.000
β / deg	97.0396(14)	96.9250(10)	96.9906(9)
γ / deg	90.000	90.000	90.000
Volume / $Å^3$	4721.3(3)	4741.2(3)	4749.9(2)
Z	4	4	4
d_{calc} / g cm^{-3}	1.756	1.747	1.736
Temperature / °C	−150	−150	−150
μ (Mo Ka) / cm^{-1}	16.868	15.938	15.085
max 2θ / deg	55.0	54.8	54.9
Reflections	21629	21833	22274
Independent refle	9599	10146	9993
R_1	0.0528	0.0266	0.0306
wR_2	0.1426	0.0540	0.0660

[a] $R_1 = \sum ||F_o| - |F_c|| / \sum |F_o|$. [b] $wR_2 = [\sum w (F_o^2 - F_c^2)^2 / \sum w (F_o^2)^2]^{1/2}$.

Chapter 7

Summary and outlook

Abstract

In this thesis, the author discussed the design of organic bridging ligands to control the entire moieties of assembled Ln(III) coordination compounds and their photophysical, thermal, and mechanical properties. These molecular designs provide strong luminescence upon ligand excitation (Chapter 2), tunable emission colors (Chapter 3), glass-formability (Chapters 4, 5), and mechanical stress-sensitivity (Chapter 6) depending on the geometrical structures of organic bridging ligands and incorporated Ln(III) ions. In this chapter, a summary of the results, possible applications, and future perspectives are presented.

7.1 Summary of the results

The author aimed to systematically control the assembled structures of Ln(III) coordination compounds for achieving novel photophysical, thermal, and mechanical properties. The design of a series of organic bridging ligands to control the entire moieties of Ln(III) complexes and to exploit the advantages of strong luminescent $Ln(hfa)_3$ units is described in this thesis.

In Chapter 1, a brief history of luminescent materials was given. The scientific background of the development of luminescent lanthanide complexes and achievements such as strong luminescence and thermal stability were described.

A novel packing system, “coordination zippers,” for improving the efficiency of the photo-sensitization process was introduced in Chapter 2. Densely packed structures were provided by bent-angled thiophene-based bridging ligands, and characteristic low-lying absorption bands that arose from the stabilized energy level of antenna ligands were observed. Higher energy transfer efficiency (η_{sens} = 80%) and thermal stability (d.p. = 322˚C) were achieved by reducing the intra-chain hfa-hfa distances and increasing intermolecualr CH/F and CH/π interactions.

In Chapter 3, energy transfer between Ln(III) ions was systematically investigated using biphenylene-bridged coordination polymers with various Tb(III)/Eu(III) mixture ratios. The energy transfer efficiencies were found to depend on the mixture ratios, which varied from 99% to 8.2% at room temperature (Tb/Eu = 1-500). Unusual negative energy transfer efficiency was estimated for Tb/Eu = 750, indicating the different dominating concentration quenching mechanisms of Tb(III) and Eu(III) ions.

In Chapter 4, molecular designs for amorphous and luminescent Ln(III) complexes were reported. *Ortho*-, *meta*-, and *para*-substituted phenylene-bridging ligands with ethynyl groups were prepared. Single crystal X-ray analyses and DFT optimizations revealed the formation of dimer, trimer, and polymer structures. The glass transition properties were found to depend on the moiety of bridging ligands (T_g = 25-96˚C). The ethynyl groups as well as *pseudo*-C_3 structures contributed to the formation of an amorphous state.

Systematic construction of Ln(III) coordination glasses using bent-angled bridging ligands with ethynyl groups was described in Chapter 5. Temperature-sensitive Ln(III) coordination compounds were prepared following the strategy described in Chapter 2 and Chapter 4. Green, yellow, orange, and red photoluminscence (PL) in a glassy state was successfully observed depending on the temperature.

In Chapter 6, triboluminescence (TL) of Ln(III) coordination polymers was focused. A series of strong TL compounds was prepared by introducing an inter-molecular face-to-face arrangement of CF_3 substituents, and relationships between packing structures and TL activity were investigated. In addition, the excitation process of TL from both ligands and Ln(III) ions was proposed, on the basis of TL observations in a Gd(III) coordination polymer and an Eu(III) coordination polymers with varied PL efficiencies. These features provided the large spectral difference between TL and PL in Tb(III)/Eu(III) mixed systems.

7.2 Outlook

The photophysical, thermal, and mechanical properties of Ln(III) coordination compounds can be controlled by organic bridging ligands (Figure 7-1). The enhancement of intermolecular interactions leads to thermal stability, and the suppression of intermolecular packing is also advantageous for the formation of glassy materials. In addition, intermolecular disordered arrangement of substituents can trigger stress-sensitive luminescence.

The novel designs of bridging ligands have further potential for the development of functional materials such as low temperature-sensitive luminescent dyes to visualize the ice-coating of super-cooled liquid on airframes, thermally stable luminescent Ln(III) coordination glasses for EL devices, and NIR-PL/VIS-TL coordination polymers for hyper-advanced security marking techniques. As well as the obvious importance of the strong luminescence, these “additional” features are attractive for next-generation functional luminescent materials.

The author hopes that the molecular designs described in this thesis break new ground for functional materials with strong luminescence and additional physical properties arising from specific assembled structures. The relationships between photoluminescence and other physical properties are also expected to provide scientific understandings of fluid dynamics in unsteady flows, thermophysics in glass transitions, and photoscience in triboluminescence.

Acknowledgements

I would like to express my sincere gratitude to Prof. Dr. **Yasuchika Hasegawa**, Laboratory of Advanced Materials Chemistry (AMS Lab) in Hokkaido University for his continuous support of my Ph.D study and related research over a period of 5 years starting from my undergraduate study.

Besides my advisor, I would like to thank Prof. Dr. **Masako Kato**, Prof. Dr. **Hajime Ito**, Dr. **Tomohiro Seki**, and Prof. Dr. **Toshifumi Satoh** in Hokkaido University for sincere guidance in experiments such as single crystal X-ray analyses and DSC measurements for suggestive discussion about the results. I am also grateful to Prof. Dr. **Kazuyoshi Tanaka**, Dr. **Hiroyuki Fueno**, Prof. Dr. **Keiji Morokuma**, and Dr. **Miho Hatanaka** (now in Kinki University) in the Fukui Institute for Fundamental Chemistry (FIFC), Kyoto University for cooperative work on quantum calculations of coordination structures and energy transfer efficiencies using a cutting-edge supercomputer and theories.

I acknowledge Assoc. Prof. Dr. **Koji Fushimi**, Dr. **Takayuki Nakanishi**, and Dr. **Yuichi Kitagawa** in AMC Lab, Hokkaido University for their kind help, suggestions, and fruitful discussions.

My sincere thanks also go to Dr. **Hirotaka Sakaue** in JAXA (now in the University of Notre-Dame) for the valuable experiments in a hypersonic wind tunnel and motivation to be a scientist with a wide vision.

I am also grateful to Prof. Dr. **Ana de Bettencourt-Dias**, Prof. Dr. **Thomas W. Bell**, Dr. **Andres Zavaleta**, Dr. **Jeff Rossini** and other laboratory members in University of Nevada, Reno for motivation, immense knowledge, experimental techniques, and how it feels like to be an internationalist out of Japan.

I express my thanks to **RIGAKU Co.** and **SHIMADZU Co.** for single crystal X-ray analyses of micro-sized crystals, DSC measurements, and SPM observations.

I would like to acknowledge support by the Japan Society for the Promotion of Science (Grants-in-Aid for JSPS fellows), Grants-in-Aid for Scientific Research on Innovative Areas of “New Polymeric Materials Based on Element-Blocks,” and Frontier Chemistry Center Akira Suzuki “Laboratories for Future Creation” Project.

I would like to thank everyone I met in domestic and international conferences, overseas study, internship, etc. who gave me great motivation and opportunities to access the latest research and topics in different fields.

Finally, the biggest thanks go to my family, **Mitsuhiro Hirai** and **Rika Hirai**, for their understanding and support.

March, 2017

Yuichi Hirai